**Inaugural dissertation**

**for**

**obtaining the doctoral degree**

**of the**

**Combined Faculty of Mathematics, Engineering and Natural Sciences**

**of the**

**Ruprecht - Karls - University**

**Heidelberg**

**Presented by**

**M.Sc. Aylin Sibel Haas**

**born in: Leonberg, Germany**

**Oral examination: 27th October 2023**

# Gene Regulatory Networks in Plant Stem Cells

-

## Investigating cell fate decision-making in the vascular cambium of *Arabidopsis*

**Referees:** **Prof. Dr. Thomas Greb**

**Prof. Dr. Jan U. Lohmann**

**In memory of those who lost their lives**

2019

2020

2021

2022

2023

# Zusammenfassung

Stammzellen faszinieren die Menschen schon lange, da sie für den Aufbau und den Erhalt vieler Lebensformen von grundlegender Bedeutung sind. Stammzellen sind in der Lage, sich zu teilen und sich selbst zu erhalten und gleichzeitig neue Zelltypen zu produzieren. Wie tierische Stammzellen sind auch pflanzliche Stammzellen ein faszinierendes Forschungsobjekt. Sie liefern die Zellen für das Pflanzenwachstum und ermöglichen es vielen Pflanzen, ihr ganzes Leben lang weiter zu wachsen, wodurch enorme Mengen an pflanzlicher Biomasse auf diesem Planeten produziert werden. Im Rahmen dieser Studie habe ich mich speziell auf die pflanzlichen Stammzellen, die Holz und Bast produzieren, konzentriert. Diese Stammzellen findet man als zylindrischen Stammzellverband, dem vaskulären Kambium, in der Wurzel, im Stamm und in dem Gewebe, das Wurzel und Stamm verbindet, dem Hypokotyl. Bei meinen Analysen habe ich mich auf das Hypokotyl der Modellpflanze *Arabidopsis thaliana* fokussiert, da dort die Holz- und Bastproduktion sehr aktiv ist und der Gewebeaufbau dem vaskulären Kambium von Bäumen ähnelt.

Eine vaskuläre Kambiumstammzelle produziert sowohl Holzvorläuferzellen nach innen als auch Bastvorläuferzellen nach außen. Daher muss sie zwischen den folgenden Zellschicksalen „wählen“: Holzvorläuferzelle werden, Bastvorläuferzelle werden oder Stammzelle bleiben. Auf Grundlage welcher Mechanismen diese erste Zellschicksalsentscheidung getroffen wird, ist bisher nicht geklärt. Um diesen Entscheidungsprozess besser zu verstehen, habe ich in einem ersten Schritt in Zusammenarbeit mit dem Mironova Labor Genregulationsnetzwerke mathematisch modelliert. Dies hat gezeigt, dass ein Netzwerk aus nur drei Genen, die sich gegenseitig auf spezifische Weise regulieren, ausreicht, um die oben genannten drei Zellschicksalsoptionen herbeizuführen. Ich habe anschließend die Hypothese aufgestellt, dass dieses Netzwerk aus zwei sich gegenseitig hemmenden Komponenten des Auxin- und des Cytokininsignalwegs bestehen könnte. Zusätzlich könnten diese Komponenten von WUSCHEL-RELATED HOMEOBOX4 (WOX4), einem wichtigen Transkriptionsfaktor für Stammzellregulation im vaskulären Kambium, reguliert werden. Integriert in ein 1D-Modell generierte dieses Netzwerk bidirektionales

Wachstum. Ich konnte durch in planta Analysen zeigen, dass die Auxin- und Cytokininsignaltransduktion spezifisch im vaskulären Kambium niedrig ist. Um meine Hypothese zu testen, habe ich untersucht, welche Gene der Auxin- und Cytokininsignalwege durch WOX4 reguliert werden, auch im Vergleich zu WUSCHEL, einem Stammzellregulator des Sprossapikalmeristems. Im Rahmen meiner Untersuchungen konnte ich spezifische Typ-A *ARABIDOPSIS RESPONSE REGULATORs* (*ARRs*), die den Cytokininsignalweg negativ regulieren, als mögliche WOX4-Ziele identifizieren. Ich fand heraus, dass die Expression der Typ-A *ARR* Gene *ARR5*, *ARR6*, *ARR7* und *ARR15* im vaskulären Kambium des Hypokotyls reduziert ist. Darüber hinaus habe ich beobachtet, dass die Expression von *ARR6* und *ARR15* durch WOX4 herunterreguliert wird. Diese Art der Regulation von Typ-A *ARRs* wird auch durch WUSCHEL im Sprossapikalmeristem ausgeübt und könnte daher ein generelles Konzept der pflanzlichen Stammzellregulation darstellen. Zusätzlich deuten Ergebnisse dieser Studie darauf hin, dass WOX4 möglicherweise selbst durch Cytokinin über das DNA BINDING WITH ONE FINGER2.1 (DOF2.1) Protein reguliert wird. Von zentraler Bedeutung ist, dass die Mutation von *ARR7* und *ARR15* die Zellschicksals-Entscheidungen der vaskulären Kambiumstammzelle verändert und mehr Holzzellen produziert werden als in Wildtyppflanzen. Zusammenfassend legt diese Studie nahe, dass ein Mechanismus der Zellschicksals-Entscheidungen von vaskulären Kambiumstammzellen auf der Regulierung des Cytokininsignalwegs durch WOX4 und durch Typ-A ARRs basiert.

# Abstract

Stem cells have fascinated humans for a long time because of their fundamental importance in building and sustaining many forms of life. Stem cells are able to divide and maintain themselves while producing new cell types. Like animal stem cells, plant stem cells are a fascinating research object. They provide the cells for plant growth and allow many plants to continue growing throughout their lives, thereby producing enormous amounts of plant biomass on this planet. In this study, I specifically focussed on the plant stem cells that produce wood and bast. These stem cells form a cylindrical stem cell niche, the vascular cambium, which is found in the root, the stem and the tissue that connects the root and stem, the hypocotyl. In my analyses, I focused on the hypocotyl of the model plant *Arabidopsis thaliana*, since wood and bast production is very active there and the tissue patterning resembles the patterning of the vascular cambium of trees.

A vascular cambium stem cell produces both, wood progenitor cells inward and bast progenitor cells outward. Thus, it needs to “choose” between the following cell fates: becoming a wood progenitor cell, becoming a bast progenitor cell, or remaining a stem cell. The basis on which this first cell fate decision is made has not yet been clarified. To better understand this decision-making process, in a first step I mathematically modelled gene regulatory networks in collaboration with the Mironova laboratory. This has shown that a network of just three genes that regulate each other in a specific way is sufficient to bring about the three cell fate possibilities mentioned above. I then hypothesized that this network could consist of two mutually inhibitory auxin and cytokinin signalling pathway components. Furthermore, these components could be additionally regulated by WUSCHEL-RELATED HOMEOBOX4 (WOX4), an important transcription factor for stem cell regulation in the vascular cambium. Integrated into a 1D model, this network generated bidirectional growth. Using in planta analysis, I was able to show that both auxin and cytokinin signalling levels are low specifically in the vascular cambium. To test my hypothesis, I investigated which genes of the auxin and cytokinin pathways are regulated by WOX4, also in comparison to WUSCHEL, a stem cell regulator of the shoot apical meristem. In the course of my investigations, I

identified specific type-A *ARABIDOPSIS RESPONSE REGULATORs* (*ARRs*), which negatively regulate cytokinin signalling, as putative WOX4 targets. I found that the expression of the type-A *ARR* genes *ARR5*, *ARR6*, *ARR7* and *ARR15* is reduced in the hypocotyl vascular cambium. Furthermore, I observed that the expression of *ARR6* and *ARR15* is downregulated by WOX4. WUSCHEL also exerts this type of regulation on type-A *ARRs* in the shoot apical meristem and therefore this could represent a general concept for the regulation of plant stem cells. In addition, findings in this study propose that WOX4 itself is regulated by cytokinin via the DNA BINDING WITH ONE FINGER 2.1 (DOF2.1) protein. Importantly, when *ARR7* and *ARR15* are mutated, the cell fate decisions of vascular cambium stem cells are altered and more wood cells are produced than in wild type plants. In conclusion, this study suggests that a mechanism of cell fate decision making in vascular cambium stem cells is based on the regulation of cytokinin signalling by WOX4 and by type-A ARRs.

# Contributions

Some unpublished plant lines and datasets I used and analyzed in this thesis were contributed by the following collegues: **Dr. Viriginie Jouannet** (COS, Heidelberg University) generated the *pWOX4:WOX4-GR* line in the *wox4-1* background. The *pUBI10:mCherry-GR* line was provided by the **Jan Lohmann Lab** (COS, Heidelberg University). **Dr. Dongbo Shi** (COS, Heidelberg University) generated the cambium domain-specific RNA-seq dataset and performed its analysis. **Dr. Eliana Mor** (VIB, Ghent, Belgium) generated the *pRPS5A:WOX4-GR* RNA-seq dataset (analysed and published in Mor, 2020), and provided the raw files for re-analysis. All published material used are referenced accordingly.

Some results presented in this thesis were done in collaboration with the following colleagues: Together with **Dr. Marjorie Guichard** (Heinrich-Heine-University, Düsseldorf, Germany) I worked on the idea of accelerated analysis of hypocotyl cross-sections. Marjorie wrote the first draft of the Fiji macro for the semi-automated high-throughput phenotyping of hypocotyls, with subsequent modifications and finalization by me. **Dr. Michael Gebert** (COS, Heidelberg University) supported me in generating the *pUBI10:mCherry-GR-WOX4* line by performing some of the steps necessary to establish the line and supporting the characterization of the line. Together with **M.Sc. Inés Hidalgo Prados** (COS, Heidelberg University) I characterized the *pUBI10:mCherry-GR-WUS*, *pUBI10:mCherry-GR-WOX4* and *pUBI10:mCherry-GR* lines and performed the RNA-seq experiment. The subsequent RNA-seq analysis for comparing *WOX4* and *WUS* effects was performed entirely by myself.

## Mathematical Modelling

The mathematical modelling results presented in this thesis were generated in collaboration with the following colleagues: **Prof. Dr. Victoria V. Mironova** (Radboud University, Nijmegen, The Netherlands) introduced me to mathematical modelling and guided the modelling part of my thesis. Together with Victoria, **M.Sc. Daria Azarova** (Novosibirsk State University, Novosibirsk, Russia) and **Dr. Viktoriya Lavrekha** (Institute of Cytology and Genetics/ Novosibirsk State University, Novosibirsk, Russia)

I performed the modelling and analysis of the gene regulatory networks (GRNs) and the 1D cambium growth model. In detail, the equations of the GRN model 1 were constructed jointly by Victoria, Daria and me. Parameter optimization of the GRN model 1 was done jointly and iteratively by me and Daria. The equations of the improved GRN model 2 were constructed jointly by me, Daria and Victoria. The code for the phase portraits was constructed first by Daria and then improved iteratively together with me. The first draft of the equations of the core GRN for the 1D cambium growth model was generated by me. Improvements were made by Daria, Victoria and Viktoriya. The basis of the MATLAB script for the 1D model was generated by Victoria, Daria and Viktoriya based on previously published work (Mironova et al., 2010; Savina et al., 2020). **Dr. Maria Savina** (Radboud University, Nijmegen, The Netherlands) advised me on the technical aspect of the published models. Integration of the GRN and cell fate decision-making mechanism into the 1D model layout was done by Victoria and Viktoriya. Adjustment of the code was carried out by Viktoriya, me and Victoria. Parameter screening and optimization was done by Viktoriya and me, with the final parameter set being constructed by Viktoriya. The cell type counter was introduced by Daria and Viktoriya. The 1D mutant model construction was done by Viktoriya, Victoria and me, and we thank Maria for her advice. To summarize the contributions to the 1D model, I was involved in the generation of the equations describing the core GRN for the 1D model, but the 1D model layout and code was built by my afforementioned collegues, with minor input from me. All text on mathematical modeling in the respective methods, results and discussion chapters as well as the figures presented in this study were created by myself.

# Acknowledgements

Dear Thomas, thank you very much for the possibility to pursue my PhD in your lab. From the beginning you gave me the opportunity to shape my project and then you let me follow the directions I wanted to explore. Thank you for all your support and guidance. Thank you also for your patience, understanding and trust in the many difficult times of the last few years. This was fundamental to me and of immeasurable value.

Dear Victoria, I am very grateful that I had the opportunity to work with you on this project. You are a role model for me in many ways. Thank you very much for opening the world of mathematical modelling to me and welcoming me as a part of your lab for a while.

Dear Jan, thank you for agreeing to be my referee and for your guidance as thesis advisory committee member. Thank you also very much for being open to and enabling the collaboration with your lab.

Dear Karin, thank you for supporting me on my scientific journey since my masters. Thank you too for your guidance as thesis advisory committee member and for agreeing to also be an examination commission member.

Dear, Steffen (Lemke), thank you very much for agreeing to be the fourth examination commission member.

My thanks also go to all COS members, especially all former and current Greb lab members and Rausch lab members. I would like to thank a few people in particular. Thank you, Dongbo, for guiding me scientifically and personally and for sharing your dataset. Thank you Xiaomin, Jiao and Daria for all the valuable scientific and life-related discussions. I learned so much from you. Special thanks go to Ilona who has many times been of great help to me in the laboratory. Also thank you Conny, Katja,

Nina and Ann-Kathrin for additional lab managing and/ or support with the preparatory lab work. Steffen (Greiner), thank you very much for your support over the years and for answering my many questions. Angelika, thank you for helping me and all of us with organisational things. Thank you very much, Michael (Schilbach), for kindly taking care of my plants when I was away, it helped me tremendously. Thank you, David (Ibberson) for your support with the RNA-seq experiments over the years. Thank you, Moni, for your great help with teaching duties. My special thanks go to our former lab member Virginie Jouannet, who worked on WOX4 before I joined the lab and from whom I inherited a central plant line for this project. Many thanks also go to Inés and Michael (Gebert) for our collaboration.

My PhD study also involved collaborations with people outside COS, whom I would like to thank. My thanks extend to all the Mironova lab members for giving me such a warm welcome and good time during my research stay in the Netherlands. Special thanks go to Daria, Viktoriya and Maria with whom I worked with on the modelling part of the project. Special thanks also go to Yana, for all her support and Eric for devoting so much of his time to help me in the lab.
Thank you, Marjorie, for your help in automating image analysis to make life easier. My thanks also go to Bert de Rybel and Eliana Mor for the great interaction and for generously sharing seed material and datasets.

My heartfelt thanks go to my old and new friends whom I have made over the past years. Thank you for sharing my journey with me and for always supporting me even though we are scattered all over the world. How lucky I was that our paths have crossed!

Finally, I would like to express my deepest gratitude to my parents. Your love and support are exceptional and so precious. Thank you for making this possible for me.

‘We should step off the roller coaster of consumption and spend more time appreciating the wonder of life – of something so hopeful, so complex and yet so apparently effortless as saplings emerging around a tree struck down by lightning.’

*Jonathan Drori*

From ‘The world in a cedar’, Resurgence & Ecologist Magazine, July/August 2022

# Table of Contents

# 1. Introduction

## 1.1 The fascination of stem cells

Stem cells have long fascinated humans, and although research into stem cells began earlier, it was not until the late 20th century with the advent of cellular and molecular biology that a better understanding of stem cells and their functions came about (Laurenti & Göttgens, 2018; Charitos *et al.*, 2021). What is fascinating about stem cells is their ability to maintain themselves alive and in an undifferentiated state, sometimes for very long periods of time, depending on the species. At the same time, through cell division, stem cells produce daughter cells, which develop into different cell types, eventually forming a whole multicellular organism. Maintaining the function of stem cells is fundamental for plants, animals and humans throughout their lives. The driving question is therefore to understand how stem cells work and what mechanisms they rely on. Embryogenesis and haematopoiesis are important research areas for the study of stem cell maintenance, initial cell fate decision-making and further differentiation mechanisms (Haghverdi & Ludwig, 2023) (see also **Glossary Table 1**). In mammalian embryogenesis the first cell fate decisions are made at the 16-cell stage, based on the outer or inner position and cell polarity of cells (Haghverdi & Ludwig, 2023). The subsequent cell division and cell fate decision-making of the inner cells that will form the embryo is then achieved, amongst other things, by concentration gradients of instructive signals and transcriptional regulators (Haghverdi & Ludwig, 2023). As another example, the hematopoietic stem cells produces new blood cells throughout an individual's lifespan, so the stem cell pool and correct cell fate decision-making must be maintained throughout life (Haghverdi & Ludwig, 2023). An important step in understanding stem cell maintenance is the identification of key genes that can sustain cells as stem cells. For mouse embryonic stem cells, the *OCTAMER BINDING TRANSCRTIPTION FACTOR 4* (*OCT4*) gene has been shown to be one of the key factors for maintenance of stem cells whose daughter cells can differentiate into many different cell types (Wang *et al.*, 2012).

A recent study analysed the emergence of a gene regulatory network to which *OCT4* belongs and found that it can be dated back to the origin of jawed vertebrates (Sukparangsi *et al.*, 2022), around 400 million years ago. Although animal and human models are extensively researched, plant stem cells are an important area of research too: plants grow throughout their lifespan and all the biomass is produced by the stem cells. A key question in understanding stem cells is: how do stem cells make cell fate decisions? Because the underlying regulatory mechanisms of these cell fate decisions are highly complex, we may never be able to fully decipher them. Therefore, the identification of key mechanisms is a reasonable aim and is hugely important in various fields such as medicine and food or wood production.

### 1.1.1 Cell fate decision-making

A stem cell daughter can receive external or internal cues that instruct the cell fate decision-making process followed by differentiation, which ultimately leads to the emergence of a certain specialized cell type (see also **Glossary Table 1**). This process was famously represented graphically by Waddington as a rolling ball on a hilly surface, termed the Waddington Landscape (Haghverdi & Ludwig, 2023). For the ball (i.e., cell) the starting point is at the top of the hill. The cell fate decision is made at the first point where there are different valleys to roll into and only one of which is taken by the ball. In the end, the ball lands at a specific point, which represents a specific cell type that it has gradually acquired on its path through the landscape (Haghverdi & Ludwig, 2023). This progressive process was the first idea about how cell fate decision-making and differentiation can take place (Haghverdi & Ludwig, 2023), but now these processes appear to be much more fluid, and sometimes also cyclical and direct (Kelsh *et al.*, 2021; Subkhankulova *et al.*, 2023). Furthermore, the suitability of the fixed valleys in the Waddington Landscape for the visualization of cell fate induction has been questioned, as it can be argued that cell fate decisions rather eliminate valleys, meaning that the landscape itself changes (Ferrell, 2012).

Although the most common perception is that stem cells are homogenous cells at a certain location of the body, a so-called stem cell niche, over the years it has become clear that stem cells are more of a heterogenous pool comprising linage-biased cells within the stem cell nice (Haas *et al.*, 2018; Haghverdi & Ludwig, 2023). Besides the

genetic program for differentiation, asymmetric cell division leading to asymmetric distribution of cell fate determining factors, as well as stochasticity in gene expression are further possible sources of this heterogeneity (Haas *et al.*, 2018). Nevertheless, many key factors identified so far for guiding cell fate decision and differentiation, so-called differentiation factors, are often transcription factors (Enver *et al.*, 2009; Laurenti & Göttgens, 2018; Haghverdi & Ludwig, 2023). Transcription factors can change the cell state by initiation a transcriptional cascade. In general, changes of single transcription factor levels seems to be sufficient to alter the fate of a given cell (Enver *et al.*, 2009). Generally speaking, cell fate decision-making is a process where a cell restricts its capacity for potential future cell types and this restriction includes transcriptional but also epigenetic changes (Enver *et al.*, 2009; Laurenti & Göttgens, 2018). Stem cells can have a different number of possible cell fates they can go into and are therefore classified into bistable, tristable, quadrastable etc. systems, respectively (Kunze & Khalil, 2022). In the scope of this study, I focus on bistable cell fate decision-making based on transcriptional changes (**Figure 1**).

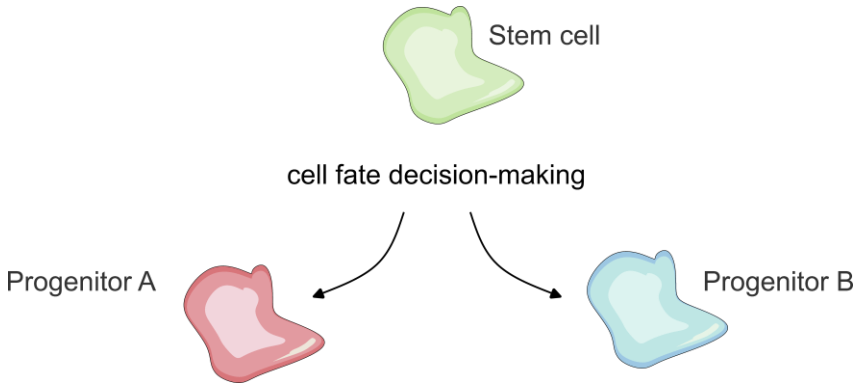


**Figure 1. Graphical illustration of the type of cell fate decision-making investigated in this study.**
Generally, a stem cell daughter is thought to attain a cell progenitor state through cell fate decision-making, and only then does complete differentiation into the final cell type occur. This initial cell fate decision does not involve change of the cell's shape or other parameters important for complete differentiation, but initially only transcriptional and epigenetic changes, which are represented here as colour changes.

By drawing gene regulatory networks (GRNs) composed of transcription factors that activate, repress or attenuate their targets, the regulatory logic of the cell's behaviour can be discovered (Enver *et al.*, 2009). For haematopoiesis, it has been shown that a minimal and simple GRN consisting of just two genes which inhibit each other and

autoactivate themselves can guide cell fate decision-making (Olariu & Peterson, 2019). This GRN was “complex” enough to cause bistability (Olariu & Peterson, 2019).

**Table 1. Glossary of terms regarding stem cells and their regulation.** The definitions presented here were taken from the indicated publications. The definition of these terms may vary in other publications or contexts, but the intention here is to clarify the meaning of the terms within this study. Direct quotations are marked as such.

| Term | Definition |
|---|---|
| Cell state | Mostly describes the given transcriptional state/ gene expression program of a certain cell [1)5)]. A stable cell state is a state which is more insensitive to changes in the environment [1)] . This could be a stem cell state or differentiated cell state. |
| Gene regulatory network | “Comprises the genes and proteins that can interact with each other within a system, or cell. Includes the underlying regulatory logic hat governs the interactions between genes and proteins.” [1)] |
| Cell fate | A term paraphrasing a future possible identify of a cell. [5)] |
| Cell fate decision-making | Describes a single cell which makes “a choice between different gene expression programs” [2)] which includes transcriptional and epigenetic changes [2)], whereby other possible fates are omitted. [5)] In my study the term refers to the decision between different progenitor cell states. |
| Progenitor | A “immediate progeny of stem cells”. [1)] A cell which is not a stem cell anymore but already lineage restricted. [4)] |
| Lineage | A gene expression program which will win over other possible gene expression programs and restrict the possibilities of cell types a cell can differentiate into. [2)] |
| Differentiation | Is “the process of acquiring the specific morphological and transcriptional markers characteristic of an individual cell type (fate)”. [6)] |
| Differentiation factor | In this study used to denote a factor that instructs the cell fate decision-making process towards a certain lineage. |
| Bifacial | The ability of a stem cell to develop two tissue progenitors in strictly opposite directions. [8)] |
| Bistability | A system “having two stable steady states” [7)], meaning that the cell has the potential of being in state A or state B. |

**1)** (Enver *et al.*, 2009)
**2)** (Laurenti & Göttgens, 2018)
**3)** (Kunze & Khalil, 2022)
**4)** (Haas *et al.*, 2018)
**5)** (Haghverdi & Ludwig, 2023)
**6)** (Kelsh *et al.*, 2021)
**7)** (Ferrell, 2012)
**8)** (Shi *et al.*, 2019)

### 1.1.2 Plant stem cells

When referring to stem cells, the term is most often associated with animal or human stem cells. But as mentioned above, plant stem cells also play an important role, basically feeding the world and producing vast amounts of plant biomass which sequester $CO_2$ since millions of years. Plants are particularly fascinating since they exhibit a high developmental plasticity over their lifespan. In plants the shape of organs such as leaves, roots and flowers in mostly predetermined in a species but the abundance of the organs and the final overall shape of the plant is very flexible.

In this study I used *Arabidopsis thaliana* (*Arabidopsis*) as a plant model organism to investigate plant stem cells. Here, plant stem cells are clustered in stem cell niches called meristems. The apical meristems are the shoot apical meristem (SAM) and root apical meristem (RAM), and they ensure longitudinal growth of shoots and roots, respectively (**Figure 2**). Remarkably, the oldest root meristem fossil of a then actively growing plant, already reminiscent of today's cellular layout of the *Arabidopsis* RAM, was identified to be more than 300 million years old (Hetherington *et al.*, 2016). A key lateral meristem is the vascular cambium, which promotes lateral growth, i.e., increasing the thickness of roots and stems, by producing wood (xylem) inward and bast (phloem) outward. It is known that vascular cambium stem cells are bifacial, producing xylem phloem in opposite directions (Bossinger & Spokevicius, 2018; Shi *et al.*, 2019; Smetana *et al.*, 2019) (see also **Glossary Table 1**). The vascular cambium is highly active also in the hypocotyl which is the connection of root and stem below the leaves rosette in *Arabidopsis* (Ragni & Greb, 2018) (**Figure 2**). Within the meristems, the stem cells need to maintain themselves. In addition, the cell fates of their daughter cells need to be tightly regulated. This happens in different cellular arrangements within the SAM, RAM and vascular cambium (**Figure 2**). Generally, it is important to differentiate between primary growth, which means the establishment of growth axes, and secondary growth, which refers to the continued radial growth.

### 1.1.3 WOX transcription factors orchestrate stem cell regulation in plants

In the *Arabidopsis* SAM, RAM and vascular cambium, the stem cells are regulated by transcription factors of the *WUSCHEL-RELATED HOMEOBOX* (*WOX*) gene family (Laux *et al.*, 1996; Sarkar *et al.*, 2007; Hirakawa *et al.*, 2010; Ji *et al.*, 2010; Etchells *et*

*al.*, 2013). The plant specific *WOX* gene family consists of 15 members which are transcription factors. All members contain a highly conserved domain, the homeobox. The homeobox is a protein motif of around 40 amino acids that can bind DNA and is found in both plants and animals (van der Graaff *et al.*, 2009). Importantly, *WOX* genes differ from other homeobox transcription factors because they possess additional domains and are phylogenetically related (Haecker *et al.*, 2004). One example of an additional domain is the eight amino acid long WUS-box, which has been shown to be important for stem cell regulation (Ikeda *et al.*, 2009). Interestingly, *WOX* genes are already important for cell fate decision-making in the embryo (Haecker *et al.*, 2004).

*WUSCHEL* (*WUS*) is the *WOX* gene, which is the key meristem regulator of the SAM and is expressed in the organizing centre (**Figure 2**, marked in yellow). The organizing centre is a subdomain in the SAM where cells are maintained in a quiescent state and which is needed for the regulation of the above localized stem cells. WUS is important for stem cell maintenance, as *wus-1* mutants cannot maintain the stem cells and stop growing (Laux *et al.*, 1996; Mayer *et al.*, 1998). An important meristem regulator of the vascular cambium is *WUSCHEL RELATED HOMEOBOX 4* (*WOX4*), which is expressed in the cambium and xylem. WOX4 promotes proliferation of the cambium stem cells as indicated by *wox4-1* mutants which display reduced cambium activity (Hirakawa *et al.*, 2010; Suer *et al.*, 2011). The *wox4-1* mutant allele was suggested to be a null allele (Hirakawa *et al.*, 2010). In the RAM, *WOX5* is a key regulator and is expressed in the quiescent centre, a specialized subdomain of cells which divide rarely. WOX5 regulates the root cap stem cells distal to the quiescent centre (Sarkar *et al.*, 2007). Interestingly, common regulatory principle among WUS, WOX4 and WOX5 were found. For example, HAIRY MERISTEM transcription factors are important for stem cell proliferation and interact with all three above-mentioned WOX proteins in their respective stem cell niche (Pi *et al.*, 2015; Zhou *et al.*, 2015).

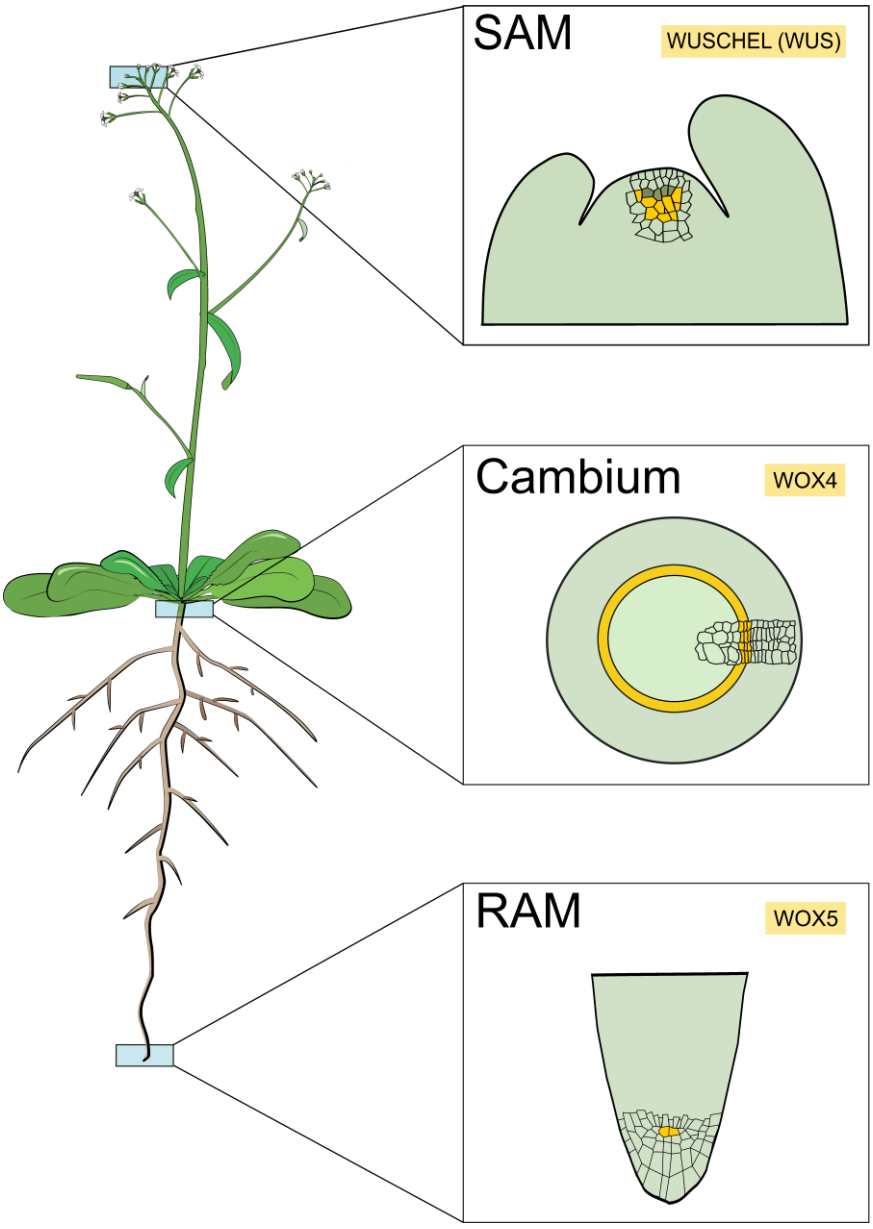


**Figure 2. Plant stem cell niches in *Arabidopsis*.**
The main stem cell niches of *Arabidopsis thaliana* are the shoot apical meristem (SAM), the root apical meristem (RAM) and the vascular cambium (here cambium). The members of the *WOX* gene family are expressed in the cells highlighted in yellow. *WUS* is expressed in the organizing centre in one layer of the stem cells (marked in brown). *WOX4* is expressed in the cambium and xylem. *WOX5* is expressed in the quiescent centre. The cellular layouts are taken from Greb & Lohmann (2016) with permission. The drawing of the *Arabidopsis* plant was modified after Bouché, Frédéric (2018), 2018_Arabidopsis_growing_on_soil. figshare. https://doi.org/10.6084/m9.figshare.7159961.v1.

In this study, I focussed on the vascular cambium since the bifacial differentiation of vascular cambium stem cells makes it ideally suited for the study of cell fate decision-making. Furthermore, the hypocotyl is a site of high vascular cambium activity and the concentric patterning of xylem, cambium and phloem resembles the cambium architecture found in trees (Chaffey *et al.*, 2002).

## 1.2 The vascular system in plants

The vascular system is a system of transporting tissues in a specific group of plants called vascular plants to which *Arabidopsis* belongs to (Woudenberg *et al.*, 2022). Most likely vascular tissues evolved gradually from conductive tissues present in earlier plant forms (Woudenberg *et al.*, 2022). The development of the vascular system proceeds from primary growth to secondary growth which is accompanied by differences in tissue anatomy and regulatory mechanisms (De Rybel *et al.*, 2016). In this study, I mainly describe the vascular system generated during the secondary growth phase but will also include insights from primary growth.

### 1.2.1 Xylem and phloem

Xylem (wood) and phloem (bast) are the transporting tissue of *Arabidopsis* and consist of different cells with specialized functions. Water transport occurs through xylem, specifically xylem vessel cells. These dead cells have a thickened cell wall and form tubes that connect the whole plant body, i.e., the root, the hypocotyl, the stem and leaves. The xylem furthermore consists of xylem parenchyma cells and, in the second phase of xylem development, xylem fibre cells. Phloem consists of phloem parenchyma, companion cells and sieve elements, the latter also form tubes and transport assimilates and nutrients. Since sieve elements lose their nucleus and other organelles during differentiation, companion cells are needed to keep the sieve elements alive. In secondary growth the vascular cambium gives rise to xylem and phloem tissues, which are then called secondary xylem and secondary phloem. What has not yet been mentioned is that on the outside of the phloem another lateral meristem is present, the so-called periderm, which gives rise to the cork and phelloderm, which are protective tissues against water loss and external influences (Ragni & Greb, 2018). In this study, I solely focus on the vascular cambium.

### 1.2.2 The vascular cambium

As mentioned earlier, the vascular cambium produces xylem inward and phloem outward (**Figure 3**). For the sake of simplicity, the vascular cambium will only be referred to as cambium. Previous research has shown that secondary growth initiation, forming the cambium from the procambial tissue, occurs already around five to six days after germination, but this time is variable depending on growth conditions (Smetana

*et al.*, 2019; Turley & Etchells, 2022). Importantly, the cambium can be divided into three spatial domains (**Figure 3**, Inset 1). The proximal domain (depicted in light green) is close to xylem and contains the xylem progenitors (see Glossary Table 1). The central domain (depicted in white) harbours the cambium stem cell and is mostly made up of just one stem cell in each radial cell file (Shi *et al.*, 2019). The third domain is the distal domain, which is close to phloem and contains the phloem progenitors (depicted in light purple). Interestingly, it is assumed that also in trees there is only one stem cell per radial cell file (Bossinger & Spokevicius, 2018). So far it is known that after the cambium stem cell (CSC) divides, one daughter cell will turn into a xylem or phloem progenitor (Shi *et al.*, 2019; Smetana *et al.*, 2019) (**Figure 3**, Inset 2). The other daughter cell remains as a stem cell and can then produce new progenitor cells as it continues to divide. The progenitor cells will differentiate into the final xylem and phloem cell types described above (**Figure 3**, depicted in darker green and purple). The described activity of the CSCs leads to the thickening of the hypocotyl and is the origin of all secondary xylem and secondary phloem produced during secondary growth.

Importantly, the three cambium domains can be distinguished by visualizing the *PHLOEM INTERCALATED WITH XYLEM* (*PXY*) and *SUPPRESSOR OF MAX2 1-LIKE5* (*SMXL5*) expression domains (Shi *et al.*, 2019). *PXY* encodes a receptor important for normal vascular patterning as in *pxy* mutants phloem and xylem are not separated in concentric areas anymore but are intercalated, as the name suggests (Fisher & Turner, 2007). The *SMXL5* gene encodes a protein which has been shown to be important in secondary phloem formation (Wallner *et al.*, 2017, 2020). The three cambium domains in the hypocotyl were already investigated at different developmental stages using lines the *pPXY* and *pSMXL5* reporters (Lebovka *et al.*, 2023) and they reliably enabled the distinction of the cambium domains and hence the identification of the of CSC location as well as the location of xylem and phloem progenitor cells. Details on the function of PXY and SMXL5 in the cambium and further molecular players are discussed in detail in chapter 1.4.

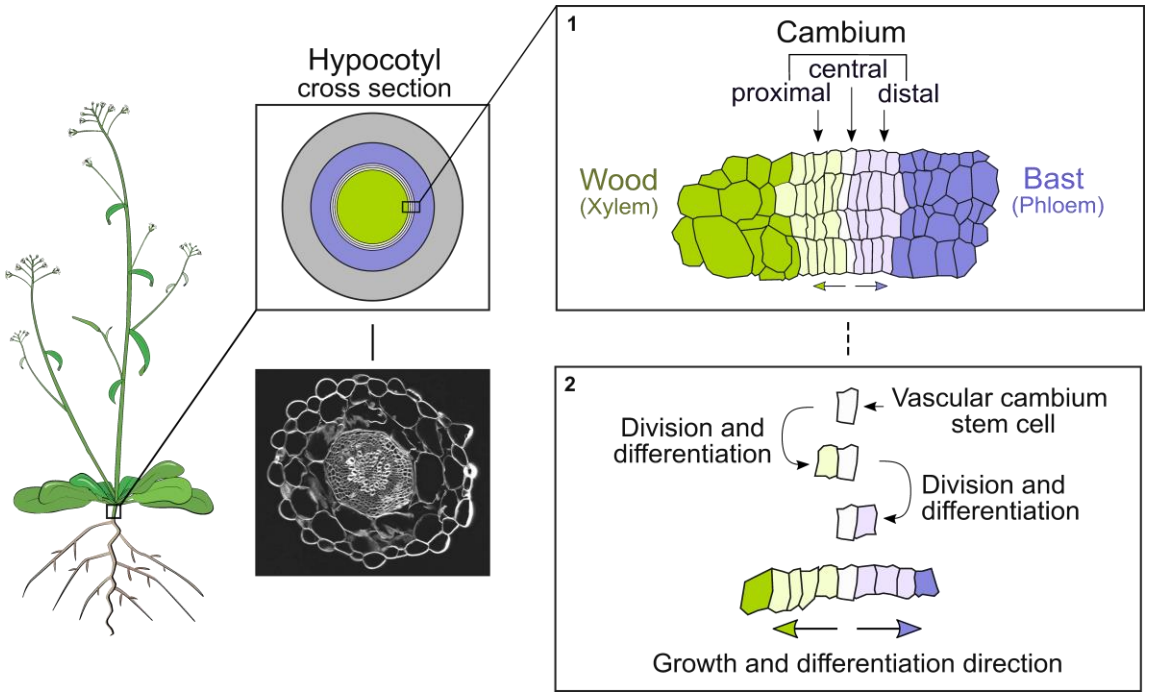


**Figure 3. The hypocotyl cambium in *Arabidopsis*.**
The vascular cambium in the *Arabidopsis* hypocotyl and its function are presented. A microscopy image shows a cross-section of the hypocotyl of a 19-day old plant (stained with Direct Red 23). The cambium produces secondary xylem (green) inward and secondary phloem (purple) outward. Inset 1: The cambium can be divided in the proximal, central and distal domain. Inset 2: The vascular cambium stem cell divides and one daughter cell acquires a progenitor cell fate while the other daughter cell remains in the stem cell state (white). The progenitor cells then fully differentiate into the different xylem and phloem cell types. Through continued division of the stem cell bidirectional growth occurs. This figure was created by me and was published in this form in Haas *et al*., 2022. The cellular cambium layout was taken from Greb & Lohmann (2016) with permission. The drawing of the *Arabidopsis* plant was modified after Bouché, Frédéric (2018), 2018_Arabidopsis_growing_on_soil. figshare. https://doi.org/10.6084/m9.figshare.7159961.v1

The question of vascular cell fate decision-making has been addressed early on and as early as the late 19$^{th}$ century it was hypothesized that a single CSC produces both xylem and phloem fated cells (Sanio, 1873). Since it has now been confirmed that the CSCs make bifacial cell fate decisions (Bossinger & Spokevicius, 2018; Shi *et al.*, 2019; Smetana *et al.*, 2019) they serve as an ideal model system to further investigate cell fate decision-making. Although many processes and factors involved in the differentiation of xylem and phloem cell types are known (De Rybel *et al.*, 2016; Fischer *et al.*, 2019), it still largely remains unclear how the first cell fate decision is made. So far, the cambium can be divided into domains. But as mentioned earlier, it is not yet clear if the central cambium domain can be further subdivided and if there is heterogeneity among the CSCs (Haas *et al.*, 2022). A possibility is that also fluctuating cell states occur (Haas *et al.*, 2022), similar to so-called cyclical fate restriction

hypothesized for neural crest cells, where cells cycle between cell fate biased states (Kelsh *et al.*, 2021).

As mentioned, cell fate decision-making is highly complex and can be influenced by many other processes. Among these processes are sucrose signalling (Narutaki *et al.*, 2023), the circadian rhythm (Torii *et al.*, 2022) and hormone signalling (for example Gordon *et al.*, 2009; Bishopp *et al.*, 2011a; Kondo *et al.*, 2014; Smetana *et al.*, 2019; Salvi *et al.*, 2020; Mäkilä *et al.*, 2023). In this study I focus on the influence of hormone signalling on cell fate decision-making.

## 1.3 Plant hormones and their action in vascular development

Plant hormones are chemical substances that act as signalling molecules and travel through the plant body to regulate a multitude of processes such as germination, flowering and seed maturation (Santner *et al.*, 2009). Furthermore, plant hormones are crucial for the regulation of the plant meristems (Greb & Lohmann, 2016). I will focus here on describing their involvement in the regulation of vascular development.

Many different plant hormones have been shown to be involved in the maintenance and regulation of the cambium as well as xylem and phloem differentiation (Fischer *et al.*, 2019). For example, gibberellic acid, together with auxin, regulates xylem differentiation, lignification and the phase of xylem expansion (Ragni *et al.*, 2011; Denis *et al.*, 2017; Ben-Targem *et al.*, 2021). Furthermore, ethylene (Etchells *et al.*, 2012), strigolactones (Agusti *et al.*, 2011), as well as jasmonic acid (Sehr *et al.*, 2010) promote cambium activity. Auxin and cytokinin are two hormones that have been shown to be central to meristem regulation and their concentration gradients are instructive for plant development (Sachs, 1991; Uggla *et al.*, 1996; Bhalerao & Fischer, 2014). Both hormones are key regulators not only of the cambium but also the SAM and RAM (Zhao *et al.*, 2010; Bishopp *et al.*, 2011a,b; Suer *et al.*, 2011; Salvi *et al.*, 2020). In this study, I specifically focus on the action of the cytokinin and auxin pathways.

### 1.3.1 The phytohormone auxin

Auxin is known to impact many developmental processes in the plant, including vascular development (Bishopp *et al.*, 2011a; Brackmann *et al.*, 2018; Smetana *et al.*,

2019). Among a group of compounds, indole-3-acetic-acid (IAA) is the major natural auxin. IAA can be synthesized from a tryptophane precursor by TRYPTOPHAN AMINOTRANSFERASE OF ARABIDOPSIS (TAA) and YUCCA (YUC) biosynthetic enzymes (Zhao, 2014). Auxin is transported over long distances in the plant and also from cell to cell by diffusion and by active transport, the so-called polar auxin transport (Adamowski & Friml, 2015; Martin-Arevalillo & Vernoux, 2023). There are three main families for auxin transport across the plasma membrane: The PIN-formed (PIN) efflux carriers, the AUX1/LIKE-AUX1 (AUX1/LAX) influx carriers, and the ATP-BINDING CASSETTE B4 (ABCB) influx and efflux carriers (Martin-Arevalillo & Vernoux, 2023). Generally, polar auxin transport can lead to auxin concentration gradients. That auxin concentration gradients are important for vascular development has been shown already a long time ago in trees (Uggla *et al.*, 1996). In trees auxin concentration peaks in the cambium and is important for cambium activity (Uggla *et al.*, 1996; Immanen *et al.*, 2016). Another interesting gene family is the *SMALL AUXIN UP-REGULATED RNA* (*SAUR*) gene family. *SAUR* genes which were shown to be involved in cell expansion in the hypocotyl through mechanisms of cell wall loosening (Leyser, 2018).

### 1.3.2 Auxin signalling

Auxin is perceived by plant cells, leading to the initiation of downstream processes in various ways (Caumon & Vernoux, 2023). Here, I focus on the nuclear auxin pathway, which results in the regulation of transcription. Auxin is perceived by TRANSPORT INHIBITOR RESPONSE1/ AUXIN F-BOX (TIR1/AFB) family proteins and Aux/IAA family members, where the latter act as auxin signalling repressors (Bhalerao & Fischer, 2014; Leyser, 2018). Auxin responsive genes contain DNA motifs termed auxin-responsive elements (AREs) in their promoter regions, and regulation of their transcription is controlled as follows: ARABIDOPSIS RESPONSE FACTORS (ARFs) are bound to AREs (Leyser, 2018) and can act as transcriptional activators or repressors (Martin-Arevalillo & Vernoux, 2023). When auxin is not present, the ARFs are bound by one of the 29 Aux/IAA proteins in *Arabidopsis* to inactivate the auxin response together with the TOPLESS family of co-repressor (Bhalerao & Fischer, 2014; Leyser, 2018). But as soon as auxin binds to the TIR1/AFB F-Box receptor, Aux/IAAs are ubiquitinated and degraded via the proteasome pathway. Since Aux/IAAs now can no longer inhibit the action of ARFs, the signalling cascade can continue (Leyser, 2018). As previously mentioned, other pathways of auxin signalling are

known. Recently, a preprint showed that there is much faster auxin response by identifying that upon auxin treatment over 1700 proteins are altered in their phosphorylation state within as little as 30 seconds (Roosjen *et al.*, 2022, bioRxiv preprint).

To visualize auxin signalling in planta, reporters were constructed using a synthetic promoter containing various repeats of the AREs (Rienstra *et al.*, 2023). A unidirectional repeat (**d**irect **r**epeat) of several AREs with a spacer of five nucleotides was called “DR5” and was integrated into a minimal 35S promoter (Ulmasov *et al.*, 1997; Rienstra *et al.*, 2023). Today, the *pDR5* reporter is a main auxin signalling reporter and a version with reversed motifs (*pDR5rev*) as well as more sensitive versions (*pDR5v2* or *pDr5revV2*) were constructed (Friml *et al.*, 2002; Liao *et al.*, 2015; Brackmann *et al.*, 2018). These synthetic promoters usually drive a marker such as a fluorescent protein. Thus, when auxin signalling is present, the downstream response is activated and fluorescence becomes detectable at different intensity levels depending on the auxin signalling levels (Liao *et al.*, 2015).

### 1.3.3 The phytohormone cytokinin

Cytokinins are known to be important for cell division (Kieber & Schaller, 2018; Yang *et al.*, 2021) and it is well established that cytokinins play a major role in cambium regulation in *Arabidopsis* and in tree species (for example Matsumoto-kitano *et al.*, 2008; Nieminen *et al.*, 2008; Smet *et al.*, 2019; Smit *et al.*, 2020; Yang *et al.*, 2021; Ye *et al.*, 2021). Also in the SAM and RAM, cytokinins are crucial for stem cell regulation (Gordon *et al.*, 2009; Zhang *et al.*, 2013; Pernisova *et al.*, 2018).

Cytokinins are a group of different molecules. Among them zeatin was the first natural cytokinin to be identified (Kieber & Schaller, 2014). The various versions of cytokinins are adenine derivatives synthesized from adenosine mono-, di-, or tri- phosphate (AMP, ADP, ATP) and dimethylallyl pyrophosphate (DMAPP) by the ISOPENTYL TRANSFERASE (IPT), CYP735A and LONELY GUY (LOG) biosynthetic enzymes. The removal of a ribose-5-phosphate group by LOG enzymes creates trans-zeatin, a form which is called the “free base” which is the active cytokinin version (**Figure 4**) (Kieber & Schaller, 2014). The *LOG* gene family consists of nine predicted members out of which seven LOGs were shown to have relevant enzymatic activities (Kuroha *et*

*al.*, 2009). Cytokinin catabolism by CYTOKININ OXIDASES (CKXs) irreversibly inactivates cytokinin, among other metabolic pathways such as reversible inhibition through conjugation (Kieber & Schaller, 2014). Cytokinins are transported over long distances from shoot to root or vice versa (Matsumoto-Kitano *et al.*, 2008) and also from cell to cell by diffusion and active transport. Active transport is mainly realized by three families of transporters: the PURINE PERMEASES (PUPs); EQUILIBRATIVE NUCLEOSIDE TRANSPORTERS (ENTs) and G SUBFAMILY ATP-BINIDNG CASETTE (ABCGs) (Durán-Medina *et al.*, 2017). Cytokinins are mainly perceived in the ER-lumen but also in the apoplast (Zürcher *et al.*, 2016; Durán-Medina *et al.*, 2017). The PUP family consists of 21 members which localize to the plasma membrane as well as to the membrane of the endoplasmic reticulum (ER). When localized to the plasma membrane, PUPs can import apoplastic cytokinin and thus deplete cytokinin from the apoplast and hence reduce cytokinin signalling (**Figure 4**) (Durán-Medina *et al.*, 2017).

### 1.3.4 Cytokinin signalling

Cytokinin signalling occurs via a phosphorelay pathway in which a phosphoryl group is passed between multiple proteins until transcriptional changes are induced in the nucleus (Kieber & Schaller, 2014). First, the cytokinins are sensed by ARABIDOPSIS HISTDINE KINASE (AHK) receptors on the plasma membrane or ER membrane via a specific extracytosolic domain to which the cytokinins bind (**Figure 4**). In the case of ER membrane-localized AHKs, this extracytosolic domain is located in the ER lumen (Kieber & Schaller, 2018). Upon cytokinin binding, the autophosphorylation in the cytosolic domain of the AHK takes place and is relayed within the protein from the transmitter to the receiver domain (Kieber & Schaller, 2014). The phosphoryl group is then transferred to cytoplasmic ARABIDOPSIS HISTIDINE PHOSPHOTRANSFER (AHP) proteins (**Figure 4**). An exception is AHP6, which is a pseudo-AHP and acts as a negative regulator of cytokinin signalling, likely by inhibiting phosphotransfer (Mähönen *et al.*, 2006a; Bishopp *et al.*, 2011b).

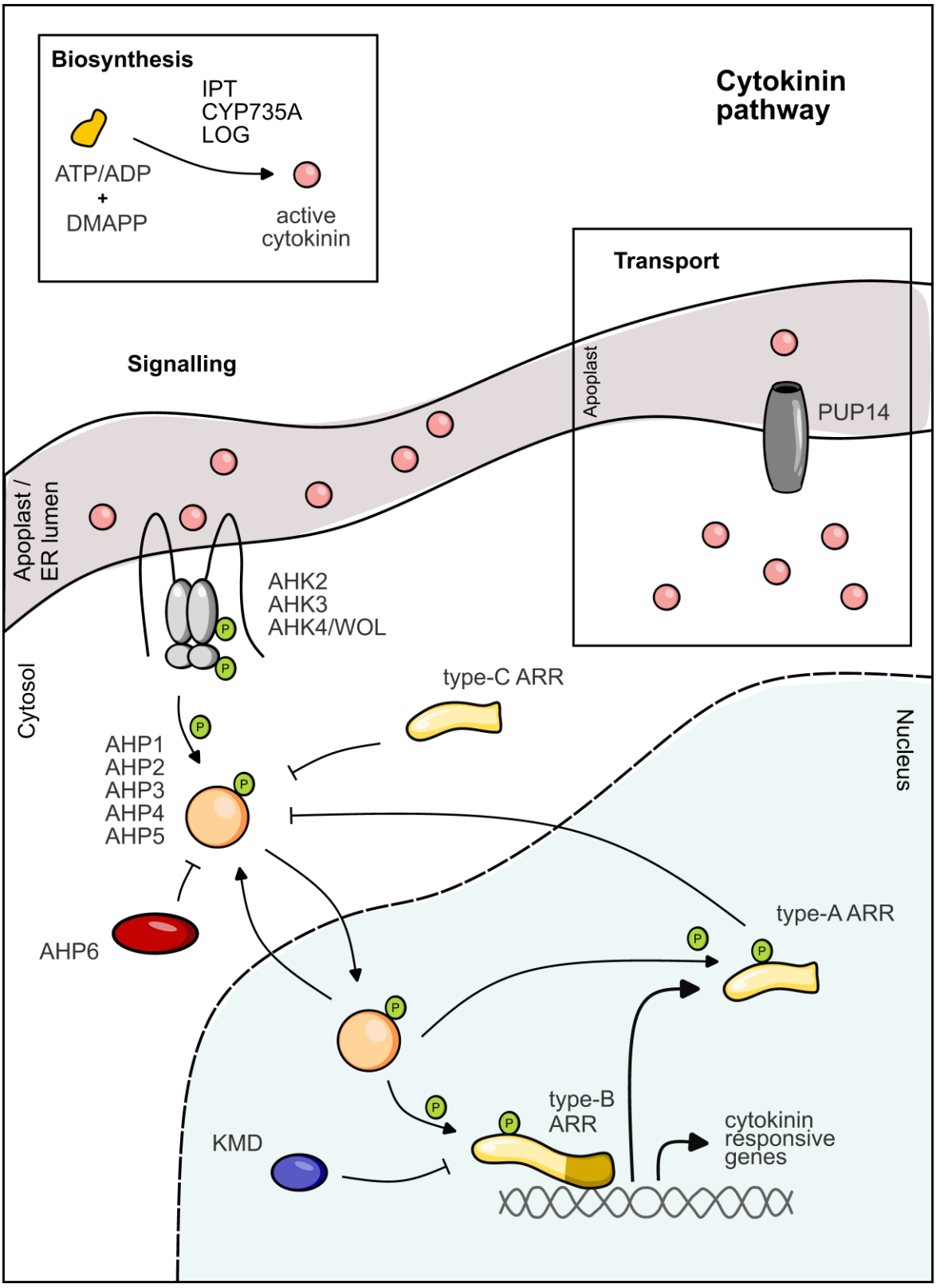


**Figure 4. Schematic overview of parts of the cytokinin pathway relevant to this study.**
An exemplary visualization of parts of the biosynthetic, transport and signalling pathways of cytokinin is shown. Active cytokinin is synthesized and can be transported across the membrane. Cytokinin signalling leads to a phosphorelay cascade, that ultimately modulates transcriptional activities. The cytokinin signalling pathway is feedback regulated in multiple ways. See the main text for protein names. This figure was generated by myself inspired by drawings from the following publications: Santner *et al.*, 2009; Durán-Medina *et al.*, 2017; Kieber & Schaller, 2018.

Importantly, APH6 was shown to be involved in cell fate decisions, as it counteracts the repression of protoxylem formation by cytokinin and thus promotes the differentiation of procambium cells to protoxylem cells (Mähönen *et al.*, 2006a).

### 1.3.5 The A-B-C of Arabidopsis Response Regulators

In a next step of the cytokinin signalling cascade, the AHPs cycle into the nucleus. In the nucleus, the phosphoryl group is transferred from the AHPs to the receiver domain of type-B ARABIDOPSIS RESPONSE REGULATOR (ARR) transcription factors and only then do the type-B ARRs bind to the DNA with their DNA-binding domain (**Figure 4**, DNA-binding domain depicted in brown). More specifically, the type-B ARRs bind a certain DNA motif in the promoter of cytokinin-responsive genes, thereby activating transcription of those genes (Kieber & Schaller, 2014; Zubo *et al.*, 2017). KISS ME DEADLY (KMD) F-box proteins can interact with and degrade type-B ARRs by conferring type-B ARR specificity on an E3-ubiquitin ligase complex (Kieber & Schaller, 2014).

In addition to the eleven type-B *ARR* genes encoded in the *Arabidopsis* genome, there are ten type-A *ARRs*. These type-A ARRs play an important role in the negative regulation of cytokinin signalling, which is described in the following. Type-A ARRs are among the first responding genes whose transcription is activated by the type-B ARRs and additionally type-A ARRs are stabilized by cytokinin (Hwang & Sheen, 2001; Naito *et al.*, 2007; To *et al.*, 2007; Kieber & Schaller, 2018; Ye *et al.*, 2021). In contrast to type-B ARRs, type-A ARRs only possess a phosphoryl group-receiving domain but no DNA-binding domain (**Figure 4**) Thus, type-A ARRs are no transcription factors. Negative regulation of cytokinin signalling by type-A ARRs is well demonstrated, but how this regulation occurs is not yet clear (Kieber & Schaller, 2014). Interestingly, there are five pairs of closely related ARRs, including the pair of ARR5 and ARR6 as well as ARR7 and ARR15. This is believed to be due to a duplication event around probably 24 to 40 million years ago (To *et al.*, 2004; Zhang *et al.*, 2011). All of these four aforementioned ARRs (ARR5, ARR6, ARR7 and ARR15) are cytokinin responsive (To *et al.*, 2004; Lee *et al.*, 2007). Type-B and type-A ARRs have been shown to be involved in the regulation of various developmental processes. Interestingly, type-B ARRs directly activate *WUS* (Zhang *et al.*, 2017; Xie *et al.*, 2018) and WUS represses

specific type-A *ARRs* (*ARR5*, *ARR6*, *ARR7* and *ARR15*) (Leibfried *et al.*, 2005). Furthermore, a bHLH transcription factor HECTATE1 (HEC1) was shown in the SAM to target *ARR7* and *ARR15* and to be repressed by WUS (Schuster *et al.*, 2014). This was found to be a crucial regulatory network for stem cell regulation in the SAM (Schuster *et al.*, 2014). With regard to vasculature development, ARR7 and ARR15 negatively affect cambium activity (Han *et al.*, 2018). Furthermore, type-B ARRs regulate protoxylem differentiation (Yokoyama *et al.*, 2007).

In addition to type-A and type-B ARRs, three type-C ARRs were identified which structurally resemble type-A ARRs, but their receiver domain is more similar to that of AHKs and their expression is not induced by cytokinin (Kiba *et al.*, 2004; Wybouw & De Rybel, 2019). Their role is not fully understood, but they may function as AHP phospho-histidine phosphatases and thus also negatively regulate cytokinin signalling (Horák *et al.*, 2008).

To visualize cytokinin signalling, the type-B ARR binding motif in the promoters of cytokinin responsive type-A *ARRs* was exploited (Hwang & Sheen, 2001; Sheen & Müller, 2008). Since the phosphorelay system of cytokinin signalling is a so-called two component system that also occurs in procaryotes, the cytokinin signalling reporters have been termed “Two Component signalling Sensor”. The *pTCS* reporter harbours concatemerized binding motifs in front of a minimal 35S promoter that drives a fluorescent protein, resulting in fluorescence intensity dependent on cytokinin signalling levels. A more sensitive version called “TCS new” (*pTCSn*) was then developed by Zürcher *et al.* (2013) by changing the arrangement of the binding motifs. More recently, by further changing the arrangement of the motifs, an even more sensitive version called “TCS version 2” (*pTCSv2*) was constructed (Steiner *et al.*, 2020).

### 1.3.6 Auxin and cytokinin crosstalk and mutual inhibition

There are a variety of auxin and cytokinin interactions which were shown to be important for developmental processes, a few of which I will highlight here. Auxin and cytokinin interaction already plays a key role in the embryo (Sheen & Müller, 2008). Here, auxin was shown to induce expression of *ARR7* and *ARR15*, resulting in

auxin-induced repression of cytokinin signalling, which was crucial for normal embryonic patterning of the root stem cell niche (Sheen & Müller, 2008). Furthermore, the balance of cytokinin and auxin is important for the control of cell fate decisions in the SAM (Schuster *et al.*, 2014; Greb & Lohmann, 2016; Gaillochet *et al.*, 2017). Here, cytokinin signalling is also regulated by auxin as auxin interferes with cytokinin signalling but this time through repression of *ARR7* and *ARR15* by ARF5, which mediates the effect of auxin on cytokinin signalling (Zhao *et al.*, 2010). There is also an effect of cytokinin on auxin in the SAM as type-B ARRs inhibit auxin synthesis through repression of *YUCCA* genes (Meng *et al.*, 2017).

Auxin and cytokinin crosstalk in roots was already reviewed 12 years ago describing the many components involved such as ARRs, PINs and Aux/IAAs (Bishopp *et al.*, 2011a). Furthermore, regulatory networks containing auxin and cytokinin pathway components have been constructed (Bishopp *et al.*, 2011b; De Rybel *et al.*, 2014; el-Showk *et al.*, 2015; Schaller *et al.*, 2015). In the root procambium, the bHLH proteins LONESOME HIGHWAY (LHW) and TARGET OF MONOPTEROS5 (TMO5) act downstream of auxin and induce expression of the *LOG* genes (*LOG3* and *LOG4*) (Ohashi-Ito *et al.*, 2014). Also downstream of the auxin pathway are cytokinin catabolic enzymes such as CKX that act on the cytokinin pathway in the RAM (Yang *et al.*, 2021).

Regarding vascular patterning, important work has shown that mutual inhibition of auxin and cytokinin is required for vascular patterning in primary growth (Bishopp *et al.*, 2011b; Šimášková *et al.*, 2015). Here, auxin induces AHP6, which negatively affects cytokinin signalling and cytokinin regulates PINs leading to auxin efflux towards the centre of the root (Bishopp *et al.*, 2011b; Šimášková *et al.*, 2015). PIN1 has been shown to be expressed in the procambium of stems (Fischer *et al.*, 2019) and in the cambium of roots (Mäkilä *et al.*, 2023). Importantly, Mäkilä *et al*. could show that GA positively affects auxin efflux by PIN1, altering the position of the auxin maximum and influencing stem cell fate decisions in the root cambium. Specifically also type-A ARRs impact PIN proteins and alter auxin patterning in the root tip (Zhang *et al.*, 2011).

## 1.4 The vascular cambium gene regulatory network

As described above, auxin and cytokinin pathways are linked in a variety of ways and this is part of the gene regulatory network in the cambium that ultimately enables stem cell maintenance, cell fate decision-making and bidirectional growth. In this chapter, I

give a brief overview of further key factors of the cambium GRN known so far, which have not yet been described in the previous chapters. It should be noted that here findings from primary and secondary growth as well as roots, hypocotyl and stems are merged and may not take place as such in the respective growth phase or organ.

As mentioned early *PXY* expression marks the proximal and central cambium domain containing the xylem progenitors and CSC, respectively (**Figure 5**) (Shi *et al.*, 2019). The PXY receptor binds CLAVATA3/EMBRYO SURROUNDING REGION- related (CLE) peptides and activates *WOX4* and *WOX14* expression promoting cambium proliferation (**Figure 5**) (Hirakawa *et al.*, 2010; Suer *et al.*, 2011; Etchells *et al.*, 2013). Furthermore, CLE peptides were shown to supress xylem cell fate (Ito *et al.*, 2006). PXY signalling moreover regulates, through WOX14 and TMO6, the expression of the LATERAL ORGAN BOUNDARIES DOMAIN4 (LBD4) transcription factor and this marks the phloem-procambium boundary (Smit *et al.*, 2020). LBDs were further shown to be downstream of cytokinin and to be targeted by BREVIPEDICELLUS/KNOTTED-1LIKE1 (BP/KNAT1) (Zhang *et al.*, 2019; Ye *et al.*, 2021).

Investigation of the cambium GRN has identified BP/KNAT1, ANTEGUMENTA (ANT), and NAC DOMAIN CONTAINING PROTEIN 15 (ANAC015) as key factors (Zhang *et al.*, 2019). ANAC015 itself is also regulated by LBD4 (Zhang *et al.*, 2019). Furthermore, LBD3 and LBD11 repress *ARR4*, *ARR5*, *ARR6*, *ARR7*, *ARR8*, *ARR9* and *ARR15* (Ye *et al.*, 2021) (**Figure 5**). Interestingly, BP/KNAT1 together with STM are necessary for xylem fibre differentiation (Liebsch *et al.*, 2014). HOMEODOMAIN LEUCIN ZIPPER III (HD-ZIP III) transcription factors promote xylem differentiation downstream of ARFs (Baima *et al.*, 2001; Smetana *et al.*, 2019). High auxin levels are thought to specify the xylem cells adjacent to the cambium as stem cell organizers (Smetana *et al.*, 2019). HAM4 and WOX4 proteins interact and this interaction increases cambium activity (Zhou *et al.*, 2015).

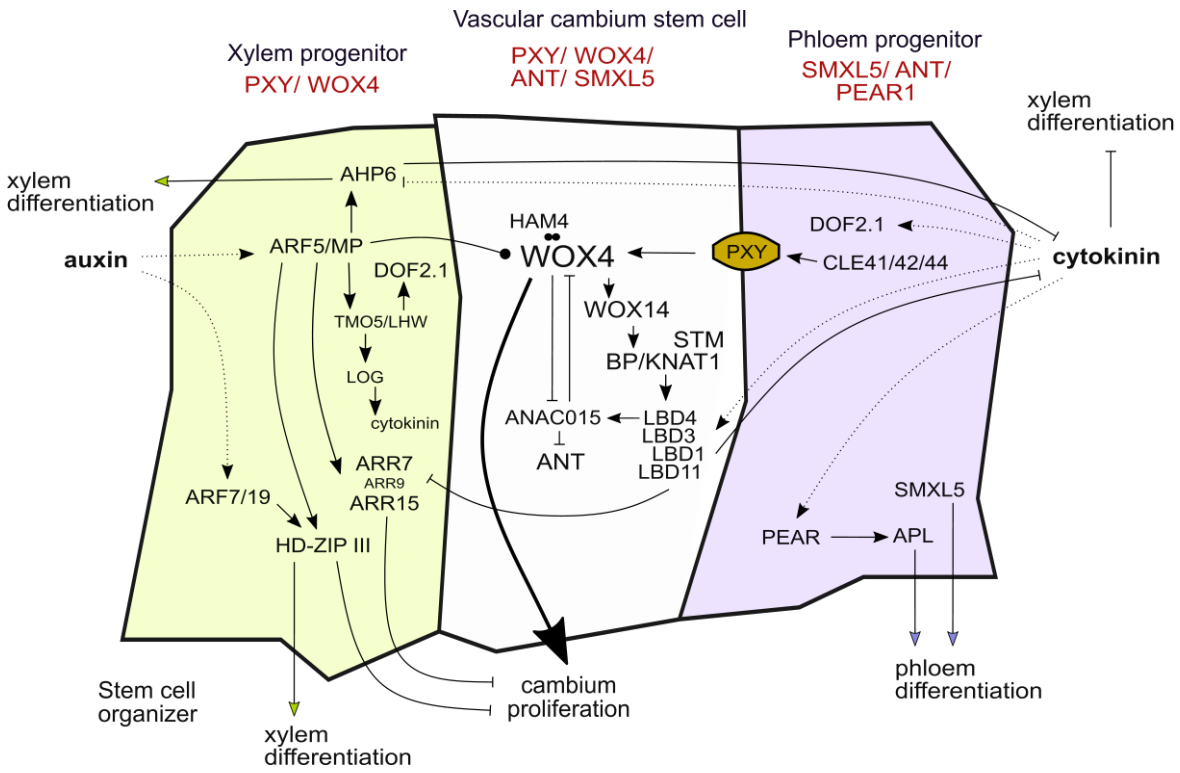


**Figure 5. The vascular cambium gene regulatory network orchestrates cambium proliferation and xylem and phloem differentiation.**
Components of the cambium gene regulatory network associated with the auxin and cytokinin pathways are shown against the background of the three cambium domains, here represented as cells (xylem progenitor, vascular cambium stem cell and phloem progenitor). See the main text for protein names. The expression of genes marked in red is commonly used to differentiate between the cambium domains. Dotted arrows indicate hormone action, ARF5 attenuates *WOX4*, and WOX4 and HAM4 protein-protein interaction is indicated. In addition, the positioning of components in specific cambium domains is mostly variable and in many cases the components are present in all three domains in planta. This figure was created by me and published in Haas *et al*., 2022 and subsequently modified by me.

Importantly, ARF5/ MONOPTERPS (ARF5/ MP) attenuates *WOX4* to maintain normal cambium patterning (**Figure 5**) (Brackmann *et al.*, 2018). ARF5 also induces *ARR7* and *ARR15* expression which represses cambium proliferation (Han *et al.*, 2018). Moreover, ARF5 induces expression of *TMO5*, and TMO5 together with LHW induces the expression of *LOG3* and *LOG4* genes, leading to xylem located cytokinin biosynthesis (De Rybel *et al.*, 2013, 2014; Ohashi-Ito *et al.*, 2014). Also downstream of TMO5/LHW, the DNA-BINDING WITH ONE FINGER2.1 (DOF2.1) transcription factor acts to induce cell division in the procambium (**Figure 5**) (Smet *et al.*, 2019). DOF2.1 is additionally cytokinin inducible (Smet *et al.*, 2019). Phloem differentiation has been shown to be guided by the PHLOEM EARLY DOF transcription factors PEAR1 and PEAR2 (Miyashima *et al.*, 2019). PEARS upregulate *ALTERED PHLOEM DEVELOPMENT* (*APL*) to regulate phloem differentiation, with the steps leading to full

differentiation having sharp transitions in cell states (Roszak *et al.*, 2021). As previously mentioned, SMXL5 proteins also guide phloem differentiation (Wallner *et al.*, 2017, 2020). Taken together, many components of the cambium GRN influencing vascular patterning and cambium activity have already been identified and many more that are not described here.

## 1.5 Mathematical modelling of vascular patterning and cambium activity

In general, it is difficult to fully understand how numerous components work together to control a given process. Therefore, mathematical models are developed that describe the interactions of selected components involved. Often these models are based on differential equations, which describe the components and their interactions over time (Tomlin & Axelrod, 2007). The differential equations include parameters such as synthesis and degradation rates, activation thresholds and diffusion of the individual components (Tomlin & Axelrod, 2007). When modelling GRNs, these components can be genes or gene products, the concentrations of which represent the variables of the system (Elahi & Hasan, 2018).

Mathematical modelling has been used to better understand vascular patterning and cambium activity. Four key examples are briefly described here to provide an overview of how modelling has advanced our understanding of the underlying GRNs that control these processes. De Rybel *et al.* (2014) used modelling to better understand embryonic vasculature formation. By modelling auxin and cytokinin synthesis and degradation and their interaction along with PIN concentrations in a 2D model of a heart stage embryo, the authors were able to show that this underlying network can create high auxin signalling in the xylem and high cytokinin signalling in the procambium (De Rybel *et al.*, 2014). In a 2D model of a primary root cross-section, mutual inhibition of auxin and cytokinin was modelled showing that this type of interaction can act as the patterning mechanism (Muraro *et al.*, 2014). Recently, a 2D model of a hypocotyl cross-section in the secondary growth phase was constructed which included inactive and active PXY and CLE peptides as components, amongst others (Lebovka *et al.*, 2023). This model could explain the previously described the *pPXY* and *pSMXL5* based patterning of cambium domains and generate wild-type-like cambium activity and could furthermore show that xylem vessel development must

occur independently from the PXY/CLE41 mechanism (Lebovka *et al.*, 2023). Another model involving auxin, cytokinin, CLE, PXY and ARF5 as components was established to investigate how their interaction can influence cambium stem cell divisions and suggests a feedback loop from PXY to ARF5 (Bagdassarian *et al.*, 2023). However, no cellular layout was used and growth was not simulated (Bagdassarian *et al.*, 2023).

## 1.6 Aims of this study

In this study, I aimed to investigate cell fate decision-making in the vascular cambium in the *Arabidopsis* hypocotyl, with a focus on gene regulatory networks. Since the discovery of the *WOX* genes, our understanding of how plant stem cells maintain themselves while giving rise to various cell types has tremendously increased. However, there are unanswered questions about how those gene regulatory networks work and exploring them will contribute to our understanding.

In this study, I asked the following questions:

1) **How can gene regulatory networks convey the bifacial cell fate decisions of stem cells and guide the resulting bidirectional growth observed in the vascular cambium?** To address this question, I used mathematical modelling. I hypothesized that in the vascular cambium, as shown in primary growth, secondary growth is regulated by mutual inhibition of auxin and cytokinin signalling, which in turn is regulated by WOX4.
2) **How are WOX4 and WUS similar or different in terms of their regulatory mechanisms of plant stem cells?** I aimed to identify the genes regulated by the transcription factors WOX4 and WUS and subsequently compare them to deduce how they regulate specifically the auxin and cytokinin pathways. This comparison could then allow a better understanding of general concepts of plant stem cell maintenance or cell fate decisions.
3) **How does WOX4 exhibit its regulatory potential of the vascular cambium?** Based on the hypothesis set out in the first question, I aimed to investigate whether auxin and cytokinin signalling are affected by WOX4. Importantly, I aimed to identify WOX4 downstream targets as well as their function within cell fate decision-making within the cambium.

.

# 2. Material

## 2.1 Plant material

*Arabidopsis thaliana* (*Arabidopsis*) was used as the model organism in this study and the *Col-0* ecotype was used throughout. The individual *Arabidopsis* T-DNA insertion mutant lines as well as reporter lines used in or generated in this study are listed in Table 2.

**Table 2. *Arabidopsis* lines used in this study.** The lines were either obtained from the Nottingham Arabidopsis Stock Centre (NASC) or kindly gifted by the person indicated.

| Genotype | Gene locus | Construct or T-DNA Identifier | Origin | Reference |
|---|---|---|---|---|
| **WT** | - | - | NASC | - |
| ***arr6*** | *AT5G62920* | *SALK_008866* | NASC (N508866) | To *et al*., 2004 |
| ***arr5***<br>***arr6*** | *AT3G48100*<br>*AT5G62920* | *SALK_052900*<br>*SALK_008866* | NASC (N25757) | To *et al*., 2004 |
| ***arr7-2*** | *AT1G19050* | *WiscDsLox485B15* | NASC (N864807) | Jeon *et al*., 2010 |
| ***arr15-2*** | *AT1G74890* | *WiscDsLox334D02* | NASC (N851593) | Han *et al.,* 2018 |
| ***arrr7-1***<br>***arr15-2*** | *AT1G19050*<br>*AT1G74890* | *Wisc KO line &*<br>*WiscDsLox334D02* | Bruno Müller | Zhang *et al*., 2011 |
| ***wox4-1*** | *AT1G46480* | *GABI462G01* | NASC (N376572) | Hirakawa *et al.,* 2010 |
| ***wox4-1*** | *AT1G46480* | *pWOX4:WOX4-GR (pSS4)* | Greb lab | unpublished |
| **WT** | - | *pWOX4:ER-YFP (pPS11)* | Greb lab | Suer *et al*., 2011 |
| **WT** | - | *pARR5:n3YFP* | Bert de Rybel | Andersen *et al.*, 2018 |
| **WT** | - | *pARR6:n3YFP* | Bert de Rybel | Andersen *et al.*, 2018 |
| ***wox4-1*** | *AT1G46480* | *pARR6:n3YFP* | this study | unpublished |
| ***wox4-1*** | *AT1G46480* | *pARR6:n3YFP*<br>*pWOX4:WOX4-GR (pSS4)* | this study | unpublished |

| | | | | |
|---|---|---|---|---|
| **WT** | - | *pARR7:ER-mTurquoise-HDEL (pAH38)* | this study | unpublished |
| **WT** | - | *pARR15:n3YFP* | Bert de Rybel | Andersen *et al.*, 2018 |
| ***wox4-1*** | *AT1G46480* | *pARR15:n3YFP* | this study | unpublished |
| ***wox4-1*** | *AT1G46480* | *pARR15:n3YFP, pWOX4:WOX4-GR (pSS4)* | this study | unpublished |
| **WT** | - | *pPXY:H4-GFP (pPS24); pSMXL5:H2B-RFP (pIL53)* | Greb lab | Shi *et al*., 2019 |
| ***wox4-1*** | *AT1G46480* | *pPXY:H4-GFP (pPS24); pSMXL5:H2B-RFP (pIL53)* | this study | unpublished |
| **WT** | - | *pPXY:mTurquoise2-ER_pSMXL5:Venus-ER (pVL78)* | Greb lab | Shi *et al*., 2019 |
| **WT** | - | *pTCSv2:3Venus* | Maya Bar | Steinert *et al.,* 2020 |
| ***wox4-1*** | *AT1G46480* | *pTCSv2:3Venus* | this study | unpublished |
| ***wox4-1*** | *AT1G46480* | *pTCSv2:3Venus, pWOX4:WOX4-GR (pSS4)* | this study | unpublished |
| **WT** | - | *pDr5revV2:YFP (pKB46)* | Greb lab | Brackmann *et al*., 2018 |
| ***wox4-1*** | *AT1G46480* | *pDr5revV2:YFP (pKB46)* | this study | unpublished |
| **WT** | - | *pUBI10:mCherry-GR-linker-WUS (ID #7.4.xx)* | Jan Lohmann | Ma *et al*., 2019 |
| **WT** | - | *pUBI10:mCherry-GR (ID #1.4.x)* | Jan Lohmann | unpublished |
| **WT** | - | *pUBI10:mCherry-GR-linker- WOX4 (ID 22-1314)* | this study | unpublished |

## 2.2 Bacteria

*Escherichia coli* (*E.coli*) strain DH5α and *Agrobacterium tumefaciens* (*Agrobacterium*) strain C58C1 (with pSoup), or strain ASE (with pSoup+) were used for cloning and *Arabidopsis* transformation procedures throughout the study.

## 2.3 Primers

The following primers listed in Table 3 have been used in this study.

**Table 3. Primers used in this study.** All primers were purchased from Eurofins (Luxembourg City, Luxembourg).

| Purpose | Primer Name | ID | Sequence (5'→ 3') |
|---|---|---|---|
| Cloning *pAH37* | *pARR7_fw* | 135A1 | AACAGGTCTCAACCTGTCTCTCGCATATCAGG |
| | *pARR7_rev* | 135A2 | AACAGGTCTCATGTTTGTCAAACTCAGAATAAAAAAG |
| Sequencing *pAH37* | *pARR7_middlePart* | 135B7 | CCAATGTTTTGTTTGGCACGA |
| | *seq_GG1_for* | 86A1 | GTTGTGTGGAATTGTGAGC |
| | *seq_GG2_rev* | 86A2 | GTTTTCCCAGTCACGACG |
| Sequencing *pAH38* | *seq_GG_Z00_fwd* | 88C3 | ACCTCTCGGGCTTCTGG |
| | *seq_GG_Z00_rvs* | 88C4 | CCTTTTTACGGTTCCTG |
| | *hygroRVS* | 92E10 | CATGTAGTGTATTGACC |
| | *mTurquoise2-SPER_R* | 119C8 | TCGCCCTTGCTCACCATTGTTG |
| | *rbscT_seq* | 120C9 | ATAATACTCAAACTCAGTAGGATTCTGG |
| Genotyping *wox4-1* | *Gabi_462G01_LP* | 14D7 | TTTTTAGCGTGGTTCATGTCC |
| | *WOX4_rev2* | 132C2 | GTCAAAGTATTAGGTATGCCGC |
| | *o8474* | 87C5 | ATAATAACGCTGCGGACATCTACATTTT |
| | *Gabi-H16* | 87C6 | GGTTCTGGAACCAATAGAACACAT |
| Detecting *WOX4-GR* (pSS4) | *WOX4for5* | 15A1 | CCCAACTGGATATCACCAATGATATC |
| | *GR_Stop_R* | 20C10 | ACTAGGATCCTCATTTTTGATGAAACAGAAGCT |
| Genotyping *arr7-1* | *JL202* | 62B8 | CATTTTATAATAACGCTGCGGACATCTAC |
| | *arr7-1_for* | 62B6 | GCCGTCGATGATAGTATTGTG |
| | *arr7-1_rev* | 62B7 | ATTCCTCAGCTTCATTCCTCA |
| Genotyping *arr7-2* | *WiscDsLox-LB-p745* | 12A7 | AACGTCCGCAATGTGTTATTAAGTTGTC |
| | *WiscDsLox485-488B15_LP* | 62B4 | TCATATCCTGAAAGTCCTGGC |
| | *WiscDsLox485-488B15_RP* | 62B5 | TAATTGAGCAATAACCACCGG |
| Genotyping *arr15-2* | *WiscDsLox-LB-p745* | 12A7 | AACGTCCGCAATGTGTTATTAAGTTGTC |
| | *WiscDsLox334D02-LP* | 11C6 | TTCAATTGATTCACCTCATGAAG |
| | *WiscDsLox334D02-RP* | 11C7 | TTCATATCCTGTTAGTCCCGG |

## 2.4 Vectors and plasmids

All plasmids in this study were generated by Green Gate cloning (Lampropoulos *et al.*, 2013) using the entry vector backbone *pGGA000* or destination vector backbone *pGGZ003*. *pGGA000* carries an Ampicillin resistance (AmpR) and *pGGZ003* carries a Spectinomycin resistance (SpecR) (Lampropoulos *et al.*, 2013).

Entry modules for *pAH001* generation were obtained from the Jan Lohmann lab (COS, Heidelberg University) or were generated by Virginie Jouannet (*pVJ44*). Entry modules used for generation of *pAH038* were generated by Vadir López-Salmerón (pVL), Dongbo Shi (pDS) or me (pAH). *pAH038* carries a Hygromcyin resistance cassette (HygroR) for plant selection (*pDS08*). All plasmids relevant to this study are listed in Table 4.

**Table 4. Plasmids created in this study.** All vectors and modules used are described in Lampropoulos *et al.,* 2013 or in the plasmid database repository of the Jan Lohmann lab and Thomas Greb lab.

| ID | Enty modules used | Backbone | Description | Usage |
|---|---|---|---|---|
| *pAH001* | *pUBI10* (*pA006*), mCherry-GR-linker (*pB069*), WOX4 (*pVJ44*), dummy (*pD017*), rbscT (*pE001*), BastaR (*pF001*) | *pGGZ003* | *pUBI10:mCherry-GR-linker- WOX4* | *Arabidopsis* transformation |
| *pAH037* | - | *pGGA000* | *pARR7* (2.7 kb) | A-Module for cloning |
| *pAH038* | *pARR7* (*pAH037*), ER signal peptide (*pVL63*), mTurquoise (*pVL67*), HDEL (*pVL71*), rbscT (*pVL66*), HygroR (*pDS08*) | *pGGZ003* (*pVL11*) | *pARR7:ER-mTurquoise-HDEL* | *Arabidopsis* transformation |

## 2.5 Reagents, consumables and kits

All reagents and kits used in this study are listed below with the source and identifier indicated (Table 5). Consumables which were crucial for conducting the experiments in this study are also listed. All reagents were purchased from Merck (Darmstadt, Germany with the brand Sigma-Aldrich), Duchefa (Harleem, Netherlands), Carl Roth (Karlsruhe, Germany), QIAGEN (Venlo, Netherlands), ibidi (Gräfeling, Germany), 3M

(Saint Paul, USA), SERVA (Heidelberg, Germany), AppliChem (Darmstadt, Germany), Greiner bio-one (Kremsmünster, Austria), Lehle Seeds (Round Rock, USA) and ThermoFischer Scientific (Waltham, USA). The items are sorted into respective categories and some items were used in multiple categories. For usage details see Methods chapter 3. All kits and enzymes were used according to the manufacturer's protocols.

**Table 5. Regents, consumables and kits used in this work.**

| Category | Reagent | Source | Identifier |
|---|---|---|---|
| **Hormone treatment** | Dexamethasone | Sigma-Aldrich | Cat# D4902 |
| | Ethanol (EtOH) absolute 99.8% | ThermoFischer Scientific | Cat# 10342652 |
| | 35 mm petri dishes | Greiner bio-one | Cat# 627102 |
| **Antibiotics & Herbicides** | Ampicillin (Amp) | SERVA | Cat# 13399.03 |
| | Chloramphenicol (Cam) | SERVA | Cat# 16785 |
| | Glufosinatammonium (Basta) | Sigma-Aldrich | Cat# 45520 |
| | Hygromycin B (Hygro) | Carl Roth | Cat# 1287.2 |
| | Kanamycin (Kan) | Sigma-Aldrich | Cat# K4000 |
| | Methotrexate hydrate (MTX) | Sigma-Aldrich | Cat# A6670 |
| | Rifampicin (Rif) | Duchefa | Cat# R0146 |
| | Spectinomycin (Spec) | Duchefa | Cat# S0188 |
| | Sulfadiazine (Sulf) | Sigma-Aldrich | Cat# S8626 |
| | Tetracycline (Tet) | Duchefa | Cat# T0150 |
| **Bacteria growth** | Bacto-tryptone | ThermoFischer Scientific | Cat# 211705 |
| | Bacto-yeast extract | Carl Roth | Cat# 2363.3 |
| | NaCl | ThermoFischer Scientific | Cat# S/3161/60 |
| | Bacto agar | ThermoFischer Scientific | Cat# 214010 |
| **PBS buffer** | NaCl | ThermoFischer Scientific | Cat# S/3161/60 |
| | $NaH_2PO_4 \cdot H_2O$ | Sigma-Aldrich | Cat# S9638 |
| | $Na_2HPO_4 \cdot 2H_2O$ | Sigma-Aldrich | Cat# 04272 |

| | | | |
|---|---|---|---|
| **Cell wall staining dyes** | Direct Red 23 | Sigma-Aldrich | Cat #212490 |
| | Calcofluor White | Sigma-Aldrich | Cat# 18909 |
| **DNA staining dyes** | Ethidium bromide | Carl Roth | Cat# HP47.1 |
| | Gel Red | Carl Roth | Cat# 0984.1 |
| **Genotyping** | Isopropanol | Honeywell | Cat# 33539 |
| | Ethanol absolute 99.8% | ThermoFischer Scientific | Cat# 10342652 |
| | Tris, pH7.5 | AppliChem | Cat# A1087 |
| | SDS | AppliChem | Cat# A0675 |
| | EDTA | AppliChem | Cat# A3553 |
| | NaCl | ThermoFischer Scientific | Cat# S/3161/60 |
| **Plant care** | Nematodes | Sautter Stepper | Nemaplus50 |
| **Sterile plant growth** | Phyto agar | Duchefa | Cat# M1002 |
| | MES | Sigma-Aldrich | Cat# M3671 |
| | Murashige and Skoog | Duchefa | Cat# M0222 |
| | Saccharose | Carl Roth | Cat# 4621.1 |
| | Micropore tape | 3M | Cat# 1530-1 |
| **Plant transformation** | Silwet L-77 | Lehle Seeds | Cat# VIS-02 |
| | Saccharose | Carl Roth | Cat# 4621.1 |
| **Hypocotyl cross-sectioning** | Paraformaldehyde | Sigma-Aldrich | Cat# P6148 |
| | Low melting (LM) agarose | Sigma-Aldrich | Cat# A9414 |
| | Razor blades | Wilkinson Sword | Classic |
| **Microscopy** | 2-well glass-bottom dish | ibidi | Cat# 80287 |
| **Kits** | RNAeasy Mini Kit | QIAGEN | Cat# 74106 |
| | QIAshredder | QIAGEN | Cat# 79564 |
| | QIAprep Spin Miniprep Kit | QIAGEN | Cat# 27106 |
| | QIAquick PCR Purification Kit | QIAGEN | Cat# 28106 |
| | QIAquick Gel Extraction Kit | QIAGEN | Cat#28704 |
| **Enzymes** | Phusion High-Fidelity DNA Polymerase | ThermoFischer Scientific | Cat# F530S |
| | T4 DNA Ligase 5U (for entry module) | ThermoFischer Scientific | Cat# EL0011 |

| | | | |
|---|---|---|---|
| | T4 DNA Ligase HC 30U (for destination module) | ThermoFischer Scientific | Cat# EL0013 |
| | JumpStart REDTaq ReadyMix | Sigma-Aldrich | Cat# P0982 |
| | Eco31I FastDigest | ThermoFischer Scientific | Cat# FD0924 |

## 2.6 Buffers, media and solutions

The following buffers, media and solutions (Table 6) were made using the reagents specified in Table 5.

**Table 6. List of buffers, media and solutions used in this study.**

| Category | Name | Ingredients | Information |
|---|---|---|---|
| **Buffer** | 10x Phosphate buffered saline (PBS) | 1.3 M NaCl<br>30 mM $NaH_2PO_4$<br>70 mM $Na_2HPO_4$<br>in $ddH_2O$ | pH 7.0 adjusted with 1 % HCl, autoclaved |
| | DNA Extraction buffer | 200 mM Tris (pH7.5)<br>25 mM NaCl<br>0,5 % SDS<br>25 mM EDTA<br>in $ddH_2O$ | - |
| **Media** | Lysogeny broth (LB) medium | 10 g Bacto-Tryptone<br>5 g Bacto-yeast extract<br>5 g NaCl<br>in 1 L $ddH_2O$ | pH 7.0 adjusted, autoclaved. For solid medium add 20 g Bacto agar before autoclaving |
| | Half strength Murashige and Skoog (½ MS) medium | 2.2 g MS<br>10 g Saccharose<br>0.5 g MES<br>in 1 L $ddH_2O$ | pH 5.7 adjusted with 1 M KOH, autoclaved, for solid medium add 8 g Phyto agar before autoclaving |
| **Solutions** | Dexamethasone | 10 µM or 20 µM Dex<br>in 99.8 % Ethanol | - |
| | Mock solution | 99.8 % Ethanol | - |

| | | | |
|---|---|---|---|
| | LM agarose | 5 % or 7 % LM agarose in 1x PBS | Mix well before heating, heat briefly |
| | PFA | 4 % PFA in 1xPBS | let solve at 60°C in a water bath |
| | Direct Red 23 | 0.5 % Direct Red 23 in 1x PBS | - |
| | Calcofluor white | 0.1 % Calcofluor white in ClearSee | - |

It should be noted that using a tablet to prepare PBS solution is not recommended as this will result in the LM agarose consistency being less suitable for hypocotyl cross-sections.

## 2.7 Software and web resources

Throughout the study the following scientific software and web resources were used (Table 7).

**Table 7. List of software and web resources used in this study.**

| Category | Name | Source | Version and/or web address |
|---|---|---|---|
| **Software** | MS Office | Microsoft | 2013, Professsional Plus 2019 |
| | Leica Application Suite X | Leica Microsystems, Wetzlar, Germany | 4.5.0.2553 |
| | Geneious | Biomatters, Auckland, New Zealand | 10.2.6 |
| | CLC Main workbench 21 | QIAGEN, Venlo, Netherlands | 21.0.3 |
| | R | R project | R-4.2.2 https://cran.r-project.org/ |
| | RStudio | posit | 2022.12.0 https://posit.co/download/rstudio-desktop/ |
| | MATLAB | The MathWorks, Natick, Massachusetts | R2021a |

| | | | |
|---|---|---|---|
| | Inkscape | The Inkscape Project | 1.2 https://inkscape.org/ |
| | Fiji/ ImageJ | National Institute of Health (NIH), Bethesda, USA | 1.53t |
| | Filemaker Pro | Claris International, Santa Clara, USA | 14 |
| | Mendeley | Elsevier, Amsterdam, The Netherlands | 1.19.8 |
| **Web resources** | TAIR | TAIR | https://www.arabidopsis.org/index.jsp |
| | NASC | NASC, University of Nottingham, United Kingdom | https://arabidopsis.info/ |
| | ShinyGO 0.77 | South Dakota State University, Brookings, USA | http://bioinformatics.sdstate.edu/go/ |
| | Venn diagram drawing tool | VIB / UGent, Zwijnaarde, Belgium | https://bioinformatics.psb.ugent.be/webtools/Venn/ |

## 2.8 Further technical equipment

Further crucial technical equipment used for this study, which is not commonly available in molecular biology laboratories, is listed in Table 8.

**Table 8. List of additional technical equipment.**

| Usage | Name | Source |
|---|---|---|
| **Agrobacterium transformation** | MicroPulser Electroporator | Bio-Rad Laboratories (Hercules, USA), provided by Karin Schumacher Lab, COS |
| **RNA extraction** | TissueLyserII | Retsch (Haan, Germany), provided by Karin Schumacher Lab, COS |
| **Confocal Microscopy** | Leica Stellaris 8 | Leica Microsystems (Wetzlar, Germany), provided by Greb lab |

| | | |
|---|---|---|
| **Modelling and RNA-seq analysis** | Dell Laptop Precision5540, Microsoft Windows 10 Pro 64-bit | Dell Technologies (Round Rock, USA), provided by Greb lab |

# 3. Methods

It should be noted that some work was carried out jointly with others. Please see the Contributions chapter for more details.

## 3.1 Mathematical modelling

Mathematical modelling was performed using MATLAB software and in collaboration with the Mironova Lab (see Contributions chapter).

### 3.1.1 GRN models

To model the GRN model 1, first, the following systems of Ordinary Differential Equations (ODEs) was created:

$$\frac{d[A]}{dt} = \frac{ka\left(\frac{[A]}{qa}\right)^h}{1+\left(\frac{[A]}{qa}\right)^h+\left(\frac{[B]}{qb}\right)^h} - kda[A] \quad (1)$$

$$\frac{d[B]}{dt} = \frac{ka\left(\frac{[B]}{qb}\right)^h}{1+\left(\frac{[A]}{qa}\right)^h+\left(\frac{[B]}{qb}\right)^h} - kdb[B]$$

These equations describe the gene product level of gene A $[A]$ or gene B $[B]$ depending on the initial expression level of A and B, the synthesis rate constant of A ($ka$) and B ($kb$), the synthesis functions that depend on the expression levels of both entities as well as the degradation rate constant ($kd$). The regulatory influences are exerted, when the thresholds for A-dependent ($qa$), and B-dependent ($qb$) regulation are reached. The Hill coefficient *h*, a way to describe cooperative action, was set to *h*=2. The equations were entered as a function in MATLAB where A is donated as ‘x’ and B is denoted as ‘y’. The initial concentrations were chosen to range from zero to two. The functions were then solved using the ode45 solver and the results were visualized with a phase portrait to assess end point solutions. By variation of the

parameter values a final set of parameters for the GRN model 1 was established which allowed three endpoint solutions. The MATLAB code is shown in **Figure 6**.

```
%%Analysing a gene regulatory network with two genes A (denoted as x) and B (denoted as y)
%with mutual inhibition by making a phase portrait depicting initial conditions
%and end point solutions of the ODE system calculation.

function PhasePortraitCambium
close all
clc

%calculation time span
tspan=[0 1000];
% figure()
hold on

for x0=0:0.5:2 %Defining the range of the initial concentration of x
    for y0=0:0.5:2 %Defining the range of the initial concentration of y

                XYinitial =[x0;y0]; %Array with the initial data

                [tout,stateout]=ode45(@Derivatives,tspan,XYinitial);
                %Runs a solver that will integrate the "@Derivatives" system of equations

                xout=stateout(:,1);
                %find in the solutions the concentration values of the first substance "x"
                yout=stateout(:,2);
                %find in the solutions the concentration values of the second substance "y"

                %Draw the phase portrait graph
                %depicted in red are points of stability into which x and y fall
                %these points of stability will reflect the progenitor or stem cell state
                plot(xout,yout,'color', [0.5 0.5 0.5])
                plot(stateout(1:2,1),stateout(1:2,2),'Linewidth',3,'Color','b')
                plot(stateout(end-20:end,1),stateout(end-
20:end,2),'Linewidth',5,'Color','r')
                xlabel('x'); ylabel('y');
                xlim([0 10])
                ylim([0 10])

                drawnow
     end
    end
end
%Giving the system of differential equations that will be solved
function dstatedt= Derivatives(t,state)
x=state(1);
y=state(2);
%passing parameters of the model
Kda=0.33; %Gene degradation constant for A
Kdb=0.33; %Gene degradation constant for B
h=2; %Hill coefficient
qa=0.58; %Threshold for A-dependent regulation
qb=0.58; %Threshold for B-dependent regulation
ka=3; %Gene synthesis constant for A
kb=3; %Gene synthesis constant for B

% Differential equations
dx= (ka*((x/qa)^h))/(1+((x/qa)^h)+((y/qb)^h))-(Kda*x);
dy= (kb*((y/qa)^h))/(1+((x/qa)^h)+((y/qb)^h))-(Kdb*y);

%finishing the calculation of one integration step
dstatedt=[dx;dy];
end
```

**Figure 6. MATLAB code of GRN model 1.**
This MATLAB code was used to describe and solve the GRN model 1 shown in Figure 10A and yields the phase portrait shown in Figure 10B. The code was jointly generated with Prof. Dr. Victoria V. Mironova and M.Sc. Daria Azarova.

For the second and improved GRN model (model 2), a factor C was introduced that governs expression of A and B. The GRN of model 2 was described with the following differential equations:

$$\frac{d[A]}{dt} = \frac{ka\left(\frac{[C]}{qc}\right)^h}{1+\left(\frac{[C]}{qc}\right)^h+\left(\frac{[B]}{qb}\right)^h} - kda[A] \quad (2)$$

$$\frac{d[B]}{dt} = \frac{kb\left(\frac{[C]}{qc}\right)^h}{1+\left(\frac{[C]}{qc}\right)^h+\left(\frac{[A]}{qa}\right)^h} - kdb[B]$$

$$\frac{d[C]}{dt} = kc\left(1-\frac{|\,[A]-[B]\,|}{[A]+[B]}\right) - kdc[C]$$

As in model 1, here the gene product level of A and B was dependent on the initial condition, the gene synthesis constant, the synthesis function, and the gene degradation rates. Additionally factor C was introduced which depends on the gene expression level of A and B described by

$$\left(1-\frac{|\,[A]-[B]\,|}{[A]+[B]}\right)$$

The gene product level of factor C is furthermore dependent on its synthesis constant and degradation constant. In the synthesis function for A and B, the autoregulation of the expression levels has been replaced by the C-dependent activation with the threshold $qc$. Again, using ode45 the system was solved and end point solutions were portrayed in a phase portrait. **Figure 7** shows the respective MATLAB code.

```
%%Analysing a gene regulatory network with two genes A (denoted as x) and B (denoted as y)
%which are regulated by a master regulator C (here denoted as z) by making a phase portrait
%depicting initial conditions and end point solutions of the ODE system calculation.

function PhasePortraitCambium
close all
clc

%calculation time points
tspan=[0 1000];
% figure()
hold on

for x0=0:0.5:2 %Defining the range of the initial concentration of x
    for y0=0:0.5:2 %Defining the range of the initial concentration of y
        for z0=0:0.25:2 %Defining the range of the initial concentration of z

                XYZinitial =[x0;y0;z0]; %Array with the initial data

                [tout,stateout]=ode45(@Derivatives,tspan,XYZinitial);
                %Runs a solver that will integrate the "@Derivatives" system of equations

                xout=stateout(:,1);
                %find in the solutions the concentration values of the first substance "x"
                yout=stateout(:,2);
                %find in the solutions the concentration values of the second substance "y"
                zout=stateout(:,3);
                %found in the solutions the concentration values of the third substance "z"

                %Draw the phase portrait graph
                %depicted in red are points of stability into which x and y fall
                %these points of stability will reflect the progenitor or stem cell state
                plot(xout,yout,'color', [0.5 0.5 0.5])
                plot(stateout(1:2,1),stateout(1:2,2),'Linewidth',3,'Color','b')
                plot(stateout(end-20:end,1),stateout(end-
20:end,2),'Linewidth',5,'Color','r')
                xlabel('x'); ylabel('y');

                drawnow
     end
    end
end
end
%Giving the system of differential equations that will be solved
function dstatedt= Derivatives(t,state)
%we transfer the values of the concentrations of substances into the calculated variables
x=state(1);
y=state(2);
z=state(3);
%passing parameters of the model
Kda=0.33; %Gene degradation constant for A
Kdb=0.33; %Gene degradation constant for B
Kdc=0.5; %Gene degradation constant for C
h=2; %Hill coefficient
qa=0.58; %Threshold for A-dependent regulation
qb=0.58; %Threshold for B-dependent regulation
qc=1; %Threshold for C-dependent regulation
ka=3; %Gene synthesis constant for A
kb=3; %Gene synthesis constant for B
kc=5; %Gene synthesis constant for C
%the gene synthesis constant for z is described by the stemness factor


% Differential equations
dx= (ka*((z/qc)^h))/(1+((z/qc)^h)+((y/qb)^h))-(Kda*x);
dy= (kb*((z/qc)^h))/(1+((z/qc)^h)+((x/qa)^h))-(Kdb*y);
dz= kc*(1-(abs(x-y)/(x+y)))-(Kdc*z);

%finishing the calculation of one integration step
dstatedt=[dx;dy;dz];
end
```

**Figure 7. MATLAB code of the second and improved GRN model 2.**
This MATLAB code was used to describe the GRN model 2 shown in Figure 10C and yields the phase portrait shown in Figure 10D. Factor C is denoted as Z in the code. The code was jointly generated with Prof. Dr. Victoria V. Mironova and M.Sc. Daria Azarova.

The parameter values were kept identical to the first GRN model and newly introduced parameters were manually varied in reasonable ranges until a parameter set was found that allowed the existence of three endpoint solutions. The final set of parameter values of both GRN models is listed in **Table 9**.

**Table 9. Final parameter values used for the first GRN model 1 and the improved GRN model 2.**. *tu* - time unit, *cu* – concentration unit, *dl* – dimensionless. Parameter values were optimized jointly with M.Sc. Daria Azarova.

| Parameter | Dimension | Values GRN Model 1 | Values GRN Model 2 |
|---|---|---|---|
| *kda* | *1/tu* | 0.33 | 0.33 |
| *kdb* | *1/tu* | 0.33 | 0.33 |
| *kdc* | *1/tu* | - | 0.5 |
| *h* | *dl* | 2 | 2 |
| *qa* | *cu* | 0.58 | 0.58 |
| *qb* | *cu* | 0.58 | 0.58 |
| *qc* | *cu* | - | 1 |
| *ka* | *1/tu* | 3 | 3 |
| *kb* | *1/tu* | 3 | 3 |
| *kc* | *1/tu* | - | 5 |

### 3.1.2 1D cambium growth model

To investigate whether the improved GRN model 2 can guide cell fate decision-making in the tissue context and lead to bidirectional growth, the GRN was supplemented by further factors and embedded in a cellular layout using a 1D model approach. First, it was hypothesized that *WOX4* might be factor C and that factors A and B are cytokinin signalling (here abbreviated as '*CS*') and auxin signalling (here abbreviated as '*AS*'), respectively. Therefore, the GRN was supplemented to include the influence of cytokinin on *CS* and auxin on *AS* levels (see Results chapter 4.3 **Figure 12**B for graphical illustration of the GRN). The interaction of *WOX4*, *AS*, *CS*, auxin and cytokinin were described with the following system of ODEs:

$$\frac{d[WOX4]}{dt} = aWOX4\left(1 - \frac{|\,[AS]-[CS]\,|}{[AS]+[CS]}\right) - kdWOX4[WOX4] \quad (3)$$

$$\frac{d[AS]}{dt} = aAS\,\frac{\left(\frac{[WOX4]}{q\_WOX4\_AS}\right)^h + \left(\frac{[AUXIN]}{q\_Auxin\_AS}\right)^h}{1+\left(\frac{[WOX4]}{q\_WOX4\_AS}\right)^h + \left(\frac{[AUXIN]}{q\_Auxin\_AS}\right)^h + \left(\frac{[CS]}{q\_CS\_AS}\right)^h} - kdAS[AS]$$

$$\frac{d[CS]}{dt} = aCS\,\frac{\left(\frac{[WOX4]}{q\_WOX4\_CS}\right)^h + \left(\frac{[CYTOKININ]}{q\_Cytokinin\_CS}\right)^h}{1+\left(\frac{[WOX4]}{q\_WOX4\_CS}\right)^h + \left(\frac{[CYTOKININ]}{q\_Cytokinin\_CS}\right)^h + \left(\frac{[AS]}{q\_AS\_CS}\right)^h} - kdCS[CS]$$

In this system, *WOX4* is balanced by auxin and cytokinin signalling levels (*AS* and *CS*). Furthermore, *WOX4* levels are dependent on the synthesis rate constant $aWOX4$ and the degradation rate constant $kdWOX4$. *AS* levels depend on the synthesis constant $aAS$ and are positively influenced by *WOX4* and *AUXIN*, when the concentration threshold for the *WOX4* dependent ($q\_WOX4\_AS$) or *AUXIN* dependent ($q\_AUXIN\_AS$) regulation is reached. Also, *AS* levels depend on the degradation constant $kdAS$. Importantly, as *CS* only appears in the denominator, *CS* negatively regulates *AS* upon reach of the respective threshold level ($q\_CS\_AS$). *CS* levels are dependent on the synthesis rate constant $aCS$ and are positively influenced by *WOX4* and *CYTOKININ*, when the concentration threshold for the *WOX4* dependent ($q\_WOX4\_CS$) or *CYTOKININ* dependent ($q\_CYTOKININ\_CS$) regulation is reached. Also, *CS* levels depend on the degradation constant $kdCS$. In a mutual inhibition, *CS* also negatively regulates *AS* upon reach of the respective threshold level ($q\_AS\_CS$). The Hill coefficient was kept equal to 2. All degradation rates were assumed to be similar.

This system of ODEs was introduced into a 1D model layout. The model was called '1D cambium growth model'. The calculations for the 1D cambium growth model were performed in MATLAB and the codes can be found in Appendix chapter 8.1.2. The basis of the 1D cambium growth model including the initial parameter values was constructed by the Mironova Lab based on previously published work (Mironova *et al.*, 2010; Savina *et al.*, 2020). The rationale of the 1D cambium growth model (hereafter called 1D model) was as follows: The CSC produces two daughter cells. One daughter cell is specified either as xylem or phloem progenitor cell, with the xylem progenitor cells being proximal to the CSC while the phloem progenitor cell is distal. After a certain time, in which the first progenitor cells acquire a certain distance from the CSC due to

newly generated progenitor cells, these first progenitor cells differentiate into the individual xylem or phloem cell types. This described spatial organization and dynamics can be captured within just one cell file. This cell file formed the basis of the 1D model, where each cell is depicted as a rectangle (see Results chapter 4.3 **Figure 12**A for illustration). At the beginning of the calculations, the 1D model consisted of eleven cells that were assigned to the three cambium domains. Since the three cambium domains can be distinguished using *pPXY* and *pSXML5* reporters (Shi *et al.*, 2019), this annotation was used in the model to describe the xylem progenitor cells (PXY+), the phloem progenitor cells (SMXL5+) and the CSC (SMXL5+ and PXY+ double-positive). Additionally, the individual cell positions were described with artificial cell coordinates (see Results chapter 4.3 **Figure 12**A). It was assumed that only the CSC can divide. Furthermore, individual xylem and phloem progenitor cells could grow until they reached a certain size threshold and were then considered to be differentiated. Upon cell differentiation, the cells were not represented in the model anymore to avoid display problems.

The original model in Savina *et al.* (2020) described auxin concentration based on auxin inflow, synthesis, degradation, and diffusion in a 1D cell file and the cells grew, divided, and differentiated depending on the auxin concentration in the cell. Here, in this study, cytokinin, *AS*, *CS* and *WOX4* were introduced as additional regulators to provide for bifacial stem cell activity. The 1D model has the following rules: Auxin and cytokinin are synthesised with the synthesis rate constants $Aks$ or $Cks$. Both auxin and cytokinin move via diffusion with the diffusion rate constants $aD$ and $cD$. Since auxin also is actively transported in planta, which was not accounted for in this model, the value of the diffusion rate of auxin was set higher than the diffusion rate of cytokinin. Furthermore, there is a constant inflow of auxin and cytokinin into the system with the inflow rate constants of $\alpha$ and $\beta$, where $\alpha$ is the auxin inflow intensity to the most proximal cell of the xylem progenitors and $\beta$ is the cytokinin inflow intensity to the most distal cell of the phloem progenitors. The hormone movement outside of the 1D layout is laterally compensated by the subsequent inflow of auxin and cytokinin, respectively, with $A\ lateral\ comp$ or $C\ lateral\ comp$. Auxin and Cytokinin are degraded with the degradation rate constants $Akd$ or $Ckd$. Furthermore, and importantly, the model made the following assumptions on the cell fate decision-making process: *WOX4* acts on *AS* and *CS*. The levels of *AS* and *CS* define the cell state as follows: PXY+ cells are

specified if *AS* > *CS* + *tau*, SMXL5+ cells are specified if *AS* + *tau* < *CS*, CSCs are specified if *CS -tau* < *AS* < *CS* + *tau.* Here *tau* defines the sensitivity of the cell to the differences between the auxin and cytokinin levels. The 1D model calculates the levels of auxin, cytokinin, *AS*, *CS* and *WOX4* for each cellular position. A plot for each factor and calculation step is returned. From these calculated results, a video file is constructed as the final output of the 1D model.

The parameters and their corresponding values were taken from the aforementioned models and were adapted by parameter screening. The final set of parameter values is displayed in Table 10. To simulate the *wox4-1* mutant, the value of the synthesis rate constant $aWOX4$ was halved. This resulted in the so called '*wox4* model'.

**Table 10. Parameters used in the 1D cambium growth model for the wild type and *wox4* model.** All shown parameters are identical between the models, but *aWOX4* is reduced in the *wox4* model. The parameters were jointly optimized with Dr. Viktoriya Lavrekha. This final parameter set was generated by Dr. Viktoriya Lavrekha.

| **Kinetic parameter** | **Dimension** | **Values for wild type model** | **Values for *wox4* model** |
|---|---|---|---|
| *Akd* | *1/tu* | 0.006 | 0.006 |
| *Aks* | *1/tu* | 0.01 | 0.01 |
| *A lateral comp* | *1/tu* | 0.85 | 0.85 |
| *alpha* | *1/tu* | 1.1 | 1.1 |
| *aD* | *1/tu* | 0.40 | 0.40 |
| *Ckd* | *1/tu* | 0.007 | 0.007 |
| *Cks* | *1/tu* | 0.0036 | 0.0036 |
| *C lateral comp* | *1/tu* | 0.9 | 0.9 |
| *betta* | *1/tu* | 0.18 | 0.18 |
| *cD* | *1/tu* | 0.085 | 0.085 |
| ***aWOX4*** | *1/tu* | **0.4** | **0.2** |
| *aAS* | *1/tu* | 1 | 1 |
| *aCS* | *1/tu* | 1 | 1 |
| *h* | *dl* | 2 | 2 |
| *kd* | *1/tu* | 1 | 1 |
| *q_Auxin_AS* | *cu* | 1 | 1 |
| *q_WOX4_AS* | *cu* | 1 | 1 |
| *q_CS_AS* | *cu* | 1 | 1 |
| *q_Cytokinin_CS* | *cu* | 1 | 1 |
| *q_WOX4_CS* | *cu* | 1 | 1 |
| *q_AS_CS* | *cu* | 1 | 1 |
| *tau* | *cu* | 0.001 | 0.001 |

## 3.2 Molecular cloning

Molecular cloning was performed with the GreenGate cloning system according to Lampropoulos *et a.* (2013) following the protocol described in detail in López-Salmerón *et al.* (2019). To generate the A-Module containing the *ARR7* promoter (of 2.7 kb length), respective primers (see Table 3) were designed in Geneious software and a PCR fragment was generated. The entry vector was assembled according to the protocol using the *pGGA000* empty entry vector with AmpR. To generate the *pARR7:ER-mTurquoise-HDEL* (*pAH038*) and *pUBI10:mCherry-GR-linker-WOX4* (*pAH001*) construct, the entry modules listed in Table 4 were used and the protocol was followed using the kits and enzymes specified in Table 5. The *pGGZ003* empty destination vector carried a SpecR. Fast-Digest restriction enzymes for analysis of the destination vector were selected in Geneious. Plasmids were sent to Eurofins for sequencing with the primers indicated in Table 3.

### 3.2.1 *E.coli* transformation

Chemically competent *E.coli* were transformed using heat shock. A 50 µl aliquot of cells in a microcentrifuge tube was thawed and 2 µl of plasmid was added and mixed. After 25 to 35 min incubation on ice, the microcentrifuge tube was placed in a water bath at 42°C for 30 sec and afterwards immediately cooled down by adding 950 µl LB medium without antibiotics. After one hour of shaking at 37°C, 100 µl of bacteria were plated on LB plates with respective antibiotics and incubated at 37°C over night. For plasmid extraction, 5 ml of overnight culture was grown at 37°C at 180 rpm in liquid LB medium with respective antibiotics. Plasmid was extracted using the QIAprep Spin Miniprep Kit.

### 3.2.2 *Agrobacterium* transformation

Correct destination vector plasmids were transformed into *Agrobacterium* using either electro competent ASE strain (with KanR, TetR, CamR, and SpecR for *pAH001*) or chemically competent C58C1 strain (with RifR, TetR, and SpecR for *pAH38*). Electro competent *Agrobacteria* were transformed via electroporation using a MicroPulser Electroporator with the pre-set Bacteria program. Chemically competent *Agrobacteria* were transformed using heat shock. Briefly, a 100 µl aliquot of cells in a microcentrifuge tube was thawed on ice, 500 ng of plasmid was added and incubated on ice for 5 min.

The microcentrifuge tube was then incubated in liquid nitrogen for 5 min and subsequently incubated at 37°C for 5 min. Immediately afterwards 800 µl LB medium without antibiotics was added and *Agrobacteria* were incubated for 2 to 4 hours at 28°C at 180 rpm. Next, after a brief centrifugation (30 sec, 7000 rcf), 800 µl of the supernatant were discarded, the remaining 100 µl were resuspended and plated on LB plates with respective antibiotics. Plates were incubated at 28°C for 2 to 4 days.

## 3.3 Plant Work

### 3.3.1 Seed sterilization

*Arabidopsis* seeds were surface sterilized in microcentrifuge tubes with 70 % EtOH for 10 minutes on a rotating wheel followed by treatment with 99.8 % EtOH for one minute and drying on filter paper under sterile conditions.

### 3.3.2 Growth conditions

For analysis of 19-day old seedlings, seeds were dispersed onto sterile agar plates containing ½ MS solid medium supplemented with 1 % sucrose if not indicated otherwise (see Table 5 and Table 6). Seeds were stratified at 4°C in darkness and then grown vertically under long day conditions (16 h light, 8 h darkness, 23ºC, 100 µE m-2 s-1, 65% relative humidity). Plates sealed with Micropore tape twice. For analysis of 30-day old plants, seeds were stratified at 4°C in darkness, then sown on soil and grown under long day conditions (16 h light, 8 h darkness, 22ºC, 100 µE m-2 s-1, 50 % relative humidity). Plants grown for seed production were kept at slightly different conditions (16 h light, 8 h darkness, 22ºC, 100 µE m-2 s-1, 65 % relative humidity). Plants on soil were treated with Nematodes on a weekly basis.

### 3.3.3 DNA extraction and genotyping

For genotyping, DNA was extracted using DNA extraction buffer (see Table 5 and Table 6). All steps were performed at room temperature (RT). One or two leaves were grinded in 400 µl extraction buffer in a microcentrifuge tube and tubes were inverted several times. After 5 min centrifugation at maximum speed, the supernatant was transferred to a new microcentrifuge tube containing 350 µl Isopropanol and incubated 5 to 10 min. Subsequently, the sample was centrifuged at maximal speed for 5 min

and the supernatant was discarded. After adding 300 µl 70 % Ethanol, the sample was centrifuged at maximal speed for 1 min, supernatant was discarded and the pellet was air-dried. Finally, the DNA was resuspended in 50 µl DNase free water by incubation for 10 min at 65°C with shaking. Genotyping PCRs were performed with JumpStart REDTaq ReadyMix (see Table 5) using 1 µl of DNA. The primers used for genotyping were designed in Geneious and are listed in Table 3. The PCR program used is shown in Table 11.

**Table 11. Genotyping PCR program.**

| Temperature | Time | Cycles |
|---|---|---|
| 94°C | 3 min | 1 |
| 94°C | 30 sec | 35 |
| 58°C | 30 sec | |
| 72°C | 2 min | |
| 72°C | 10 min | 1 |
| 10°C | Hold | 1 |

## 3.4 Generation of transgenic plant lines

In this study transgenic *Arabidopsis* plants were generated through *Agrobacterium* mediated transformation or through crossing.

### 3.4.1 *Agrobacterium* mediated *Arabidopsis* transformation

*Agrobacterium* mediated transformation was performed based on the floral dip method (Clough & Bent, 1998). Shortly, *Agrobacteria* containing the respective plasmid were grown for 48 hours in 100 ml liquid LB medium supplemented with respective antibiotics. The culture was centrifuged for 20 min at 3000 rcf at RT. The supernatant was discarded and the pellet was resuspended in 100 ml deionized water containing 5 g saccharose and 50 µl Silwet L-77. Aerial parts of the plants were dipped into the solution for minimum 2 min. Dipped plants were kept in dark at RT for overnight and were then transferred back to long day growth conditions.

### 3.4.2 Crossing of *Arabidopsis* lines

When generating reporter lines through crossing, the *wox4-1* mutant plant acted as the mother and the respective reporter line as the father. Briefly, immature anthers were removed from the inflorescence of the mother plant and then the stigma was pollinated with the pollen of the father line. The pollinated inflorescence was bagged with a small paper bag and allowed to mature under long day conditions.

### 3.4.3 Selection of transgenic lines

Transgenic lines were selected on ½ MS plates containing the respective herbicide or antibiotic as specified in Table 12.

**Table 12. Resistance markers for selection of transgenic lines.**

| Construct | Resistance marker |
|---|---|
| *wox4-1* T-DNA insertion | SulfR |
| *pWOX4:WOX4-GR (pSS4)* | BastaR |
| *pARR5:n3YFP* | MTXR |
| *pARR6:n3YFP* | MTXR |
| *pARR15:n3YFP* | MTXR |
| *pARR7:ER-mTurquoise-HDEL (pAH038)* | HygroR |
| *pPXY:H4-GFP (pPS24); pSMXL5:H2B-RFP (pIL53)* | BastaR, SulfR |
| *pPXY:mTurquoise2-ER_pSMXL5:Venus-ER (pVL78)* | BastaR |
| *pTCSv2:3Venus* | KanR |
| *pDr5revV2:YFP (pKB46)* | HygroR |
| *pUBI10:mCherry-GR-linker- WOX4 (pAH001)* | BastaR |

## 3.5 Dexamethasone treatments

Dexamethasone was used at different concentrations to induce translocation of GR-tagged proteins into the nucleus. Dex treatment procedures varied between the experiments and are therefore described seperately below.

To identify WUS and WOX4 targets, seedlings were grown for seven days on ½ MS plates (without saccharose) on nylon mesh. The seedlings were then harvested from the plate and washed with dd$H_2O$ to remove seed coats. The seedlings were transferred to several falcon tubes with liquid ½ MS. When all seedlings were dispersed, either Dex or mock stock solution was added to achieve a final concentration of 10 µM (see Table 6). Seedlings were incubated in the falcon for four hours lying horizontally under long day conditions. The seedlings were then washed again with dd$H_2O$, dried on a paper towel and frozen in liquid nitrogen.

For phenotyping of the *pWOX4:WOX4-GR* line, seeds were directly sown onto ½ MS plates containing either 20 µM Dex or mock solution. Seedlings were transferred to new plates every seven days. After 19 days, the hypocotyls were harvested.

In the *pWOX4:WOX4-GR* RNA-seq experiment, seeds were sown directly into small petri dishes (see Table 5) containing liquid ½ MS medium (4 ml of medium was used for 20 seeds). Petri dishes were sealed with parafilm and grown in liquid culture for seven days under long day conditions with gentle shaking (120 rpm). The position of the petri dishes was randomly changed every three days. For treatment, the petri dishes were opened, and Dex or mock stock solution was added to obtain a final concentration of 10 µM and the petri dishes were resealed. Seedlings were treated under long day conditions with gentle shaking for three hours and then harvested, dried on paper towel and frozen in liquid nitrogen.

For analysis of *WOX4-GR* lines crossed with *pARR* or *pTCSv2* reporters, seedlings were grown on ½ MS plates for 18 days (for 24-hour treatment) or 19 days (for six-hour treatment). Then the seedlings were transferred to ½ MS plates containing either 10 µM Dex or mock solution for 24 hours or six hours before the hypocotyls were harvested.

### 3.6 RNA extraction, sequencing and analysis

For identification of downstream targets, RNA was extracted from Dex- or mock-treated seedlings of the respective lines. Three biological replicates were collected per genotype and treatment condition.

### 3.6.1 RNA extraction and sequencing

Seedlings were ground in microcentrifuge tubes containing glass beads of different sizes using the TissueLyserII (30 Hz, for 2 min). RNA was extracted using the RNAeasy Mini Kit together with the QIAshredder columns (see Table 5). No ß-Mercaptoethanol was used for the RNA-seq described in chapter 4.6. Otherwise, all steps were performed according to the manufacturer's protocol and at RT. The extracted RNA was handed over to David Ibberson from the Heidelberg University's Deep Sequencing core facility. There, the RNA quality was checked with either an Agilent Tapestation (Agilent, Santa Clara, USA) using the RNA ScreenTape assay or an Agilent 2100 Bioanalyzer with the RNA 6000 assay. After the quality check, total RNA was quantified with the Quibit instrument (Invitrogen, now ThermoFisher Scientific) using the Qubit Broad Range RNA assay. The NGS libraries were created with theTruSeq RNA Sample Preparation Kit (Illumina, San Diego, USA). The quality control of the libraries was then performed with either the Agilent Tapestation (Agilent, Santa Clara, USA) using the DNA 1000 ScreenTape assay or the Agilent 2100 Bioanalyzer with the DNA 1000 assay. Next, the concentrations were measured using the Qubit instrument with the Qubit HS DNA assay. Finally, the libraries were equimolar pooled and loaded on a high output flow cell using the NextSeq 550 platform (75 cycles, Illumina) for sequencing.

### 3.6.2 RNA-seq analysis and visualization

The sequencing raw data was obtained from the Deep Sequencing core facility. First, the read quality was checked using FastQC (Andrews, 2010). RNA-seq analysis was performed using a combination of Linux terminal commands and R with RStudio. The reads were mapped to the *A. thaliana* TAIR10 genome using the STAR alignment (v2.5.0a) (Dobin *et al.*, 2013) with the command '--alignIntronMax 10000 --alignMatesGapMax 10000 -- outFilterMultimapNmax 1'. Further analysis was conducted in R and RStudio. The Araport11 gene annotation file was used (Cheng *et al.*, 2017) which was adapted to the TAIR10 genome dataset by Dr. Dongbo Shi. Read counts were generated using the summarizeOverlaps with mode ="Union", ignore.strand = TRUE options in the GenomicAlignments package (v1.16.0) (Lawrence *et al.*, 2013). After filtering of low expressed genes (>=5), differentially expressed genes were extracted using the DESeq2 package (v1.38.3) (Love *et al.*, 2014) with Wald test. To obtain the list of differentially expressed genes a two-factor model was

used (design = ~Condition) with Condition being specified as Genotype + Treatment. Principal component analysis (PCA) was conducted in R with RStudio using log2 transformed counts generated with the rlogTransformation function and visualized with ggplot2 (Wickham, 2016). GO term analysis was conducted using ShinyGO 0.077 and Venn diagrams were drawn with the VIB/ UGhent web tool (see Table 7).

## 3.7 Generating hypocotyl cross-sections

Generating free hand hypocotyl cross-sections required the following preparation. First 1x PBS buffer was made from a 10x stock. It is highly recommended to follow the PBS recipe specified in Table 5 and Table 6. Hypocotyls were harvested in the afternoon between 3 and 4 pm and collected in a microcentrifuge tube containing 1x PBS. PBS was then exchanged with 4 % PFA. Samples were subjected to vacuum (- 900 mbar) for 10 min. Air bubbles in the sample were then removed by vigorously tapping the closed microcentrifuge tube 35 times on a stable surface. Subsequently, samples were stored in the 4% PFA solution at 4°C over night. The next day, PFA was removed, and samples were washed once with 1x PBS. Next, the samples were embedded in Low Melting agarose in a small plastic weighing cup. For 19-day old plants 5 % LM agarose, for 30-day old plants 7 % LM agarose was used. After solidification of the agarose (around 20 min), blocks containing one hypocotyl each were cut with a razor blade. The block shape was corrected so that the hypocotyl lied parallel to the cutting board surface. Finally, cross-sections were made using fresh and sharp razor blades. For phenotyping analysis, plants of the same growth stage (defined by a leave number of 8 to 10 leaves and with a maximum leave size of 1 to 2 cm) were selected and hypocotyls were harvested.

## 3.8 Microscopy

### 3.8.1 Staining procedures

For staining of hypocotyl cross-sections either 0.5 % Direct Red 23 or 0.1 % Calcofluor White staining solutions were used (see Table 6). The staining protocols were adapted from Ursache *et al.*, 2018. For Direct Red 23, staining was conducted for a minimum of 10 min, then cross-sections were washed once in 1x PBS. For Calcofluor White, staining was conducted for 30 to 40 min with a subsequent washing step of 30 min in

ClearSee. Finally, stained cross-sections were transferred to a 2-well glass-bottom dish with 1x PBS or ClearSee as mounting medium.

### 3.8.2 Confocal Microscopy

A Leica Stellaris 8 confocal microscope with the LASX Software was used for microscopy. The 20x air objective (HC PL APO CS2, N.A. 0.75) was used in this study. The Diode 405 nm and WLL lasers were used for excitation of fluorescent proteins or dyes. Excitation and emission wavelengths were chosen as specified in Table 13 with additional settings indicated. The settings changed depending on the fluorescent proteins and dyes that were to be visualized in parallel within a sample.

**Table 13. Excitation and emission wavelengths for the visualization of fluorescent proteins or dyes.** Further settings are specified. For Direct Red 23, setting A was used when imaged together with YFP or mTurquoise and setting B was used when imaged together with RFP.

| FP or dye | Excitation | Emission | Specification |
|---|---|---|---|
| GFP | 488 nm | 494 – 547 nm or<br>520 – 525 nm | Operating Mode: Counting<br>TauMode: Tau-Gating with<br>1.7 – 6.3 ns or 1.7 – 5.2 ns |
| RFP / mCherry | 587 nm | 592 – 633 nm | Operating Mode: Counting<br>TauMode: Tau-Gating with<br>1.7 – 5.3 ns |
| YFP / Venus | 514 nm | 520 – 550 nm or<br>524 – 534 nm | Operating Mode: Counting<br>TauMode: Tau-Gating with<br>1.7 – 6.3 ns or 1.9 – 5.2 ns |
| mTurquoise /<br>mTurquoise2 | 458 nm | 470 – 479 nm or<br>465 – 509 nm | Operating Mode: Counting<br>TauMode: Tau-Gating with<br>1.7 – 6.3 ns |
| Calcofluor White | 405 nm | 425 – 490 nm | Operating Mode: Analog<br>TauMode: Intensity |
| Direct Red 23<br>Setting A | 561 nm | 580 – 615 nm | Operating Mode: Counting<br>TauMode: Intensity |
| Direct Red 23<br>Setting B | 553 nm | 558 – 581 nm | Operating Mode: Counting<br>TauMode: Intensity |

All images shown in this study are maximum intensity projections of Z-stacks. When reporter lines were analysed, Z-stacks with 1 µM z-step interval and 15 steps were

taken. If no quantification was done Z-stack size was varied. Image acquisition was performed with the following settings: 0.75x or 1x zoom, pinhole 1AU, 1024x1024 pixel scanning field, 400 Hz scanning speed, HyD detectors, sequential mode with bidirectional scanning and 4x line average. Tau-Gating was used to separate background signal of signal form the fluorescent proteins, with the settings indicated in Table 13. All settings were kept identical when images were to be compared.

## 3.9 Image processing and analysis

All images were analysed using the Fiji (Image J) open-source software application (Schindelin *et al*., 2012). If necessary, composite images were created using the plugin '*Pairwise stitching'.* Z-stacks were projected to one plane using the projection type 'Max intensity'.

### 3.9.1 Fluorescence intensity profiling in hypocotyl cross-sections

To assess fluorescence intensity across tissues of the hypocotyl vasculature, intensity profiles were generated with the 'Radial profile angle' tool and the x-axis representing the normalized radial coordinates. For normalization of the radial coordinates the centre of the section was determined in the cell wall staining channel (Direct Red 23). From this centre a line was drawn which was double the length of distance of the xylem centre to the end of the xylem vessel area. The length of this line (in pixel) was used as input for the 'Radial profile angle' plugin (Philippe Carl, Paul Baggethun) to determine the radius of the circle. The data obtained by running the plugin was stored in Excel and the fluorescence intensity as well as the measured length was normalized to 1. The normalization of the measured length allowed to centre the start of the cambium at shortly after x = 0.5. Generally, for all quantifications, the x-axis represents only an approximation as not all xylem vessel areas represent a perfect circle, thus not all end at exactly x = 0.5. The data were then plotted using R and RStudio using ggplot2 (Wickham, 2016) and the geom_point and geom_smooth functions.

### 3.9.2 High-throughput phenotyping of hypocotyl cross-sections

Together with Dr. Marjorie Guichard, I developed an image analysis pipeline for semi-automated high-throughput phenotyping of *Arabidopsis* hypocotyl cross-sections (please see Contributions chapter).

First, images from a project saved in the LASX application as *.lif* file were opened in ImageJ and saved as individual *.tiff* files in a respective folder with an ImageJ macro generated by Dr. Marjorie Guichard (**Figure 8**).

```
//MACRO_Save_as_Tiff

//Macro for saving images from a .lif project as individual .tiff files

//1) First drag and drop the .lif file into the Fiji console.
//2) Select all images and open all images
//3) Get image IDs of all open images and save them as tiff in the same
// folder by running the following code:
dir = getDirectory("Choose a Directory");
ids=newArray(nImages);
for (i=0;i<nImages;i++) {
        selectImage(i+1);
          title = getTitle;
          print(title);
          ids[i]=getImageID;

          saveAs("tiff", dir+title);
  }
//4) Close Fiji and open it again to start your analysis
```

**Figure 8. Macro for saving .lif projects as individual .tiff files.** This code was generated by Dr. Marjorie Guichard.

Next, the images were analysed following the instructions of the macro called ‘Macro_Phenotyping_Hypocotyl_CrossSections’. The code of this macro can be found in the Appendix chapter 8.1.1. This macro will extract the hypocotyl area, vasculature area, xylem vessel area, xylem area and phloem+cambium area as shown in **Figure 9**. In the following, a brief overview of the usage of the macro is given: First the macro must be opened in ImageJ. When the macro is run, as a first step, the storage location of the images must be specified. The script then asks for the genotype and sample number. Next, the hypocotyl area is automatically measured with ImageJ’s *Threshold* tool using the *Huang* threshold method (**Figure 9** step 1 to 2.1). To homogenise the ‘hypocotyl’ object recognition, an iterative pixel dilation is carried out. Then the user must specify the vascular area manually with the freehand selection tool (**Figure 9** step 3). After confirmation of the user whether the selected area was analysed correctly by the script, the user must select the xylem vessel area with the freehand selection tool (**Figure 9** step 4). After confirmation of correct measurement of the vessel area, the script estimates the xylem area by making a convex hull of the xylem vessel area (**Figure 9** step 4.2 and 4.3). Furthermore, it automatically calculates the phloem+cambium area by subtracting the xylem area from the vasculature area (**Figure 9** step 5 and 5.1). All measured values are stored in a .csv results table in the

respective folder. Furthermore, all analysed images and all measures ROIs are stored in a ZIP folder, which enables precise traceability of the measurements. The next images are loaded automatically, until all images of the chosen folder were analysed. The code of the macro can be found in Appendix chapter 8.1. Attention must be paid for correct decimal input when importing to the csv results table to Excel for further analysis. With the obtained data, boxplots were generated in R and RStudio using ggplot2. The centre lines of the boxplots show medians; box limits indicate the 25th and 75th percentiles. The whiskers extend 1.5 times the interquartile range from the 25th and 75th percentiles.

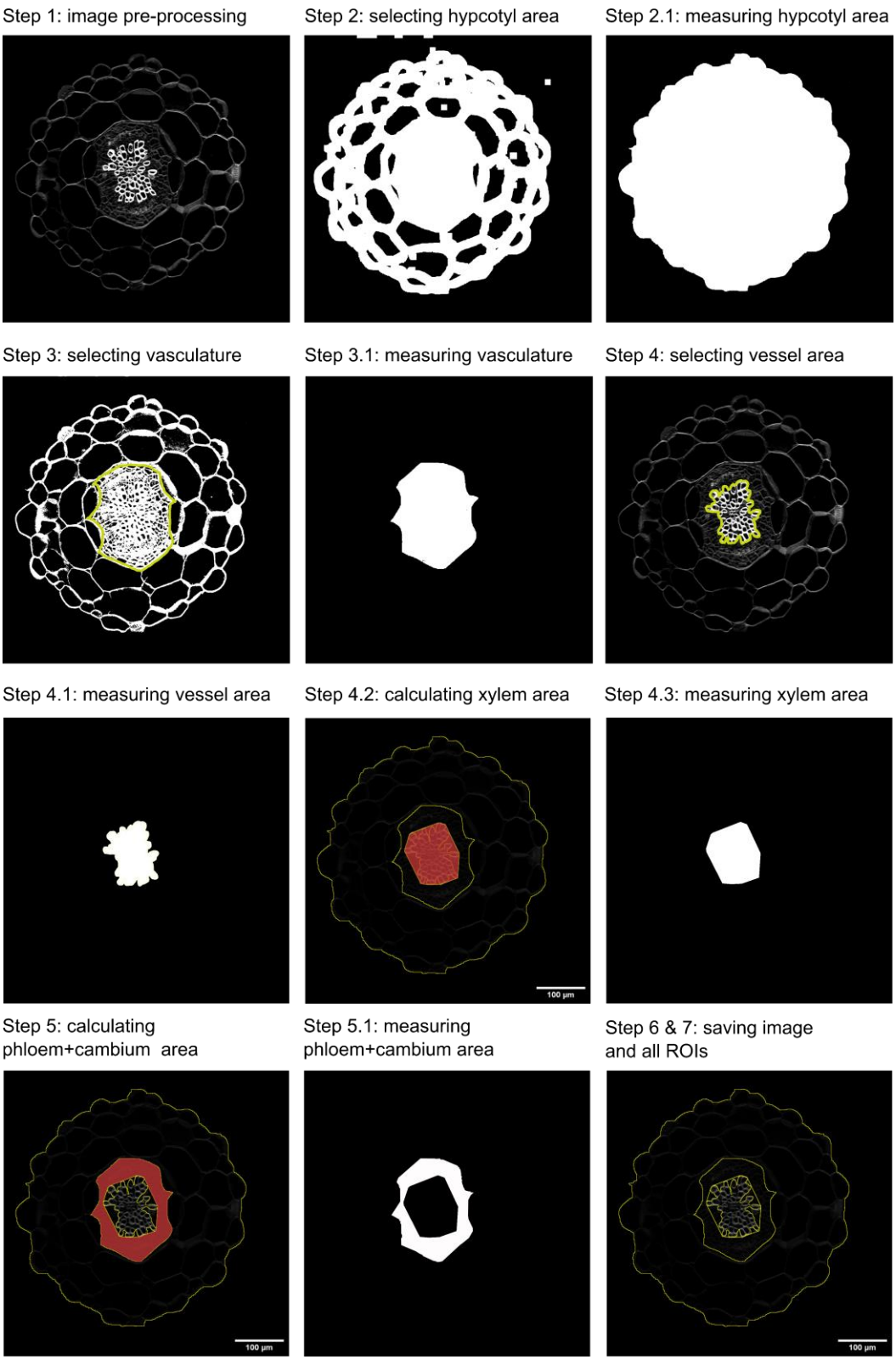


**Figure 9. Semi-automated high-throughput phenotyping of *Arabidopsis* hypocotyl cross-sections using an ImageJ macro.** The steps of the measurements are visualized. The code of the macro can be found in Appendix chapter 8.1.1. The macro was generated by Dr. Marjorie Guichard with contributions and finalization by me.

### 3.9.3 Counting fluorescent nuclei in hypocotyl cross-sections

To analyse the number of fluorescent nuclei in a hypocotyl cross-section, first Z-stacks (1 µm step size, 15 steps) were taken in the respective channels. Here, RFP and GFP marked nuclei were analysed in a Direct Red 23 stained cross-section. The specific microscopy settings are listed in Table 13. For quantification of these images in ImageJ, first a given Z-stack was projected using the maximum intensity projection and was changed from a greyscale to a composite image. Next, a manual threshold of 10 was applied to remove low fluorescent nuclei and background signal. The region of interest, here the vasculature area, was selected in the Direct Red 23 channel. Subsequently, the nuclei in the RFP and GFP channel were counted using the 'Analyse particles' function in ImageJ with a particle size range of 1.8 – 60 µm$^2$ and a circularity of 0.1 to 1.00. To identify double ´-positive nuclei, i.e. nuclei that fluoresce in both the RFP and GFP channels, all nuclei in one channel were selected and projected as ROIs on the other channel. Overlapping regions were then displayed in red by the software and the nuclei marked in red were counted as double-positive nuclei.

### 3.9.4 Analysing fluorescence intensities of nuclei

To assess the fluorescent intensity of nuclei, first Z-stacks (1 µm step size, 15 steps) were taken in the respective channels of a Direct Red 23 stained cross-section. A given Z-stack was projected with the maximum intensity projection and the channels were kept separate. For the analysis of 30-day old plants, a circular ROI in the Direct Red 23 channel was used to capture either A) the xylem area, defined by the outermost xylem vessel elements, B) the cambium area, defined as the area of low intensity of the Direct Red 23 cell wall staining minus the area previously defined as the xylem, or C) the phloem area, defined as the total vasculature area minus the previously defined areas of xylem and cambium. A threshold was employed to remove background signal. Then, using the 'Analyse particles' function in ImageJ, the nuclei in the respective channel and area were identified and the mean gey value of each nucleus was measured, omitting the Direct Red 23 channel. Thus, each biological replicate consists of multiple measurements of nuclei fluorescent intensities.

For 19-day old plants, the *WOX4* expression area was defined as the 1.2-fold of the xylem area, which was defined by connecting the outermost vessel elements in the

shortest path possible using the freehand tool. The cambium area was then defined as the *WOX4* expression area minus the xylem area. The analysis of mean grey values of the nuclei was then performed as described above.

### 3.10 Statistical analysis

For statistical analysis R with RStudio was used. When comparing two groups an unpaired two-tailed Student's *t*-test or Welch's *t*-test were used. When comparing multiple groups, a one-way ANOVA with a post hoc Tukey HSD test was performed ($p<0.05$). The groups are indicated with letters and distinct letters indicate significant differences.

### 3.11 Figure generation

All figures were generated using Fiji/ImageJ, R with RStudio and Inkscape. GO term analysis and Venn diagrams were generated using the web resources specified in Table 7.

# 4. Results

## 4.1 A minimal gene regulatory network creates three stables states

To understand how cell fate decision-making processes unfold, it is crucial to study the underlying gene regulatory mechanisms. One approach is to start as simple as possible. Regarding the cambium system, so far, it is assumed that there are three distinct cell types: the cambium stem cells (CSCs), the xylem progenitor cells, and the phloem progenitor cells (Shi *et al.*, 2019). Furthermore, it is known that both progenitor cell types are produced by single bifacial CSCs (Bossinger & Spokevicius, 2018; Shi *et al.*, 2019; Smetana *et al.*, 2019). Interestingly, a similar situation is observed in the mammalian blood system in the context of hematopoietic stem cells. These stem cells produce two lineages, the common myeloid progenitor and the common lymphoid progenitor cells (Laurenti & Göttgens, 2018). This differentiation mechanism relies on bistability of the hematopoietic stem cells and can be explained by a very simple GRN. A circuit with two differentiation factors, 'A' and 'B', which inhibit each other but activate themselves, is enough to create such a bistable system (Enver *et al.*, 2009; Bhattacharya *et al.*, 2011; Olariu & Peterson, 2019) (**Figure 10**A). In my study, I hypothesized that the basis for the bifacial cell fate decision-making process in the cambium is based on a simple core GRN conveying bistability.

To investigate such a core GRN in more detail, I used mathematical modelling. The modelling was performed in collaboration with Daria Azarova and Victoria Mironova (see Contributions chapter). First, the previously published GRN was reconstructed using ordinary differential equations. The interactions of A and B were modelled as GRN Model 1 (**Figure 10**A) with the ordinary differential equations (ODEs) described in detail in Methods chapter 3.1.1. In the cambium context, gene A can be defined as a phloem differentiation factor and gene B as a xylem differentiation factor. This generated GRN Model 1 (based on the model described in Olariu & Peterson, 2019) is described as follows: The concentrations of the two gene products A $[A]$ or B $[B]$ are affected by the initial gene expression level of A and B (the initial condition), as well as

the synthesis constants of A ($ka$) and B ($kb$) and the degradation rate ($kd$), respectively. Furthermore, A and B mutually inhibit each other with the threshold concentration of ($qa$) and ($qb$), describing the threshold for A-dependent and B-dependent regulation, respectively. The parameter values were subsequently optimized by variation (see Methods chapter **Table 9**). To conclude, from a set of initial conditions, under the identified parameter set, the GRN model 1 calculated three endpoint solutions (marked in red, hereafter called states) (**Figure 10**B). Based on the assigned function of A and B, the states in which only A or B are expressed represent the phloem progenitor and xylem progenitor cells, respectively. The third state with an exact equal amount of A and B represents the stem cell state.

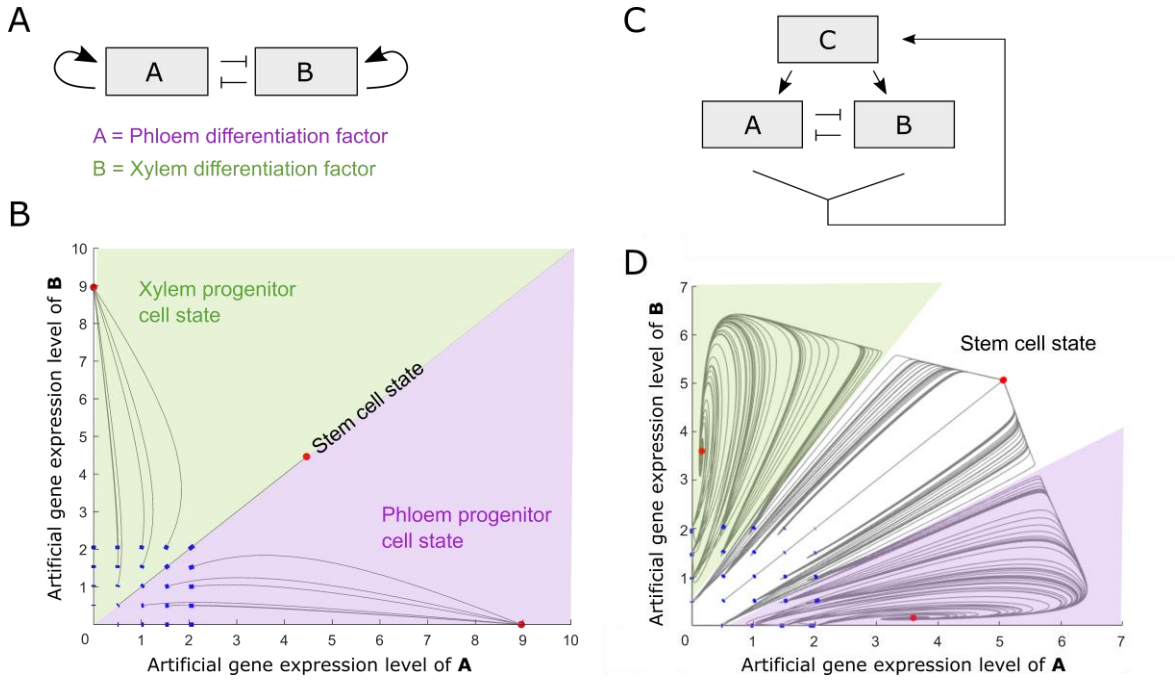


**Figure 10. A simple gene regulatory network conveys bistable behaviour and improvements lead to a more robust stem cell state.**
**A)** GRN model 1. Graphical representation of a simple GRN including two genes, A and B, with mutual inhibition and autoregulation. **B)** Phase portrait of the model depicted in A). The model leads from a range of initial conditions (blue) to three endpoint solutions (states, depicted in red) when solved. A is considered a phloem differentiation factor, B is considered a xylem differentiation factor, therefore the gene expression space is divided into the phloem progenitor cell state (lilac space) and the xylem progenitor cell state (green space). If the gene expression of A and B is exactly equal, the system stays in an undifferentiated state, interpreted as the stem cell state. **C)** GRN model 2. Graphical representation of an improved GRN model which includes an additional factor C, that regulates the expression of genes A and B and includes a feedback loop. **D)** Phase portrait of the GRN in C). This model also leads to three endpoint states. However, the CSC state (white space) arises from a broader range of initial gene expression values and is therefore considered to be more robust. The modelling was jointly performed with M.Sc. Daria Azarova and Prof. Dr. Victoria V. Mironova.

Considering that the CSCs need to be maintained over a long period of time, I expected that the range of initial conditions in which the stem cell state arises would be broader than suggested by the GRN model 1, since tolerating a broader range of initial gene expression will make the CSC state more resistant to fluctuations. In an updated model, GRN model 2, a broadened space for the CSC state was achieved by adding additional coordinated regulation of the factors A and B through a newly introduced factor C. This factor C also replaced the autoregulation of A and B (**Figure 10**C). This GRN model 2 was modelled with the system of ODEs described in detail in Methods chapter 3.1.1. As in the previous model, A and B gene products were synthesized with the gene synthesis constant of A ($ka$) and B ($kb$) as well as the degradation rate $kd$. Again, as in model 1, A and B mutually inhibit each other with the threshold concentration of ($qa$) and ($qb$). Instead of autoregulation of A and B, factor C now coordinatively activated A and B with the threshold concentration qc (set to 1). Factor C was degraded with a rate described by ($kdc$). Importantly, the synthesis of the factor C was described in a way that it is maximal when the concentrations of the gene products A and B are in balance using the function $\left(1-\frac{|\,[A]-[B]\,|}{[A]+[B]}\right)$ together with the synthesis rate ($kc$). This means that when the gene expression of both genes A and B is within a certain range (stem cell state), it positively influences factor C, which positively feedbacks to A and B. The GRN model 2 again calculated three states (**Figure 10**D). But now, importantly, the range of initial gene expression that resulted in the CSC state was much broader, suggesting that the CSC state was more robust. In the cambium context, WOX4 maintains cambium activity (Hirakawa *et al.*, 2010; Suer *et al.*, 2011). Therefore, I hypothesized that WOX4 might be involved in maintaining stem cell proliferation in a role similar to that of factor C. GRN model 1 (Figure 10B) could thus molecularly describe what happens when the system lacks a stem cell niche regulator: the stem cell state becomes less stable. This predicts that eventually cambium activity would diminish or stop altogether. In the GRN model 2 genes A and B must be still expressed in a balanced ratio in the cambium area to allow the stem cell state to occur. To summarize, a simple mathematical GRN model was constructed to explore a possible underlying mechanism of the bifacial cell fate decision-making process in the cambium stem cells. By introducing a third factor into a well-known GRN model, the robustness of the stem cell state could be increased. Therefore, I concluded that this GRN model 2 might be more suitable to describe cell fate decision mechanisms in the cambium context.

In both described models, the two genes A and B and their mutual negative interaction form the core of the bistable system (Bhattacharya *et al.*, 2011). Therefore, I looked for factors that are known to be important in the cambium context and as well exhibit mutual inhibition. I found that auxin and cytokinin signalling are good candidates, since their mutual inhibitory interaction is well known to be important in cambium regulation in roots and stems (Bishopp *et al.*, 2011b; De Rybel *et al.*, 2014; Brackmann *et al.*, 2018; Smetana *et al.*, 2019; Ye *et al.*, 2021). Thus, I next aimed to investigate auxin and cytokinin signalling in the cambium of the hypocotyl and to see whether predictions made by the models are a central aspect of cambium regulation.

## 4.2 Auxin and cytokinin signalling are at low levels in the hypocotyl cambium

The output of auxin and cytokinin signalling can be visualized by genetically encoded reporters which employ the *DR5* or *TCS* promoters, respectively (see Introduction chapter). So far, cytokinin signalling patterns were analysed using the *pTCS*, *pTCSn* or *pARR* reporters (Sheen & Müller, 2008; Bishopp *et al.*, 2011b; Zürcher *et al.*, 2013) (see Introduction chapter). The reporter *pTCSv2* was shown to be more sensitive in the *Arabidopsis* SAM and in tomato (Steiner *et al.*, 2020). To date, none of the cytokinin signalling reporters mentioned above were used for analysis of the cambium in the hypocotyl. In contrast, low but existing auxin signalling in the cambium was already shown to be necessary to maintain normal cambium function (Suer *et al.*, 2011; Brackmann *et al.*, 2018). Furthermore, auxin signalling in stems, hypocotyls and roots is higher in the xylem and phloem area than in the cambium area (Brackmann *et al.*, 2018; Smetana *et al.*, 2019; Zhao, 2022; Mäkilä *et al.*, 2023). To investigate auxin and cytokinin signalling patterns in the hypocotyl, I used lines carrying the *pDR5revV2:YFP* (Brackmann *et al.*, 2018) as well as the *pTCSn:GFP* (Zürcher *et al.*, 2013) and *pTCSv2:3nVenus* reporters (Steiner *et al.*, 2020).

To be able to analyse signal intensities of the *pDR5* and *pTCS* reporter activities in relation to the xylem, cambium and phloem area, I developed a new quantification method based on a previously published approach (Lebovka *et al.*, 2023). In contrast to this approach, I did not analyse the entire vasculature, but a circular area whose radius is twice the radius of the xylem vessel area. With this new approach, I was able to centre the cambium area to start just after x = 0.5, under the assumption that there

are a few cell layers of developing xylem cells distal to the xylem vessel area. This is illustrated in **Figure 11**A, with the cambium area indicated in red. To conclude, using the developed method I was able to differentiate fluorescence intensities of a given reporter according to tissue types and at the same time, identify intensity fluctuations within a tissue type.

To analyse auxin signalling patterns in the hypocotyl, I quantified the *pDR5revV2:YFP* reporter-derived fluorescence intensity. I observed that *pDR5revV2* reporter activity in the hypocotyl is high in the xylem area, and also present in the phloem area, although to a lesser extent (**Figure 11**A). The analysis of auxin signalling in the hypocotyl cambium using the *pDR5revV2:YFP* reporter was already conducted in a previous study (Zhao, 2022). In that study, auxin signalling was also reported to be high in the xylem area and weak in the phloem area; however, no quantification was conducted. Using the above-described quantification method, I could identify a clear fluorescence intensity peak within the xylem and the phloem area, respectively (**Figure 11**D). Furthermore, I identified a local fluorescence intensity minimum in the cambium area (**Figure 11**D cambium area marked in red, and G). While the fluorescence intensity minimum is visible even without quantification, the quantification allowed for a better understanding of the course of the fluorescence intensity levels at both edges of the minimum. Based on the *pDR5revV2:YFP* reporter, it appeared that in all samples examined, auxin signalling increased in a similar fashion on both the xylem and phloem side of the cambium, but the reached intensity peak was lower in the phloem area. This auxin signalling pattern discovered here contributes to a better understanding of the auxin signalling requirements in the xylem, cambium and phloem area during secondary growth in the hypocotyl. To summarize, analysis of the *pDR5revV2:YFP* reporter suggested an auxin signalling maximum in the xylem area, a local auxin signalling minimum in the cambium area, and a local auxin signalling maximum with lower intensity in the phloem area.

To explore cytokinin signalling in the hypocotyl, I first analysed the *pTCSn* reporter. I detected low reporter activity in the xylem area, with a local minimum in the most distal part of the xylem area (**Figure 11**B and E). Furthermore, there was a steady increase of reporter activity from the distal part of the xylem area to the phloem area. To conclude, analysis of the *pTCSn* reporter indicated a cytokinin signalling gradient along

the cambium area with a prominent signalling peak in the phloem area (**Figure 11**E and H).

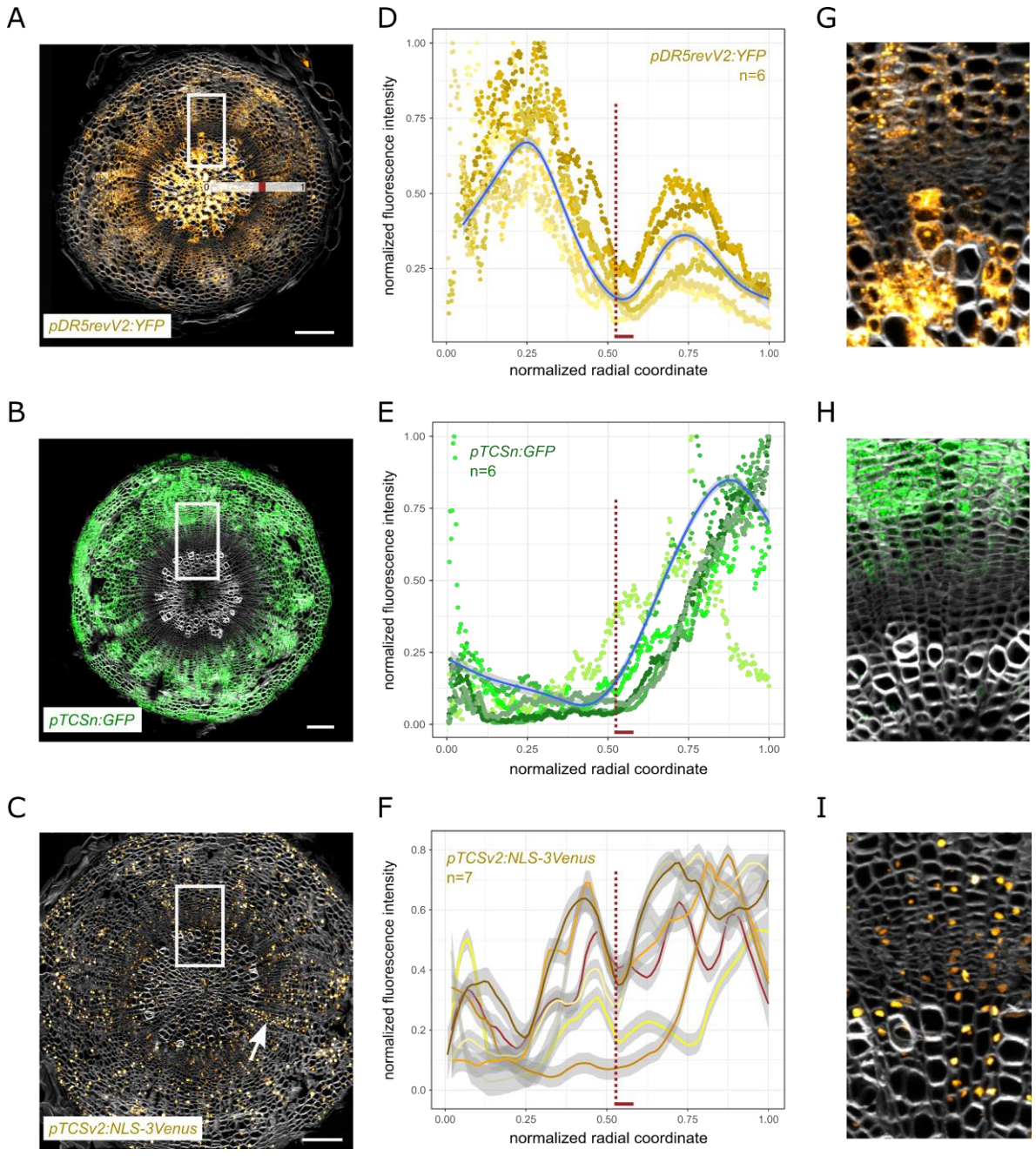


**Figure 11. Auxin and cytokinin signalling are low in the cambium.**
**A) to C)** Hypocotyl cross-sections of the auxin signalling reporter *pDR5revV2:YFP*, and the cytokinin signalling reporters *pTCSn:GFP* and *pTCSv2:NLS-3Venus*, respectively. Plants were grown for four weeks in long day conditions. In A) the quantification method is exemplarily visualized with a white rectangle. The quantification method results in the cambium being centred to start shortly after x=0.5, marked in red. In C) an area with high signal intensity in the cambium is marked with an arrow. Sections were stained with Direct Red 23 (grey). Scale bars represent 100 µm. **D) to F)** Quantification of signal intensities of respective lines using the 'Radial Profile Angle' plugin of Fiji. The radial coordinates were normalized with the xylem centre representing 0, the most outer position of xylem vessels aligning at 0.5 and 1 representing twice this distance, reaching into the phloem area. The signal intensity was normalized to 1 by dividing by the maximum intensity of the respective sample. One sample which best represents all samples was picked and additionally shown as a smoothed

curve to better guide the eye in panel D) and E). In panel F) only smoothed lines are shown since individual data points would be hard to distinguish. For all smoothed curves grey areas indicate confidence intervals. Shown are the quantifications of two or three independent experiments for each line. Respective sample size is indicated. **G) to I)** Enlargement of the areas indicated in A) to C) for better visualization of the cambium area.

Next, I analysed how cytokinin signalling patterns are reported using the more sensitive *pTCSv2* reporter. Due to the nuclear localization of the Venus protein and since not all nuclei aligned to one optical plane, the quantification resulted in noisier signal distribution compared to the *pTCSn* reporter. Therefore, only smoothed intensity curves and no datapoints are shown for the *pTCSv2* line (**Figure 11**C and F). In contrast to the *TCSn* reporter, *pTCSv2* analysis revealed high cytokinin signalling in xylem area. The fluorescence intensity was highest in the distal xylem area adjacent to the cambium, likely since this area contains fewer dead xylem vessel cells. Additionally, as for the *pTCSn* reporter, signalling was high in the phloem area. The signal intensities also varied within the xylem and phloem areas (**Figure 11**F). However, this is likely caused by the nuclear localization of the signal and the chosen quantification method. To interpret nuclear localized signal radially more faithfully, the quantification method would have to be adapted. Nevertheless, the current analysis still revealed a local fluorescence intensity minimum in the cambium area for most samples (**Figure 11**C, F and I). Furthermore, I observed that the fluorescence intensity increases at the cambium area boarders (**Figure 11**F and I). In some cases, small parts of the cambium area did not show a local fluorescence intensity minimum (**Figure 11**C indicated by the arrow). This observation reduces the concern that the fluorescence intensity minimum could have technical reasons, but also raises the question how these specific areas come about and whether they fulfil a certain function. Taken together, the analysis of the *pTCSv2* reporter revealed high cytokinin signalling in the phloem area, but in contrast to the *pTCSn* reporter also a substantial signalling in the xylem area. Strikingly, a local signalling minimum in the cambium area was observed in the *pTCSv2* reporter.

To conclude, my analyses of the *pDR5revV2* and *pTCSv2* reporter lines indicated that there is a local minimum of auxin and cytokinin signalling in the cambium area of the hypocotyl. The *pTCSn* line suggested that there is a cytokinin signalling gradient increasing from the proximal xylem to the phloem area, whereas the *pTCSv2* reporter suggested a local signalling minimum in the cambium area. Although, these two results

appeared to be contradictory when looking at the entire vasculature radius, when focussing solely on the cambium area, the results of both reporters were similar, as both reporters showed lower reporter activity in the proximal cambium domain and higher activity in the distal cambium domain. Due to the clear *pTCSv2* reporter activity in the xylem area, describing the result as local cytokinin signalling minimum in the cambium area may be more accurate. Similarly, the *pDR5revV2* reporter clearly showed a local minimum instead of an one-sided auxin gradient from the distal towards the proximal side of the cambium, as reported in other studies with other *pDR5* reporter lines (Mäkilä *et al.*, 2023).

To better understand how auxin and cytokinin signalling could interact to guide cell fate decision-making and bidirectional growth in the hypocotyl cambium, I aimed to generate a one-dimensional computational model based on the previously described GRN model 2 (see Results chapter 4.1).

## 4.3 Modelling bifacial differentiation and growth in one dimension

Since the hypocotyl cambium lies deep within the tissue, it is not easily accessible for live imaging and live-cell tracking, therefore, cambium dynamics are very hard to capture. Mathematical modelling provides a tool to circumvent this difficulty. Therefore, it can also aid to better understand how the dynamics of auxin and cytokinin signalling could direct the cell fate decision-making process in the cambium. The improved GRN model 2 (see chapter 4.1) explained a possible underlying core gene regulatory mechanism of the bifacial cell fate decision-making process. Mutual inhibition and bistability mechanisms appear to be core motifs in cell fate decision-making and stable patterning and more and more of these motifs are being detected in plant morphogenesis (Moret *et al.*, 2020; Guan *et al.*, 2022). A very recent study has shown that a mutual inhibitory interaction between WUS and WOX13 occurs when pluripotent callus cells take cell fate decisions in order to produce shoots (Ogura *et al.*, 2023).

As a next step, it was of central importance to understand how this GRN can guide cell fate decision-making in the tissue context leading to bidirectional growth and how it can influence tissue production rates. For this, a cambium growth model was constructed in one dimension in collaboration with the Mironova lab (Prof. Dr. Victoria

Mironova, M.Sc. Daria Azarova and Dr. Viktoriya Lavrekha, see the Contributions chapter for details). The here constructed 1D cambium growth model (1D Model) was based on previous models that described a one-directional meristem activity in the root meristem (Mironova *et al.*, 2010; Savina *et al.*, 2020). The rationale of the 1D model layout is described in detail in the Methods chapter 3.1.2. Briefly, a single cell file showing xylem progenitors (PXY+), CSCs (PXY+ and SMXL5+ double-positive) and phloem progenitors (SMXL5+) was depicted as an approximation of the radial organization of the cambium (illustrated in **Figure 12**A). It was assumed that only the CSCs (**Figure 12**A, marked with an asterisks) can divide. Furthermore, individual xylem and phloem progenitor cells grew until a certain size threshold was reached and were then considered to be differentiated xylem or phloem cells. Differentiated cells were not represented in the model anymore to avoid display problems. But by establishing a counter for the numbers of stem cell divisions, produced PXY+ cells, PXY+/SMXL5+ double-positive cells, SMXL5+ cells, as well xylem and phloem cells, the differentiation dynamics could be still tracked over time. As described in the respective methods section, the model assumes auxin inflow to the cambium from the xylem side and cytokinin inflow from the phloem side. The 1D model was based on the GRN model 2, but now genes A and B were assigned to represent auxin signalling (*AS*) and cytokinin signalling (*CS*), respectively (**Figure 12**B). Thus, the mutual negative interaction of A and B was represented by the mutual inhibition of auxin and cytokinin signalling. Since factor C was assigned to represent *WOX4*, an influence of *WOX4* on auxin and cytokinin signalling was hypothesized. The core GRN was then extended to include the influence of auxin and cytokinin on auxin signalling and cytokinin signalling, respectively (**Figure 12**B). Consequently, additional factors were introduced to describe these dynamics (see Methods chapter 3.1 for details). Importantly, in the 1D model xylem progenitors (PXY+ cells) were specified if auxin signalling levels were higher than cytokinin signalling levels, whereas phloem progenitors (SMXL5+ cells) were specified if cytokinin signalling levels were higher than auxin signalling levels. CSCs were specified if auxin and cytokinin signalling levels were balanced. To summarize, a 1D model layout was constructed, depicting the proximal, central and distal cambium including a GRN with mutual inhibition of auxin and cytokinin signalling governed by WOX4.

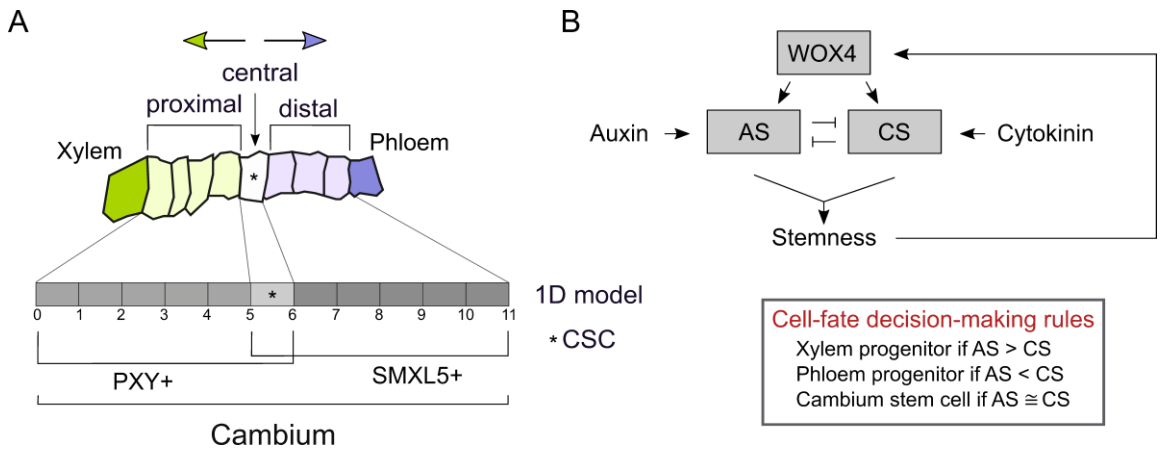


**Figure 12. Rationale and build-up of the 1D cambium growth model.**
**A)** Graphic representation of a radial cell file of the hypocotyl cambium and visualization of the corresponding representation in the 1D model. In the model the proximal cambium domain is labelled as PXY-positive (PXY+), the distal domain as SMXL5-positive (SMXL5+), and the central domain as double-positive (SMXL5+/PXY+). The central domain consists of the cambium stem cell (CSC), which is marked with an asterisk. **B)** Scheme of the core GRN used for the 1D model and the cell fate decision-making rules used within. In the GRN WOX4 as factor C is hypothesized to target auxin and cytokinin signalling. Auxin signalling (AS) and cytokinin signalling (CS) levels are influenced by the respective hormones and a stem cell state occurs when signalling levels are balanced, leading to a positive influence on *WOX4*. This GRN was implemented into the cellular model illustrated in A), which included cell division and growth. The GRN and 1D cambium growth model were jointly generated with Prof. Dr. Victoria Mironova, M.Sc. Daria Azarova and Dr. Viktoriya Lavrekha.

Next, the parameter space was screened for a parameter set which allowed for both, a continuous maintenance of the CSC as well as bidirectional tissue production (for parameter values see Methods chapter 3.1.2). Using a suitable parameter set, the 1D model could maintain the CSC over time and, crucially, daughter cells differentiated in a bidirectional manner into either xylem or phloem progenitor cells. The output of the 1D model was visualized in a video which displays the radial cell file with division and differentiation. The first and last frame of the generated video are shown in **Figure 13**, the video itself can be generated following the instructions and using the code listed in chapter 8.1.2. In the video, the corresponding auxin and cytokinin levels of each cell, as well as auxin signalling levels (*AS*) and cytokinin signalling levels (*CS*) and *WOX4* expression levels were depicted. The generated video showed a timeframe in which the CSC divided 25 times and 12 xylem cells as well as 12 phloem cells differentiated (**Figure 13**). In the 1D model, *WOX4* (**Figure 13**, line depicted in red) is expressed the highest in the CSC, where the balancing of the auxin and cytokinin signalling levels occurs due to the wiring of the GRN (shown in light blue and magenta). To summarize, it was shown that the core GRN, which explained a possible cell fate decision-making process in the CSC based on auxin and cytokinin signalling, when integrated into a 1D

cambium layout, could generate the bifacial differentiation and bidirectional growth observed in the cambium in planta.

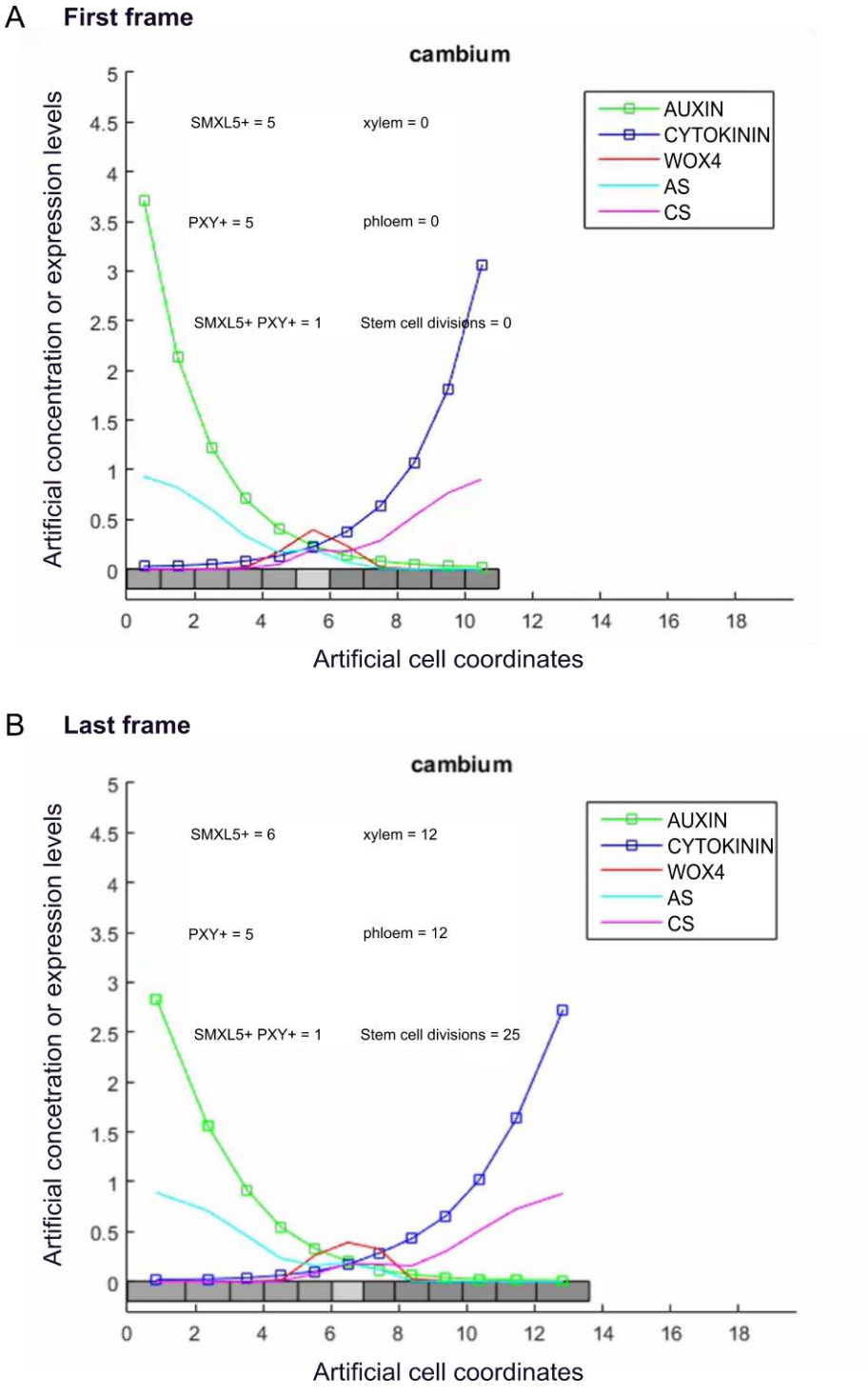


**Figure 13. The 1D cambium growth model showed cambium specific bifacial differentiation and growth based on a core GRN with mutual inhibition of auxin and cytokinin signalling.**
The first **(A)** and last **(B)** frame of the video of the 1D cambium growth model is depicted. The y-axis represents the artificial gene expression or concentration levels of a given substance along the artificial cell coordinates. The x-axis represents artificial cell coordinates. Each rectangle represents a cell. The light grey cell represents the CSC, the cells left of it represent the proximal cambium domain and the dark grey cells right of it represent the distal cambium domain. The CSC is counted

as SMXL5+PXY+. During the model runtime new xylem (PXY+) or phloem (SMXL5+) progenitors were generated, which differentiated into xylem or phloem cells upon reaching a size threshold. The differentiated xylem or phloem cells were no longer represented in the model, but the differentiation dynamics could be tracked with the cell type counter. The levels of auxin, cytokinin, auxin signalling (AS), cytokinin signalling (CS) and WOX4 are shown with respect to the cells. The 1D cambium growth model was jointly generated with Prof. Dr. Victoria Mironova, M.Sc. Daria Azarova and Dr. Viktoriya Lavrekha.

The focus on auxin and cytokinin signalling based cell fate decision-making makes this model a useful addition to a recently published 2D cambium model (Lebovka *et al.*, 2023). In this fundamental study the authors defined xylem and phloem differentiation to be dependent on cell size as well as active PXY levels or generally *PXY* expression. Using a 2D layout depicting hypocotyl cross-sections, the authors could show that an ODE system describing PXY and CLE41 interaction and the addition of a further phloem-derived factor plus a differentiation factor were sufficient to explain the cambium activity observed in planta (Lebovka *et al.*, 2023). Although the presented 2D models contained many informative interactions, auxin or cytokinin signalling as well as *WOX4* were not considered. Therefore, the construction of the 1D model presented here was necessary. By creating this 1D cambium growth model, it is now possible to study the influence of *WOX4* as well as auxin and cytokinin signalling on the cell fate decision-making process and vascular tissue patterning in the context of secondary growth in silico. Furthermore, the 1D model generated in this study enables to draw parallels from secondary growth to primary growth, where it was shown that the interaction of auxin and cytokinin was sufficient to create the bisymmetric tissue pattern of the root vasculature (Bishopp *et al.*, 2011b; De Rybel *et al.*, 2014).

### 4.3.1 The 1D model allowed modelling of cambium stem cell loss

Establishing changes in gene expression and hormone signalling in planta takes time or is sometimes even experimentally infeasible. However, the generated 1D model now enabled a rapid initial investigation of the influence of the factors represented in the model on cambium activity.

To assess the effect of the loss of functional *WOX4* in the 1D model, the value of the synthesis rate constant of WOX4 ($aWOX4$) was reduced. This model variant was termed "*wox4* model" (for details and parameter values see Methods chapter 3.1.2). The first and last frame of the generated *wox4* mutant video are shown in **Figure 14**. The video of this *wox4* model can be generated following the instructions and using the code

listed in chapter 8.1.2. The initial conditions of the *wox4* model were identical to the wild type model (**Figure 14**A). The reduction synthesis rate constant of WOX4 led to the complete loss of the CSC (SMXL5+PXY+ = 0) and thus of cambial activity in the 1D model. Since the CSC was not maintained, the existing xylem and phloem progenitors differentiated to xylem and phloem cells respectively without further progenitors being produced (**Figure 14**B). This observed effect of the in silico *wox4* mutation on cambium activity was much stronger than the effect of non-functional *WOX4* on cambium activity reported in planta (Hirakawa *et al.*, 2010; Suer *et al.*, 2011). Importantly, *wox4-1* was shown to be a null allele (Hirakawa *et al*., 2010). Since already a reduction of synthesis rate constant of WOX4 produced a strong effect, I concluded that the factor in the core GRN hypothesized to be *WOX4* (**Figure 12**B) might rather represent a pool of core stem cell regulators with a combined effect on cambium activity. According to literature, a complete loss of cambium activity was only observed in the *bp-9,wox4,pxy* triple mutant (Zhang *et al.*, 2019). In summary, when *WOX4* expression was reduced in the 1D model, cambium activity was eliminated. The established 1D *wox4* model represents a first step in investigating perturbations of cambium activity in silico. However, further investigations are needed to fully exploit the possibilities offered by the 1D cambium growth model, which must also be done in conjunction with experimental investigations.

A **First frame**

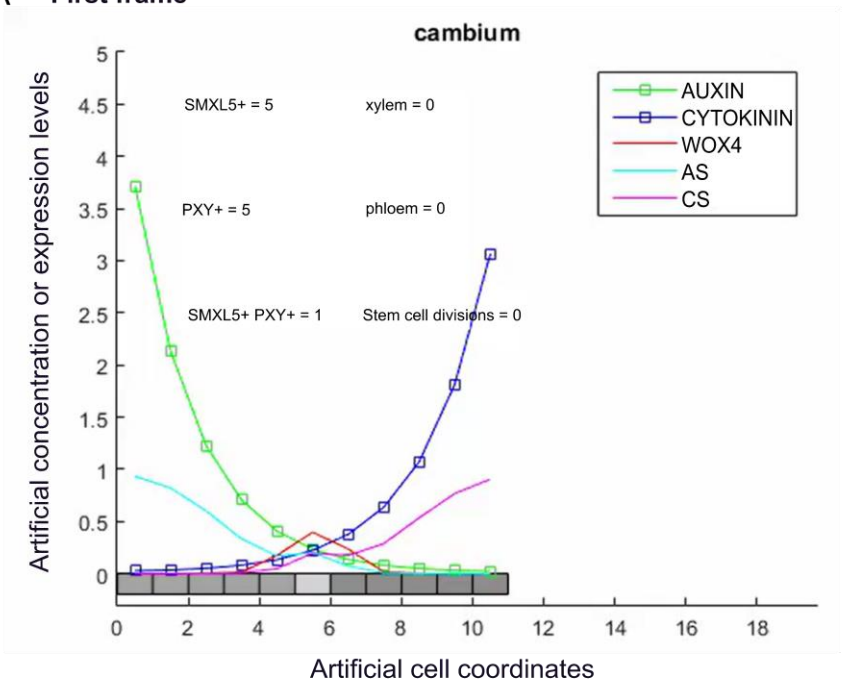


B **Last frame**

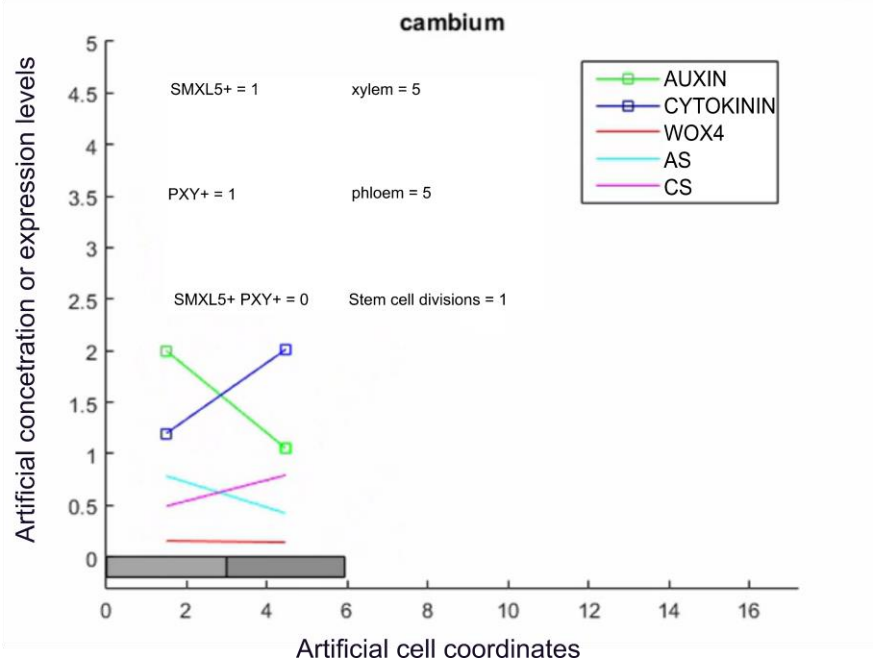


**Figure 14. A 1D *wox4* mutant model showed loss of bifacial differentiation and growth.**
The first **(A)** and last **(B)** frame of the 1D cambium growth *wox4* mutant model video is depicted. The y-axis represents the artificial gene expression or concentration levels of a given substance along the artificial cell coordinates on the x-axis. In the model shown here, the synthesis rate constant of *WOX4* was reduced. The 1D *wox4* model was jointly generated with Prof. Dr. Victoria Mironova, M.Sc. Daria Azarova and Dr. Viktoriya Lavrekha.

## 4.4 Investigating auxin and cytokinin signalling in the *wox4-1* mutant

Auxin signalling in the cambium is required for normal cambium activity and WOX4 has previously been shown to be important in conveying auxin responses in the stem cambium (Suer *et al.*, 2011; Brackmann *et al.*, 2018). Analysis of the *DR5rev:GFP* reporter line revealed that auxin signalling was still present in the interfascicular region in the stems of *wox4-1* mutants, therefore, indicating a role of WOX4 downstream of auxin (Suer *et al.*, 2011).

Here, to investigate whether auxin signalling is altered in the hypocotyl cambium when WOX4 is non-functional, I crossed the more sensitive auxin signalling reporter *pDR5revV2:YFP* (Brackmann *et al.*, 2018) with the *wox4-1* mutant. I analysed hypocotyls of 30-day old wild type and *wox4-1* mutant plants. I observed that, similar to the situation in stems, in the hypocotyl cambium of *wox4-1* mutants fluorescence, thus auxin signalling, was still present (**Figure 15**A). Similar to wild type plants, *wox4-1* mutants also showed a local fluorescence intensity minimum in the cambium (**Figure 15**A). The mean fluorescence intensity in the cambium and phloem area, measured as mean grey value (for details, see methods chapter 3.9.4), was not significantly dampened or elevated in the *wox4-1* mutant compared to wild type plants (**Figure 15**B). Since I could not obtain plants which were homozygous for the construct, the fluorescence intensity was normalized to the highest fluorescence intensity value within a given sample. As fluorescence intensity was always highest in the xylem area in each sample all values were equal to one in the xylem area (**Figure 15**B). Also, without normalization, no significant difference between *wox4-1* mutant and wild type plants was apparent (Supplemental Figure 1). Interestingly, when analysing the radial distribution of the *pDR5revV2:YFP* derived signal, I observed a small but significant distal shift of the local fluorescence intensity minimum in the cambium in the *wox4-1* mutant compared to wild type (**Figure 15**C, marked by vertical lines). The local fluorescence maximum in the phloem was not significantly shifted. I did not analyse a possible shift of a local fluorescence intensity maximum in the xylem area since xylem vessels show no fluorescent signal and therefore the location of a fluorescence maximum would be based on xylem vessel distribution and hence not meaningful. It is important to note that in 30-day old *wox4-1* mutant plants the *wox4-1* phenotype reported earlier for 19-day old plants (i.e., reduced cambium activity and therefore smaller vasculature area) was no longer present. Nevertheless, there may still be

changes at the molecular level which may cause the observed distal shift of the local fluorescence intensity minimum in the cambium in the *wox4-1* mutant. To summarize, the analysis of the *DR5revV2* reporter in *wox4-1* background revealed that overall auxin signalling levels in the *wox4-1* mutant are comparable to the wild type and that the local auxin signalling minimum in the hypocotyl cambium can be maintained without functional WOX4. Hence, WOX4 is not necessary to generate a local auxin signalling minimum in the cambium. However, the observed distal shift of the auxin signalling minimum in the *wox4-1* mutant could indicate that WOX4 might be necessary for the correct (more proximal) positioning of the auxin signalling minimum in the hypocotyl cambium.

To examine whether the lack of functional WOX4 impacts cytokinin signalling levels, I crossed the *pTCSv2:NLS-3Venus* cytokinin reporter with the *wox4-1* mutant. I obtained F3 lines which were homozygous for the construct and mutation. Interestingly, I found that cytokinin signalling levels were elevated in the xylem and cambium area in the *wox4-1* mutant (**Figure 15**D and E). Here, due to the nuclear localization of the signal, the mean grey values of nuclei within the xylem, cambium or phloem area were measured (see methods chapter 3.9.4). As the lines were homozygous for the construct, absolute values are shown. No significant difference could be detected in the phloem area between the wild type and *wox4-1* mutant (**Figure 15**E). The nuclear nature of the signal did not allow to compare the radial distribution of the *pTCSv2* signal between wild type and *wox4-1* mutants, as the analysis method produced too noisy results (see **Figure 11**F). A different analysis method developed in this study, once established, might circumvent this issue. To conclude, the analysis of the *pTCSv2:NLS-3Venus* reporter in wild type and *wox4-1* mutant background indicated that cytokinin signalling was elevated when WOX4 was non-functional. Although this result must be viewed with caution due to small sample size and lack of independent repetition it can nevertheless serve as a first indication that WOX4 might negatively affect the cytokinin signalling pathway.

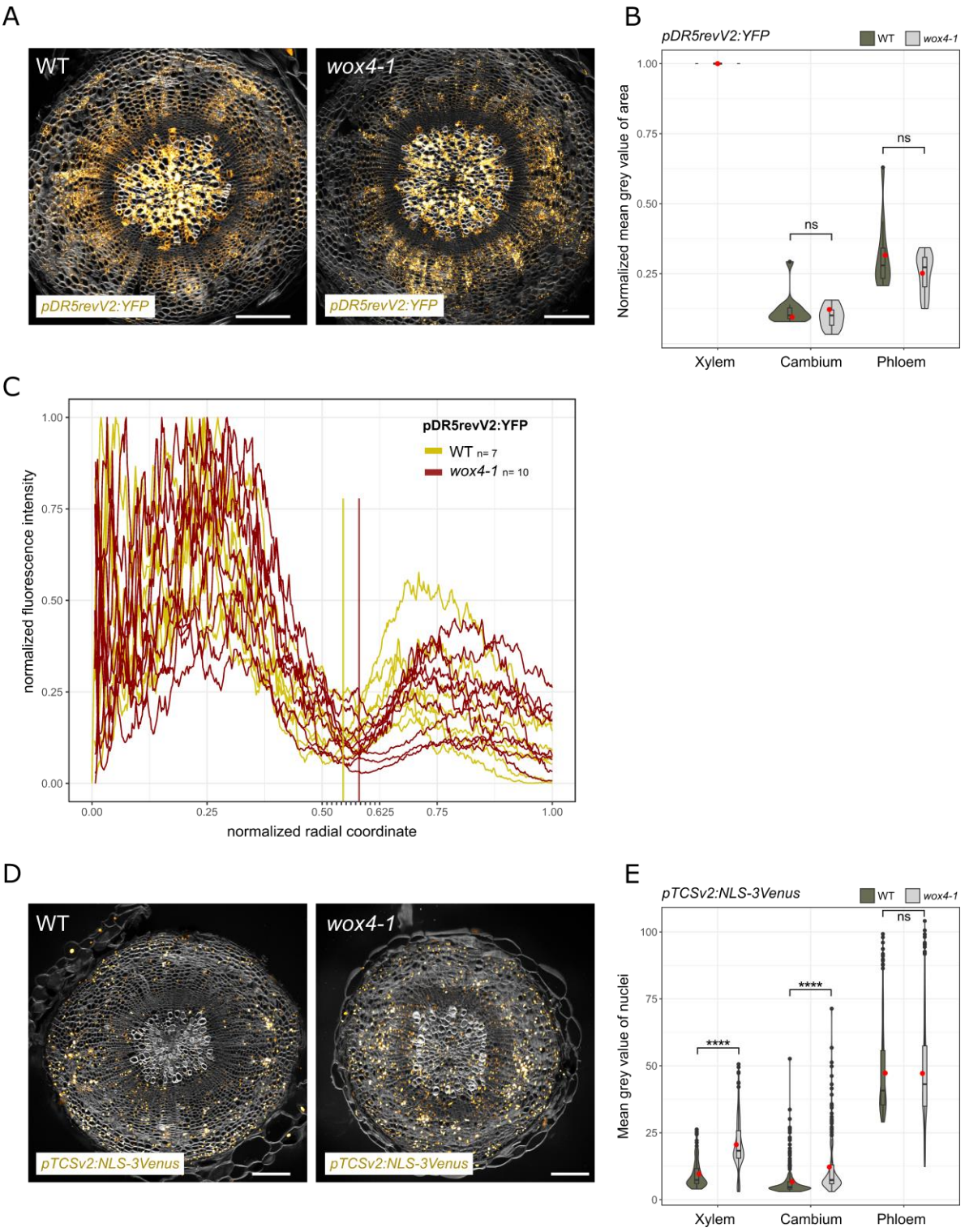


**Figure 15. Comparison of auxin and cytokinin signalling in wild type and *wox4-1* background. A) and D)** Exemplary hypocotyl cross-sections of lines harbouring the *pDR5revV2:YFP* or *pTCS:NLS-3Venus* transgene (displayed in the *Orange Hot* look-up table where white/ light yellow represent high fluorescence intensity and dark yellow represents lower fluorescence intensity). Sections were stained with Direct Red 23 (grey). Plants were grown for 30 days in long day conditions. Scale bars represent 100 µm. **B) and E)** Quantification of fluorescent signal intensities of the p*DR5revV2:YFP* reporter (B) or *pTCS:NLS-3Venus* reporter (E) in hypocotyl cross-sections of wild type and *wox4-1* mutants in the xylem, cambium and phloem area. Significant differences were identified using Welch's *t*-test (95% CI), ****p<0.0001. The violin plots graphically indicate the distribution of datapoints and additionally the boxplots show the medians (centre lines of boxes). The red dots indicate the mean. For B) the data was collected in two independent experiments. Sample

size for wild type was n=11 and for *wox4-1* n=14. The mean grey values were normalized within one sample to the highest fluorescence intensity since the plants were not homozygous for the construct. Highest fluorescence intensity was always located in the xylem area; thus, all data points are equal to 1 in the xylem area. For E) the data was collected in one experiment and biological replicates for wild type were n=3 and for *wox4-1* n=4. Absolute mean grey values of the nuclei of are displayed as the lines were homozygous for the construct. **C)** Radial quantification of fluorescent signal intensities of the *DR5revV2:YFP* reporter in hypocotyl cross-sections in wild type and *wox4-1* mutants. Sample size is indicated. The fluorescent intensity as well as the radial coordinates were normalized. Here, x = 0 represents the xylem centre and x = 1 represents twice the distance of the xylem centre to the end of the xylem vessel area. Thus, the cambium is centred to start shortly after x=0.5 in all samples. Quantification of signal intensities was performed using the 'Radial Profile Angle' plugin of Fiji. Significance was determined using the Welch's t-test, p=0.044.

## 4.5 Analysis of cambium domain pattern in the *wox4-1* mutant

In the 1D *wox4-1* mutant model discussed above, the *wox4-1* phenotype was simulated such that the cambium stem cells (CSCs) disappeared at the end of the simulation. In planta, however, in the *wox4-1* mutants, the CSCs cannot have completely disappeared as lateral growth is reduced but still maintained (Hirakawa *et al.*, 2010; Suer *et al.*, 2011). I hypothesized that nevertheless in the *wox4-1* mutant there must be a change regarding the stem cells, hence the central domain, that then leads to the described reduced cambium activity. Furthermore, I hypothesized that if *WOX4* regulates xylem and phloem differentiation factors, a change in the patterning of the proximal and distal cambium domains might be observed. The *pPXY:H4-GFP;pSMXL5:H2B-RFP* reporter line described in Shi *et al*., 2019 allowed labelling of the proximal cambium domain by expressing GFP under the *PXY* promoter while the distal cambium domain was labelled through expressing RFP under the *SMXL5* promoter (Shi *et al.*, 2019). Where both signals overlap, the central cambium domain, where the CSCs reside, is located (Shi *et al.*, 2019). Thus, this reporter allowed visualization of cambium domain patterns.

To better understand how stem cells were influenced when WOX4 was non-functional, I investigated the *wox4-1* mutant in terms of cell fate decision-making processes by analysing its cambium domain pattern. To assess whether *WOX4*-deficiency causes a change in the cambium domain pattern in the hypocotyl, I introgressed the *pPXY:H4-GFP; pSMXL5:H2B-RFPs* marker (consisting of two transgenes*)* into the *wox4-1* mutant. I then investigated hypocotyl cross-sections of 19-day old plants (**Figure 16**A). Since both, the wild type and the generated *wox4-1* cross, were not homozygous for the reporters, I focussed only on the hypocotyl cross-sections that showed both RFP

and GFP signals. Double-positive nuclei are depicted in white and exemplarily marked with an arrow (**Figure 16**A). Since the reporter's fluorescent signal was located to the nucleus, it allowed counting of individual nuclei, and thus cells, belonging to each of the domains. Because the *wox4-1* mutant exhibits a phenotype with reduced cambium activity and hence reduced vasculature size, I normalized the number of nuclei in a domain to the total number of nuclei counted. Using this analysis method, I observed that in the wild type background, the relative amount of *pPXY:H4-GFP* positive (PXY+) nuclei ranges from 1 to 35 %, while *pSMXL5:H2B-RFP*-positive (SMXL5+) nuclei account for 51 up to 94 % of all counted nuclei within a sample. Double-positive nuclei accounted for 3 to 38 % of all nuclei (**Figure 16**B). These large variations are most likely caused by the nuclear localization of the signal, as not all nuclei are within one optical plane leading to variation of the total number of captured nuclei between individual cross-sections. Nonetheless, by focussing on the resulting median of all analysed samples, I found that in wild type plants, SMXL5+ nuclei accounted for about two thirds of all counted nuclei, and the other third was distributed between PXY+ and double-positive nuclei (**Figure 16**B). In contrast to the wild type, the *wox4-1* mutant showed an approximately 30% reduction in double-positive nuclei, i.e., stem cells. However, this trend was not significant. I also did not observe any significant change in the relative number of PXY+ or SMXL5+ nuclei, although a trend towards more SMXL5+ and less PXY+ nuclei was visible. An extreme case is shown in **Figure 16**A. The finding that the relative number of PXY+ or SMXL5+ nuclei does not change significantly in the *wox4-1* mutant could indicate that *WOX4* function does not go beyond regulation of cambium activity. But it could also be that processes of cell fate decision-making and thus the patterning of the cambium domains is well buffered and the mutation of *WOX4* alone is not sufficient to cause significant changes. To conclude, the *wox4-1* mutant trended to have fewer stem cells compared to wild type, which may explain the reduced cambium activity reported for the mutant (Hirakawa *et al.*, 2010; Suer *et al.*, 2011). But no significant change in the ratio of nuclei belonging to the proximal, central or distal cambium domain was observed applying the chosen analysis method. These results again support the notion, that WOX4 alone does not induce large phenotypic changes.

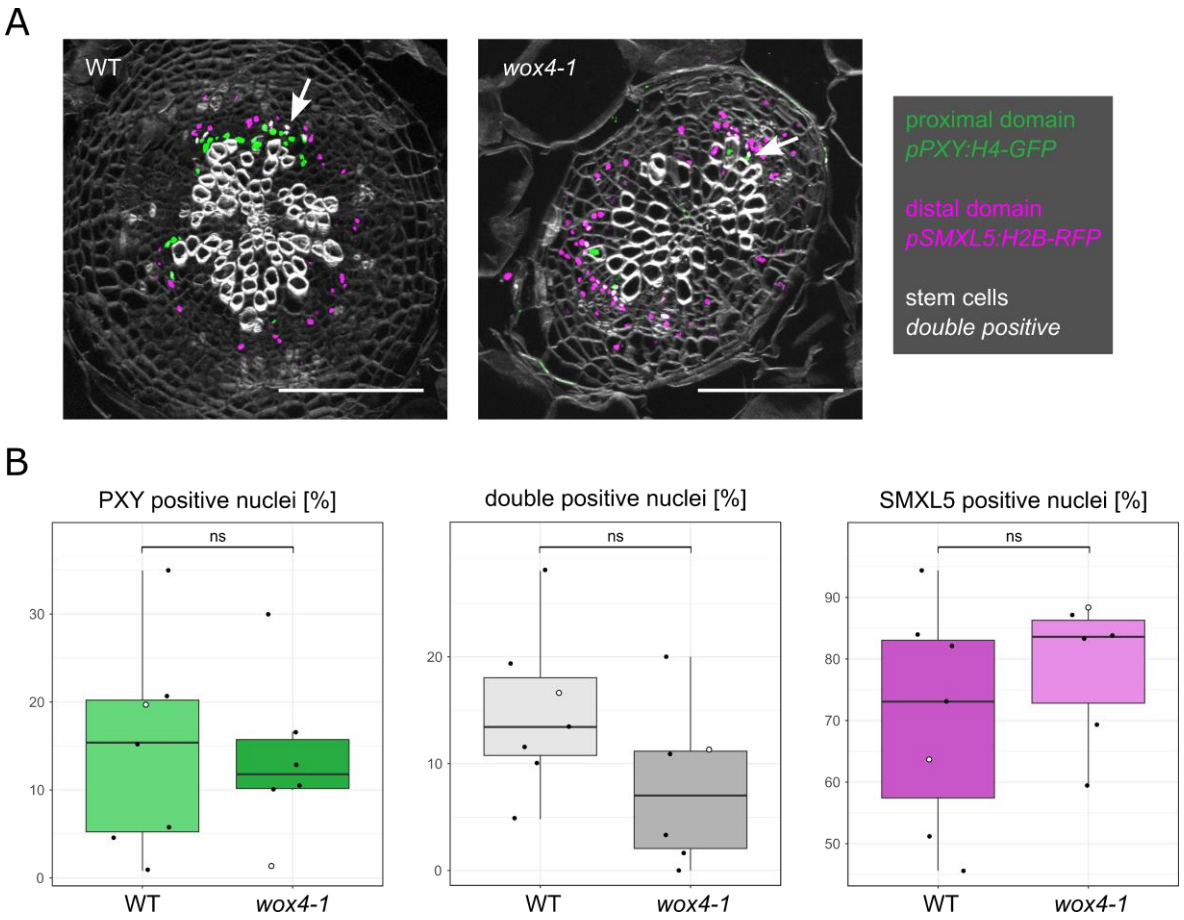


**Figure 16. Analysis of cambium domain pattern in wild type and *wox4-1* mutant hypocotyl cross-sections.**
**A)** Hypocotyl cross-sections of 19-day old wild type or *wox4-1* mutant plants harbouring the *pPXY:H4-GFP* (green, marks proximal cambium domain) and *pSMXL5:H2B-RFP* (magenta, marks distal cambium domain) transgenes. Nuclei which are positive for both the RFP and GFP signals (here depicted in white) make up the central cambium domain, thus marking the CSCs. Sections are stained with Direct Red 23 (grey). Scale bars represent 100 µm. **B)** Quantification of PXY-positive, double-positive or SMXL5-positive nuclei relative to the total amount of nuclei counted in each cross-section in wild type and *wox4-1* background. Significance was tested using Welch's *t*-test (95% CI). Sample size was n=7 for wild type and n=6 for the *wox4-1* mutant.

To better assess whether WOX4 function might influence cell fate decision-making processes, it is necessary to understand which processes are regulated by WOX4 in the first place. Therefore, in a next step I analysed the transcriptional signature of WOX4 in comparison to WUS.

## 4.6 WUS and WOX4 share targets in the auxin and cytokinin pathways

It is known that WUS interacts with the auxin and cytokinin signalling pathways (Leibfried *et al.*, 2005; Gordon *et al.*, 2009; Busch *et al.*, 2010; Ma *et al.*, 2019) and Leibfried *et al*. (2005) revealed that WUS integrates cytokinin response by targeting genes of the cytokinin signalling pathway. Based on RNA-seq and ChIP-seq experiments, Ma *et al*. (2019) identified the downstream targets of WUS. In addition to cytokinin-related genes, the authors found that WUS directly controls genes of the auxin response pathway to maintain a local auxin signalling minimum in the stem cells of the SAM, which is needed to maintain the apical stem cells. During my work, I hypothesized that, like WUS, WOX4 plays a role in integrating auxin and cytokinin signalling in the cambium context. Therefore, I aimed to compare the genes regulated by these two transcription factors. Although WOX4 is an important WOX family member, shown to maintain stem cell proliferation in the cambium (Hirakawa *et al.*, 2010; Suer *et al.*, 2011), the WOX4-dependent transcriptome has not been extensively studied so far.

To compare WUS and WOX4 function in terms of auxin and cytokinin pathway regulation, identified the downstream targets of both TFs using RNA-seq in collaboration with Michael Gebert and Inés Hidalgo Prados (see Contributions chapter). For this, I established a *pUBI10:mCherry-GR-linker-WOX4* line in an otherwise wild type background (here termed *pUBI10:GR-WOX4* line) (done in collaboration with Michael Gebert) following the strategy of the *pUBI10:mCherry-GR-linker-WUS* line (here termed *pUBI10:GR-WUS* line) published in Ma *et al*. (2019). The fusion of the glucocorticoid receptor (GR) to the respective protein allows its translocation from the cytoplasm to the nucleus upon Dexamethasone (Dex) treatment (Lloyd *et al.*, 1994), leading to transcript alterations of downstream targets. First, a *pUBI10:GR-WOX4* line with comparable expression strength to the *pUBI10:GR-WUS* line was identified by investigating the mCherry signal strength (**Figure 17**) (done in collaboration with Michael Gebert and Inés Hidalgo Prados). Using the ubiquitously active *UBI10* promoter allowed for identification of the general transcriptional effects of the WUS and WOX4 proteins, irrespective of their natural site of expression.

To (re-) check the functionality of the *pUBI10:GR-WUS* and *pUBI10:GR-WOX4* line, Dex treatments were performed including wild type and a *pUBI10:GR* line provided by the Jan Lohmann lab as controls. As expected, the mCherry-GR-linker-WUS protein as well as the mCherry-GR control protein were cytoplasmic in mock conditions and translocated to the nucleus upon Dex treatment. Contrarily, the mCherry-GR-linker-WOX4 protein already localized to the nucleus under mock conditions (**Figure 17**). However, phenotypic analyses of this line showed that Dex application still led to a prominent effect on the overall plant phenotype (**Figure 17**). The plants were smaller than under mock conditions, the leaf development was delayed and leaves turned yellowish. Although was not as prominent as in the *pUBI10:GR-WUS*, it nevertheless indicated that Dex application still induced substantial transcriptome changes. To summarize, in a first step, Dex-inducibility of the *pUBI10:GR-WUS* and *pUBI10:GR-WOX4* line was validated.

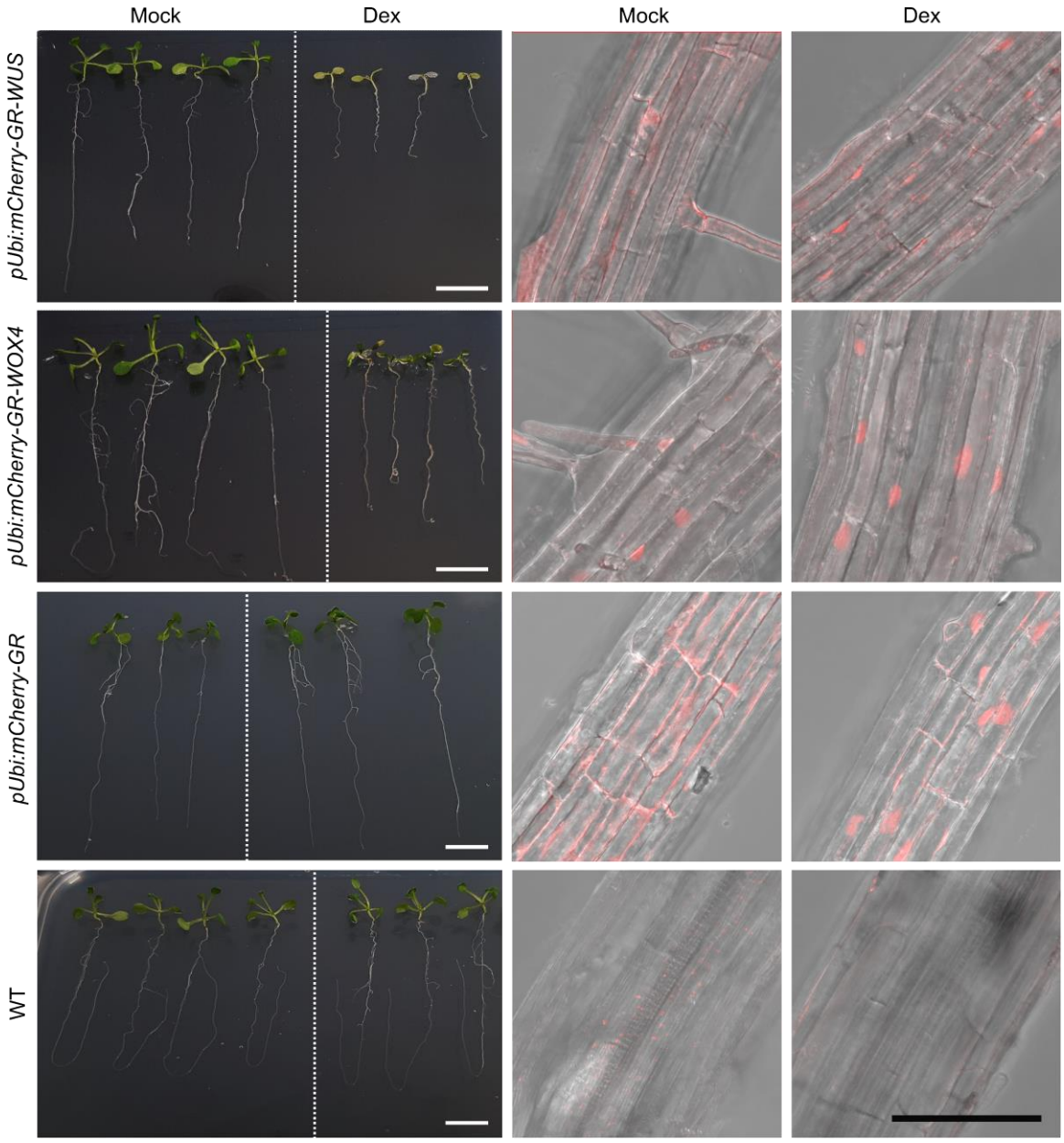


**Figure 17. Characterization of inducible WUS and WOX4 lines.**
Characterization of the lines harbouring the *pUBI10i:mCherry-GR-WUS*, *pUBI10:mCherry-GR-WOX4* or *pUBI10:mCherry-GR* control construct as well as wild type (WT). The plant growth phenotype was analysed using 11-day old plants treated with 10 µM Dex for the last four days (left panels). Localization of the construct was analysed using 7-day old roots after four hours of 10 µM Dex treatment (right panels). mCherry signal is depicted in red. White scale bars represent 1 cm, black scale bar represents 100 µm and are valid for all microscopy images. The data was produced jointly with M.Sc. Inés Hidalgo Prados.

Next, to identify genes targeted by both WUS and WOX4, I performed RNA-seq of all three validated lines together with Inés Hidalgo Prados. By re-including the *pUBI10:GR-WUS* line in this experiment, a faithful comparability of the WUS and WOX4 RNA-seq results was ensured. For the RNA-seq experiment, seedlings were grown on ½ MS plates for seven days and then treated with mock or Dex solution in

liquid culture for four hours. After this period, RNA was extracted and sequenced. The principal component analysis of the obtained RNA-seq datasets showed that the mock- and Dex-treated samples of the *pUBI10:mCherry-GR* control line clustered together (**Figure 18**A). In this cluster also the samples from the mock-treated *pUBI10:GR-WOX4* line were present. But also one Dex-treated sample from the *pUBI10:GR-WOX4* line clustered together with these controls. I concluded that Dex induction failed for this sample. This sample was therefore excluded from further analysis. The cluster of the mock-treated *pUBI10:GR-WUS* line samples was distinct from the described 'control' cluster but a clear difference to the cluster of the Dex-treated *pUBI10:GRWUS* line was visible. By including the *pUBI10:mCherry-GR* control line, genes generally responding to the Dex treatment could be identified by comparing the mock-treated and Dex-treated samples. To identify the differentially expressed genes (DEGs) in the *pUBI10:GR-WUS* line, I removed the Dex-responsive genes identified by analysing the control line from the DEG list of the *pUBI10:GR-WUS* line and then applied a threshold for the p-adjusted value (padj=0.005) as well as a log2 Fold Change threshold (logFC=1). With this approach, I identified in total 3630 WUS-responsive DEGs in the *pUBI10:GR-WUS* line, which represented potential WUS downstream targets. Using the same analysis pipeline, I identified 3303 DEGs as potential WOX4 downstream targets. Out of the WOX4 and WUS DEG lists, 1781 genes were overlapping (48 % and 53 % of the respective target lists) (**Figure 18**B). To conclude, based on these results, WUS and WOX4 share about half of their putative downstream targets when activated irrespectively from their endogenous expression domain. This indicated a possible substantial functional overlap between the two transcription factors.

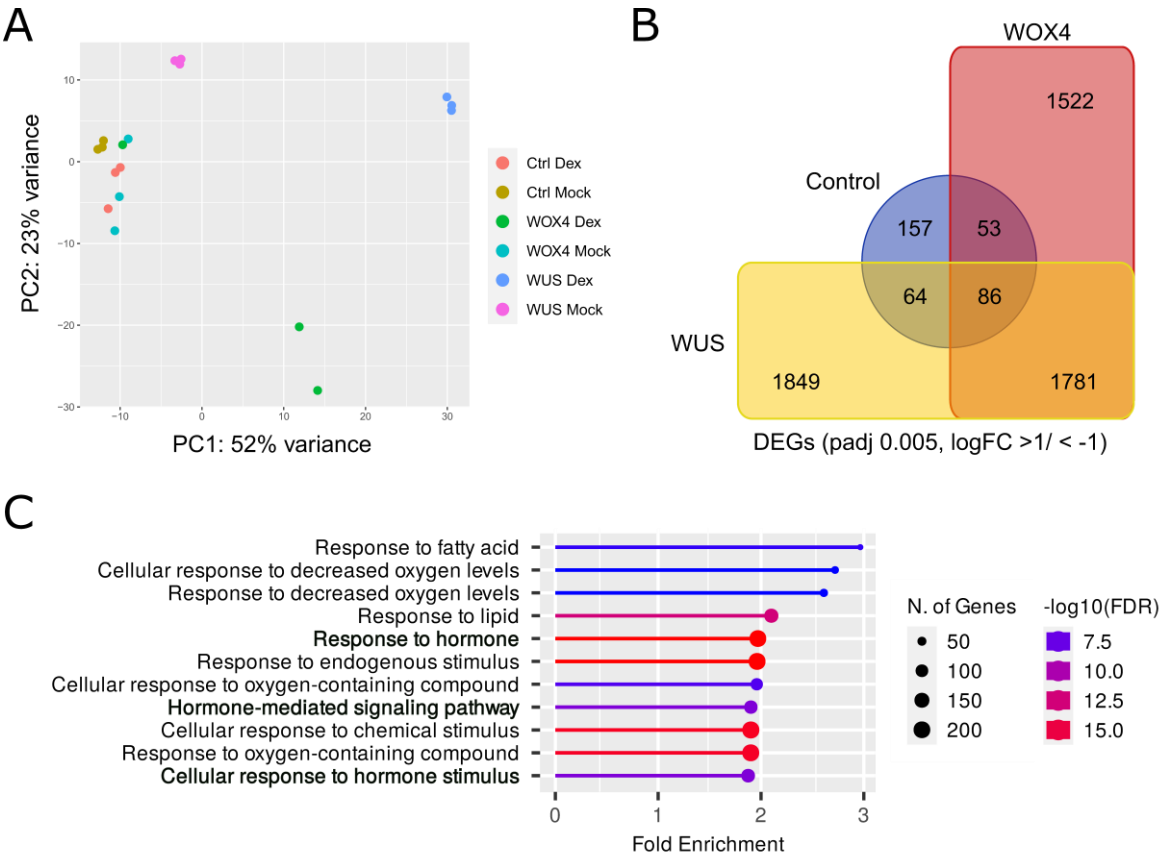


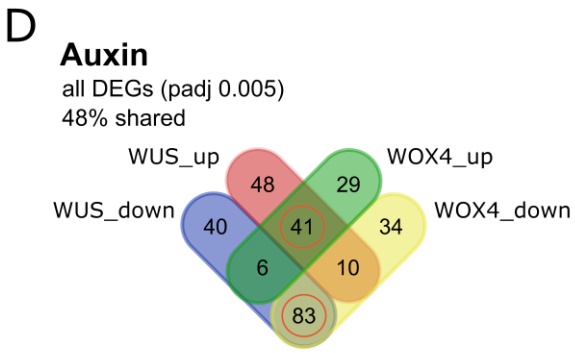


88% of shared targets regulated in same direction

| upregulated | downregulated |
|---|---|
| *YUC9* | *YUC2* |
| *SAUR34* | *YUC3* |
| *SAUR46* | *YUC6* |
| *PIF4* | *YUC8* |
| *PID* | *ARF6* |
| *PILS5* | *IAA4* |
| *PILS6* | *IAA13* |
| *ILR1* | *IAA29* |

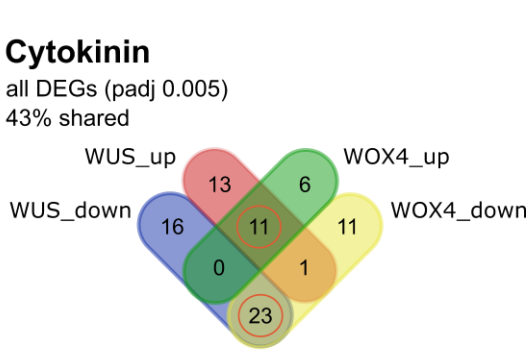


98% of shared targets regulated in same direction

| upregulated | downregulated |
|---|---|
| *ARR2* | *ARR7* |
| *ARR9* | *ARR11* |
| *ARR10* | *KNAT2* |
| *AHP2* | *LOG1* |
| *AHP5* | *LOG8* |
| *WOL1* | *AHP4* |
| *IPT7* | *IPT9* |
| *CKH1* | *IPT5* |

**Figure 18. Comparison of putative WUS and WOX4 downstream targets using a ubiquitous promoter.**
**A)** Principal component analysis of bulk RNA-seq using wild type lines harbouring the inducible constructs *pUBI10:mCherry-GR-WUS*, *pUBI10:mCherry-GR-WOX4* or *pUBI10i:mCherry-GR* (control), respectively. **B)** Venn diagram showing the overlap of DEGs comparing mock and Dex conditions of the respective lines after applying the thresholds for the padj and log2FC values indicated in the panel. **C)** GO term analysis of biological processes of the targets shared by WUS and WOX4. The line length shows the fold enrichment of the respective process. The colour indicates the -log10 of the False Discovery Rate (FDR). The size of the dots represents the number of genes which fall into the respective process. This graph was generated using ShinyGO0.77. **D) and E)** Venn diagrams showing all targets with an associated GO term related to the auxin or cytokinin pathways without applying a log2FC threshold. The Venn diagrams were generated by using the website

https://bioinformatics.psb.ugent.be/webtools/Venn/, then their geometric form was slightly adjusted. The RNA-seq experiment was jointly performed with M.Sc. Inés Hidalgo Prados. All analyses were conducted by myself.

To identify the top biological processes regulated by WUS and WOX4, I visualized the top gene ontology (GO) terms in the list of overlapping target genes using ShinyGO 0.77 (Ge *et al.*, 2020) (**Figure 18**C). Interestingly, GO terms related to hypoxia or reduced oxygen levels showed up prominently. The importance of reactive oxygen species for plant stem cell fate regulation in the SAM in connection with *WUS* was previously reported (Zeng *et al.*, 2017). Additionally, the GO terms 'Response to hormone', 'hormone-mediated signalling pathway' and 'Cellular response to hormone stimulus' were among the top GO terms, which indicated that WOX4 and WUS have the capacity to regulate a high number of genes which fall into these categories. A separate analysis of top GO terms of either WUS or WOX4 target gene lists showed that additional processes were individually upregulated, such as secondary metabolic processes for WUS and defence response for WOX4 (Supplemental Figure 2). To conclude, the GO term analysis revealed that many genes involved in hormone related processes were differentially regulated by WUS and WOX4.

Since in this study I hypothesized that WOX4 might play a similar role to WUS in integrating auxin and cytokinin pathways, I focussed my further analysis on these two pathways. To break down which possible targets of WOX4 and WUS encode components of the auxin or cytokinin pathway, I investigated this specific overlap without filtering for the log2FC to also include weakly regulated genes (**Figure 18**D and E, **Supplemental Table 1** and **Supplemental Table 2**). For this analysis, I furthermore differentiated between up- and downregulated genes. This revealed that 43 % to 48 % of the targets which are connected to the auxin or cytokinin pathway are shared between WUS and WOX4 respectively and that a high number (88 % and 98 %, respectively) of these shared targets are regulated in the same direction by both transcription factors. This suggests that WUS and WOX4 might in parts similarly affect the auxin and cytokinin pathways. In summary, this analysis allowed me to identify putative common WUS and WOX4 target genes which encode components of the auxin and cytokinin pathways or are regulated by these hormones. Importantly, the shared target genes were largely regulated in the same direction by WUS and WOX4.

Since WOX4 targets have not yet been further validated as it is the case for WUS targets (Ma *et al.*, 2019), I rationalized that a more refined analysis of WOX4 targets was required.

## 4.7 Refined identification of WOX4 target genes

First, I used the *pWOX4:ER-YFP* reporter (Suer *et al.*, 2011) to confirm that *WOX4* expression localized to the vascular cambium of the hypocotyl and that its expression domain reached into the xylem area as described before (Shi *et al.*, 2019) (**Figure 19**). Additionally, the *WOX4* promoter was active in the periderm as described previously in the root (Xiao *et al.*, 2020) (**Figure 19**).

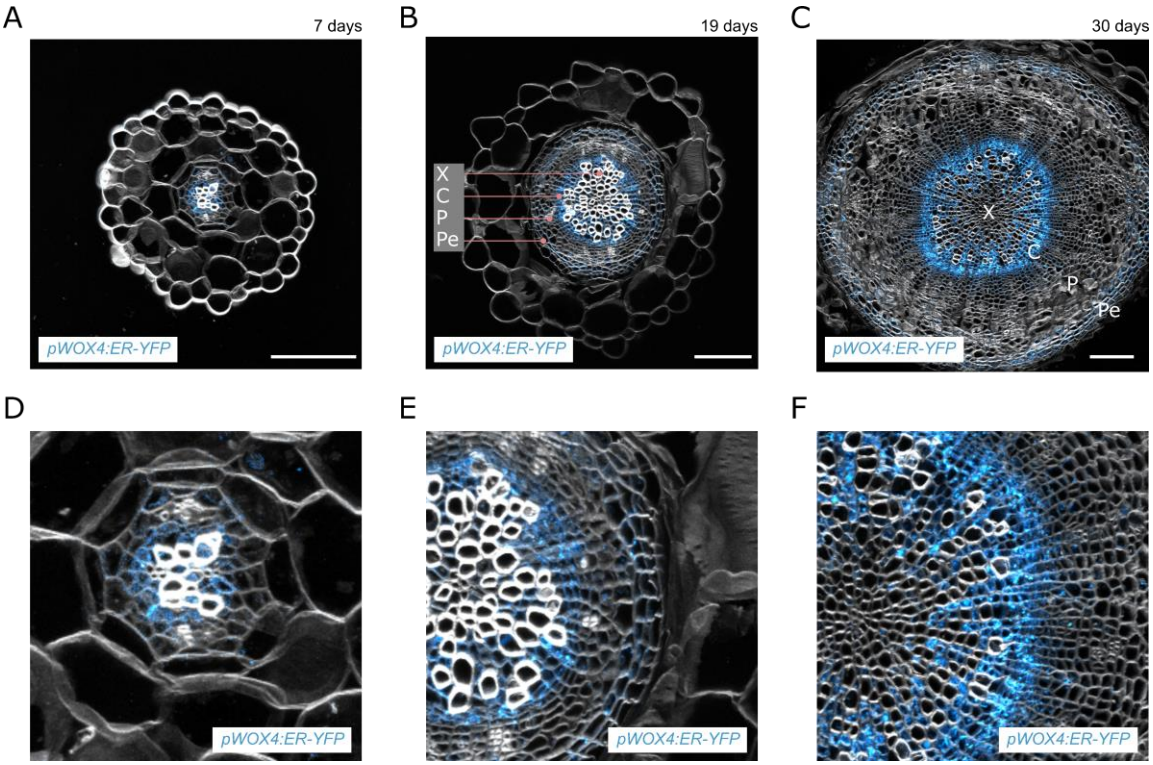


**Figure 19. *WOX4* expression domain visualized by the *pWOX4:ER-YFP* reporter.**
**A) to C)** Hypocotyl cross-sections of 7-day (A), 19-day (B) and 30-day old (C) plants harbouring the *pWOX4:ER-YFP* transgene, whose activity is displayed in blue. This line was described in Suer *et al*. (2011). Sections were stained with Direct Red 23 to visualize cell walls (grey). X = Xylem, C = Cambium, P = Phloem, Pe = Periderm. Scale bars represent 100 µm. Here the progression from primary growth (A) to continuing secondary growth (B and C) becomes visible. **D) to F)** Enlarged images of the sections shown in A to C).

To refine the list of potential WOX4 downstream targets, I again used an inducible WOX4-GR line, but this time expression was driven by the endogenous *WOX4* promoter (*pWOX4:WOX4-GR*) in the *wox4-1* (Hirakawa *et al.*, 2010; Suer *et al.*, 2011) mutant background (here termed *pWOX4:WOX4-GR* line). The *pWOX4:WOX4-GR* line was previously generated in the Greb Lab by Virginie Jouannet. By using the *pWOX4:WOX4-GR* line for an RNA-seq experiment, a more refined identification of gene regulation is possible, due to the usage of the endogenous promoter and the absence of wild type levels of a functional WOX4 protein.

First, to investigate whether the *pWOX4:WOX4-GR* construct was functional, I analysed hypocotyl cross-sections of Dex- and mock-treated 19-day old plants. To see whether WOX4-GR rescued the *wox4-1* defects in a Dex-dependent manner, I quantified the hypocotyl area and vasculature area as well as the xylem vessel and phloem area. To be able to analyse large amounts of hypocotyl sections quickly, I established of a Fiji Macro for semi-automated high-throughput phenotyping with extensive help from Marjorie Guichard (please see Contributions chapter and for details see Methods chapter 3.9.2). Since the *pWOX4:WOX4-GR* line was in the *wox4-1* background I used both wild type and the *wox4-1* mutant as controls. As a first result, I was able to recapitulate the previously reported *wox4-1* mutant phenotype, with a significant reduction in the vasculature area in comparison to wild type despite no significant change in the hypocotyl area (**Figure 20**A, B and F) (Hirakawa *et al.*, 2010). The reduction of the vasculature area was likely caused by a reduction of both the phloem+cambium and xylem vessel area (**Figure 20**C and D). Additionally, I observed a trend of reduced xylem vessel area was significant when normalized to the overall hypocotyl area (**Figure 20**D and E). Surprisingly, in the *pWOX4:WOX4-GR* line Dex treatment did not lead to a significant increase of the production of vascular tissues (**Figure 20**B). The lack of significance was likely caused by the high variability within genotypes and treatments. But importantly, for the xylem vessel area a significant increase was detected in the Dex-treated *pWOX4:WOX4-GR* line compared to mock-treated plants arguing for the functionality of the *pWOX4:WOX4-GR* transgene (**Figure 20**D). Additionally, the analysis could clearly confirm that the *pWOX4:WOX4-GR* construct is not leaky. Taken together, my phenotypic analysis revealed that Dex treatment was able to restore wild type tissue area proportions in the

*pWOX4:WOX4-GR* line indicating that the expressed WOX4-GR protein was functional.

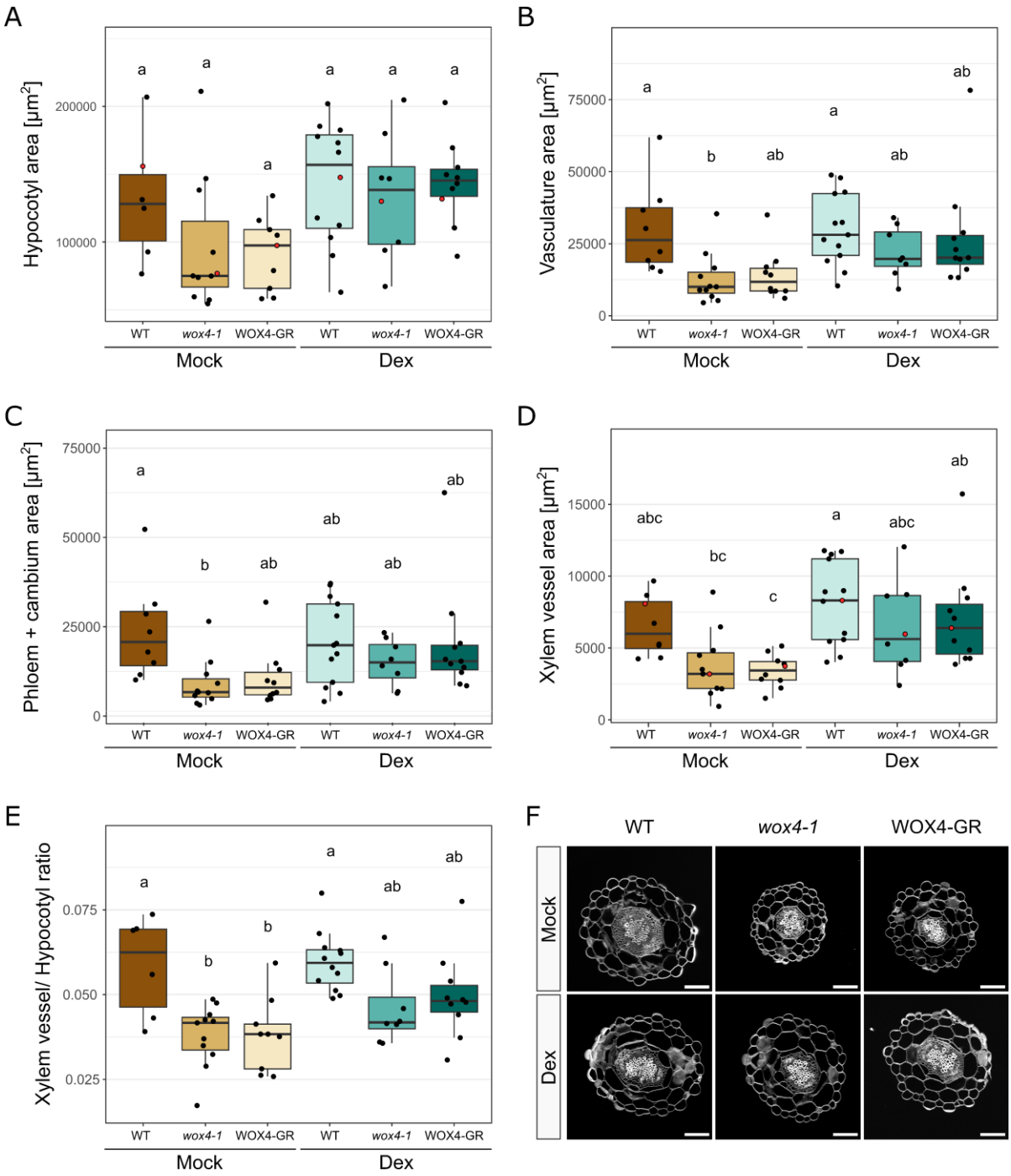


**Figure 20. Phenotyping of the *pWOX4:WOX4-GR* line using hypocotyl cross-sections.** Phenotyping of hypocotyl cross-sections of 19-day old wild type, *wox4-1* and *pWOX4:WOX4-GR* plants (in *wox4-1* background). Plants were treated for the whole growth period with either Dex (20 µM) or mock (ethanol). **A) to E)** Quantification of hypocotyl, vasculature, phloem plus cambium and xylem vessel area. Sample sizes equal to or are larger than n=6 for each genotype-treatment combination. Statistic groups are indicated by letters based on one-way ANOVA followed by a post-hoc Tukey HSD test (95% CI). **F)** Representative hypocotyl cross-sections, which correspond to the datapoints marked in red in panel A) and D). Sections were stained with Direct Red 23 (grey). Scale bars represent 100 µm.

To reveal the WOX4-GR-dependent transcriptome changes induced by Dex treatments, I performed RNA-seq analyses using seven-day old seedlings treated for three hours with either 20 µM Dex or mock solution. The three hour time point was chosen since it was found to be an optimal treatment duration to observe short term gene activity effects in the cambium context (Brackmann *et al.*, 2018). The principal component analysis of the RNA-seq data showed that the individual samples were less distinctly clustered than observed for the RNA-seq data described in chapter 4.6. However, this is to be expected as this time WOX4 was expressed endogenously and not ubiquitously, thus a minor change was induced by the different genotype and different treatment conditions (**Figure 21**A). Although one sample of the *wox4* mock and WOX4-GR Dex condition were distinct from the other replicated, the analysis included all samples. First, I identified the DEGs in the *wox4-1* and *pWOX4:WOX4-GR* line respectively comparing Dex- and mock-treated samples and applying thresholds for the padj value (padj= 0.1) as well as the logFC (logFC = 0.5). These newly identified putative WOX4 targets were to a large extent already identified in the *pUBI10:GR-WOX4* analysis (**Figure 21**B). For the *pWOX4:WOX4-GR* line (**Supplemental Table 3**), the percentage of genes identified in both approaches (around 56 %) is substantial. By subtracting the DEGs found for the *wox4-1* control from the DEG list identified for the *pWOX4:WOX4-GR* line, I identified 219 WOX4-GR specific DEGs, representing the sought refined list of putative WOX4 targets (**Figure 21**B and **Supplemental Table 4**). Out of the 219 DEGs, 99 genes were upregulated, and 120 genes were downregulated (**Figure 21**C). This was in line with my previous conclusion that WOX4 can act as both, a transcriptional activator and repressor. The most enriched pathway in this gene list was the ‘circadian rhythm’ pathway with a 13.3-fold enrichment (identified using ShinyGO0.77). This is very interesting as the circadian clock has been shown to be an important factor in the regulation of vascular cell differentiation (Torii *et al.*, 2022). In the context of this work, though, I focused on the auxin and cytokinin pathways. By filtering for auxin- and cytokinin-related genes, I identified in total 14 auxin and seven cytokinin pathway genes as putative WOX4 targets (**Figure 21**D). In order to get an overview that is as complete as possible, these lists also include genes that appear as DEGs in the *wox4-1* control (marked in red in **Figure 21**D) and therefore must be taken with some caution. *Aux/IAA29*, *ARR7*, *REVEILLE1* (*RVE1)*, *MYB DOMEIN PROTEIN31* (*MYB31)* and *KMD1* are the auxin- or cytokinin- regulated genes that I could already previously identify using the *pUBI10:GR-WOX4* line. To

conclude, by performing RNA-seq upon endogenous WOX4-GR induction, I generated a refined putative WOX4 target gene list consisting of 219 genes, out of which 21 genes encode auxin or cytokinin pathway related or regulated genes. Moreover, the results indicated that WOX4 acts as a transcriptional activator as well as repressor, also within its endogenous domain.

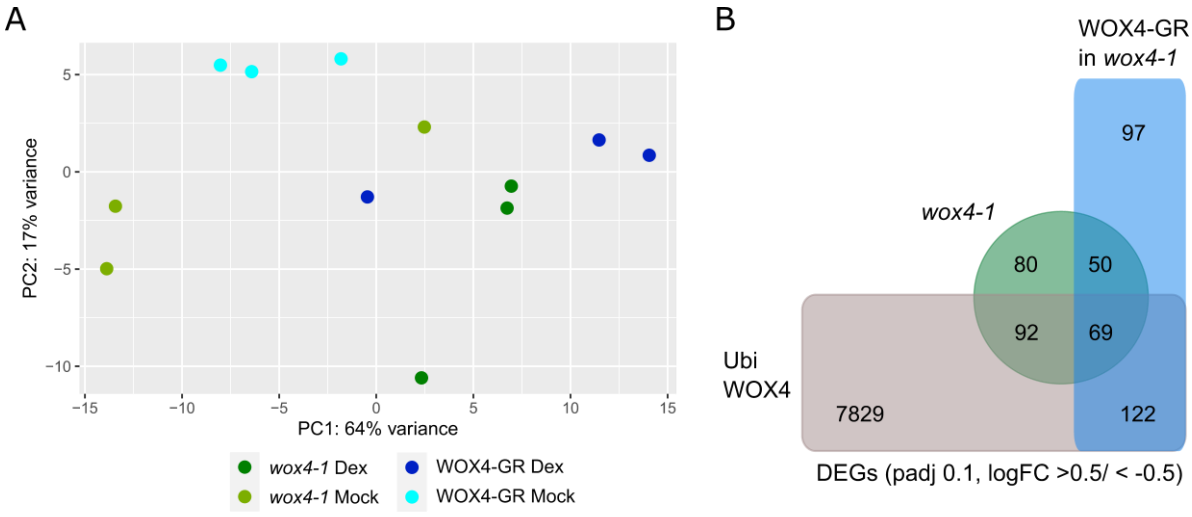


| upregulated | downregulated |
|---|---|
| *HEC1* | *NIT2* |
| ***IAA29*** | ***RVE1*** |
| ***SAUR1*** | *bt5* |
| *SAUR5* | *TCH2* |
| *SAUR7* | *TCH4* |
| *ARGOS* | *AT5G41900* |
| ***MYB31*** | *AT1G19000* |

| upregulated | downregulated |
|---|---|
| *ARR6* | *PUP2* |
| *ARR7* | *PRR9* |
| *HEC1* | ***KMD1*** |
| *SAUR7* | |

**Figure 21. Refined analysis of WOX4 transcriptional signature using the endogenous WOX4 promoter.**
**A)** Principal component analysis of bulk RNA-seq using the *pWOX4:WOX4-GR* line in *wox4-1* background as well as the *wox4-1* mutant as control. **B)** Venn diagram showing the overlap of the DEGs of the respective line as well as the previously identified DEG list of the ubiquitously expressed WOX4 line. The applied thresholds for the padj and log2FC values are indicated. The website https://bioinformatics.psb.ugent.be/webtools/Venn/ was used to generate the Venn plot. **C)** Visualization of the number of up- and downregulated DEGs after subtracting the DEGs of the *wox4-1* line from the WOX4-GR target list. **D)** Full lists of auxin and cytokinin related DEGs which are putative downstream targets of WOX4.

### 4.7.1 Inducible, meristem specific *WOX4* expression in the root

To evaluate the robustness of my results, I took advantage of another recently published WOX4-GR dataset. In her thesis, Eliana Mor used a line expressing WOX4-GR under the control of a meristem-specific promoter (*pRPS5A:WOX4-GR* in wild type background, termed *pRPS5A:WOX4-GR* in this study). She harvested root

tips of five day old plants after one hour, two hours and four hours Dex treatment and conducted RNA-seq to analyse WOX4 downstream regulation in primary growth (Mor, 2020). I was provided with the raw data of this RNA-seq experiment. By re-analysing this dataset applying my RNA-seq analysis pipeline, I was able to compare the *pRPS5A:WOX4-GR* dataset with the *pWOX4:WOX4-GR* RNA-seq dataset. The principal component analysis revealed four distinct clusters for each treatment condition (**Figure 22**A). I focussed on the comparison between the mock treatment and the four-hour time point since my RNA-seq was conducted with seedlings treated for three hours with Dex or mock. In this comparison, I identified in total 941 DEGs as potential WOX4 downstream targets using a less stringent filtering than used for the *pWOX4:WOX4-GR* RNA-seq, i.e. no logFC filtering was applied. This allowed me to get a better impression, which genes of the *pWOX4:WOX4-GR* dataset might be reappearing in this dataset but maybe with a changed logFC value. The padj value has been retained the same to allow for comparison. I found that out of the 338 genes identified in the *pWOX4:WOX4-GR* RNA-seq (which includes also DEGs identified in the *wox4-1* control), 33 genes (around 10 %) were re-identified in the *pRPS5A:WOX4-GR* RNA-seq dataset (see **Supplemental Table 5**). This was less than expected and I speculated that this rather small overlap is caused by either using different promoters or the focus on root tissues versus harvesting whole seedlings. However, similar to my previous observations around half of the DEGs were up- or downregulated, indicating for the third time that WOX4 acts as transcriptional activator as well as repressor (**Figure 22**B). Within the *pRPS5A:WOX4-GR* gene list, I identified 33 auxin regulated and 12 cytokinin regulated genes (**Figure 22**C and **Supplemental Table 6**). Importantly, these lists largely consisted of newly identified targets. But some of the newly identified genes belong to the same family of previously identified genes, e.g., the *Aux/IAA*, *ARR*, *PRR*, *MYB* or *SAUR* gene family. To summarize, the analysis of the *pRPS5A:WOX4-GR* RNA-seq dataset confirmed the action of WOX4 as transcriptional activator and repressor. Furthermore, focussing on the auxin and cytokinin pathway, this analysis strengthened the classification of some previously identified gene families as possibly downstream of WOX4.

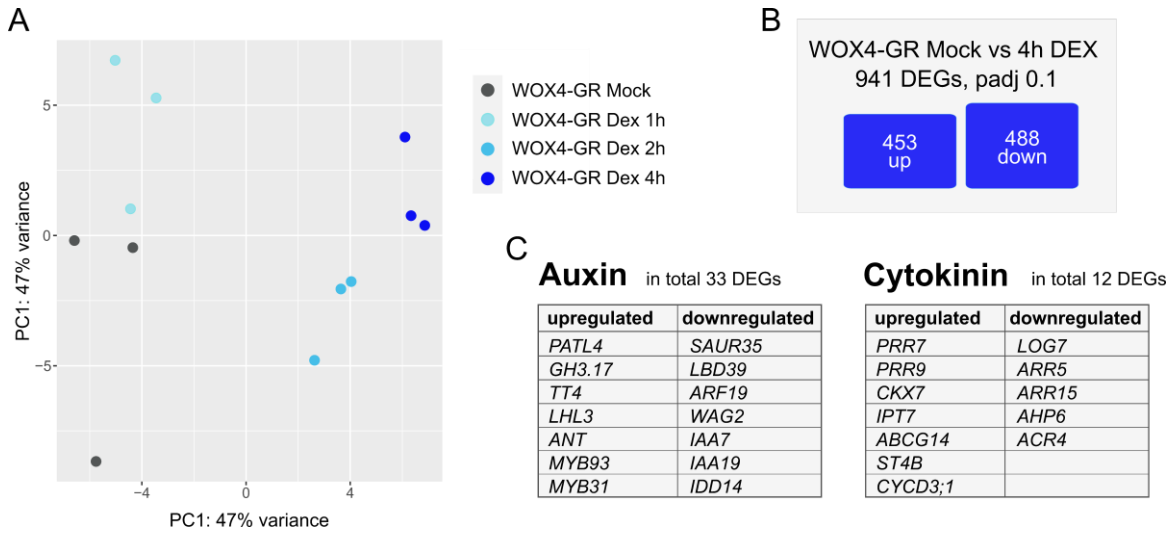


| upregulated | downregulated |
|---|---|
| *PATL4* | *SAUR35* |
| *GH3.17* | *LBD39* |
| *TT4* | *ARF19* |
| *LHL3* | *WAG2* |
| *ANT* | *IAA7* |
| *MYB93* | *IAA19* |
| *MYB31* | *IDD14* |

| upregulated | downregulated |
|---|---|
| *PRR7* | *LOG7* |
| *PRR9* | *ARR5* |
| *CKX7* | *ARR15* |
| *IPT7* | *AHP6* |
| *ABCG14* | *ACR4* |
| *ST4B* | |
| *CYCD3;1* | |

**Figure 22. Re-analysis of WOX4 transcriptional signature in the root using a meristematic promoter.**
**A)** Principal component analysis of bulk RNA-seq of using the *pRPS5A:WOX4-GR* line in wild type background after mock or Dex treatment. **B)** Visualization of the number of up- and downregulated DEGs after applying a padj threshold. **C)** Tables listing a selection of auxin related DEGs and the full list of cytokinin related DEGs which are putative downstream targets of WOX4. The RNA-seq data was produced by Dr. Eliana Mor, the re-analysis was conducted by myself.

## 4.8 Analysing cambium domain-specific gene expression data

So far, I identified putative WOX4 downstream target genes encoding components of the auxin and cytokinin pathways using bulk RNA-seq datasets. But it remained unclear, whether and how these genes are expressed in the cambium area. Dr. Dongbo Shi generated a cambium domain-specific expression dataset of hypocotyl tissue by using a previously published double marker line (Shi *et al.*, 2019). This line contained a *pPXY:H4-GFP* and a *pSMXL5:H2B-RFP* construct marking the proximal and distal domains of the cambium, respectively as described earlier. Nuclei which are double-positive for both fluorescent signals are considered to mark the central cambium domain harbouring the cambium stem cells (Shi *et al.*, 2019). Via Fluorescence Activated Nuclei Sorting followed by RNA-seq analyses, Dr. Dongbo Shi generated a domain-specific expression dataset in which gene expression intensities were mapped to the proximal, central and distal cambium domains, respectively. This unpublished dataset was provided to me by Dr. Dongbo Shi.

First, to investigate WOX4, PXY and SMXL5 expression within the cambium, I analysed the cambium domain-specific expression dataset. This analysis revealed that WOX4 was highly expressed in the central domain of the cambium relative to the other

domains (**Figure 23**). As expected, *SMXL5* was relatively higher expressed in the distal domain in the cambium than in the proximal domain and the opposite was the case for *PXY* expression (**Figure 23** and **Supplemental Table 7**).

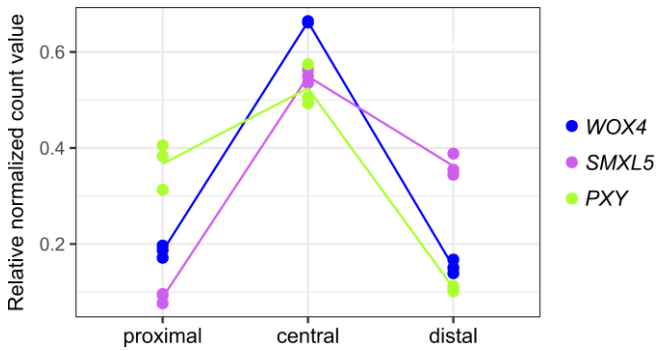


**Figure 23. Relative expression of *WOX4*, *PXY* and *SMXL5* across cambium domains.**
The graph shows the relative normalized count values of *WOX4*, *PXY* and *SXML5* in the proximal, central and distal cambium domains. The relative normalized count values indicate the ratio at which a gene is expressed in a certain domain relative to its expression across all domains. The RNA-seq data and analysis was produced by Dr. Dongbo Shi. The analysis and visualization of *WOX4*, *PXY* and *SMXL5* was conducted by myself.

### 4.8.1 Putative WOX4 target gene expression across cambium domains

To investigate how the auxin and cytokinin pathway related or regulated putative WOX4 targets are expressed in the three cambium domains, I filtered this cambium domain-specific dataset for my genes of interest and visualized their relative expression based on normalized count values using heatmaps (**Figure 24**). By setting a threshold for expression (sum of normalized count value >10) similar to previous studies (Ye *et al.*, 2021), I found that 321 genes out of the 338 genes (= 90 %) identified in the *pWOX4:WOX4-GR* RNA-seq are expressed in the cambium domains (see **Supplemental Table 8**). I visualized a selection of the relative expression of the putative auxin or cytokinin regulated WOX4 targets of the *pWOX4:WOX4-GR* and *pRPS5A:WOX4-GR* RNA-seq separately (**Figure 24**A and B respectively). Most interestingly, members of the same gene family seemed to have distinct expression patterns. For example, *ARR6* and *ARR7* expression was highest in the distal cambium, whereas *ARR15* expression was elevated in the proximal domain. The same was true for members of the *Aux/IAA* and *SAUR* gene families.

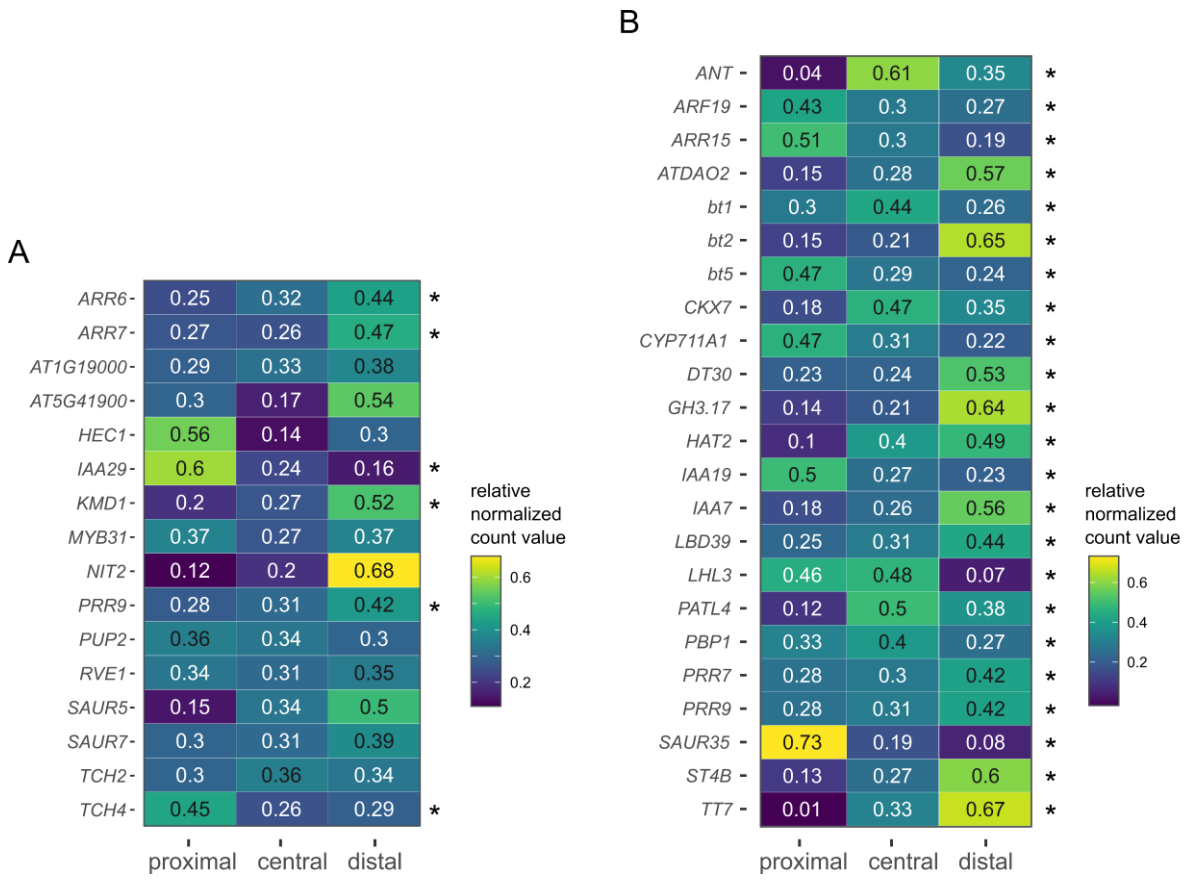


**Figure 24. Relative expression of putative auxin and cytokinin regulated WOX4 targets across cambium domains.**
Heatmaps showing the relative expression of the DEGs identified in the RNA-seq of the *pWOX4:WOX4-GR* line **(A)** as well as a selection of genes identified in the *pRPS5A:WOX4-GR* line **(B)** in the proximal, central and distal cambium domains. The relative normalized count values are shown, which indicate the ratio at which a gene is expressed in a certain domain relative to its expression across all domains. Genes which are significantly differentially expressed across domains (determined using a likelihood ratio test) are marked with an asterisk. For genes which show a high difference across domains but are not marked as significantly differentially expressed, the normalized count values of the biological replicates varied substantially and therefore must be taken with precaution. The RNA-seq data and analysis was produced by Dr. Dongbo Shi. The analysis and visualization of *WOX4* targets was conducted by myself.

I hypothesized that a gene which acts as a xylem or phloem differentiation factor is expressed at higher levels in the proximal or distal domain than in the central domain. Furthermore, this expression difference would need to be significant. To determine whether the difference in the normalized count value is significant across cambium domains, Dr. Dongbo Shi used a likelihood ratio test (LRT) within the DESeq2 package. The LRT is more suitable than the Wald test when comparing three or more levels (here the cambium domains) (Love *et al.*, 2014). Out of the 21 putative WOX4 target genes acting in the auxin or cytokinin pathway identified in the *pWOX4:WOX4-GR* RNA-seq, six genes were significantly differentially expressed across the cambium domains (**Figure 24**A, marked with asterisks). Out of the 45 putative WOX4 target

genes encoding auxin or cytokinin pathway components which were identified in the *pRPS5A:WOX4-GR* RNA-seq, 23 genes were significantly differentially expressed across the cambium domains (**Figure 24**B). By combining these two datasets, in total 29 genes were found to be significantly differentially expressed across the cambium domains. By focussing on significantly differentially expressed genes with an expression peak either in the distal or proximal cambium, I identified 23 genes of high interest. In summary, I found that most of the so far identified putative WOX4 targets are expressed in the cambium area and a large amount of these genes are significantly differentially expressed across the proximal, central and distal cambium domains. Furthermore, I was able to narrow down the candidate genes for potential cytokinin or auxin associated phloem or xylem differentiation factors downstream of WOX4, to a list of 23 genes.

### 4.8.2 Auxin and cytokinin pathway gene expression in cambium domains

To investigate whether the auxin and cytokinin pathways (including biosynthesis, metabolism, signalling and transport) are associated with different cambium domains, I filtered the cambium domain-specific expression dataset for genes encoding components of the auxin and cytokinin pathway and visualized their expression using heatmaps. I identified genes which encode auxin or cytokinin pathway components or genes regulated by these hormones by associating the ‘biological process’ GO terms to all genes of the RNA-seq dataset and then filtering for respective GO terms and manually completing this initial list with genes which were lacking the GO term annotation.

For auxin, out of the 620 genes encoding auxin pathway components or genes regulated by auxin, 192 genes were significantly differentially expressed along the cambium domains and a selection is shown in **Figure 25**. The full list containing the 620 genes is available in **Supplemental Table 9** including the non-relative mean of normalized count values. These genes are involved in the biosynthesis, degradation, signalling or transport of auxin. I could not identify a clear assignment of these processes to a certain cambium domain. Interestingly, among the significantly differentially expressed genes related to the auxin pathway, many belonged to *ARF* or *Aux/IAA* or *PIN* gene families, indicating that auxin signalling and transport might have

to be precisely regulated across the cambium domains, which supports previous findings (Brackmann *et al.*, 2018). In general, only very few genes displayed a peak of expression in the central domain. Among those, strikingly *YUCCA1* was almost solely expressed in the central domain, however at very low levels (Supplemental Table 9). But in contrast to *YUCCA1*, *YUCCA6* expression was highest in the proximal domain at considerably high level. To summarize, the general impression based on this analysis is that the auxin pathways are indeed differentially regulated across cambium domains. However, it appears that the auxin pathway processes are spatially modulated rather than confined to a certain domain.

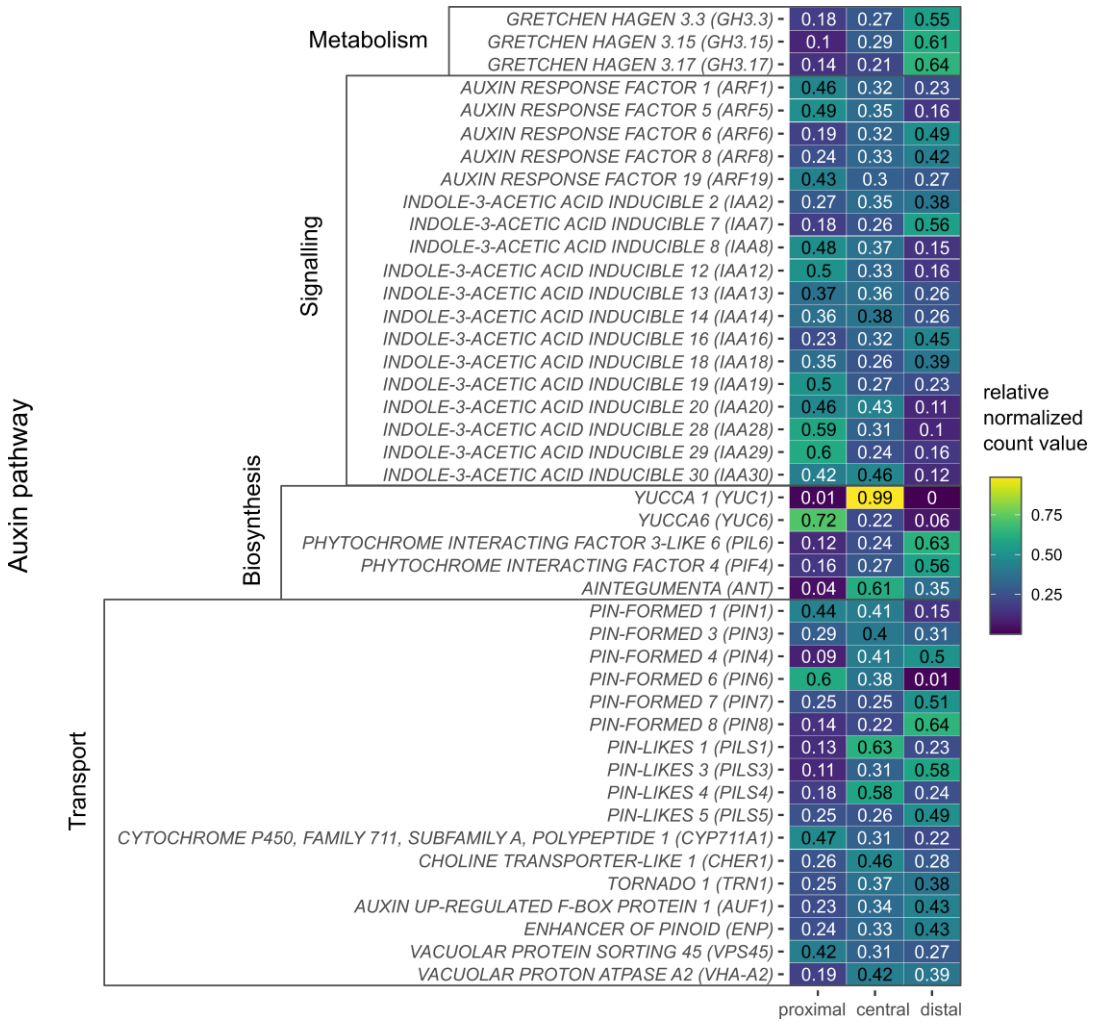


**Figure 25. Auxin pathway genes are differentially expressed across the cambium domains.** Heatmap showing the relative expression of a selection of genes in the auxin pathways that are significantly differentially expressed across cambium domains (determined using a likelihood ratio test). The relative normalized count values are shown, which indicate the ratio at which a gene is expressed in a certain domain relative to its expression across all domains. The RNA-seq data and analysis was produced by Dr. Dongbo Shi. The analysis and visualization of auxin pathway genes was conducted by myself.

Next, I conducted the same investigation for the cytokinin pathway. Here, 54 genes out of 198 genes encoding components of the cytokinin pathway or cytokinin regulated genes were significantly differentially expressed along the cambium domains and a selection is shown in **Figure 26**. Interestingly, *ARR1*, *ARR4*, *ARR5*, *ARR7*, *ARR9*, *AHK4/ WOODEN LEG (WOL)*, *LOG6* and *SMXL7* belonged to the 20 highest cytokinin-related genes in the cambium area (see **Supplemental Table 10** for the full list of genes and non-relative means of the normalized count values). Regarding the cytokinin biosynthetic pathway, it stands out that many members of the *LOG* gene family were identified. These *LOG* genes were higher expressed in the proximal and central cambium domain than in the distal domain. This was in line with analyses in the root where for example *LOG4* was shown to be active along the xylem axis and in the protoxylem associated pericycle (Smet *et al.*, 2019). The *LOG* family members *LOG2*, *LOG5* and *LOG7*, which are not significantly differentially expressed (thus not depicted in Figure 26, but see Supplemental Table 10), are evenly expressed across the domains. Thus, one cannot conclude that cytokinin biosynthesis preferentially happens on the proximal side of the cambium. Furthermore, the non-significantly differentially expressed *IPT* members either have a high variance in their biological replicates or are also evenly expressed across the domains (Supplemental Table 10). The only significantly differentially expressed gene involved in cytokinin transport, *PURINE PERMEASE 18* (*PUP18*), (Gillissen *et al.*, 2000; Bürkle *et al.*, 2003) showed a slightly higher expression in the proximal domain, but other members of the *PUP* gene family, including *PUP14*, were uniformly expressed. Also, expression of genes involved in cytokinin metabolism and signalling could not be assigned to a certain domain. Regarding the genes of the cytokinin signalling pathway, all three cytokinin receptors (*AHK1*, *AHK3* and *WOL*) were differentially expressed but show different domain preferences. The only differentially expressed *Histidine Phosphotransfer protein* gene, *AHP1,* is clearly expressed at higher levels in the distal domain than in the proximal and central domain. The remaining *AHP* members are evenly expressed (*AHP2*, *AHP3*, *AHP5*) (Supplemental Table 10) or varied substantially in their expression values within biological replicates (*AHP6*). Out of 23 members in the *ARR* gene family, seven were significantly differentially expressed across the cambium domains. In addition to *ARR6*, *ARR7* and *ARR15*, which were identified as putative WOX4 targets, the type-A *ARRs ARR3*, *ARR4*, *ARR9* were differentially expressed, preferentially at higher levels in the proximal domain. The remaining type-A *ARRs*

which are not depicted here (*ARR5*, *ARR16*, *ARR17*) were evenly expressed across the domains. For *ARR8* no data were available. The only differentially expressed type-B *ARR, ARR2,* was higher expressed in the central domain and thus was unique compared to the other *ARRs*. The remaining, non-significantly differentially expressed type-B *ARRs* are either high in variance within biological replicates (which holds true for *ARR13*, *ARR19* and *ARR21*) or are also evenly expressed across the domains (*ARR1*, *ARR2*, *ARR10*, *ARR11*, *ARR12*, *ARR14*, *ARR18*, *ARR20*) (Supplemental Table 10). To conclude, according to the expression values of cytokinin related genes, the cytokinin pathway processes are modulated across cambium domains but, based on this analysis cannot be assigned to certain cambium domains.

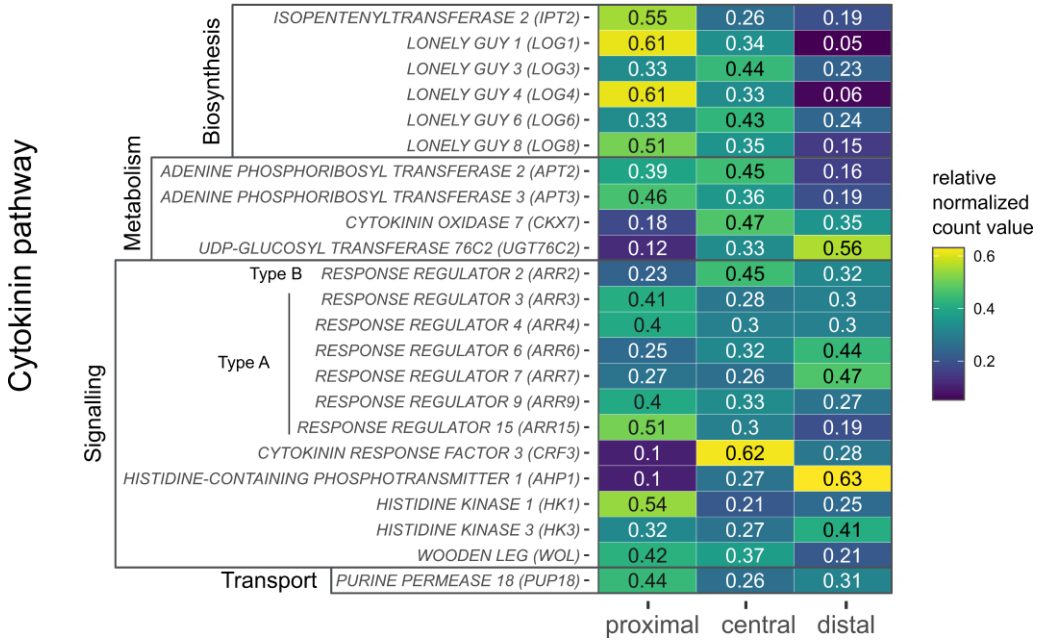


**Figure 26. Cytokinin pathway genes are differentially expressed across the cambium domains.** Heatmap showing the relative expression of a selection of genes in the cytokinin pathways that are significantly differentially expressed across cambium domains (determined using a likelihood ratio test). The relative normalized count values are shown, which indicate the ratio at which a gene is expressed in a certain domain relative to its expression across all domains. The RNA-seq data and analysis was produced by Dr. Dongbo Shi. The analysis and visualization of cytokinin pathway genes was conducted by myself.

With the aim to understand cell fate decision-making processes in the cambium, I focussed only on the cytokinin signalling pathway, as it is less well understood and studied in the context of WOX4 in comparison to the auxin signalling pathway (Suer *et al.*, 2011; Brackmann *et al.*, 2018).

## 4.9 Cytokinin signalling and *WOX4* may be linked through *DOF2.1*

It is known that cytokinin initiates secondary growth in the root (Ye *et al.*, 2021) and that members of the *DNA BINDING WITH ONE FINGER* (*DOF*) transcription factor family act downstream of cytokinin (Brenner *et al.*, 2005; Miyashima *et al.*, 2019; Smet *et al.*, 2019; Qian *et al.*, 2022). Moreover, *DOF* genes are involved in vascular cambium regulation. For example, *HCA2* (*DOF5.6*) controls divisions of the interfascicular cambium (Guo *et al.*, 2009). Interestingly, *DOF2.1* was shown to be important for the cytokinin-dependent proliferation of procambial cells (Smet *et al.*, 2019). The authors of the study generated a *pRPS5A:DOF2.1-GR* line to investigate whether *DOF2.1* was sufficient to induce divisions in the vasculature of the root meristem. Indeed only six hours after induction, *DOF2.1* induced radial divisions in the root meristem vasculature (Smet *et al.*, 2019). In her thesis, Eliana Mor investigated how *DOF2.1* could mediate this regulation (Mor, 2020). For this, Eliana Mor identified downstream targets of *DOF2.1* using the *pRPS5A:DOF2.1-GR* line focussing on root tissues. Surprisingly, her data suggested that *WOX4* functions downstream of *DOF2.1* in the root (Mor, 2020). So far, I found that cytokinin signalling levels might be dampened by WOX4. This observation raised the question whether *WOX4* itself could be regulated by cytokinin signalling.

To investigate whether DOF2.1 also plays a role in linking cytokinin signalling to WOX4 action in the context of the hypocotyl cambium, I analysed the localization of the DOF2.1 protein and investigated the cambium domain-specific expression dataset. First, I analysed 19-day and 30-day old hypocotyl cross-sections of the *pDOF2.1:DOF2.1-YFP* reporter line published in Smet *et al*. (2019). I observed that the DOF2.1 protein localized to nuclei in epidermal, cortical and vascular tissues (**Figure 27**A). Within vascular tissue types, the DOF2.1 protein was found in both xylem and phloem tissues as well as in the cambium and the periderm. To investigate *DOF2.1* expression in more detail within the cambium area, I examined the previously described cambium domain-specific RNA-seq dataset generated by Dr. Shi. I found that of the 37 putative members of the *DOF* TF family (Yanagisawa, 2002), 13 genes (about 35 %) were significantly differentially expressed across the cambium domains (**Figure 27**B). It is important to note that some genes in the dataset do not appear to be significantly differentially expressed since the biological replicates were very variable. These genes are marked in red in Supplemental Figure 3. Regarding the

genes identified as significantly differentially expressed, it is striking that *DOF2.1* was the *DOF* with the highest relative expression value in the central domain, the domain where *WOX4* also peaks (**Figure 27**B and **Figure 19**C). To conclude, I found that DOF2.1 protein was present in the cambium of 19-day and 30-day old plants and that relative *DOF2.1* expression was highest in the central cambium domain. These were two indications that DOF2.1, as previously demonstrated for primary growth in the root tissue (Smet *et al.*, 2019; Mor, 2020), plays a role in cambium regulation and links the cytokinin signalling pathway to WOX4. Interestingly, the data of the *pUBI10:GR-WOX4* RNA-seq furthermore suggest that WOX4 might target *DOF2.1* in a feedback loop.

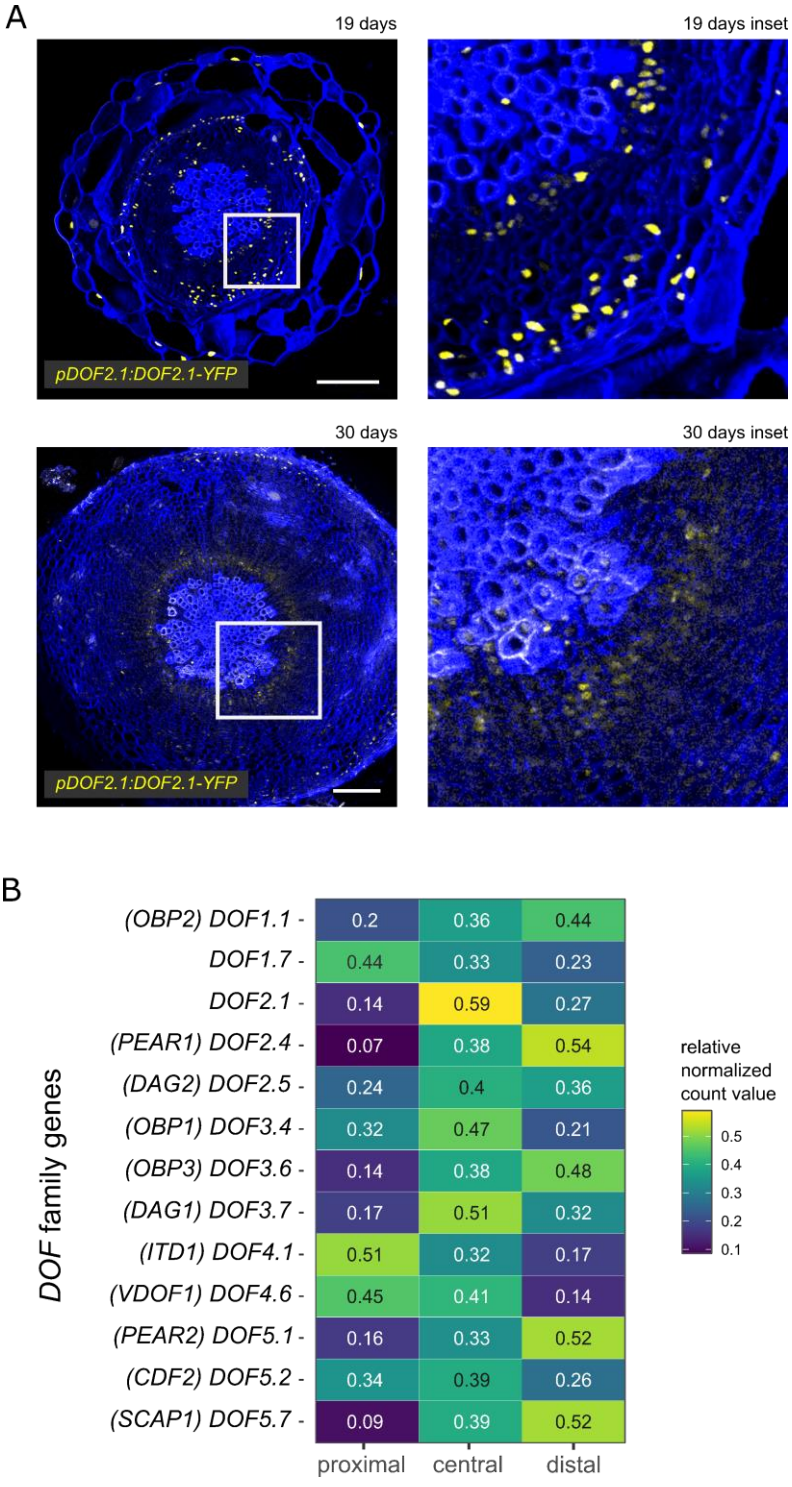


**Figure 27. DOF2.1 protein localized to the cambium and the DOF2.1 gene was preferentially expressed in the central cambium domain.**
**A)** Hypocotyl cross-sections of 19-day and 30-day old plants harbouring the *pDOF2.1:DOF2.1-YFP* transgene. This line was described in Smet *et al*. (2019). DOF2.1 protein localization is displayed in yellow. Signal which is not nuclear localized represents background signal. Sections were stained with Calcofluor white in Clear See (blue). Scale bars represent 100 µm. Enlarged areas of the sections are shown. **B)** Heatmap showing the relative expression of significantly differentially expressed *DOF* family members across cambium domains (determined using a likelihood ratio test). The relative normalized count values are shown, which indicate the ratio at which a gene is expressed in a certain domain relative to its expression across all domains. The RNA-seq data and analysis was produced by Dr. Dongbo Shi. The analysis and visualization of *DOF* genes was conducted by myself.

To further evaluate the action of cytokinin signalling in cambium regulation downstream of WOX4, I looked for genes which were shown to be regulated by WUS as this would enable to compare the stem cell regulatory processes of apical and lateral meristems. I found type-A *ARRs* as putative targets in all three RNA-seq datasets and *ARR5*, *ARR6*, *ARR7* and *ARR15* are known to be directly regulated by WUS (Leibfried *et al.*, 2005). Moreover, the *ARR* gene family members, specifically type-A *ARRs*, were largely differentially expressed across the cambium domains. Thus, I chose to investigate the type-A *ARR* genes *ARR5*, *ARR6*, *ARR7* and *ARR15* in more detail in the cambium.

## 4.10 Type-A *ARRs* are expressed at low levels specifically in the hypocotyl cambium

To further examine type-A A*RRs*, I investigated the expression pattern of *ARR5*, *ARR6*, *ARR7* and *ARR15* in the hypocotyl of 19-day and 30-day old plants. For this, I was provided with the *pARR5:n3YFP*, *pARR6:n3YFP* and *pARR15:n3YFP* lines generated by Brecht Wybouw (unpublished, provided by Bert de Rybel). Additionally, I generated a *pARR7:ER-mTurquoise-HDEL* line. I found that all four investigated reporters were active in all vascular tissue types throughout development (**Figure 28**). 19-day old plants of the *ARR5*, *ARR6* and *ARR15* reporter lines also showed expression in the cortex and epidermis. Notably, some nuclei in the cambium area showed lower signal intensities than nuclei of cells in xylem and phloem tissues (**Figure 28**A, B and D), but, at this growth stage, no general trend of expression intensities for tissue types could be observed. Interestingly, in 30-day old plants, where the cambium area is broader, the reduced expression in the cambium area became more evident (**Figure 28**E to H). Although fluorescence intensities varied within the xylem and phloem tissues, the cambium area was still clearly distinguishable due to the general lower signal intensities of the reporters. Importantly, the activity patterns of the nuclear localized *pARR5*, *pARR6* and *pARR15* reporters were reminiscent to the activity pattern of the *pTCSv2* reporter (see chapter 4.2). Since *pARR* reporters are also used to report cytokinin signalling levels (Bishopp *et al.*, 2011b), this supported the finding of low cytokinin signalling in the cambium area.

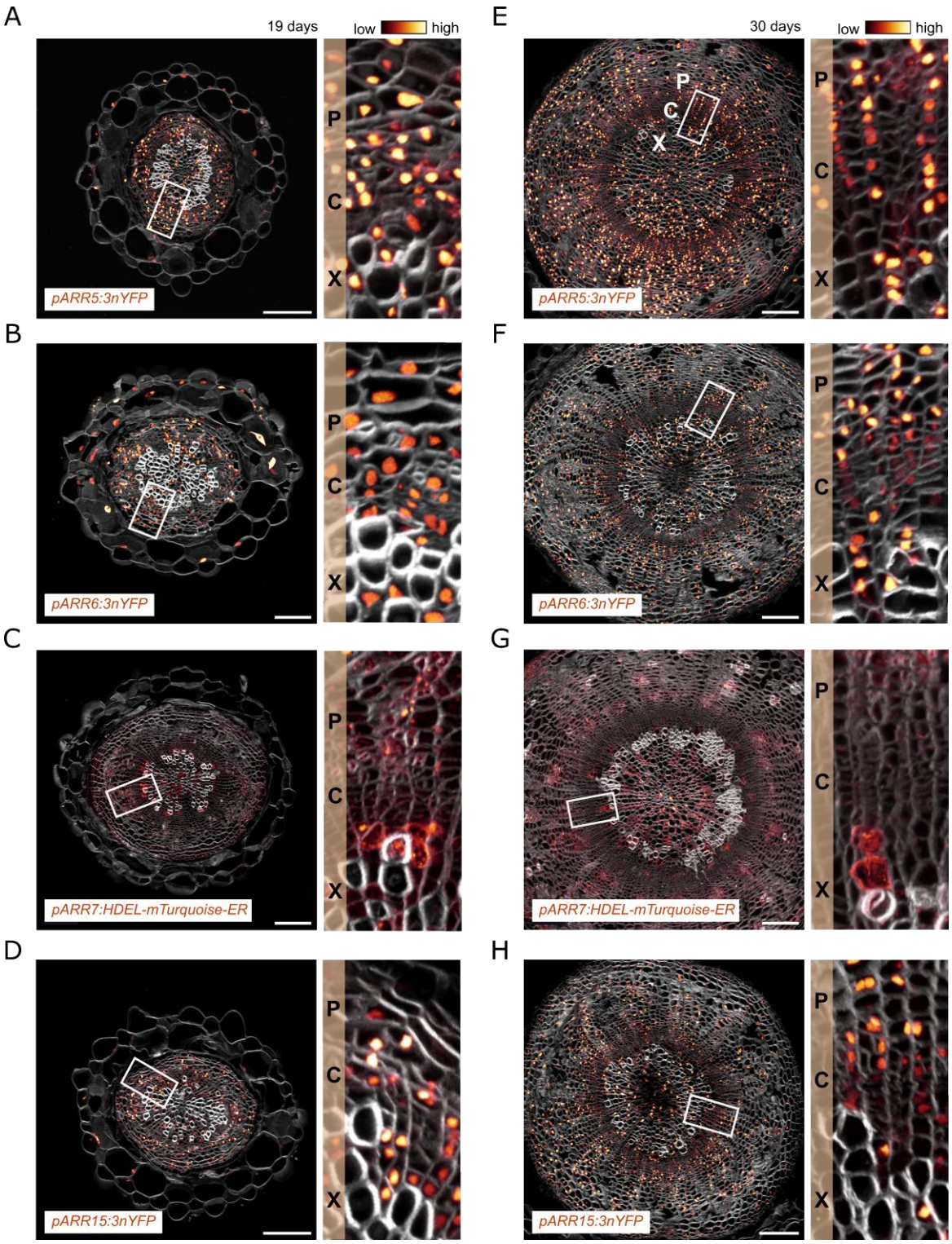


**Figure 28. Type-A *ARR* reporters show low expression in the cambium area.**
Hypocotyl cross-sections of plants harbouring the *pARR5:3nYFP*, *pARR6:3nYFP*, *pARR7:HDEL-mTurquoise-ER* and *pARR15:3nYFP* transgene, whose activity is displayed with the Leica glow lookup table, indicating fluorescence intensities (dark red represents low intensity, light yellow represents high intensity). Sections were stained with Direct Red 23 to visualize cell walls (grey). X = Xylem, C = Cambium, P = Phloem. Scale bars represent 100 µm. The white rectangles indicate the areas that are enlarged in the right image of each panel. **A) to D)** Hypocotyl cross-sections of 19-day old plants. **E) to H)** Hypocotyl cross-sections of 30-day old plants.

Also, in the generated *ARR7* reporter activity was more pronounced in the xylem and phloem area than in the cambium area. (**Figure 28**C and G). Although this pattern was true for all cross-sections investigated, signal intensities were fluctuating among individual samples. In some cross-sections of the *ARR7* reporter, I observed relatively high expression specifically in cells that I identified to be developing xylem vessel cells (**Figure 28**C and G, marked by arrows). Taken together, the analysis of hypocotyl cross-sections of the *ARR5*, *ARR6*, *ARR7* and *ARR15* reporters, indicated that these *ARRs* were expressed at low levels in the cambium area. This could indicate a possible role of these *ARRs* in cambium regulation, where their low expression might be necessary to maintain normal cambium function.

## 4.11 Analysis of *ARR* expression levels upon WOX4 activity changes

To directly study whether type-A *ARRs* are downstream of WOX4, I investigated their expression level when WOX4 activity was altered.

### 4.11.1 *ARR* expression levels might increase in the *wox4-1* mutant

First, to find support for the conclusion that WOX4 acts on type-A *ARR* expression, I investigated their expression level in the *wox4-1* mutant background. As described above, I found that in wild type *ARR5*, *ARR6*, *ARR7* and *ARR15* were expressed throughout the vasculature, but expression was low in the cambium area. This was best visible in 30-day old plants and therefore, I focussed on analysing plants at this growth stage. I introgressed the *pARR6:3nYFP* and *pARR15:3nYFP* markers into the *wox4-1* mutant and identified F3 lines homozygous for the mutation as well as the transgenes. Identification of differences in fluorescence intensities by eye was difficult although an intensity look-up table was used, thus quantification was needed. Due to the nuclear localization of the signal, I did not create radial profiles of the fluorescence intensity of the respective reporter lines but quantified the fluorescence intensity of nuclei (as mean grey value) located in the xylem, cambium or phloem area (for details, see methods chapter 3.9.4). By quantifying the mean grey values of individual nuclei, I observed that the fluorescence intensity of the *pARR6:3nYFP*-tagged nuclei was higher in the *wox4-1* mutants compared to wild type in the xylem, cambium and phloem area (**Figure 29**A, C and E). For the *pARR15:3nYFP* reporter I observed a similar trend of increased fluorescence intensity in the *wox4-1* mutants compared to wild type for

the xylem and cambium area, but no intensity change was detected in the phloem area. (**Figure 29**B, D and E). To summarize, these results were a first hint towards a possible function of WOX4 as a repressor of *ARR6* and *ARR15*, similar to the function reported for WUS (Leibfried *et al.*, 2005).

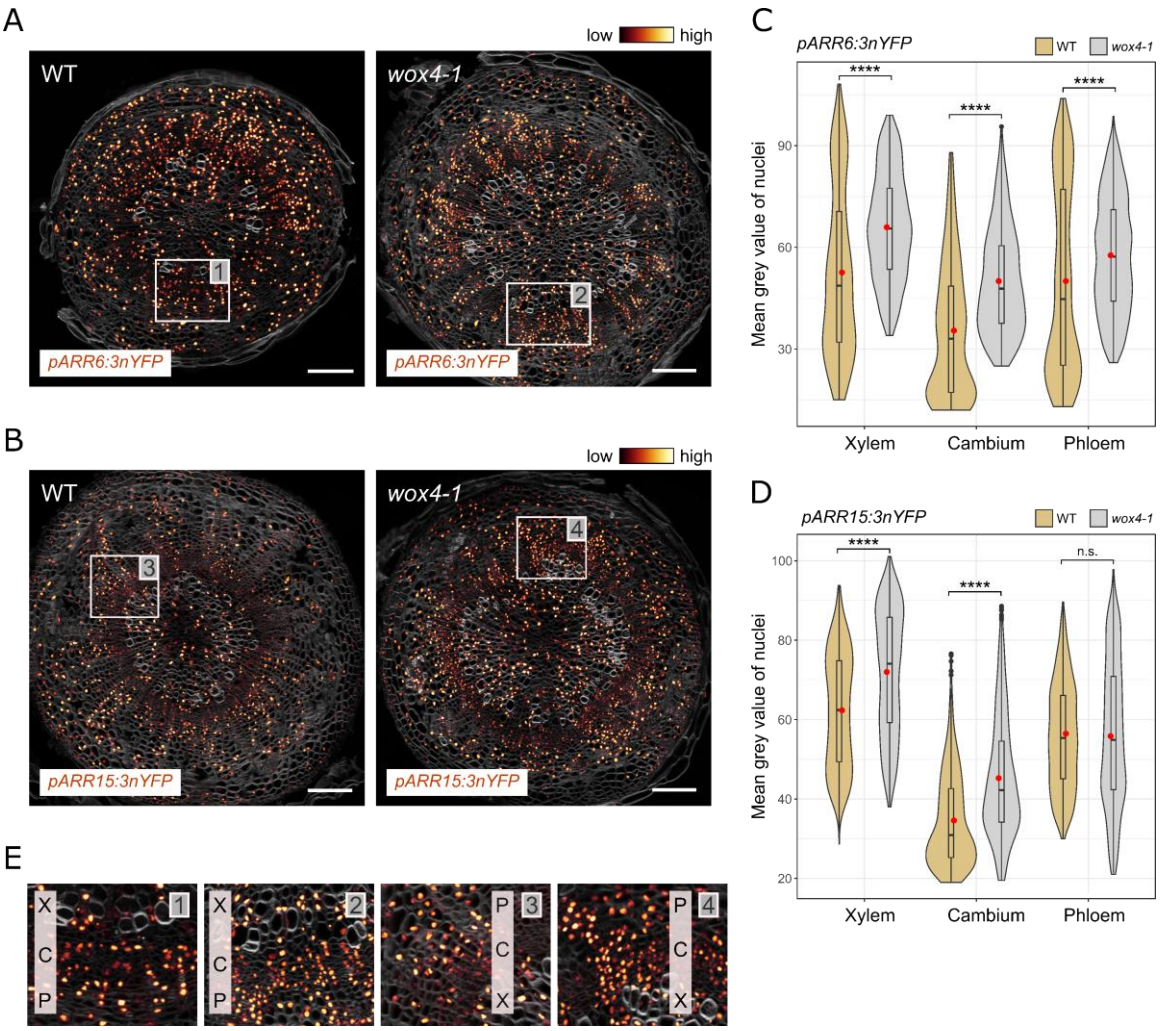


**Figure 29. Comparison of type-A *ARR* expression in wild type and *wox4-1* mutant background reveals increased *ARR* expression in the absence of functional WOX4.**
**A) and B)** Hypocotyl cross-sections of 30-day old plants harbouring the *pARR6:3nYFP* or *pARR15:3nYFP* transgene in either wild type or *wox4-1* mutant background. The fluorescence of the reporters is displayed with the Leica glow lookup table, visualizing fluorescence intensities (dark red represents low intensity, light yellow represents high intensity). Sections were stained with Direct Red 23 to visualize cell walls (grey). Scale bars represent 100 µm. **C) and D)** Quantification of fluorescent signal intensities of nuclei respective to their location in the xylem, cambium or phloem area. Significant differences were identified using Welch's *t*-test (95% CI), ****p<0.0001. The violin plots graphically indicate the distribution of datapoints and additionally the boxplots show the medians (centre lines of boxes). The red dots indicate the mean. For panel C) the fluorescence intensity of nuclei was measured from three biological replicates for wild type and four biological replicates for *wox4-1*. For panel D) the fluorescence intensity of nuclei was measured from three biological replicates for wild type and five biological replicates for *wox4-1*. **E)** Enlarged areas of sections indicated in A) and B). X = Xylem, C = Cambium, P = Phloem.

The presented observations must be taken with caution, though, due to the rather small number of biological replicates and the lack of independent repetitions of the experiment. Nevertheless, as both investigated type-A *ARRs* can be taken as a proxy for cytokinin signalling activity levels, the observations of the *ARR6* and *ARR15* reporters corroborate each other in the xylem and cambium area, where *WOX4* is expressed. Furthermore, these observations are consistent with the finding of increased *pTCSv2* reporter activity in the xylem and cambium area of *wox4-1* mutants described earlier (see chapter 4.4). Regarding the increase in *pARR6:3nYFP* fluorescence intensity levels in the phloem in the *wox4-1* background (**Figure 29**C), one could speculate that *ARR6* expression levels are sensed and buffered throughout the vasculature and therefore upon expression level increase in the xylem and cambium area, the expression levels in the phloem are adjusted to restore the radial pattern with the overall expression minimum in the cambium area. To summarize, based on my analysis, it appears that WOX4 negatively regulates *ARR6* and *ARR15* expression since their expression levels were elevated in the *wox4-1* mutant background.

### 4.11.2 *ARR* expression levels might respond to WOX4 activation in different time frames

To further investigate the possible regulation of *ARR6* and *ARR15* by WOX4, I used the *pWOX4:WOX4-GR* transgene in the *wox4-1* background, by which it is possible to induce WOX4 activity through Dex treatment. For this, I introgressed the *pARR6:3nYFP* and the *pARR15:3nYFP* transgenes into the *pWOX4:WOX4-GR* background, respectively. I identified F3 lines which were homozygous for the *wox4-1* mutation as well as for the *ARR* reporters and the *pWOX4:WOX4-GR* transgene, respectively. Since the functionality of the *pWOX4:WOX4-GR* line was established in 19-day old plants, I analysed plants at this growth stage. I treated plants with 10 µM Dex for six hours or 24 hours to see if there were any buffering effects after 24 hours of treatment. Since *WOX4-GR* expression was driven by the endogenous *WOX4* promoter, I estimated the *WOX4* expression domain based on the *pWOX4:YFP* reporter activity shown above (Figure 19B) and analysed the nuclei located in this domain. To rule out the possibility that the inclusion of the xylem area masks possible effects in the cambium area, I also specifically analysed only the nuclei in the cambium area (for details on the analysis method, see methods chapter 3.9.4). When

investigating the fluorescence intensities of *pARR6:3nYFP*-tagged nuclei, I found that there was no significant difference between Dex- and mock-treated plants after six hours of treatment in both areas analysed (**Figure 30**A). If buffering was happening, I expected the 24-hour timepoint to also show so significant changes. But strikingly, after 24 hours of Dex treatment, the fluorescence intensity of *pARR6:3nYFP*-tagged nuclei was significantly reduced in the Dex-treated plants in both, the *WOX4* expression area and the cambium area alone (**Figure 30**B and C). Taken together, *ARR6* expression levels were dampened 24 hours after Dex-induced WOX4 activation.

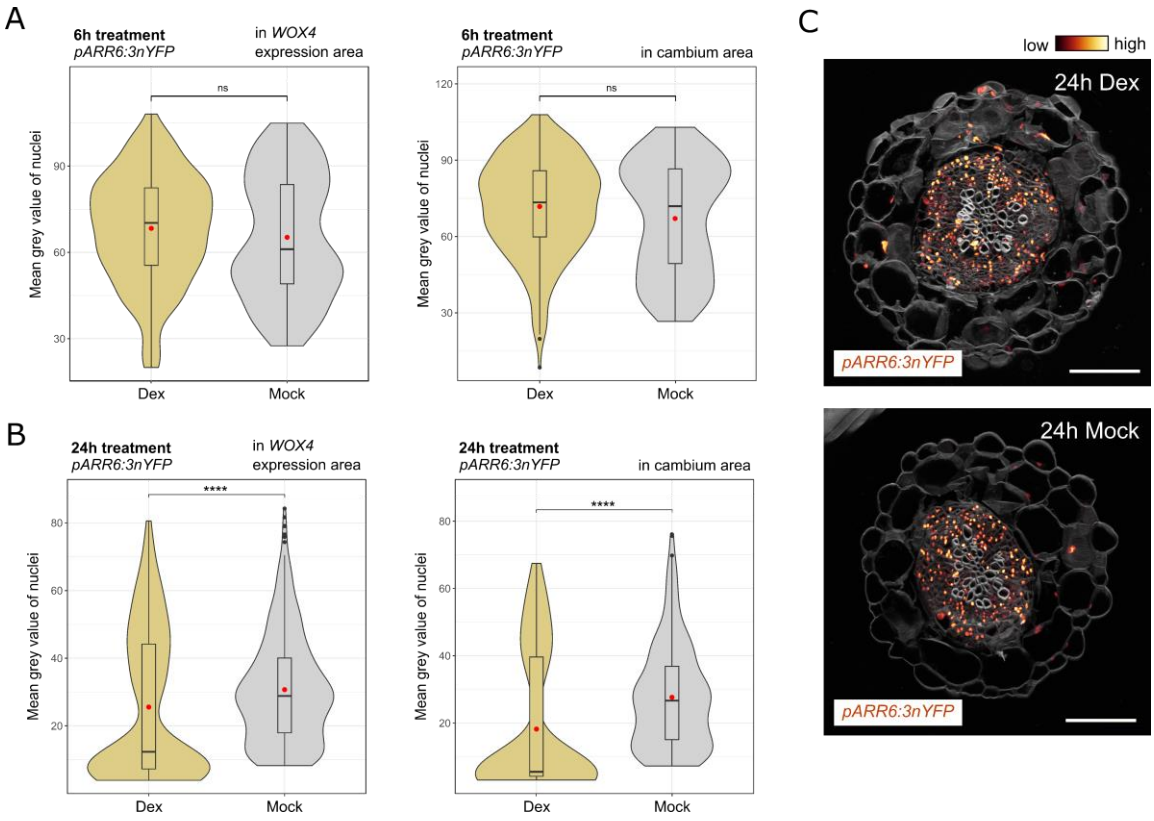


**Figure 30. Analysis of *ARR6* expression in *pWOX4:WOX4-GR* plants in *wox4-1* mutant background.**
**A) and B)** Quantification of fluorescent signal intensities of nuclei in hypocotyl cross-sections of Dex- or mock-treated 19-day plants harbouring the *pARR6:3nYFP* and the *pWOX4:WOX4-GR* transgene in *wox4-1* mutant background. The violin plots graphically indicate the distribution of datapoints and additionally the boxplots show the medians (centre lines of boxes). The red dots indicate the mean. Plants were treated for either six hours (A) or 24 hours (B) with 10 µM Dex or mock. Either all nuclei located in the estimated *WOX4* expression domain (xylem and cambium area, see Figure 19B), or only the nuclei located in the estimated cambium area were quantified. For A) biological replicates were n=5 for Dex- and n=3 for mock-treated plants. For B) biological replicates were n=4 for Dex- and n=4 for mock-treated plants. Significant differences were identified using Welch's *t*-test (95% CI), ****p<0.0001. **C)** Exemplary hypocotyl cross-sections of 19-day old plants harbouring the *pARR6:3nYFP* and the *pWOX4:WOX4-GR* transgene in *wox4-1* mutant background. Plants displayed here were treated with 10 µM Dex or mock for 24 hours. The fluorescence of the reporters is displayed with the Leica glow lookup table, visualizing fluorescence intensities (dark red represents low intensity, light yellow represents high intensity). Sections were stained with Direct Red 23 to visualize cell walls (grey). Scale bars represent 100 µm.

I conducted the same analysis for *pARR15:3nYFP*-tagged nuclei. I found that in this case the fluorescence intensity of the nuclei in both, the *WOX4* expression area and the cambium area alone, was already significantly reduced after six hours of Dex treatment compared to mock-treated plants, indicating a repression of *ARR15* expression through WOX4 (**Figure 31**A and B). However, this effect was not observable any more after 24 hours of treatment (**Figure 31**C). Taken together, although the described findings should be confirmed by adding more biological replicates, it is interesting to conclude that there were different time frames in which WOX4 regulates the expression of different *ARR* genes. In both cases, restoration of WOX4 activity caused a reduction of the fluorescence intensity of *pARR6:3nYFP* and *pARR15:3nYFP* tagged nuclei in the *WOX4* expression area and the cambium area alone. These results were the second indication that WOX4 negatively regulates the expression of *ARR6* and *ARR15* in the hypocotyl.

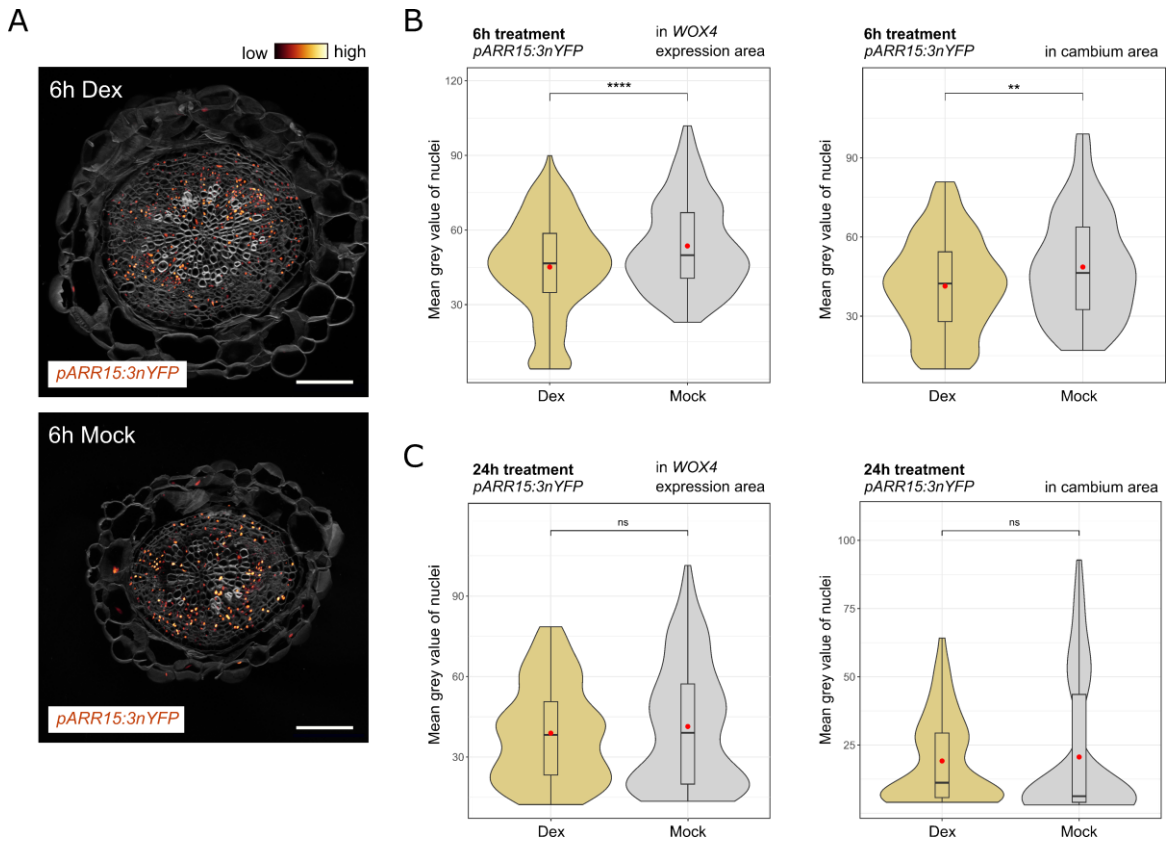


**Figure 31. Analysis of *ARR15* expression in *pWOX4:WOX4-GR* plants in *wox4-1* mutant background.**
**A)** Exemplary hypocotyl cross-sections of 19-day old plants harbouring the *pARR15:3nYFP* and the *pWOX4:WOX4-GR* transgene in *wox4-1* mutant background. Plants displayed here were treated with 10 µM Dex or mock for six hours. The fluorescence of the reporters is displayed with the Leica glow lookup table, visualizing fluorescence intensities (dark red represents low intensity, light yellow represents high intensity). Sections were stained with Direct Red 23 to visualize cell walls (grey). Scale bars represent 100 µm. **B) and C)** Quantification of fluorescent signal intensities of nuclei in

hypocotyl cross-sections of Dex- or mock-treated plants. The violin plots graphically indicate the distribution of datapoints and additionally the boxplots show the medians (centre lines of boxes). The red dots indicate the mean. Plants were either treated for six hours (B) or 24 hours (C) with 10 µM Dex or mock. Either all nuclei located in the estimated *WOX4* expression domain (xylem and cambium area, see Figure 19B), or only the nuclei located in the estimated cambium area were quantified. For B) biological replicates were n=6 for Dex- and n=3 for mock-treated plants. For C) biological replicates were n=4 for Dex- and n=3 for mock-treated plants. Significant differences were identified using Welch's *t*-test (95% CI), ****p<0.0001.

While cytokinin signalling is regularly reported using *ARR* reporters (Sheen & Müller, 2008; Bishopp *et al.*, 2011b; Zürcher *et al.*, 2013), I aimed to investigate cytokinin signalling based on the *pTCSv2* reporter upon Dex induced WOX4 activation to better understand how WOX4 might act on cytokinin signalling.

### 4.11.3 Investigating cytokinin signalling upon WOX4 activation

To examine cytokinin signalling reported by the *TCSv2* reporter upon WOX4 activity changes, I introgressed the *pTCSv2:NLS-3Venus* transgene into the *pWOX4:WOX4-GR*; *wox4-1* background. I could not obtain F3 lines which were homozygous for both transgenes, however, I selected *wox4-1* homozygous plants harbouring the *pWOX4:WOX4-GR* transgene and all investigated plants were positive for the NLS-3Venus signal. Again, I focussed my analysis on 19-day old plants. Interestingly, at this growth stage, the *pTCSv2* signal was confined to the phloem poles (**Figure 32**A). This contrasted with the signal distribution observed within all vascular tissue types in 30-day old plants (**Figure 11**C). I analysed the fluorescence intensity of the nuclei of the whole vasculature in Dex- and mock-treated plants and observed that Dex treatment dampened the fluorescence intensity of the *pTCSv2:NLS*-3Venus-tagged nuclei (**Figure 32**B). This indicated that cytokinin signalling reported by *pTCSv2* is dampened by Dex-induced WOX4 activity. This finding was in line with my findings on the *ARR6* and *ARR15* reporters whose activity levels also were reduced upon WOX4 activation (**Figure 30** and **Figure 31**). To conclude, the finding of reduced cytokinin signalling reported by *pTCSv2* upon WOX4 activation provided a third piece of evidence that WOX4 negatively regulates components of the cytokinin signalling pathway.

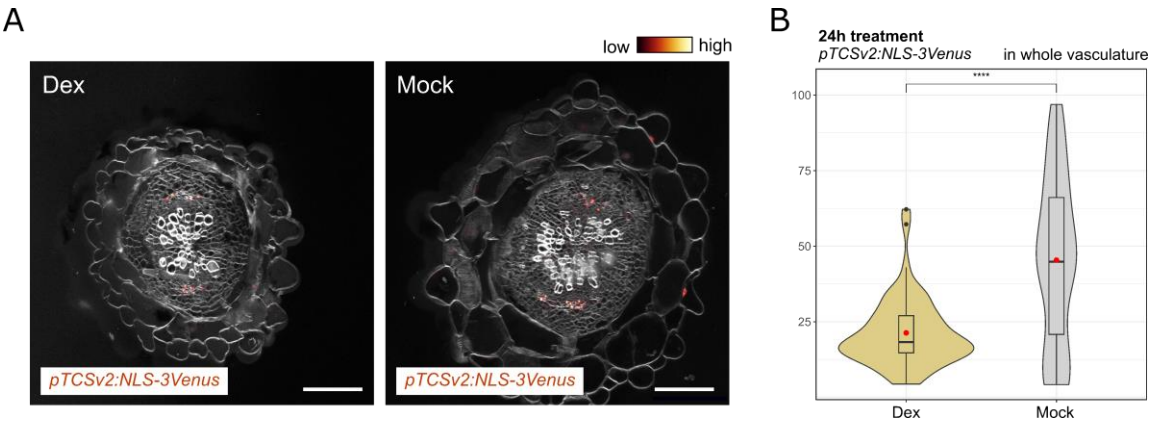


**Figure 32. *pTCSv2* reporter activity in *pWOX4:WOX4-GR* plants in *wox4-1* mutant background.** **A)** Exemplary hypocotyl cross-sections of 19-day old plants harbouring the *pTCSv2:NLS-3Venus* and the *pWOX4:WOX4-GR* transgene in *wox4-1* mutant background. Plants displayed here were treated with 10 µM Dex or mock for 24 hours. The fluorescence of the reporters is displayed with the Leica glow lookup table, visualizing fluorescence intensities (dark red represents low intensity, light yellow represents high intensity). Sections were stained with Direct Red 23 to visualize cell walls (grey). Scale bars represent 100 µm. **B)** Quantification of fluorescent signal intensities of nuclei in hypocotyl cross-sections of Dex- or mock-treated plants. The violin plots graphically indicate the distribution of datapoints and additionally the boxplots show the medians (centre lines of boxes). The red dots indicate the mean. All nuclei located in the vasculature area were quantified. Biological replicates were n=5 for Dex- and n=6 for mock-treated plants. Significant differences were identified using Welch's *t*-test (95% CI), ****p<0.0001.

Although the results of the individual experiments in this chapter have to be interpreted with caution due to small sample size, all the results consistently indicated that WOX4 might have a role similar to that of WUS (Leibfried *et al.*, 2005) in repressing specific type-A *ARRs* to ensure normal meristem function. To investigate the possible functions of *ARR5, ARR6, ARR7* and *ARR15* in the hypocotyl cambium, I investigated different *arr* mutants.

## 4.12 Investigating type-A *ARR* function in the cambium

So far, in my study, I found the type-A *ARRs ARR5*, *ARR6*, *ARR7* and *ARR15* to be potentially downstream of *WOX4* and to be significantly differentially expressed across cambium domains. Furthermore, I observed that they are expressed at lower levels in the cambium area compared to mature xylem and phloem tissues. I gained indication that *ARR6* and *ARR15* expression as well as *pTCSv2* reported cytokinin signalling was dampened by WOX4. Interestingly, *ARR7* and *ARR15* were already studied in the cambium context (Han *et al.*, 2018). The authors showed that phosphorylation of *ARF5* through *BIL1* is important to increase *ARR7* expression in the stem (Han *et al.*, 2018). Through analysis of stem and hypocotyl cross-sections of single mutants as well as

overexpression lines, the authors found that *ARR7* and *ARR15* act negatively on cambium activity (Han *et al.*, 2018). Importantly, *WOX4* expression was insensitive to TDIF signalling in the *ARR7* overexpression line, indicating that *ARR7* dampens TDIF-PXY stimulated cambium activity (Han *et al.*, 2018). Furthermore, *ARR7* and *ARR15* were shown to be expressed in the fascicular and interfascicular cambium in the stem (Han *et al.*, 2018).

I aimed to further investigate type-A *ARR* function in the hypocotyl cambium. For this, I selected single and double *arr* mutants (T-DNA insertion lines) (**Figure 33**A) and analysed hypocotyl cross-sections of 19-day old plants using the generated semi-automated high-throughput phenotyping pipeline. I included the analysis of *wox4-1* mutants as control for altered vasculature phenotypes. Firstly, I found that in this analysis the vasculature area in *wox4-1* mutants were reduced compared to wild type, however not significantly (**Figure 33**B). Interestingly, the vasculature area was tentatively increased in the *arr6* mutant was well as in the *arr15-2* mutant, although not significantly (**Figure 33**B). When analysing the xylem and phloem areas normalized to the vasculature area, I observed that *wox4-1* and wild type had similar xylem and phloem production ratios (**Figure 33**E). This indicated that although cambium activity is reduced in the *wox4-1* mutant, this did not result in a shift in xylem or phloem tissue production rates (**Figure 33**B, C, D and E). I hypothesized that since in the *wox4-1* mutant no shift in the xylem and phloem production ratio was observed, it could be that the lack of functional WOX4 could be buffered by other redundant genes. For the *arr6* and the *arr5;6* mutant (To *et al.*, 2004) as well as for the *arr7-2* mutant (Jeon *et al.*, 2010) and the *arr15-2* mutant no significant mutant phenotype was observed (**Figure 33**), which could also be caused by the redundancy of the genes.

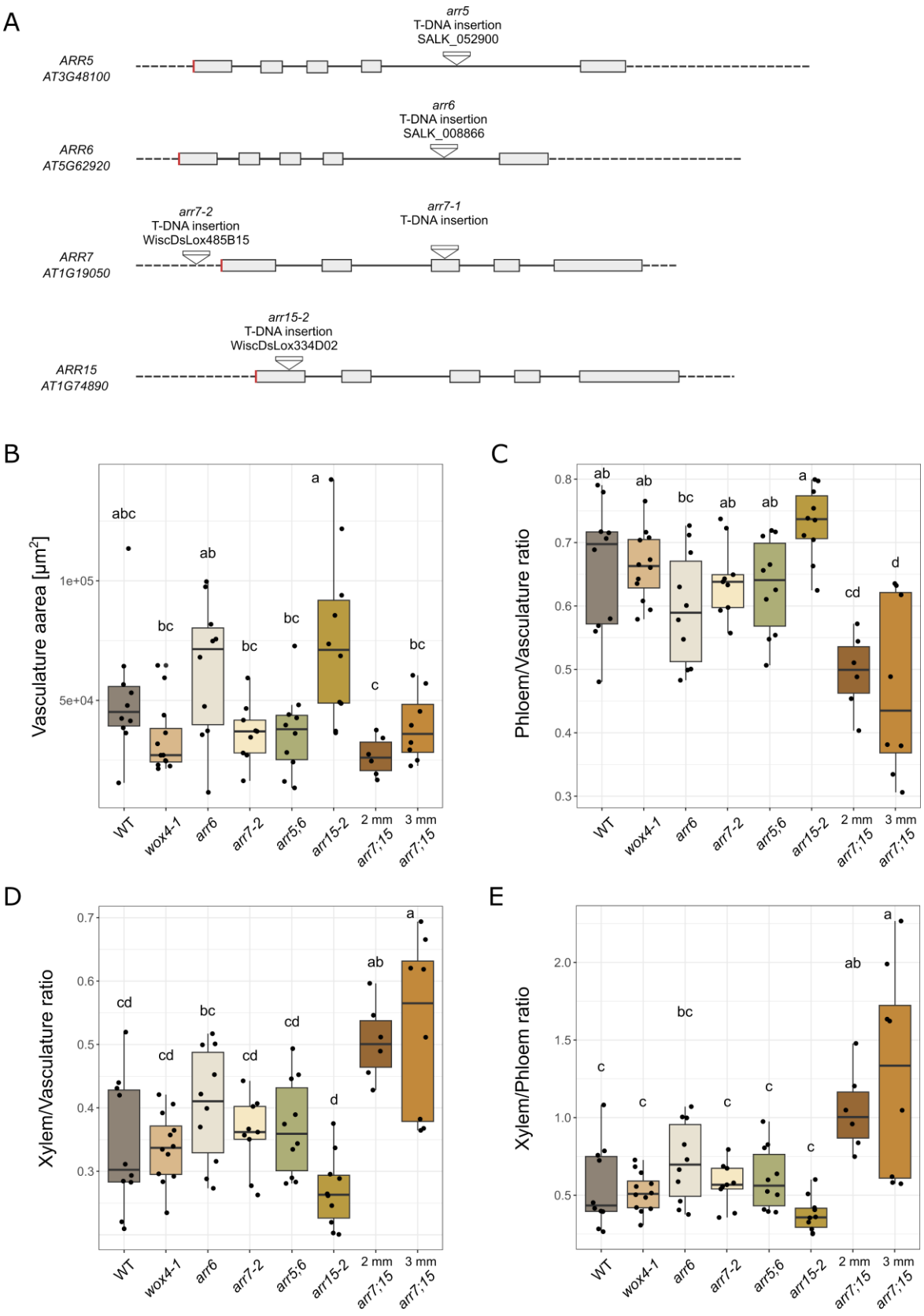


**Figure 33. Analysis of multiple *arr* single and double mutants using hypocotyl cross-sections.** **A)** Graphical illustration of T-DNA insertion sites of the investigated mutant lines. Dashed lines represent untranslated regions, boxes represent exons and lines represent introns. The start of the genes (ATG) is marked in red. The site of the T-DNA insertion is indicated by a triangle. **B) to E)** Quantification of vasculature area, phloem/vasculature ratio, xylem/vasculature ratio and xylem/phloem ratio, respectively. Sample sizes equal to or are larger than n=6 for each genotype.

Statistic groups are indicated by letters based on one-way ANOVA followed by a post-hoc Tukey HSD test (95% CI).

Strikingly, the *arr7-1;15-2* double mutant (hereafter called *arr7;15*) (Zhang *et al.*, 2011) showed a strong decrease in phloem production and an increase in xylem production (normalized to the vasculature area), resulting in a significantly higher xylem/phloem ratio (**Figure 33**C, D and E). Interestingly, the *arr7;15* mutant plants simultaneously showed an approximately 1 mm longer elongated hypocotyl phenotype compared to wild type and *wox4-1* plants. Therefore, I investigated the *arr7;15* hypocotyls at 2 mm above the root hypocotyl junction and also at 3 mm above the root hypocotyl junction (**Figure 33**), as the 3 mm cutting height might be more comparable to the developmental stage of the wild type and *wox4-1* samples at 2 mm. I observed that at a cutting height of 3 mm the *arr7;15* mutant phenotype was even stronger than at the 2 mm cutting height (**Figure 33**). It is to note that the *arr7* mutant alleles differ in the single *arr7* mutant (*arr7-2*) compared to the *arr7;15* double mutant (*arr7-1*) (**Figure 33**A). The *arr7-2* allele has a T-DNA insertion in the promoter region and was shown to have a 20-fold reduction in *ARR7* transcript levels and thus is not a null allele (Jeon *et al.*, 2010). In contrast, the *arr7-1* allele was effectively found to be a null allele (Zhang *et al.*, 2011). Therefore, the analysis of the *arr7-2* single mutant does not allow a statement regarding a possible concerted action of *ARR7* and *ARR15* in balancing xylem and phloem tissue production. To summarize, the mutant analysis revealed that the *arr7;15* double mutant showed a significant shift in xylem and phloem production rates with higher xylem and lower phloem production. This result suggested that *ARR7* and *ARR15* (or possibly *ARR7* alone) might be involved in cell fate decision-making processes within the hypocotyl cambium.

### 4.12.1 *arr7;15* mutation causes mutant phenotypes of varying degrees

Based on the previous interesting finding, I investigated the observed *arr7;15* phenotype in detail by examining the hypocotyl cross-sections more closely. The analysis of hypocotyl cross-sections of different *arr* mutants revealed a shift in the xylem and phloem production ratio in the *arr7;15* mutant. When analysing the individual cross-sections of the *arr7;15* mutant, I observed that the intensity of the xylem/phloem ratio shift compared to wild type and *wox4-1* varied between individual samples (**Figure 34**, also visible in the boxplots of **Figure 33**). Rarely, in extreme cases, xylem

production was increased to such an extent that in parts of the vasculature neither cambium nor phloem tissue remained (**Figure 34**D, Category 2, marked with asterisks). However, this was not observed in all cases (**Figure 34**C, Category 1). Upon simultaneous mutation of *ARR7* and *ARR15* it seemed that the effect of the single mutant as described in Han et al., 2018 changed from an alteration in tissue production to an alteration in cell fate decision-making. Taken together, the altered vasculature phenotype of the *arr7;15* mutant was not uniform, but enhanced xylem vessel production occurred to varying degrees. This finding could hint towards a complex thresholding function of *ARR7* and *ARR15*.

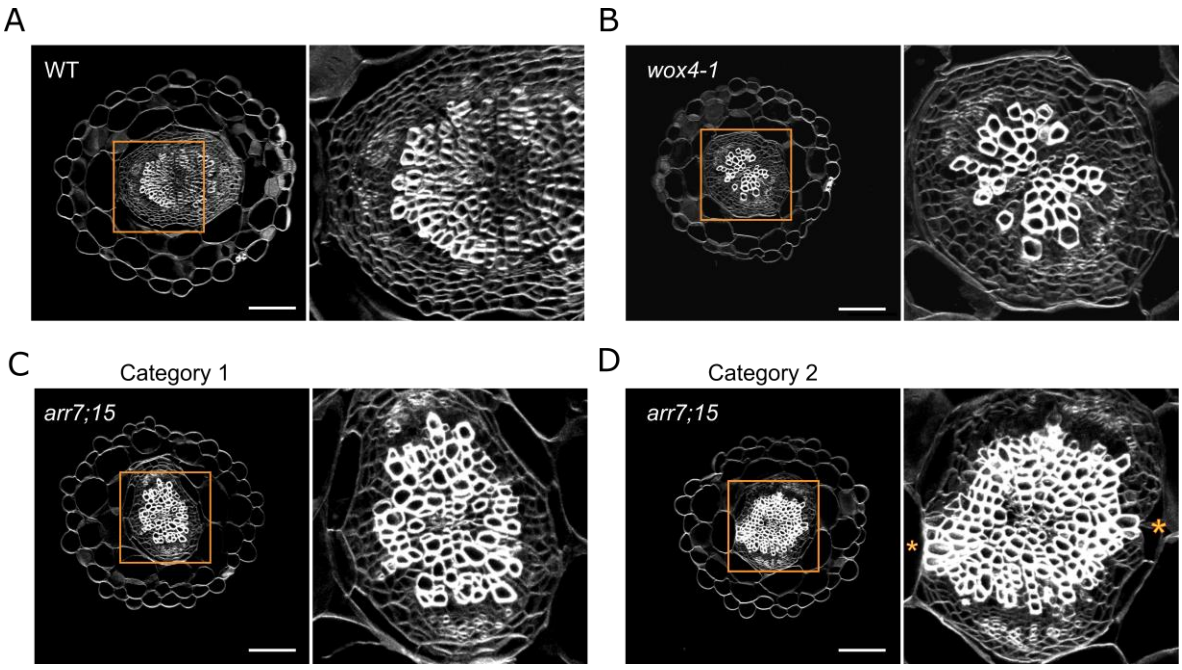


**Figure 34. *arr7;15* mutants showed a varying degree of mutant phenotype severity.**
Hypocotyl cross-sections of 19-day old plants. Sections were stained with Direct Red 23 (grey). The rectangles indicate the enlarged areas shown on the right side of each panel. Scale bars represent 100 µm. **A) and B)** Images of wild type and the *wox4-1* mutant, respectively. **C) and D)** Images of the *arr7;15* mutant. The individuals are exemplarily classified into two different severity categories of the phenotype. In D) the areas with a complete loss of cambium and phloem tissues are indicated with an asterisk.

# 5. Discussion

In this study I aimed to answer three main questions. First, I asked how GRNs can guide bifacial cell fate decisions of the cambium stem cells ultimately leading to bidirectional growth. I collaborated with the Mironova Lab to establish mathematical models and found that a hypothesised mutual inhibition of auxin and cytokinin signalling governed by WOX4 is sufficient to enable bifacial cell fate decision-making. Furthermore, the proposed GRN was furthermore able to produce bidirectional growth when implemented into a 1D model layout. Additionally, I found that auxin and cytokinin signalling levels were low in the cambium. Second, I raised the question to what extent WUS and WOX4 are similar or different in terms of their downstream regulatory mechanisms. By analysing WUS and WOX4 downstream targets, I found that both transcription factors, share the concept of type-A *ARR* repression. This may be a general concept for regulation of plant stem cells in addition to general concepts already known. Third, I asked how WOX4 exerts its regulatory potential on the cambium. I found that WOX4 targets both auxin and cytokinin related genes and likely affects auxin and cytokinin signalling levels in the hypocotyl. Furthermore, *WOX4* might itself be regulated by cytokinin via DOF2.1. Specifically, I identified that the type-A *ARRs ARR6*, *ARR7* and *ARR15* are targets of WOX4, and are expressed at low levels in the hypocotyl cambium. Moreover, WOX4 dampens ARR6 and ARR15 expression levels. Importantly, I found that ARR7 and ARR15 together are crucial for normal cell fate decision-making in the hypocotyl cambium. In the following I discuss my findings in more detail.

## 5.1 Mathematical modelling of cambium processes

Mathematical modelling can describe the temporal-spatial dynamics of biological processes with its involved factors and their relationship to each other as well as external influences on the process. Thus, it is a great tool to understand the underlying regulatory mechanisms of a given biological processes and their evolution in time (Tomlin & Axelrod, 2007). Modelling is also widely used in plant developmental biology.

Especially the modelling of GRNs using differential equations is of key importance when aiming to understand the dynamical nature of biological processes (Lavedrine *et al.*, 2015). Moreover, morphogens, like the hormones auxin and cytokinin, are known to provide further cues that are fundamental to coordinate growth on a tissue scale and are thus implemented in many models (Lavedrine *et al.*, 2015). However, the downside of mathematical modelling is that in the world of biology, most processes are immensely complex, even those we perceive as simple. For it to be possible to better understand a process using mathematical models, the system must be simplified by reducing internal factors and external influences. But this simplification then again is an advantage, as it allows us to understand how a process can be explained in the most minimal way. Regarding GRNs, this allows us to identify design principles for the creation of transcriptional networks. Here, I used mathematical models to develop approaches that improve our understanding of the cell fate decision-making process specific to CSCs.

### 5.1.1 A simple GRN can provide for cell fate decision-making and stem cell maintenance

It was already known that a minimal GRN consisting of two mutual inhibitory genes with auto activation of each gene is sufficient to create a system with bistability with a switch like behaviour where one gene (i.e. fate) “wins” over the other (Ferrell, 2012; Olariu & Peterson, 2019). Here, this was shown again by constructing ODEs (GRN model 1) describing this specific interaction of genes which led to three endpoint solutions/ states consisting of two differentiated states and one undifferentiated state (Figure 10). It is possible that the specific bifacial differentiation behaviour of the CSC occurs through a bistable switch that has also been shown for animal models (Chickarmane *et al.*, 2006). A key finding related to vascular differentiation is that for protophloem differentiation cell fate decision-making or developmental transitions happen rapidly with sharp transcriptomic changes within the differentiating cell, caused by mutual inhibition (Roszak *et al.*, 2021), the same design principle discussed in my study.

The range of initial conditions in which the undifferentiated cell state (CSC state) occurred in GRN model 1 was very narrow. Importantly, in this study, it was found that

by adding a governing factor C (GRN model 2) the stem cell state could be stabilized (Figure 10). A stable stem cell state is more likely to occur in the cambium, as the CSC can maintain itself during quite drastic changes of vascular tissue size during secondary growth. I conclude from the GRN model 2 presented here, that theoretically not more than three factors are needed to convey stem cell regulation and bifacial cell fate decision-making in the cambium. Recently, further models investigated the action of PXY along with additional factors showing that the interaction of just a few factors is sufficient to constitute cambium activity and bidirectional growth (Bagdassarian *et al.*, 2023; Lebovka *et al.*, 2023). When compared to animal models, surprisingly, the core network for pluripotency of mouse embryonic stem cells seems to be made up of just six genes (Lackner *et al.*, 2021). Approaches to identify the core transcriptional regulatory network of CSCs have also been conducted (Zhang *et al.*, 2019). However, a clear picture of the core genes network important for CSC maintenance is still lacking.

### 5.1.2 Heterogeneity of cambium stem cells?

A very crucial but so far unanswered question remains whether CSCs are homogenous or exhibit heterogenous transcriptional cell states (Haas *et al.*, 2022). In mouse embryonic stem cell models, *NANOG* together with *OCT4* and *SRY-BOX2* (*SOX2*) are the core pluripotency genes and each gene was shown to represses specific cell fates and promote other cell fates (Thomson *et al.*, 2011; Wang *et al.*, 2012). Importantly, it has been shown that one of the core pluripotency genes, *NANOG* expression needs to fluctuate in a regulated manner in order to allow cell fate decisions (Kalmar *et al.*, 2009). The authors propose that not a distinct cell state with fixed gene expression but rather a dynamic heterogeneity of stem cells is the key to pluripotency (Kalmar *et al.*, 2009). As dynamic observations in the cambium are difficult, uncovering such a heterogeneity in CSCs remains a tricky task.

### 5.1.3 Modelling of cambium dynamics based on auxin and cytokinin interaction

With regard to plants, modelling of auxin and cytokinin interaction has already greatly improved our understanding of vascular differentiation (De Rybel *et al.*, 2014; Muraro *et al.*, 2014). In contrast to previous approaches that focussed on pattern formation (Bagdassarian *et al.*, 2023; Lebovka *et al.*, 2023), the 1D model presented in this study serves the purpose of examining the cell fate decision-making capacity of the proposed

GRN model 2 in a cellular context. Importantly, auxin and cytokinin influence on auxin and cytokinin signalling respectively was included to form the core GRN of the 1D model (Figure 12). This resulting core GRN was implemented in the 1D model as a function which defined cell-fate decision-making. With this GRN continuous bifacial differentiation and growth was indeed obtained (Figure 13). Moreover, a continuous balance of auxin and cytokinin signalling levels in the CSCs could be maintained. Also, a high expression of *WOX4* within the CSCSs can be sustained over time. The *WOX4* expression pattern in the 1D model resembles the pattern identified in planta by the cambium domain-specific RNA-seq analysis. In the 1D model the parameters have been adjusted to obtain high auxin signalling in the proximal domain decreasing towards the distal domain and the opposite case for cytokinin signalling. Thus, the model can be adapted further to accommodate the valley-like distribution of auxin and cytokinin signalling identified in this study. A disadvantage of the current layout of the model is that cells are not easy to follow visually. This could be improved by fixing the stem cell to a certain position. In the scope of this work, the construction of a 2D model was not necessary. However, when implementing the core GRN into a 2D model layout, this would offer the opportunity to analyse cell fate decision-making not only in a single radial cell file but in multiple radial cell files investigating how the cell files work together to maintain the concentric structure of the cambium.

### 5.1.4 The 1D model allows in silico perturbation of cell fate decision-making

In this study, the 1D model was used to simulate a WOX4-deficiency. However, when expression of factor C (hypothesized to be WOX4) was reduced, the CSC was lost (Figure 14). Thus, factor C most likely rather represents a core group of regulators acting together to ensure cambium functions as *wox4-1* mutants still have CSCs (Figure 16). This core group may consist of the *PXY*, *BP*/*KNAT1* and *WOX4* genes as mutant analyses have shown that the combination of mutations in these genes leads to the most severe cambium defects (Zhang *et al.*, 2019). Furthermore, due to the complete CSC depletion, alterations in auxin and cytokinin hormone as well as signalling levels could not be properly tracked in the mutant model. According to my findings of in planta analysis of the *wox4-1* mutant, WOX4-deficiency causes elevated cytokinin signalling levels and a distal shift of the auxin signalling minimum. These findings should be captured in a “milder” mutant model.

## 5.2 Investigation of auxin and cytokinin pathways in the cambium

The auxin and cytokinin pathways, more specifically hormone synthesis, transport and signalling, are important in the cambium for cell proliferation, patterning and differentiation (Mähönen *et al.*, 2000, 2006a; Bishopp *et al.*, 2011a,b; De Rybel *et al.*, 2014; Ursache *et al.*, 2014). Furthermore, specific levels of synthesis and signalling are associated with specific tissue types and this highly regulated spatial distribution is crucial for normal patterning and activity (Brackmann *et al.*, 2018; Smetana *et al.*, 2019; Ye *et al.*, 2021). When components of auxin and cytokinin pathways, or the patterns they produce, are disrupted, a normally functioning cambium cannot be sustained. Many important insights into these regulatory mechanisms were derived from studies indicated above in *Arabidopsis* embryos, roots and stems. But so far, a detailed analysis of auxin and cytokinin pathway components and signalling patterns in the context of secondary growth in the hypocotyl was lacking. Therefore, I investigated and radially quantified auxin and cytokinin signalling patterns in the hypocotyl. In addition, by investigating a cambium domain-specific RNA-seq dataset provided by Dr. Dongbo Shi, I gained insights into the expression pattern of auxin and cytokinin pathway regulated genes within the cambium.

### 5.2.1 Auxin and cytokinin signalling levels are low in the cambium

When analysing auxin signalling patterns in the hypocotyls of 30-day old plants, I found that auxin signalling levels were low specifically in the cambium area (Figure 11). This indicated that, similar to roots and stems (Brackmann *et al.*, 2018; Smetana *et al.*, 2019), a low auxin signalling levels in the cambium is crucial for proper hypocotyl cambium function. Interestingly, auxin signalling is important in the SAM in several aspects and low auxin signalling is needed for proper meristem function (Ma *et al.*, 2019). Whether there are auxin signalling gradients in the stem remains unclear so far. In contrast, in roots of 14-day old plants, it has been shown that auxin signalling gradually increases from the site of the most recent cell division within the cambium towards xylem, plus a mirrored gradient towards phloem (Smetana *et al.*, 2019; Mäkilä *et al.*, 2023). For the hypocotyl, based on my quantification of auxin signalling, similar gradients may exist. However, it is to note that the chosen analysis method averages fluorescence intensities in concentric rings. This type of radial measurement also means that the x-axis represents just an approximation of the tissue area boundaries as the xylem, cambium and phloem area are not always perfectly circular in shape.

Thus, for now, it would be more accurate to speak of areas with different overall levels of auxin signalling within the hypocotyl vasculature. In a future step, the quantification of individual cell files, as performed in root studies (Smetana *et al.*, 2019; Mäkilä *et al.*, 2023) could be conducted to answer the question of the existence of a gradient. For now, upon closer inspection of the microscopy images of the *pDR5revV2:YFP* reporter, it appears that if such a gradient exists in the radial cell files of the hypocotyl vasculature, it might increase in steepness depending on whether new xylem vessels are being formed in the given cell file (see Figure 11G). This would suggest that cambium stem cells would be able to decode different auxin signalling slopes.

Like for auxin signalling, I found that the hypocotyls of 30-day old plants showed specifically low levels of cytokinin signalling in the cambium (Figure 11). This is similar to the finding of lower levels of cytokinin signalling in the procambium compared to the primary phloem (Ye *et al.*, 2021). Interestingly, I found that the type-A *ARRs* were likewise expressed at low levels in the cambium. Although, they are negative regulators of cytokinin signalling, these findings are not contradictory as type-A *ARR* expression depends on cytokinin signalling. Strikingly, Ye *et al*., (2021) showed that *LBDs* regulate the initiation of secondary growth downstream of cytokinin. LBD1, LBD3, LBD4 and LBD11 inhibit cytokinin signalling and are required for proper cambium function and stem cell maintenance (Ye *et al.*, 2021). According to the cambium domain-specific RNA-seq data presented here, these four LBDs were expressed in all cambium domains (proximal, central and distal). I suspect that the low cytokinin signalling observed in the hypocotyl cambium is partly caused by the action of LBDs. Interestingly, WOX14 activates LBD4 and modulates the phloem-procambium border downstream of PXY (Smit *et al.*, 2020).

Remarkably, the cytokinin transporter PUP14 inhibits cytokinin signalling (Zürcher *et al.*, 2016). According to the cambium domain-specific RNA-seq data, *PUP14* is among the five most highly expressed cytokinin-related genes in the cambium area. Thus, in addition to LBDs, PUP14 may play a role in maintaining low cytokinin signalling levels in the hypocotyl cambium.

As discussed previously for auxin signalling, the existence of a cytokinin signalling gradient is suggested from the data of the *pTCSn* and *pTCSv2* reporters presented

here but quantification of single cell files will help to confirm this. Nevertheless, in the scope of this study, I could clearly show that areas with different overall cytokinin signalling levels exist within the hypocotyl. The difference of the reported cytokinin signalling by the two *pTCS* reporters might lie in the different arrangement of the type-B *ARR* binding motifs of the *pTCSv2* reporter (Steiner *et al.*, 2020) rendering it more sensitive especially for cytokinin signalling in the xylem. That cytokinin signalling was present at substantial levels in the secondary xylem in the hypocotyl is supported throughout the study by the *pARR5*, *pARR6*, *pARR7* and *pARR15* reporters, respectively. The existence of cytokinin signalling in the xylem is in contrast to findings from primary growth in the root meristem, where cytokinin signalling is absent in the primary xylem due to activation of the cytokinin signalling repressor *AHP6* by *ARF5* (Mähönen *et al.*, 2006a,b; Bishopp *et al.*, 2011b; Ye *et al.*, 2021). Thus, it seems that in secondary growth, regulation of cytokinin signalling patterning is altered compared to primary growth. This is consistent with the findings of Ye *et al*. (2021) who reasoned that overall elevated cytokinin signalling in the mature roots and in hypocotyls compared to young roots is associated with the initiation of secondary growth. The question now remains whether cytokinin signalling in the secondary xylem is used as a cue for cambium regulation, or whether suppression is simply no longer necessary for correct vascular patterning. In addition, it would be interesting to find out whether activation of *AHP6* by ARF5 is maintained in the secondary xylem. If this is the case, it would suggest that *AHP6*-mediated repression of cytokinin signalling has to be counteracted by, for example, cytokinin itself (Mähönen *et al.*, 2006a) or by another factor.

In the primary growth context, *ARF5* not only activates *AHP6* in the xylem, but also *LOG* genes and hence cytokinin synthesis via the TMO5/LHW pathway (De Rybel *et al.*, 2013, 2014; Ohashi-Ito *et al.*, 2014). The xylem-produced cytokinin is then proposed to move to procambial cells where its high accumulation promotes cell divisions (De Rybel *et al.*, 2014; Ohashi-Ito *et al.*, 2014). My analysis focussed on cytokinin signalling levels, not hormone levels and analysis of cytokinin hormone levels has not yet been conducted in the *Arabidopsis* hypocotyl, nor have auxin hormone levels been investigated in this regard. Auxin and cytokinin hormone patterns could be investigated using genetically encoded auxin biosensors (Herud-Sikimić *et al.*, 2021) or fluorescent auxin analogues (Parizkova *et al.*, 2021). Thus far, similar approaches

for the visualization of cytokinins are missing. In contrast to the *Arabidopsis* hypocotyl, measurements of auxin and cytokinin levels in the cambium context were performed using mass spectrometry or antibodies in poplar stems (Immanen *et al.*, 2016; Fu *et al.*, 2021). The authors reported that IAA levels were highest in the centre of the cambial zone (Immanen *et al.*, 2016), whereas cytokinins peaked in phloem tissue (Immanen *et al.*, 2016; Fu *et al.*, 2021). It remains to be investigated, whether this is similar in *Arabidopsis*.

### 5.2.2 Domain-specific expression data reveals subtle modulation of auxin and cytokinin pathways

As part of this study, I used the cambium domain-specific expression dataset provided by Dr. Dongbo Shi to examine the auxin and cytokinin pathway in the hypocotyl cambium in detail for the first time. The gene lists of the auxin and cytokinin pathway components, or genes regulated by these hormones, presented here contain information on the cambium domain-specific expression of around 800 genes. However, it must be noted that the gene lists were generated manually based on GO term annotations and genes may be missing due to missing GO term annotations. Based on my analysis, the signalling, transport, or biosynthetic pathways could not be assigned to a distinct cambium domain but rather appear to be present throughout the cambium. This conclusion is based on the observation that the expression of individual genes similarly regulating a certain pathway peak in different cambium domains.

## 5.3 Investigation of the role of *WOX4* in the cambium

In this study, I hypothesized that WOX4 plays a role in cell fate decision-making in the vascular cambium by governing transcriptional responses of the auxin and cytokinin pathways. WOX4 has so far been mainly linked to the maintenance of cambium activity (Hirakawa *et al.*, 2010; Suer *et al.*, 2011) and with a dual role in cell proliferation and xylem differentiation, specifically xylem vessel expansion (Zhang *et al.*, 2019). A major goal of my study therefore was to better understand the role of WOX4 with a focus on its action in the hypocotyl cambium.

### 5.3.1 Is *WOX4* expression linked to cytokinin via DOF2.1?

WOX4 is long known to be involved in mediating the effect of auxin signalling (Suer *et al.*, 2011; Brackmann *et al.*, 2018), but only recently has it been linked to cytokinin by a study that found that *WOX4* is upregulated by DOF2.1 in the context of primary growth (Mor, 2020). To first investigate whether this connection exists in the hypocotyl, I analysed a DOF2.1 reporter (Smet *et al.*, 2019) and found DOF2.1 protein localization in xylem, cambium and phloem tissue, among others (Figure 27). In previous studies *DOF2.1* was also reported to be expressed in vascular tissues in the root, specifically in the xylem pole pericycle cells, procambium cells and endodermal cells (Smet *et al.*, 2019), but not in the central xylem. This contrasts with my observation of DOF2.1 localization in xylem parenchyma cells in the hypocotyl. Since HD-ZIP III transcription factors are expressed in the central vasculature, Smet *et al.* (2019) raised the question whether they might repress *DOF2.1*. If so, this regulation must be different in secondary growth as here DOF2.1 was present within the xylem area. Overall, the detected DOF2.1-YFP derived fluorescent signal pattern in hypocotyl-cross sections was patchy, which might arise from generally low fluorescence that makes it difficult to capture numerous nuclei. However, the domain-specific RNA-seq dataset confirmed expression of *DOF2.1* in the cambium. Within the cambium area, expression of *DOF2.1* was highest in the central domain, as was the case for *WOX4*. Although overlap in expression domains indicate that *WOX4* expression is linked to cytokinin via DOF2.1, this does not yet implicate a direct regulation. Experiments such as Chromatin Immunoprecipitation (ChIP) or Electrophoretic Mobility Shift Assay (EMSA) must be conducted before this conclusion can be drawn.

Interestingly, the *pUBI10:mCherry-GR-WOX4* dataset suggests that there might also be a feedback regulation from WOX4 to *DOF2.1*. According to this dataset, WOX4 represses *DOF2.1* expression which would result in a feedback loop.

### 5.3.2 Auxin and cytokinin signalling might be partially influenced by WOX4

I hypothesized that WOX4 acts on auxin and cytokinin pathways in view of the proposed GRN for cell fate decision-making. Thus, I investigated whether auxin and cytokinin signalling patterns differed when WOX4 was non-functional. It is interesting to note that high auxin signalling reported by *pDR5revV2* in putative developing xylem vessel elements as observed in wild type is not altered when WOX4 is non-functional (Figure 15), indicating that WOX4 is not involved in this process. Based on my analysis

I found that WOX4 influences the correct positioning of the local auxin signalling minimum in the cambium more proximal to the hypocotyl centre and dampen cytokinin signalling levels within the xylem and cambium. However, it might as well be, that the auxin signalling minimum is broadened and that causes a shift of the local auxin signalling minimum. Furthermore, the performed quantification of the whole vascular tissue might mask further effects within the cambium area. This can be clarified by a specific analysis of the cambium area only. Although the experiments would need to be repeated before making firm conclusions, my observations are a first hint that indeed WOX4 acts on both the auxin and cytokinin signalling pathways. It is tempting to speculate that the *wox4-1* mutant phenotype with less cambium activity is caused in part by elevated cytokinin signalling in the xylem and cambium, which together with the more distal auxin signalling minimum, could lead to a distortion of the auxin and cytokinin signalling ratios within the central domain, thereby slowing down cambium proliferation.

### 5.3.3 Cambium domain patterning is not changed in the *wox4-1* mutant

I investigated proximal, central and distal cambium domain patterns in the *wox4-1* mutant with the aim of determining whether WOX4 is directly involved in cell fate decision-making. I did not observe significant changes in the number of nuclei allocated to each cambium domain in the *wox4-1* mutant compared to wild type (Figure 16). However, a clear problem of this experiment was the large variation in nuclei counted between samples of the same genotype. I suspect that the number of cells allocated to a cambium domain normally would be rather similar between individuals of the same genotype. The variation observed here could have been caused by the nuclear localization of the signal, which does not allow to capture fluorescence for all nuclei, i.e. cells, in one plane. Furthermore, the normalization to the total number of nuclei counted could have enhanced the variation. Still, in this experiment, a trend towards a reduction of nuclei assigned to the central domain, i.e. CSCs, by about 30% was observed, which would be consistent with the observed reduced cambium activity in the *wox4-1* mutant.

An important question yet to be answer is whether the distal shift of the *pDR5revV2* fluorescence minimum observed in the *wox4-1* mutant is followed by a shift of the central cambium domain. Due to the nuclear localisation of the signal, this is not easy to answer with the here analysed line. However, existing ER-localized *pPXY* and

*pSMXL5* markers (Shi *et al.*, 2019) could be introgressed into the *wox4-1* mutant and investigated to answer this open question. Furthermore, the use of older growth-stages and the associated increase of detectable nuclei could contribute to a more robust analysis.

That no significant difference in the cambium domain patterning was observed in the *wox4-1* mutant could also be taken as a confirmation that the core genes that regulate cambium stem cell maintenance and cell fate decisions are in fact a group of genes working together, like previous studies showed (Etchells *et al.*, 2013; Zhang *et al.*, 2019). To investigate this in more detail, it would be helpful to analyse both the nuclear- as well as ER-localized *pPXY/pSMXL5* reporters in hypocotyl cross-sections of the *wox4-1;14-1* mutant (Etchells *et al.*, 2013) as well as further mutants (*bp-9;wox4-1*, *bp-11;wox4-1* and *bp-9 wox4 pxy*) (Zhang *et al.*, 2019). Additionally, domain-specific RNA-seq experiments could be conducted with these lines. If a significant difference in the stem cell number or domain positioning is found in one of the mutant combinations, analysis of the domain-specific expression changes could help to identify the core stem cell genes for the cambium. Along these lines, it would also be important to start investigating other *wox4* mutant alleles alongside *wox4-1* or RNA interference lines (Ji *et al.*, 2010) to increase our understanding of *WOX4* function.

### 5.3.4 Identification of the WOX4-dependent transcriptome

A main aim of this study was to investigate the WOX4-dependent transcriptome. First, I identified all potential WOX4 targets independent of the endogenous *WOX4* expression domain using the *pUBI10:mCherry-GR-linker-WOX4* line. Subsequently, I generated a refined list by employing the *pWOX4:WOX4-GR* line. Analysing the functionality of the *pWOX4:WOX4-GR* line, only a trend towards rescue of vascular area size could be observed. Nonetheless, I found that WOX4 activation rescued the reduced xylem vessel area size observed in *wox4-1* mutants, indicating that the line is nevertheless functional (Figure 20). The RNA-seq analysis of the *pWOX4:WOX4-GR* line identified 219 potential WOX4 downstream targets (Figure 21). In comparison, in the RNA-seq data of the *pRPS5A:WOX4-GR* line, I identified 914 potential downstream targets in my re-analysis (Figure 22). This stark difference could be caused by the suboptimal clustering of samples in the *pWOX4:WOX4-GR* dataset or the usage of the *RPS5A* promoter. Comparing all three RNA-seq datasets, it is noticeable that some genes appeared to be repressed in one dataset and activated in

another dataset. However, I would argue that this is not concerning, since different tissues and conditions were used. The three WOX4 RNA-seq datasets represent a valuable resource for further investigation of WOX4 function after ubiquitous, endogenous and meristem specific activation. It can now be stated with quite high certainty that WOX4 functions as both an activator and repressor as this was supported by all three RNA-seq datasets. But since no cycloheximide was used in the experiments to inhibit translation, the gene lists comprise potential primary but also secondary downstream targets. Further experiments such as ChIP-seq are needed to safely identify direct downstream targets.

### 5.3.5 *WOX4* expression gradient remains to be investigated more closely

The cambium domain-specific RNA-seq data showed a clear peak of expression of *WOX4* in the central domain and lower expression in the proximal and distal domain (Figure 23). Interestingly, WOX4 also peaks in the central zone of tree cambia (Immanen *et al.*, 2016). The *pWOX4:ER-YFP* line investigated here however indicated that *WOX4* is higher expressed in the proximal cambium domain (Figure 19). Quantification of fluorescence intensities in individual radial cell files would help to find out whether a *WOX4* expression gradient can be identified and how comparable it is to the cambium-domain RNA-seq data. Furthermore, WOX4 protein localization in the hypocotyl has not been shown yet. Moreover, it is still not known whether WOX4 protein movement occurs and if so, if it is crucial for its function, as has already been shown for WUS (Yadav *et al.*, 2011) and WOX5 (Pi *et al.*, 2015). These are important questions yet to be answered to understand the function of WOX4.

## 5.4 Analysis of type-A *ARRs* in the cambium context

### 5.4.1 Type-A *ARRs* are repressed by WOX4 in the hypocotyl

Type-A *ARRs* are important factors for the negative feedback in cytokinin signalling (To *et al.*, 2004). Their expression and function have been investigated in embryos, roots, RAM, SAM and stem but only rarely in the hypocotyl cambium context (To *et al.*, 2004; Leibfried *et al.*, 2005; Sheen & Müller, 2008; Zhao *et al.*, 2010; Zhang *et al.*, 2011; Han *et al.*, 2018). Han et al., (2018) showed that *ARR7* and *ARR15* act downstream of the BIN2-LIKE1 (BIL1)-ARF5/MP module in the inflorescence stem. Using a constitutively active ARF5 version expressed under the control of the *PXY*

promoter, the authors showed that ARF5 activates *ARR7*, *ARR9* and *ARR15* within three hours after induction. Interestingly, this did not seem to be the case for *ARR5* and *ARR6*, as they did not respond to the induction of constitutively active ARF5 (Han *et al.*, 2018). Although *ARR7* and *ARR15* are activated by ARF5, it remains to be analysed whether this regulation is direct. A main finding of my study was that *ARR6, ARR7* and *ARR15* are downstream targets of WOX4 and that *ARR6* and *ARR15* are repressed by WOX4. This is interesting because it suggests that there are parallel pathways of *ARR* regulation though ARF5 and WOX4 in the cambium. Moreover, the effect of ARF5 and WOX4 on *ARRs* could be linked since, at the same time, ARF5 regulates *WOX4* (Brackmann *et al.*, 2018). Interestingly, also in the SAM context both auxin and cytokinin pathways converge on *ARR7* and *ARR15* but here ARF5 acts negatively on the expression of these *ARRs* (Zhao *et al.*, 2010).

It is important to note again that the conclusion of *ARR* repression by WOX4 was based on the analysis of relatively few biological replicates. However, in both cases, when *WOX4* was non-functional or activated by Dexamethasone application, the results indicated a repression of *ARR6* and *ARR15* (Figure 29, Figure 30, Figure 31). The hypothesized direct regulation remains to be confirmed by using molecular techniques like EMSA or ChIP-seq. Furthermore, a focussed analysis of the cambium area can identify possible differences of *ARR* regulation between cambium domains.

### 5.4.2 Type-A *ARRs* are expressed at low levels in the cambium

The expression pattern of type-A *ARRs* was investigated in *Arabidopsis* in roots and stems so far (Zhang *et al.*, 2011; Han *et al.*, 2018). Han *et al*. showed that *ARR7* and *ARR15* are expressed in the fascicular and interfascicular cambium regions of the stem, but expression of *ARRs* in the hypocotyl was unknown so far. Here, I report the first analysis of *ARR* expression patterns in the hypocotyl. Remarkably, I found that in 30-day old plants *ARR5*, *ARR6*, *ARR7* and *ARR15* are expressed at low levels specifically in the cambium area (Figure 28). This is in line with low cytokinin signalling levels in the cambium area observed in this study. As stated above, Ye *et al*. (2021) found that cytokinins initiate secondary growth through LBDs and that LBDs repress cytokinin signalling. Additionally, the authors found that specifically LBD3 and LBD11 repress *ARR5*, *ARR6*, *ARR7* and *ARR15* (Ye *et al.*, 2021) based on the downregulation of their expression after LBD activation. Now, it is difficult to put these results together as it seems that LBDs represses cytokinin signalling and in parallel *ARRs*, the

repressors of cytokinin signalling. However, it may well be that this parallel contrasting regulation, along with other regulatory mechanisms, is necessary to maintain cytokinin signalling in the cambium at a very specific level. Hence, the ARRs may need to be repressed to allow a basal level of cytokinin signalling similar to the importance of maintaining basal auxin signalling levels in the stem cambium (Brackmann *et al.*, 2018) and stem cells in the SAM (Ma *et al.*, 2019).

The cambium-specific gene expression dataset showed an increase for *ARR6*, *ARR7* expression levels from the proximal to the distal cambium area and an opposite gradient for *ARR15* (Figure 26). *ARR5* was expressed at even levels (Supplemental Table 10). Interestingly, in trees, expression of almost all type-A and type-B *ARR*s peaks in phloem (Immanen *et al.*, 2016). It remains to be solved whether and how an expression gradient exists for type-A as well as type-B *ARRs* in the hypocotyl cambium and whether this gradient is instructive for cell fate decision-making.

All this interpretation of *ARR* expression levels in the hypocotyl cambium is based on my observations of 30-day old plants and the cambium domain-specific RNA-seq data. In 19-day old plants however, a specific downregulation of *ARR* expression in the cambium area was not apparent (Figure 28). The question therefore arises as to which specific expression levels are important in which growth stages and how these requirements change between organs. Most likely, many *ARRs* change their expression patterns and expression levels throughout development to fulfil their respective function. For example, in 5-day or 8-day old roots, *ARR5* and *ARR15* are used as cambium markers, respectively, because of their almost exclusive expression in the procambium and cambium (Zhang *et al.*, 2019; Fujiwara *et al.*, 2023), which is in stark contrast to my observations in the hypocotyl.

In contrast to the finding that expression of *ARR5*, *ARR6*, and *ARR15* was relatively constistant at low levels in the cambium area of 30-day old plants, it is striking that expressions levels in xylem and phloem tissues varied greatly between individual nuclei, thus cells, in both 19-day old and 30-day old hypocotyls. This implies that *ARR*5, *ARR6* and *ARR15* expression levels in mature secondary xylem and phloem tissues can vary from cell to cell and do not contribute to the maintenance of cell identity. However, this could be a different case for *ARR7*. I found that *ARR7* expression is

sometimes particularly pronounced in developing xylem vessel elements (Figure 28C and G). This is interesting because in the primary growth context, *ARR7* expression is highly specific for the protoxylem cells during late elongation and differentiation in the root (data from Root cell atlas, https://rootcellatlas.org/). Further investigations are needed to understand how ARR7 functions in this regard.

### 5.4.3 *arr7;15* mutants show altered cell fate decisions

Disruption of cytokinin signalling has previously been shown to cause problems in cell fate decision-making within the vasculature. The mutation of the cytokinin receptor *AHK4/WOL* caused a bias towards xylem differentiation in the primary growth context as all procambial cells differentiated into xylem cells (Mähönen *et al.*, 2000). A similar mutant phenotype was also found in *arr1;10;12* triple mutants (Yokoyama *et al.*, 2007). Additionally, the *log3;4* double mutant was shown to develop extra protoxylem (De Rybel *et al.*, 2014; Ohashi-Ito *et al.*, 2014).

Han *et al*. (2018) investigated the *arr7-2* and *arr15-2* single mutants of around 5-week-old plant and found that *ARR7* and *ARR15* repress cambium activity in the stem and in hypocotyls. To investigate the function of type-A *ARRs* in the cambium context I analysed 19-day old hypocotyls. My analysis of the same *arr7-2* and *arr15-2* single mutants as used by Han *et al.* did not show any alterations of xylem, phloem, or whole hypocotyl area size (Figure 33). It needs to be noted that in the experiments I performed, also no significant difference of the vasculature area size between wild type and *wox4-1* was observed which would have been expected. This could be due to the large variation between samples within a genotype. Hence, even though single mutants were not identified to have significantly altered tissue proportions, it might be worth repeating the analysis with older plants as performed in Han *et al.* (2018). This will help determine if some of the trends identified here in 19-day old plants are amplified in older hypocotyls.

Importantly, in my study a combination of the *arr7-1* and the *arr15-2* mutation showed an altered tissue production ratio towards increased xylem production. Although it is not clear yet how this phenotype arises, I hypothesize that this is based on an altered cell fate decision-making. Interestingly, ARR7 and ARR15 together play an important role in specifying the root stem cell niche, as only in the conditional double loss-of-

function mutants did the root stem cell niche become strongly malformed (Sheen & Müller, 2008). I thus propose a concerted action of *ARR7* and *ARR15* in the cambium. However, to give a definitive answer whether ARR7 and ARR15 act together, the *arr7-1* single mutant needs to be analysed. The *arr7;15* phenotype observed in this study varied in the severity of the altered tissue production ratio (Figure 34). This phenotype suggests that *ARR7* and *ARR15* have a function as a rheostat of cytokinin signalling levels, similar to WUS for auxin signalling (Ma *et al.*, 2019). As for the *arr7;15* mutant itself, it should be noted that it was initially identified to be gametophyte-lethal (Leibfried *et al.*, 2005). However, in a later study, Zhang *et al.* (2011) claimed that gametophyte lethality or abnormal pollen production only occurred when the plants were heterozygous for the mutations. In homozygous plants normal pollen was produced and plants were fertile (Zhang *et al.*, 2011).

To better understand how the different severity of the *arr7;15* mutant phenotypes comes about, cytokinin signalling in the mutant could be analysed by introgressing the *pTCSv2* reporter. Upon construction of a suitable analysis pipeline for nuclear signal quantification, analysis of radial patterns can be performed. This can answer the question whether a distal or proximal shift in the radial position of the local cytokinin signalling minimum happens or whether cytokinin signalling levels change in the cambium area. Furthermore, younger growth stages could be analysed to better track how the mutant phenotype evolves over time. In addition, cytokinin signalling could be analysed in a line co-overexpressing *ARR7* and *ARR15* to see if an altered tissue production rate, this time potentially favouring phloem production, could be observed. Moreover, as conducted for the *wox4-1* mutant in this study, investigation of *pPXY* and *pSMXL5* expression domains in the *arr7,15* mutant background can help to understand whether cambium domain sizes are changed, or stem cell numbers are reduced. Furthermore, the analysis of xylem vessels number and size could give valuable information whether ARR7 and ARR15 also act on xylem vessel expansion as documented for WOX4 (Zhang *et al.*, 2019).

I speculate that the *arr7;15* mutant phenotype also arises from changes in auxin signalling. Similar to recent identification of a gibberellic acid action on PIN1 (Mäkilä *et al.*, 2023), cytokinin also acts on PINs (Bishopp *et al.*, 2011b; Marhavý *et al.*, 2011). Thus, it is possible that the mutation of both *ARR7* and *ARR15* together causes an

increase in cytokinin levels which cause an increase in PIN1 derived auxin export. As shown in Mäkilä *et al.* (2023), this enhanced PIN1 action led to a broadened auxin domain. I suspect that this results in a distal shift of the local auxin minimum leading to more xylem specification. This hypothesis can be easily examined by investigating the *pDR5revV2* signal in the *arr7;15* mutant background. In general, xylem cell fate determination is a highly complex process and linked to further hormone and peptide signalling pathways (Kondo *et al.*, 2014). It therefore remains to be elucidated in detail how *ARR7* and *ARR15* are involved in the complex process of cell fate decision-making.

## 5.5 WUS and WOX4 share regulatory concepts

One aim of this study was to compare the function of WUS and WOX4 by investigating their downstream targets to derive information on possible further general concepts for plant cell fate decision-making in apical and lateral meristems (for example Zhou *et al.*, 2015).The ubiquitous expression of both transcription factors allowed me to identify the general regulatory potential of the WUS and WOX4 proteins, irrespective of their natural site of expression. However, the disadvantage of this approach is that the generated target lists are somewhat artificial and must be taken with precaution. While comparing downstream targets, I concentrated on auxin and cytokinin-related or -regulated genes based on the hypothesis that cell fate decision-making within the hypocotyl cambium is directed by these two hormonal pathways. In my analysis of putative WUS and WOX4 downstream targets, I found that 43 % to 48 % of downstream targets are shared (Figure 18). Moreover, 88% to 98 % of these shared targets are regulated in the same direction. I interpreted this result as substantial overlap and as a hint that WUS and WOX4 exert similar effects on downstream pathways.

Since the focus of my work was on type-A *ARRs*, it is important to compare my findings to previous findings in the SAM (Leibfried *et al.*, 2005; Zhao *et al.*, 2010). WUS represses *ARR5*, *ARR6*, *ARR7* and *ARR15* ensuring normal meristem function (Leibfried *et al.*, 2005). My findings hint towards a similar function for WOX4 in the cambium. Interestingly, for WUS, based on qRT-PCR experiments, *ARRs* are repressed already four hours after WUS induction and repression increases with longer

treatment time (Leibfried *et al.*, 2005). This contrasts with my observation that *ARR6* repression by WOX4 is reversed or compensated after 24 hours and that *ARR15* repression by WOX4 could not be observed after six hours of treatment. It is conceivable that, while WUS and WOX4 share the general concept of *ARR* repression in their respective stem cell niche, the fine-tuning needs to be tailored to individual stem cell niche conditions. A key difference of these conditions could be that *WUS* is expressed in the organizing centre and regulates the stem cells above, while *WOX4* is expressed in the stem cells, where a more dynamic regulation of *ARRs* might be required. The construction of the *pUBI10:mCherry-GR-linker-WOX4* line follows the same rationale as the *pUBI10:mCherry-GR-linker-WUS* line used for ChIP-seq experiments (Ma *et al.*, 2019). Thus, performing ChIP-seq using an RFP-trap for immunoprecipitation will allow a comparison of DNA regions bound by WOX and WUS. I speculate that there are more general concepts to be found when comparing auxin pathway regulation between *WUS* and *WOX4*. For example my analysis suggests that both WUS and WOX4 largely downregulate *YUCCA* genes.

When comparing the functions of WUS and WOX4, the question arises as to how interchangeable they are. This question has been raised before (Dolzblasz *et al.*, 2016) and it was shown that WOX4, when expressed in the *wus* mutant background under the control of the *WUS* promoter, failed to rescue the phenotype in stem cell maintenance in the SAM and floral meristem (Dolzblasz *et al.*, 2016). So far, it is not known whether WUS can replace WOX4. This could be answered by expressing *pWOX4:mCherry-GR-linker-WUS* in the *wox4-1* mutant background and subsequent investigation of hypocotyl cross-sections. Finally, a comparison could be made with the WOX5 function in the RAM, as this would allow a comparison of all three major plant stem cell niches. Strikingly, ubiquitous *WOX5* acts likewise negatively on *ARR5, ARR6 and ARR7* expression (Lee *et al.*, 2022). Thus, my study supports the notion that WOX dependent type-A *ARR* regulation is a general concept of WOX dependent plant stem cell regulation.

## 5.6 Final remarks and outlook

In this study, I aimed to investigate how gene regulatory networks guide cell fate decision-making in the vascular cambium of the *Arabidopsis* hypocotyl. My work has

shown that auxin and cytokinin signalling occurs at low levels in CSCs. Furthermore, auxin and cytokinin pathway are most likely fine-tuned in the hypocotyl cambium as components of the signalling, transport and biosynthetic were expressed in all cambium domains with no confinement to a certain domain. Moreover, the maintenance of low cytokinin signalling levels may be in part due to WOX4. Furthermore, my results support a role of WOX4 as a repressor of the type-A ARRs *ARR6* and *ARR15*. Analysis of the *arr7;15* mutant indicated that these type-A ARRs are important for cell fate decision-making in the hypocotyl cambium. In summary, my work revealed a new link between cytokinin, DOF2.1, WOX4 and type-A ARRs and cell fate decision-making (**Figure 35**). However, since type-A ARRs lack the DNA-binding domain, further downstream regulation does not occur at the transcriptional level, but more likely at the signalling level. It remains to be clarified whether the investigated type-A ARRs are xylem cell fate repressing factors or phloem cell fate promoting factors. Further experiments are needed to test and validate the proposed connections of this study and to identify details of DOF2.1, WOX4 and type-A ARR interaction.

Based on this study, further indications have emerged that strengthen the inclusion of interesting research directions: Since the auxin signalling pathway and its regulation downstream of WOX4 were only partially analysed, the data obtained can be used to identify further interesting auxin pathway related cell fate regulating factors. Furthermore, hypoxia response was one of the top GO terms of biological processes regulated by WUS and WOX4. Since hypoxia and ROS formation are linked and ROS signalling was shown to be in connection with auxin and cytokinin crosstalk (Tognetti *et al.*, 2017; Dang *et al.*, 2023), this line of research could provide insights into new important regulatory circuits downstream of WOX proteins. Very recently, a feedback loop between LBD11 and ROS has been identified to be important for the maintenance of normal cambium proliferation (Dang *et al.*, 2023), which could constitute a starting point for studies involving WOX4. Additionally, the ‘circadian rhythm’ was the most enriched pathway in the *pWOX4:WOX4-GR* RNA-seq dataset. Since interesting connections between cell fate decision-making and the circadian clock exist (Torii *et al.*, 2022), this research direction may open new fields to understand cell fate decision-making of CSCs in a temporal context.

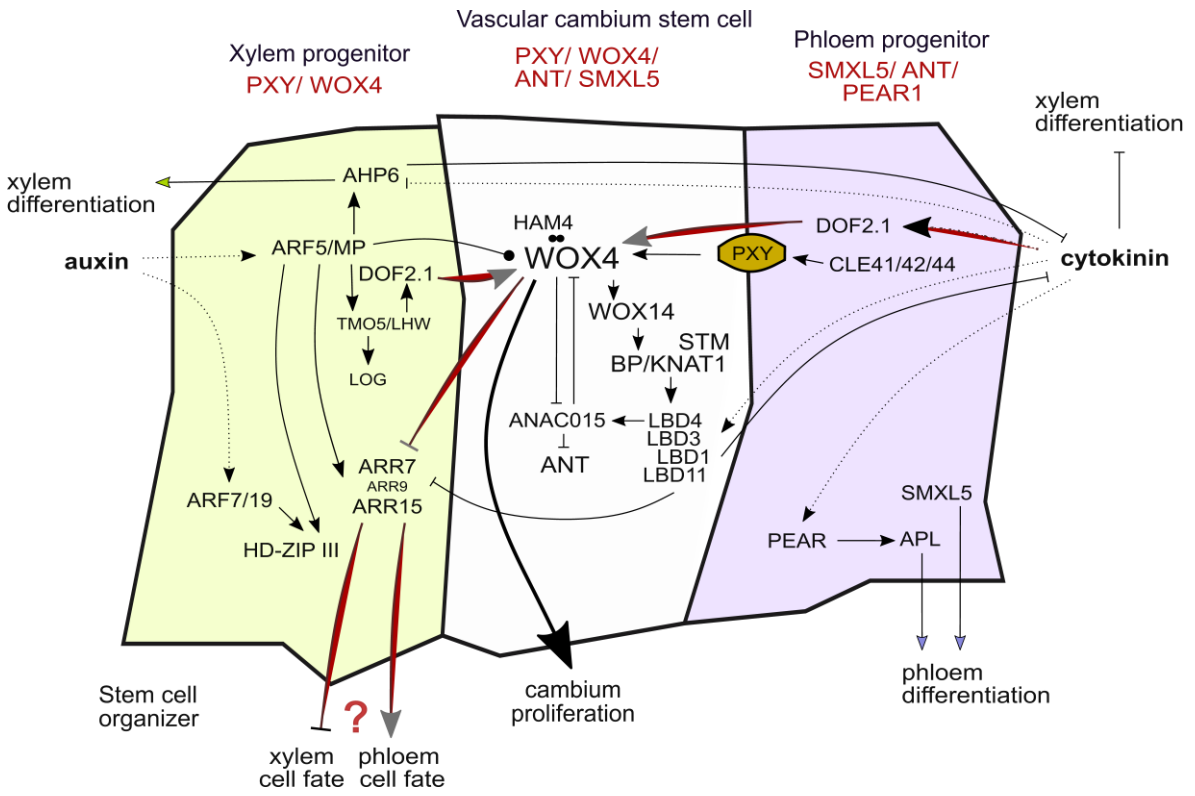


**Figure 35. This study suggest that cambium regulation is partially orchestrated through a GRN including DOF2.1, WOX4 and type-A ARRs.**
A graphical representation of the newly proposed link of cytokinin, DOF2.1, WOX4 and type-A ARRs to regulation of cell fate decision-making in the vascular cambium. This figure was created by me and published in Haas *et al.*, 2022 and subsequently modified by me.

It is important to mention that due to the focus of this study on auxin and cytokinin pathways, many other important known hormone and peptide signalling derived mechanisms of stem cell maintenance and cell fate decision-making have been neglected. These include, for example, the gibberellic acid pathway (Ben-Targem *et al.*, 2021; Mäkilä *et al.*, 2023) and the brassinosteroid pathway (Furuya *et al.*, 2021).

Finally, important studies in trees investigating WOX4 (Kucukoglu *et al.*, 2017) and auxin (Nilsson *et al.*, 2008; Immanen *et al.*, 2016) as well as cytokinin pathways (Nieminen *et al.*, 2008; Immanen *et al.*, 2016) have already demonstrated the importance of WOX4, auxin and cytokinin in cambium regulation of trees. It remains to be seen how much knowledge is transferable between the model species *Arabidopsis* and tree species such as poplar. Nonetheless, continued research on the vascular cambium may not only serve to identify and clarify fundamental concepts in biology such as cell fate decision-making, but also enhance our understanding of how wood is formed.

# 6. Supplement

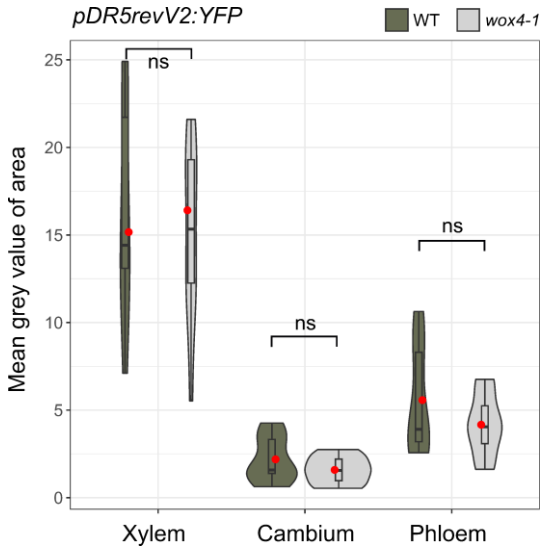


**Supplemental Figure 1. Comparison of auxin signalling in wild type and *wox4-1* background without normalization.**
Quantification of fluorescent signal intensities of the p*DR5revV2:YFP* reporter in hypocotyl cross-sections of wild type and *wox4-1* mutants in the xylem, cambium or phloem area. Significant differences were identified using Welch's *t*-test (95% CI), *ns* = not significant. The violin plots graphically indicate the distribution of datapoints and additionally the boxplots show the medians (centre lines of boxes). The red dots indicate the mean. Sample size for wild type was n=9 and for *wox4-1* n=11. The mean grey values were not normalized although the reporter is not homozygous (see main text).

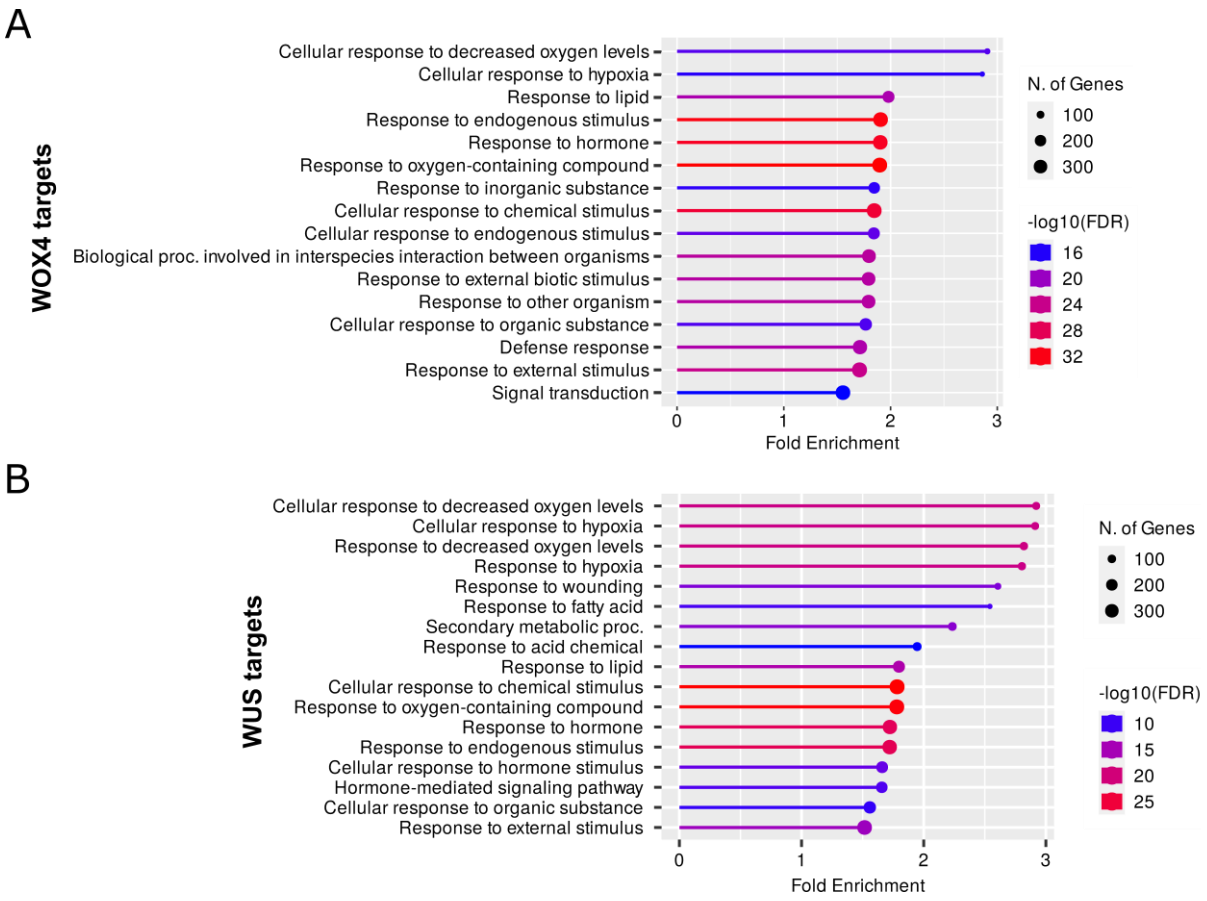


**Supplemental Figure 2. GO term analysis of individual *WOX4* and *WUS* transcriptional signature upon ubiquitous expression.**
GO term analysis of biological processes of the WOX4 targets **(A)** and WUS targets **(B)**. The line length shows the fold enrichment of the respective process. The colour indicates the -log10 of the False Discovery Rate (FDR). The size of the dots represents the number of genes which fall into the respective process. The graphs were generated using ShinyGO0.77. The RNA-seq experiment was jointly performed with Inés Hidalgo Prados. All analyses were conducted by myself.

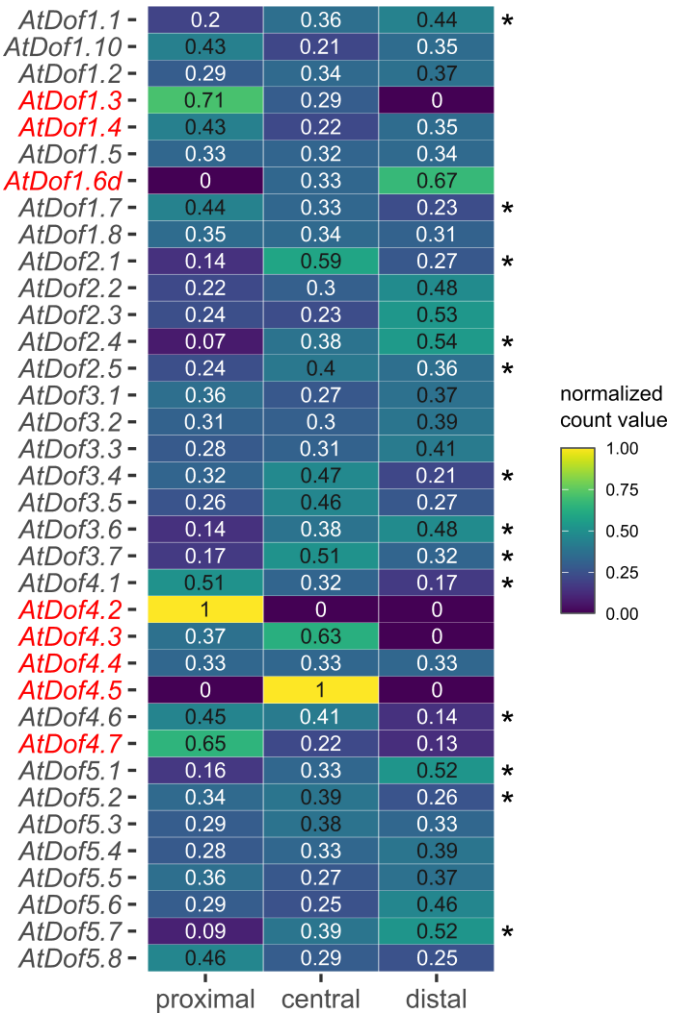


**Supplemental Figure 3. Investigation of cambium domain-specific expression of all *DOF* family members.**
Heatmap showing the expression of all 37 members of the *DOF* transcription factor family across cambium domains. The relative normalized count values are shown, which indicate the ratio at which a gene is expressed in a certain domain relative to its expression across all domains. Genes which are significantly differentially expressed across domains (determined using a likelihood ratio test) are marked with an asterisk. The genes marked in red show a high variance across domains but are not marked as significantly differentially expressed, since the normalized count values of the biological replicates vary substantially and therefore the expression of these genes must be interpreted with precaution. The RNA-seq data and analysis was produced by Dr. Dongbo Shi. The analysis of *DOF* genes and visualization were conducted by myself.

**Supplemental Table 1.** List of the 124 genes in the auxin pathway or regulated by auxin, which are shared by WUS and WOX4 and regulated in the same direction. Padj value threshold = 0.005. The RNA-seq experiment was jointly performed with Inés Hidalgo Prados. All analyses were conducted by myself.

| | ***pUBI10:mCherry-GR-WUSCHEL*** | | ***pUBI10:mCherry-GR-WOX4*** | |
|---|---|---|---|---|
| **Gene** | **log2FC** | **Padj value** | **log2FC** | **Padj value** |
| AT3G51800 | -0.52 | 6.74397E-08 | -0.39 | 0.000487004 |
| AT3G27580 | 0.64 | 9.34288E-10 | 1.20 | 5.58894E-27 |
| AT1G21410 | 1.09 | 1.02661E-23 | 0.95 | 6.22067E-15 |
| AT4G11280 | 0.65 | 8.53896E-07 | 1.38 | 1.24098E-23 |
| AT2G26260 | 0.88 | 4.42217E-11 | 1.30 | 6.70837E-20 |
| AT5G19530 | -1.33 | 7.94759E-07 | -1.91 | 2.94779E-10 |
| AT4G29140 | -1.69 | 1.85287E-17 | -0.71 | 0.001263976 |
| AT5G13790 | -0.73 | 0.000860662 | -1.29 | 9.54862E-08 |
| AT2G36910 | 0.53 | 0.000111284 | 0.72 | 2.10871E-06 |
| AT3G62150 | -2.77 | 3.76708E-39 | -3.29 | 2.83272E-43 |
| AT5G43700 | -1.27 | 5.56672E-17 | -1.02 | 4.58937E-09 |
| AT1G77850 | 0.83 | 5.16784E-13 | 0.70 | 3.62245E-08 |
| AT1G30330 | -0.47 | 0.00274188 | -1.18 | 1.60879E-12 |
| AT3G07390 | 2.23 | 3.80857E-54 | 1.50 | 4.82886E-20 |
| AT2G04160 | -0.74 | 0.000121642 | -1.21 | 8.40485E-09 |
| AT2G34680 | -1.24 | 2.66159E-09 | -1.09 | 5.3874E-06 |
| AT2G33310 | -0.97 | 5.04978E-11 | -0.73 | 1.84749E-05 |
| AT1G54200 | -2.02 | 8.34482E-11 | -0.92 | 0.001507311 |
| AT3G13980 | -1.61 | 9.87527E-17 | -2.10 | 3.79194E-21 |
| AT1G69160 | -3.32 | 4.84096E-36 | -3.72 | 1.08685E-35 |
| AT1G13670 | -3.93 | 2.08363E-20 | -3.39 | 2.00966E-12 |
| AT2G35600 | -1.55 | 0.003645505 | -1.86 | 0.002692207 |
| AT4G32810 | -1.71 | 2.93481E-07 | -3.34 | 3.67827E-15 |
| AT4G10100 | 0.50 | 0.002809011 | 0.64 | 0.000527635 |
| AT3G01490 | -1.41 | 2.50422E-13 | -0.92 | 3.04603E-05 |
| AT3G43670 | 0.78 | 6.38575E-05 | 1.11 | 2.11395E-07 |
| AT4G08920 | -1.24 | 6.35891E-33 | -0.95 | 7.17236E-16 |
| AT5G55910 | -1.23 | 6.55409E-44 | -0.49 | 1.16234E-06 |
| AT1G14130 | 0.95 | 2.78907E-08 | 1.60 | 4.12673E-18 |
| AT5G63420 | -0.65 | 9.67484E-05 | -0.58 | 0.002659174 |
| AT2G45000 | -0.31 | 0.004344578 | -0.37 | 0.001705006 |
| AT2G33860 | 0.39 | 0.000354971 | 0.51 | 1.31854E-05 |
| AT5G43870 | -2.34 | 5.06482E-29 | -1.39 | 1.06447E-11 |
| AT4G14740 | -1.02 | 7.90112E-12 | -0.51 | 0.003085939 |
| AT1G14350 | -1.83 | 7.1094E-12 | -1.31 | 2.04669E-05 |
| AT5G56860 | -3.04 | 9.99121E-30 | -1.82 | 2.50993E-10 |
| AT1G28130 | -0.44 | 0.003564405 | -0.72 | 1.11286E-05 |
| AT4G03190 | -0.76 | 0.000830128 | -1.44 | 8.37467E-09 |
| AT5G56660 | 0.55 | 3.59282E-06 | 0.53 | 6.2108E-05 |
| AT3G02875 | 1.02 | 1.47715E-14 | 1.55 | 4.85526E-26 |
| AT4G14560 | -1.03 | 1.18796E-06 | -1.73 | 3.37968E-12 |
| AT3G15540 | -1.31 | 9.61786E-05 | -1.32 | 0.001227999 |

| | | | | |
|---|---|---|---|---|
| AT4G32280 | -1.81 | 0.000153012 | -1.77 | 0.00290494 |
| AT5G65670 | -0.37 | 9.32707E-06 | -0.38 | 7.37658E-05 |
| AT3G04730 | -0.37 | 0.003449821 | -1.80 | 1.17837E-42 |
| AT1G13580 | 0.53 | 0.001482153 | 0.56 | 0.002342139 |
| AT5G14090 | -0.48 | 0.003738779 | -0.73 | 5.06476E-05 |
| AT1G27340 | -1.10 | 1.03978E-19 | -0.47 | 0.000576548 |
| AT4G37540 | -0.87 | 3.84974E-08 | -1.79 | 2.78542E-24 |
| AT3G59790 | 3.19 | 0.000369733 | 5.10 | 0.000255142 |
| AT4G29810 | 0.57 | 0.000337094 | 1.13 | 3.95053E-11 |
| AT5G45800 | 1.21 | 1.03852E-58 | 1.22 | 5.28693E-49 |
| AT5G52900 | -4.18 | 2.28892E-50 | -3.33 | 2.48847E-28 |
| AT1G10210 | 0.30 | 0.00189482 | 0.51 | 1.07408E-06 |
| AT4G04950 | 0.36 | 1.90305E-05 | 0.46 | 3.79303E-07 |
| AT2G42620 | -0.72 | 2.96585E-10 | -0.96 | 4.46861E-14 |
| AT1G08810 | -2.04 | 6.67667E-23 | -2.85 | 6.44572E-33 |
| AT5G39610 | -0.74 | 0.001006967 | -1.50 | 8.02642E-10 |
| AT4G17980 | -5.66 | 2.36544E-05 | -4.05 | 4.63668E-05 |
| AT5G11790 | 1.33 | 1.89851E-20 | 0.57 | 0.000785121 |
| AT3G05630 | -1.04 | 3.11042E-05 | -1.21 | 1.19305E-05 |
| AT3G59060 | -0.98 | 1.87201E-21 | -1.12 | 3.05607E-22 |
| AT2G43010 | 1.38 | 5.74343E-32 | 1.03 | 1.10285E-14 |
| AT3G16500 | -0.58 | 1.55829E-05 | -1.74 | 1.68071E-33 |
| AT1G70940 | -1.42 | 8.62352E-18 | -2.25 | 1.48179E-34 |
| AT1G77110 | -2.36 | 0.000836604 | -2.67 | 0.000925108 |
| AT1G76520 | -1.82 | 1.41256E-35 | -0.98 | 7.61606E-09 |
| AT2G17500 | 1.79 | 1.14699E-17 | 1.28 | 1.31188E-07 |
| AT5G01990 | 0.52 | 0.004351796 | 0.71 | 0.000479273 |
| AT2G34650 | 1.14 | 3.81341E-14 | 0.90 | 2.18937E-07 |
| AT4G07410 | -0.60 | 1.08398E-08 | -0.55 | 3.26577E-06 |
| AT3G53970 | 0.59 | 1.45104E-07 | 0.70 | 2.21996E-08 |
| AT4G38630 | 0.46 | 4.60803E-05 | 0.72 | 7.38197E-09 |
| AT5G17300 | -1.21 | 1.52183E-12 | -2.24 | 1.15235E-30 |
| AT1G80360 | 0.81 | 2.15183E-10 | 0.47 | 0.001714959 |
| AT1G78570 | 1.05 | 1.01217E-08 | 1.76 | 3.3308E-18 |
| AT5G14420 | 0.81 | 1.0695E-17 | 0.45 | 6.00425E-05 |
| AT1G07910 | 1.16 | 8.73169E-29 | 0.66 | 5.3477E-08 |
| AT5G64770 | -4.88 | 8.22659E-18 | -4.30 | 1.44218E-27 |
| AT2G31190 | 0.83 | 9.87732E-11 | 0.51 | 0.000487927 |
| AT3G25717 | -0.78 | 0.00039306 | -1.43 | 2.99681E-09 |
| AT3G53020 | -0.50 | 1.57045E-07 | -0.33 | 0.002864257 |
| AT1G16510 | -1.15 | 1.29633E-05 | -1.67 | 8.90729E-08 |
| AT1G29490 | -6.26 | 5.41247E-06 | -5.73 | 0.000955748 |
| AT4G34770 | -8.03 | 2.71219E-18 | -4.35 | 1.95829E-24 |
| AT2G18010 | -3.87 | 0.001266648 | -5.52 | 0.001038711 |
| AT4G38840 | -3.75 | 2.87083E-25 | -4.07 | 5.42453E-23 |
| AT4G22620 | 3.58 | 2.05576E-10 | 1.73 | 0.001307012 |
| AT4G34800 | -5.11 | 0.000140475 | -2.55 | 0.000222888 |

| | | | | |
|---|---|---|---|---|
| AT2G37030 | 1.97 | 1.34506E-06 | 2.84 | 1.56519E-08 |
| AT3G60690 | -1.45 | 1.50301E-11 | -2.16 | 1.1238E-19 |
| AT1G17345 | -0.83 | 9.81767E-05 | -3.16 | 4.72506E-32 |
| AT4G36110 | -1.07 | 0.003961397 | -2.30 | 5.78499E-08 |
| AT5G43270 | -1.68 | 1.33922E-19 | -1.59 | 1.7625E-14 |
| AT4G23410 | -1.99 | 1.6406E-29 | -1.70 | 1.06249E-17 |
| AT4G30430 | 2.62 | 8.27906E-06 | 2.06 | 0.004454579 |
| AT1G15750 | -0.86 | 8.1238E-15 | -0.75 | 2.37551E-09 |
| AT1G10840 | -0.24 | 0.00103415 | -0.27 | 0.00074023 |
| AT3G62980 | -0.66 | 2.24563E-08 | -0.42 | 0.002189838 |
| AT3G20630 | 0.53 | 4.55597E-08 | 0.48 | 1.10815E-05 |
| AT3G11260 | -1.52 | 0.003401672 | -1.78 | 0.001676865 |
| AT5G57740 | 0.69 | 2.07072E-08 | 0.72 | 1.74665E-07 |
| AT2G06850 | -2.26 | 3.22541E-19 | -1.47 | 4.92159E-07 |
| AT1G08410 | -0.72 | 2.22153E-10 | -0.43 | 0.000916839 |
| AT1G04610 | -1.83 | 0.002698818 | -2.28 | 0.002335279 |
| AT4G28720 | -2.21 | 3.08296E-12 | -1.60 | 1.39864E-05 |
| AT1G04180 | 1.43 | 0.00455272 | 2.01 | 0.001018618 |
| AT4G13260 | -1.58 | 5.75912E-05 | -2.90 | 3.05258E-09 |
| AT5G43890 | -2.58 | 1.21386E-07 | -2.75 | 1.56701E-06 |
| AT5G25620 | -1.03 | 0.000507503 | -1.04 | 0.002506412 |
| AT5G13750 | -1.22 | 7.86549E-13 | -0.64 | 0.001772389 |
| AT5G56840 | -1.52 | 1.30102E-05 | -3.32 | 4.71939E-11 |
| AT4G09890 | -3.35 | 3.15559E-59 | -2.59 | 1.01865E-30 |
| AT1G61255 | -3.10 | 0.000139697 | -2.56 | 1.92005E-05 |
| AT1G63420 | -2.12 | 1.623E-25 | -1.77 | 2.12186E-15 |
| AT5G49800 | -1.75 | 1.33173E-06 | -1.74 | 1.06554E-05 |
| AT5G06930 | -3.13 | 2.96825E-26 | -1.61 | 2.53529E-07 |
| AT3G51400 | -1.41 | 7.14188E-11 | -1.28 | 9.70811E-08 |
| AT1G25400 | -1.33 | 2.63697E-17 | -1.24 | 3.37116E-12 |
| AT3G07010 | -1.29 | 3.84615E-20 | -1.13 | 6.04261E-13 |
| AT5G58090 | 1.22 | 1.9954E-17 | 0.58 | 0.000741049 |
| AT1G65920 | 0.62 | 0.000171306 | 0.70 | 0.000163104 |
| AT1G14185 | 0.93 | 0.00208687 | 1.10 | 0.001197521 |
| AT4G21740 | 1.20 | 4.51243E-11 | 1.26 | 1.88394E-10 |

**Supplemental Table 2.** List of the 34 genes in the cytokinin pathway or regulated by cytokinin, which are shared by WUS and WOX4 and regulated in the same direction. Padj value threshold = 0.005. The RNA-seq experiment was jointly performed with Inés Hidalgo Prados. All analyses were conducted by myself.

| | ***pUBI10:mCherry-GR-WUSCHEL*** | | ***pUBI10:mCherry-GR-WOX4*** | |
|---|---|---|---|---|
| **Gene** | **log2FC** | **Padj value** | **log2FC** | **Padj value** |
| AT3G16360 | -5.34 | 8.5919E-05 | -5.26 | 1.4312E-05 |
| AT3G10520 | -3.07 | 1.4642E-40 | -3.22 | 4.1475E-43 |
| AT1G33170 | -2.73 | 9.4307E-16 | -2.39 | 4.3255E-10 |

| | | | | |
|---|---|---|---|---|
| AT2G28305 | -1.51 | 6.0798E-07 | -2.20 | 9.3263E-11 |
| AT5G56860 | -3.04 | 9.9912E-30 | -1.82 | 2.5099E-10 |
| AT5G11950 | -1.38 | 2.4045E-19 | -1.81 | 1.2687E-26 |
| AT2G18300 | -1.35 | 1.9353E-19 | -1.73 | 5.2508E-25 |
| AT1G66190 | -1.10 | 1.1488E-09 | -1.71 | 2.1631E-16 |
| AT4G28720 | -2.21 | 3.083E-12 | -1.60 | 1.3986E-05 |
| AT1G19050 | -2.94 | 5.2929E-24 | -1.51 | 7.5767E-10 |
| AT1G31770 | -0.95 | 2.8276E-06 | -1.49 | 4.4513E-11 |
| AT4G37790 | -0.87 | 1.2728E-11 | -1.48 | 1.3004E-25 |
| AT1G70510 | -2.30 | 1.0899E-14 | -1.40 | 3.3806E-06 |
| AT1G03850 | -0.86 | 0.00051493 | -1.40 | 3.1885E-07 |
| AT5G19040 | -0.93 | 0.00022213 | -1.39 | 9.3065E-06 |
| AT1G09250 | -0.93 | 2.7113E-13 | -1.21 | 2.805E-17 |
| AT1G67710 | -1.45 | 2.1396E-11 | -1.21 | 1.3687E-06 |
| AT3G47620 | -2.97 | 5.884E-204 | -1.20 | 1.2693E-33 |
| AT3G11540 | -0.52 | 1.8014E-05 | -0.98 | 1.8354E-13 |
| AT5G02810 | -0.47 | 0.00015652 | -0.88 | 8.6068E-11 |
| AT5G20040 | -0.44 | 6.1867E-06 | -0.70 | 4.4465E-12 |
| AT5G49720 | -0.51 | 8.4319E-05 | -0.68 | 2.4582E-06 |
| AT1G27210 | -0.38 | 0.00102045 | -0.59 | 2.9356E-06 |
| AT3G29350 | 0.87 | 2.0132E-12 | 0.42 | 0.00441259 |
| AT3G57040 | 0.42 | 0.00028577 | 0.43 | 0.00090093 |
| AT5G14420 | 0.81 | 1.0695E-17 | 0.45 | 6.0043E-05 |
| AT1G17440 | 0.69 | 1.1987E-06 | 0.54 | 0.00110801 |
| AT4G16110 | 0.86 | 1.9622E-14 | 0.63 | 1.246E-06 |
| AT4G38630 | 0.46 | 4.608E-05 | 0.72 | 7.382E-09 |
| AT1G03430 | 0.76 | 1.4346E-08 | 0.98 | 2.704E-11 |
| AT4G31920 | 0.98 | 5.4638E-19 | 1.00 | 1.8918E-16 |
| AT2G01830 | 1.16 | 9.0496E-07 | 1.08 | 7.708E-05 |
| AT2G40230 | 1.58 | 1.6109E-13 | 1.11 | 9.7657E-06 |
| AT3G23630 | 2.45 | 8.578E-07 | 2.70 | 8.231E-08 |

**Supplemental Table 3.** List of the 338 putative WOX4 downstream targets based on the RNA-seq data using the *pWOX4:WOX4-GR* line without subtraction of genes also identified in the *wox4-1* control line. Padj value threshold = 0.1, log2FC threshold = >0.5/ <-0.5.

| Gene | BaseMean | log2FC | LfcSE | Stat | Pvalue | Padj value |
|---|---|---|---|---|---|---|
| AT3G19480 | 174.720 | -0.97 | 0.2688 | -3.6259 | 0.000287968 | 0.033635881 |
| AT4G20820 | 211.746 | -0.94 | 0.2936 | -3.2123 | 0.001316598 | 0.08954532 |
| AT2G43140 | 234.693 | 1.10 | 0.2884 | 3.8136 | 0.00013694 | 0.02164058 |
| AT3G62950 | 17.675 | -2.44 | 0.7156 | -3.4115 | 0.000645962 | 0.058087897 |
| AT4G17460 | 694.361 | -0.88 | 0.1902 | -4.6401 | 3.48231E-06 | 0.001313015 |
| AT1G68670 | 460.150 | -0.98 | 0.2698 | -3.6229 | 0.000291369 | 0.033849191 |
| AT3G48870 | 487.471 | -1.17 | 0.2044 | -5.7043 | 1.16819E-08 | 1.14122E-05 |
| AT4G02800 | 363.321 | 1.67 | 0.5017 | 3.3281 | 0.000874314 | 0.070337802 |
| AT1G74930 | 30.416 | -2.08 | 0.5507 | -3.7848 | 0.000153812 | 0.023245458 |

| | | | | | | |
|---|---|---|---|---|---|---|
| AT5G63660 | 155.789 | 1.07 | 0.2346 | 4.5622 | 5.06143E-06 | 0.001699692 |
| AT1G76590 | 146.616 | -1.04 | 0.3229 | -3.2262 | 0.001254464 | 0.087919419 |
| AT5G40460 | 45.415 | -1.29 | 0.3973 | -3.2552 | 0.001133202 | 0.083122095 |
| AT5G24150 | 58.871 | -1.69 | 0.3555 | -4.7656 | 1.88249E-06 | 0.000778046 |
| AT3G14770 | 219.867 | -0.96 | 0.2234 | -4.2767 | 1.89644E-05 | 0.004882967 |
| AT1G01480 | 24.760 | 2.00 | 0.6195 | 3.2259 | 0.001255875 | 0.087919419 |
| AT1G01120 | 626.698 | -0.75 | 0.2297 | -3.2515 | 0.001147999 | 0.083636619 |
| AT1G07720 | 320.178 | -0.90 | 0.2802 | -3.2187 | 0.001287656 | 0.08869972 |
| AT4G11080 | 774.699 | 1.68 | 0.4704 | 3.5677 | 0.000360079 | 0.039483803 |
| AT1G13700 | 182.157 | -1.13 | 0.3289 | -3.4258 | 0.000612913 | 0.056293738 |
| AT1G04620 | 193.178 | 0.83 | 0.2393 | 3.4706 | 0.000519211 | 0.05026521 |
| AT2G46510 | 64.373 | -1.17 | 0.3275 | -3.5633 | 0.000366198 | 0.039749133 |
| AT4G22780 | 332.435 | 1.34 | 0.3598 | 3.7349 | 0.000187777 | 0.02563475 |
| AT1G64740 | 62.341 | -1.11 | 0.3272 | -3.3899 | 0.000699094 | 0.0604706 |
| AT4G17920 | 12.935 | -1.82 | 0.5489 | -3.3199 | 0.000900541 | 0.071155983 |
| AT3G11110 | 48.943 | -1.26 | 0.3446 | -3.6554 | 0.000256808 | 0.03153892 |
| AT5G47610 | 112.864 | -0.91 | 0.2430 | -3.7374 | 0.000185958 | 0.025619251 |
| AT3G20395 | 393.503 | 1.44 | 0.3009 | 4.7955 | 1.62276E-06 | 0.00068385 |
| AT1G22500 | 323.420 | -1.29 | 0.3527 | -3.6455 | 0.000266894 | 0.032407292 |
| AT2G23130 | 362.493 | -0.79 | 0.2341 | -3.3922 | 0.000693288 | 0.0604706 |
| AT2G44080 | 784.605 | 1.90 | 0.2736 | 6.9307 | 4.18856E-12 | 1.28601E-08 |
| AT2G33793 | 120.272 | 1.02 | 0.3212 | 3.1741 | 0.001502794 | 0.098170329 |
| AT3G28270 | 117.294 | -1.78 | 0.3585 | -4.9626 | 6.9545E-07 | 0.000347596 |
| AT1G17840 | 283.394 | -1.03 | 0.3099 | -3.3102 | 0.000932367 | 0.073132949 |
| AT3G55130 | 111.051 | -1.96 | 0.3624 | -5.4080 | 6.37184E-08 | 4.72219E-05 |
| AT3G52310 | 8.983 | -3.64 | 0.9671 | -3.7676 | 0.000164837 | 0.024053198 |
| AT1G08570 | 601.814 | -0.84 | 0.1848 | -4.5650 | 4.9947E-06 | 0.001699692 |
| AT5G61440 | 561.745 | -0.90 | 0.2140 | -4.1841 | 2.86334E-05 | 0.006617089 |
| AT4G12770 | 1101.635 | 1.19 | 0.3740 | 3.1695 | 0.001526813 | 0.09899103 |
| AT3G59900 | 254.883 | 2.19 | 0.3123 | 7.0008 | 2.54583E-12 | 9.11916E-09 |
| AT5G15830 | 85.245 | -1.37 | 0.2610 | -5.2652 | 1.40046E-07 | 9.12084E-05 |
| AT3G49760 | 13.127 | -1.81 | 0.5306 | -3.4085 | 0.000653312 | 0.058504118 |
| AT1G68520 | 2262.594 | -0.90 | 0.1564 | -5.7602 | 8.4016E-09 | 9.50354E-06 |
| AT5G62390 | 11025.907 | 1.58 | 0.4697 | 3.3576 | 0.000786248 | 0.06524344 |
| AT5G18670 | 573.568 | -0.93 | 0.1972 | -4.7299 | 2.24681E-06 | 0.000877971 |
| AT3G44450 | 126.854 | -0.92 | 0.2512 | -3.6819 | 0.000231483 | 0.02928895 |
| AT3G12920 | 374.489 | 0.66 | 0.1937 | 3.3877 | 0.000704737 | 0.0604706 |
| AT1G18400 | 509.317 | 2.08 | 0.3446 | 6.0301 | 1.63828E-09 | 2.34733E-06 |
| AT1G73830 | 488.126 | 0.84 | 0.1902 | 4.4169 | 1.00123E-05 | 0.003021566 |
| AT4G37610 | 515.620 | -2.53 | 0.3916 | -6.4719 | 9.67973E-11 | 1.89124E-07 |
| AT5G49480 | 767.788 | -0.78 | 0.2286 | -3.3947 | 0.000686926 | 0.060391472 |
| AT1G49660 | 948.615 | 0.68 | 0.2112 | 3.2395 | 0.001197461 | 0.085693329 |
| AT2G25090 | 55.166 | -1.25 | 0.3395 | -3.6774 | 0.00023566 | 0.029618761 |
| AT1G06450 | 87.444 | 2.20 | 0.5813 | 3.7839 | 0.000154364 | 0.023245458 |
| AT3G27170 | 74.957 | -0.94 | 0.2655 | -3.5462 | 0.000390811 | 0.041381643 |
| AT4G35440 | 77.208 | -1.10 | 0.2761 | -3.9777 | 6.95983E-05 | 0.013355416 |
| AT4G17090 | 383.725 | -1.22 | 0.3715 | -3.2707 | 0.001072666 | 0.080890289 |

| | | | | | | |
|---|---|---|---|---|---|---|
| AT2G37770 | 133.263 | -1.66 | 0.4349 | -3.8093 | 0.000139363 | 0.021862733 |
| AT2G30490 | 1547.031 | -0.55 | 0.1552 | -3.5681 | 0.000359548 | 0.039483803 |
| AT1G15950 | 35.133 | -1.26 | 0.3897 | -3.2292 | 0.001241317 | 0.087757863 |
| AT2G46830 | 265.412 | -1.04 | 0.1998 | -5.2221 | 1.76888E-07 | 0.000105602 |
| AT2G21660 | 20844.259 | 0.99 | 0.2736 | 3.6160 | 0.000299241 | 0.034027946 |
| AT5G53420 | 513.767 | 0.79 | 0.2430 | 3.2664 | 0.001089126 | 0.08155923 |
| AT3G02380 | 43.426 | -1.26 | 0.3850 | -3.2824 | 0.001029237 | 0.078912565 |
| AT3G21870 | 66.886 | -1.14 | 0.3343 | -3.4116 | 0.000645944 | 0.058087897 |
| AT5G62430 | 65.185 | -1.42 | 0.3269 | -4.3447 | 1.39486E-05 | 0.003893296 |
| AT3G48350 | 143.575 | -0.95 | 0.2504 | -3.7950 | 0.000147634 | 0.022826906 |
| AT4G11470 | 5.024 | 2.98 | 0.8560 | 3.4845 | 0.000493014 | 0.048382933 |
| AT5G40380 | 78.525 | -0.99 | 0.3050 | -3.2566 | 0.001127375 | 0.082977892 |
| AT5G25140 | 98.185 | -1.03 | 0.2784 | -3.6866 | 0.000227286 | 0.029110768 |
| AT1G13080 | 269.999 | -1.33 | 0.2649 | -5.0079 | 5.50284E-07 | 0.000288456 |
| AT3G26290 | 907.519 | -0.81 | 0.2553 | -3.1810 | 0.00146783 | 0.096842731 |
| AT2G34500 | 73.870 | -1.14 | 0.2766 | -4.1251 | 3.70593E-05 | 0.008296644 |
| AT3G14620 | 474.524 | -1.09 | 0.3069 | -3.5656 | 0.000362967 | 0.039598369 |
| AT4G31950 | 9.295 | 6.17 | 1.5692 | 3.9289 | 8.53525E-05 | 0.015545726 |
| AT4G00360 | 94.690 | -1.63 | 0.2931 | -5.5502 | 2.85348E-08 | 2.45308E-05 |
| AT5G66640 | 24.525 | 1.62 | 0.4951 | 3.2817 | 0.001031753 | 0.078912565 |
| AT5G17890 | 1595.612 | 1.47 | 0.4492 | 3.2629 | 0.001102605 | 0.081997214 |
| AT4G14140 | 12.129 | 1.70 | 0.4739 | 3.5897 | 0.000331113 | 0.036871955 |
| AT5G55970 | 140.603 | -1.64 | 0.4493 | -3.6464 | 0.000265959 | 0.032407292 |
| AT5G60800 | 325.437 | 1.10 | 0.3215 | 3.4137 | 0.000640916 | 0.058087897 |
| AT3G55830 | 112.020 | -0.82 | 0.2575 | -3.1992 | 0.001377935 | 0.091970716 |
| AT2G01850 | 2286.330 | -0.84 | 0.2004 | -4.2167 | 2.47854E-05 | 0.005897135 |
| AT2G20880 | 13.905 | -2.96 | 0.6850 | -4.3204 | 1.55773E-05 | 0.004292142 |
| AT5G44210 | 118.132 | 0.96 | 0.2375 | 4.0513 | 5.09317E-05 | 0.010627428 |
| AT3G23150 | 587.493 | 1.40 | 0.3044 | 4.6093 | 4.04022E-06 | 0.001447206 |
| AT2G47520 | 32.227 | 2.87 | 0.4658 | 6.1507 | 7.71211E-10 | 1.18392E-06 |
| AT2G31230 | 310.815 | 0.97 | 0.2288 | 4.2554 | 2.08645E-05 | 0.005095668 |
| AT1G26770 | 197.445 | -0.89 | 0.2630 | -3.3876 | 0.000704965 | 0.0604706 |
| AT3G29030 | 161.242 | -1.35 | 0.3721 | -3.6316 | 0.000281641 | 0.033442115 |
| AT2G40610 | 82.325 | -1.17 | 0.2874 | -4.0842 | 4.42234E-05 | 0.009375893 |
| AT2G17036 | 70.752 | 1.69 | 0.3169 | 5.3433 | 9.12873E-08 | 6.13108E-05 |
| AT5G55150 | 8.008 | 3.98 | 1.2319 | 3.2279 | 0.001246997 | 0.087870355 |
| AT5G49730 | 515.148 | -1.15 | 0.2952 | -3.9044 | 9.44599E-05 | 0.016505142 |
| AT5G49740 | 252.872 | -1.00 | 0.2444 | -4.0888 | 4.33648E-05 | 0.009319962 |
| AT1G07050 | 133.234 | 1.51 | 0.3797 | 3.9818 | 6.83863E-05 | 0.01324107 |
| AT5G46330 | 840.751 | 0.91 | 0.2431 | 3.7533 | 0.000174515 | 0.024838864 |
| AT4G28300 | 611.189 | -0.60 | 0.1829 | -3.2754 | 0.001054965 | 0.07983562 |
| AT1G43800 | 586.078 | 2.01 | 0.5539 | 3.6332 | 0.000279874 | 0.033417003 |
| AT2G25650 | 77.839 | 2.00 | 0.6221 | 3.2161 | 0.001299261 | 0.089213145 |
| AT5G56300 | 28.042 | 1.83 | 0.4760 | 3.8453 | 0.000120383 | 0.019902151 |
| AT5G59845 | 17.171 | -1.75 | 0.5152 | -3.3998 | 0.000674307 | 0.059638743 |
| AT2G24762 | 493.035 | -0.65 | 0.1866 | -3.4969 | 0.000470626 | 0.047045107 |
| AT3G30725 | 2.259 | -4.20 | 1.2879 | -3.2594 | 0.001116556 | 0.082463966 |

| | | | | | | |
|---|---|---|---|---|---|---|
| AT2G29450 | 947.732 | -0.86 | 0.2239 | -3.8430 | 0.00012156 | 0.019943341 |
| AT4G01950 | 113.725 | -1.19 | 0.2831 | -4.1875 | 2.82057E-05 | 0.006589103 |
| AT5G41080 | 1084.459 | -1.44 | 0.4061 | -3.5365 | 0.000405533 | 0.042724099 |
| AT5G44190 | 932.574 | -0.88 | 0.2541 | -3.4533 | 0.000553675 | 0.052421063 |
| AT5G28300 | 2010.694 | 1.88 | 0.4641 | 4.0423 | 5.29295E-05 | 0.010938082 |
| AT5G62020 | 99.377 | -1.17 | 0.2858 | -4.0828 | 4.44975E-05 | 0.009375893 |
| AT5G50740 | 1582.028 | 1.52 | 0.4768 | 3.1875 | 0.001435063 | 0.095192513 |
| AT5G67060 | 95.114 | 1.97 | 0.2998 | 6.5773 | 4.79022E-11 | 1.1439E-07 |
| AT2G16060 | 1129.451 | 1.41 | 0.3849 | 3.6638 | 0.00024849 | 0.031049734 |
| AT5G14570 | 880.836 | 0.75 | 0.1898 | 3.9650 | 7.33831E-05 | 0.013834647 |
| AT3G61890 | 242.514 | -0.83 | 0.2322 | -3.5714 | 0.000355116 | 0.039341047 |
| AT5G53980 | 83.943 | 1.54 | 0.4087 | 3.7590 | 0.000170563 | 0.024438294 |
| AT1G25550 | 914.001 | -0.89 | 0.2393 | -3.7340 | 0.000188456 | 0.02563475 |
| AT3G24715 | 27.052 | -1.51 | 0.3967 | -3.8027 | 0.000143155 | 0.022294826 |
| AT4G26670 | 886.130 | 0.78 | 0.2342 | 3.3244 | 0.000886062 | 0.070792763 |
| AT3G10040 | 870.625 | 2.74 | 0.4200 | 6.5230 | 6.89212E-11 | 1.48125E-07 |
| AT4G32280 | 15.272 | 1.86 | 0.5734 | 3.2427 | 0.001184135 | 0.08511512 |
| AT2G34600 | 33.873 | -2.79 | 0.6230 | -4.4735 | 7.69661E-06 | 0.002468888 |
| AT1G23390 | 1592.518 | -2.02 | 0.3003 | -6.7244 | 1.76368E-11 | 4.73813E-08 |
| AT1G80440 | 1298.312 | -1.72 | 0.4210 | -4.0910 | 4.29438E-05 | 0.009319962 |
| AT1G01060 | 119.791 | -1.51 | 0.2923 | -5.1611 | 2.45497E-07 | 0.000138848 |
| AT3G59530 | 53.135 | 1.04 | 0.3154 | 3.2840 | 0.001023457 | 0.078912565 |
| AT5G59310 | 238.404 | -1.96 | 0.5775 | -3.3941 | 0.000688438 | 0.060391472 |
| AT3G04290 | 948.419 | -0.60 | 0.1871 | -3.2231 | 0.001268051 | 0.088483588 |
| AT3G10525 | 140.209 | -0.75 | 0.2200 | -3.4140 | 0.000640058 | 0.058087897 |
| AT2G02100 | 2040.264 | 0.73 | 0.1661 | 4.4145 | 1.01225E-05 | 0.003021566 |
| AT3G08870 | 8.572 | -2.76 | 0.7621 | -3.6163 | 0.000298853 | 0.034027946 |
| AT1G26800 | 171.925 | -1.40 | 0.4161 | -3.3607 | 0.0007775 | 0.06524344 |
| AT1G09575 | 70.546 | -0.98 | 0.2999 | -3.2665 | 0.001089045 | 0.08155923 |
| AT1G70830 | 3165.125 | -1.14 | 0.3042 | -3.7324 | 0.000189675 | 0.025638374 |
| AT3G24500 | 41.933 | -1.37 | 0.3781 | -3.6341 | 0.000278935 | 0.033417003 |
| AT1G66230 | 69.253 | -1.49 | 0.4033 | -3.6937 | 0.000221031 | 0.028830212 |
| AT3G53200 | 25.634 | 2.40 | 0.4230 | 5.6629 | 1.48866E-08 | 1.39106E-05 |
| AT1G74650 | 88.841 | 1.26 | 0.3739 | 3.3645 | 0.000766747 | 0.064623263 |
| AT5G54230 | 48.726 | -1.30 | 0.4097 | -3.1636 | 0.001558301 | 0.099379848 |
| AT3G15510 | 420.622 | -0.94 | 0.2930 | -3.2123 | 0.001316591 | 0.08954532 |
| AT3G15500 | 453.037 | -1.97 | 0.3684 | -5.3600 | 8.32446E-08 | 5.77126E-05 |
| AT3G11660 | 341.327 | -1.10 | 0.2980 | -3.7053 | 0.000211157 | 0.028013482 |
| AT4G14760 | 146.596 | -0.91 | 0.2329 | -3.9256 | 8.64966E-05 | 0.015621727 |
| AT5G04950 | 777.072 | -1.35 | 0.3453 | -3.9121 | 9.14782E-05 | 0.016248349 |
| AT5G64170 | 180.593 | -1.38 | 0.2449 | -5.6464 | 1.63809E-08 | 1.46691E-05 |
| AT3G12320 | 298.737 | -0.82 | 0.1918 | -4.2830 | 1.84387E-05 | 0.004832739 |
| AT4G19170 | 493.847 | -1.32 | 0.3545 | -3.7179 | 0.000200896 | 0.02698538 |
| AT1G62580 | 45.650 | 1.37 | 0.4266 | 3.2190 | 0.001286329 | 0.08869972 |
| AT3G44300 | 71.353 | -1.43 | 0.4009 | -3.5558 | 0.000376834 | 0.040494572 |
| AT4G10380 | 984.277 | 1.07 | 0.3377 | 3.1673 | 0.001538387 | 0.09899103 |
| AT3G21670 | 245.568 | -1.77 | 0.2342 | -7.5586 | 4.07298E-14 | 2.18841E-10 |

| | | | | | | |
|---|---|---|---|---|---|---|
| AT2G41230 | 198.553 | 2.22 | 0.4063 | 5.4703 | 4.49161E-08 | 3.71284E-05 |
| AT2G40000 | 1042.659 | -2.01 | 0.4981 | -4.0257 | 5.68094E-05 | 0.01162808 |
| AT2G28120 | 218.484 | -1.29 | 0.2252 | -5.7053 | 1.16144E-08 | 1.14122E-05 |
| AT5G56550 | 280.663 | -3.06 | 0.3289 | -9.2932 | 1.49762E-20 | 3.21868E-16 |
| AT1G72150 | 13168.333 | 1.34 | 0.3923 | 3.4180 | 0.000630893 | 0.057698516 |
| AT2G14610 | 9.203 | 2.82 | 0.7256 | 3.8873 | 0.000101373 | 0.017429637 |
| AT4G19420 | 1643.727 | -1.34 | 0.3438 | -3.9049 | 9.42592E-05 | 0.016505142 |
| AT3G53260 | 1339.600 | -0.54 | 0.1605 | -3.3787 | 0.000728302 | 0.061868279 |
| AT3G61060 | 169.628 | -1.68 | 0.3830 | -4.3947 | 1.10932E-05 | 0.003221814 |
| AT1G09530 | 534.781 | 0.78 | 0.2105 | 3.6933 | 0.000221337 | 0.028830212 |
| AT4G02075 | 217.292 | -1.34 | 0.2731 | -4.8890 | 1.0135E-06 | 0.000484049 |
| AT5G15120 | 787.117 | 1.06 | 0.3356 | 3.1710 | 0.001519056 | 0.09893197 |
| AT5G39890 | 350.180 | 2.37 | 0.4527 | 5.2379 | 1.62396E-07 | 0.000102654 |
| AT3G53420 | 8153.953 | -0.77 | 0.2307 | -3.3416 | 0.00083285 | 0.068059369 |
| AT4G28460 | 17.208 | 3.88 | 0.8703 | 4.4568 | 8.31976E-06 | 0.002591425 |
| AT2G46790 | 45.588 | -1.25 | 0.3366 | -3.7026 | 0.0002134 | 0.028137362 |
| AT2G33750 | 16.131 | -1.63 | 0.4916 | -3.3224 | 0.000892567 | 0.070795211 |
| AT4G33070 | 86.740 | 2.47 | 0.2917 | 8.4555 | 2.77833E-17 | 1.9904E-13 |
| AT3G05370 | 134.039 | 1.29 | 0.2651 | 4.8480 | 1.24734E-06 | 0.000553197 |
| AT1G13260 | 986.905 | -1.41 | 0.2912 | -4.8362 | 1.32354E-06 | 0.000568909 |
| AT1G68840 | 1544.738 | -0.78 | 0.2046 | -3.8188 | 0.000134092 | 0.021506758 |
| AT1G22190 | 575.335 | -1.20 | 0.3034 | -3.9703 | 7.1781E-05 | 0.013652369 |
| AT5G62920 | 297.698 | 1.06 | 0.2648 | 3.9877 | 6.67287E-05 | 0.013037568 |
| AT1G19050 | 245.941 | 0.90 | 0.2374 | 3.7835 | 0.000154667 | 0.023245458 |
| AT5G24655 | 87.372 | 1.40 | 0.4386 | 3.2030 | 0.001360142 | 0.091350571 |
| AT5G25610 | 2312.323 | -0.66 | 0.1813 | -3.6186 | 0.00029621 | 0.034027946 |
| AT4G27410 | 311.661 | -1.35 | 0.2483 | -5.4295 | 5.65203E-08 | 4.49902E-05 |
| AT2G37180 | 605.226 | -0.95 | 0.2062 | -4.6241 | 3.76249E-06 | 0.001370568 |
| AT5G04890 | 284.636 | 1.35 | 0.4129 | 3.2605 | 0.00111222 | 0.08242698 |
| AT5G17300 | 136.170 | -1.47 | 0.3439 | -4.2675 | 1.97663E-05 | 0.004882967 |
| AT3G09600 | 121.422 | -0.83 | 0.2364 | -3.5298 | 0.00041583 | 0.043087704 |
| AT2G02990 | 31.587 | -1.83 | 0.5532 | -3.3065 | 0.00094461 | 0.073556389 |
| AT5G44280 | 569.505 | 1.64 | 0.5055 | 3.2370 | 0.001208128 | 0.085693329 |
| AT4G03510 | 601.910 | -1.30 | 0.3434 | -3.7754 | 0.000159764 | 0.023844775 |
| AT5G22920 | 3196.877 | -1.05 | 0.3118 | -3.3530 | 0.000799445 | 0.066083362 |
| AT2G17450 | 279.629 | -0.93 | 0.2671 | -3.4992 | 0.000466688 | 0.046869462 |
| AT1G13245 | 969.220 | -0.99 | 0.2934 | -3.3872 | 0.000706222 | 0.0604706 |
| AT1G67265 | 48.581 | -1.64 | 0.4946 | -3.3086 | 0.000937557 | 0.073272651 |
| AT1G07350 | 437.863 | -0.87 | 0.2161 | -4.0212 | 5.78922E-05 | 0.011737912 |
| AT4G26690 | 335.657 | -0.67 | 0.2052 | -3.2459 | 0.00117065 | 0.08442822 |
| AT1G11185 | 164.999 | 1.05 | 0.3039 | 3.4491 | 0.000562477 | 0.053020841 |
| AT3G47720 | 3.441 | 3.74 | 1.1665 | 3.2104 | 0.001325303 | 0.089853029 |
| AT1G21850 | 9.189 | 3.74 | 1.1755 | 3.1788 | 0.001478634 | 0.097005756 |
| AT4G34770 | 158.430 | 1.27 | 0.2961 | 4.3001 | 1.707E-05 | 0.004529247 |
| AT4G34810 | 169.670 | 1.19 | 0.2792 | 4.2691 | 1.96304E-05 | 0.004882967 |
| AT2G21200 | 24.528 | 1.53 | 0.4306 | 3.5495 | 0.000386035 | 0.041276917 |
| AT5G24160 | 198.219 | -1.01 | 0.2404 | -4.2151 | 2.49693E-05 | 0.005897135 |

| | | | | | | |
|---|---|---|---|---|---|---|
| AT2G46340 | 576.176 | -0.61 | 0.1730 | -3.5291 | 0.000417004 | 0.043087704 |
| AT3G22380 | 5723.573 | 1.35 | 0.4082 | 3.2957 | 0.000981748 | 0.076172317 |
| AT5G37770 | 282.565 | -0.90 | 0.2506 | -3.6074 | 0.00030923 | 0.034978846 |
| AT5G57560 | 436.550 | -1.76 | 0.3603 | -4.8710 | 1.11028E-06 | 0.000507703 |
| AT4G09820 | 17.106 | 1.65 | 0.5107 | 3.2373 | 0.001206675 | 0.085693329 |
| AT2G18700 | 782.641 | -0.91 | 0.2804 | -3.2520 | 0.001145804 | 0.083636619 |
| AT1G70290 | 1167.487 | -1.25 | 0.2791 | -4.4917 | 7.06461E-06 | 0.002300495 |
| AT2G30424 | 143.389 | 0.87 | 0.2520 | 3.4348 | 0.000592956 | 0.054930237 |
| AT4G34138 | 77.394 | -1.72 | 0.3506 | -4.8995 | 9.60591E-07 | 0.000469205 |
| AT1G22370 | 111.374 | -0.97 | 0.2990 | -3.2387 | 0.001200954 | 0.085693329 |
| AT1G79680 | 7.245 | 3.95 | 1.0661 | 3.7082 | 0.00020875 | 0.027866151 |
| AT4G33560 | 684.803 | 3.01 | 0.6031 | 4.9926 | 5.95836E-07 | 0.000304898 |
| AT5G24110 | 22.129 | 3.52 | 1.1086 | 3.1785 | 0.001480453 | 0.097005756 |
| AT3G27220 | 478.777 | 2.39 | 0.2598 | 9.1863 | 4.06463E-20 | 4.36785E-16 |
| AT5G35777 | 74.909 | -3.01 | 0.4137 | -7.2761 | 3.43673E-13 | 1.47725E-09 |
| AT5G03230 | 616.335 | -1.64 | 0.2546 | -6.4358 | 1.22818E-10 | 2.19966E-07 |
| AT5G21940 | 1511.155 | -2.09 | 0.3268 | -6.3896 | 1.66359E-10 | 2.7503E-07 |
| AT5G19190 | 533.764 | -1.27 | 0.2116 | -6.0114 | 1.83952E-09 | 2.47094E-06 |
| AT2G17850 | 30.266 | 4.04 | 0.6781 | 5.9551 | 2.59967E-09 | 3.2866E-06 |
| AT2G20670 | 2355.947 | -2.29 | 0.3893 | -5.8935 | 3.78202E-09 | 4.51573E-06 |
| AT4G24110 | 206.661 | 1.56 | 0.2721 | 5.7400 | 9.46654E-09 | 1.01727E-05 |
| AT5G28610 | 113.265 | 1.34 | 0.2470 | 5.4132 | 6.19007E-08 | 4.72219E-05 |
| AT1G02610 | 308.569 | -1.52 | 0.2835 | -5.3701 | 7.87113E-08 | 5.63888E-05 |
| AT5G60680 | 780.407 | -1.26 | 0.2415 | -5.2253 | 1.73835E-07 | 0.000105602 |
| AT2G15830 | 191.410 | 1.53 | 0.2934 | 5.2124 | 1.8642E-07 | 0.000108285 |
| AT3G07350 | 269.963 | -1.55 | 0.3019 | -5.1477 | 2.63687E-07 | 0.000141679 |
| AT4G32480 | 858.530 | -1.95 | 0.3786 | -5.1485 | 2.62641E-07 | 0.000141679 |
| AT1G49570 | 103.166 | 2.03 | 0.4162 | 4.8749 | 1.08839E-06 | 0.000507703 |
| AT4G16146 | 196.689 | 1.25 | 0.2586 | 4.8458 | 1.26124E-06 | 0.000553197 |
| AT1G60590 | 26.950 | -2.01 | 0.4248 | -4.7318 | 2.22576E-06 | 0.000877971 |
| AT2G28200 | 228.513 | -1.32 | 0.2791 | -4.7362 | 2.17737E-06 | 0.000877971 |
| AT2G28815 | 57.459 | 1.66 | 0.3524 | 4.6991 | 2.61308E-06 | 0.001002862 |
| AT3G28580 | 69.312 | 2.96 | 0.6403 | 4.6242 | 3.76086E-06 | 0.001370568 |
| AT3G19030 | 919.654 | -0.86 | 0.1865 | -4.5935 | 4.35966E-06 | 0.001536031 |
| AT1G28190 | 248.038 | 1.67 | 0.3636 | 4.5900 | 4.43271E-06 | 0.001536577 |
| AT5G19120 | 2058.730 | -1.57 | 0.3492 | -4.5100 | 6.4817E-06 | 0.002143149 |
| AT3G06435 | 51.341 | 2.25 | 0.5047 | 4.4643 | 8.03492E-06 | 0.002539508 |
| AT3G12910 | 5.448 | 6.38 | 1.4337 | 4.4486 | 8.6426E-06 | 0.002653527 |
| AT4G09630 | 142.084 | -1.01 | 0.2284 | -4.4045 | 1.06042E-05 | 0.003121995 |
| AT4G13575 | 269.447 | -0.88 | 0.2006 | -4.3807 | 1.18275E-05 | 0.003389293 |
| AT1G06420 | 90.687 | 1.20 | 0.2758 | 4.3453 | 1.391E-05 | 0.003893296 |
| AT1G13470 | 9.747 | 3.03 | 0.7024 | 4.3103 | 1.63057E-05 | 0.004389395 |
| AT1G17665 | 332.435 | 2.21 | 0.5132 | 4.3098 | 1.63387E-05 | 0.004389395 |
| AT1G12805 | 21.281 | 2.52 | 0.5896 | 4.2683 | 1.96974E-05 | 0.004882967 |
| AT3G22970 | 1167.137 | -1.03 | 0.2409 | -4.2752 | 1.90946E-05 | 0.004882967 |
| AT2G38820 | 219.846 | -1.49 | 0.3523 | -4.2224 | 2.41668E-05 | 0.005835882 |
| AT5G59000 | 112.759 | 1.71 | 0.4111 | 4.1705 | 3.03932E-05 | 0.006949052 |

| | | | | | | |
|---|---|---|---|---|---|---|
| AT2G14247 | 22.627 | 3.81 | 0.9200 | 4.1401 | 3.47192E-05 | 0.007854572 |
| AT2G17845 | 7.419 | 5.80 | 1.4093 | 4.1178 | 3.82507E-05 | 0.008475088 |
| AT1G64500 | 429.718 | -0.91 | 0.2216 | -4.1117 | 3.92682E-05 | 0.00861175 |
| AT1G23205 | 103.274 | -1.03 | 0.2560 | -4.0184 | 5.85839E-05 | 0.011767154 |
| AT1G08643 | 164.751 | 2.70 | 0.6743 | 3.9975 | 6.40264E-05 | 0.012741258 |
| AT2G41250 | 495.392 | -0.76 | 0.1903 | -3.9933 | 6.51716E-05 | 0.01285017 |
| AT1G05035 | 67.936 | 2.02 | 0.5125 | 3.9421 | 8.07834E-05 | 0.015097365 |
| AT3G54520 | 15.076 | 2.84 | 0.7218 | 3.9363 | 8.27609E-05 | 0.015333598 |
| AT5G03890 | 91.520 | 1.40 | 0.3552 | 3.9298 | 8.50234E-05 | 0.015545726 |
| AT2G25200 | 166.306 | -1.85 | 0.4733 | -3.9133 | 9.10368E-05 | 0.016248349 |
| AT5G54300 | 90.611 | -1.25 | 0.3203 | -3.8888 | 0.000100741 | 0.017429637 |
| AT5G54170 | 461.642 | -0.98 | 0.2540 | -3.8623 | 0.000112313 | 0.019157433 |
| AT2G03750 | 346.023 | -0.92 | 0.2404 | -3.8469 | 0.000119639 | 0.019902151 |
| AT2G04495 | 7.360 | 4.93 | 1.2817 | 3.8476 | 0.000119303 | 0.019902151 |
| AT4G14500 | 167.818 | -0.91 | 0.2358 | -3.8505 | 0.000117879 | 0.019902151 |
| AT2G24240 | 118.059 | -1.21 | 0.3145 | -3.8386 | 0.000123714 | 0.019991423 |
| AT4G30570 | 86.562 | 1.00 | 0.2598 | 3.8387 | 0.000123695 | 0.019991423 |
| AT5G57510 | 6.702 | 3.78 | 0.9902 | 3.8156 | 0.000135857 | 0.021628415 |
| AT2G24550 | 825.450 | -1.03 | 0.2711 | -3.7879 | 0.000151956 | 0.023245458 |
| AT3G51340 | 41.408 | 1.24 | 0.3286 | 3.7727 | 0.000161479 | 0.023934593 |
| AT1G78450 | 76.660 | -1.31 | 0.3484 | -3.7647 | 0.000166756 | 0.024053198 |
| AT3G49790 | 374.137 | -1.19 | 0.3163 | -3.7666 | 0.000165477 | 0.024053198 |
| AT3G63445 | 112.007 | 1.01 | 0.2690 | 3.7661 | 0.000165802 | 0.024053198 |
| AT1G55960 | 333.771 | -0.87 | 0.2316 | -3.7477 | 0.000178472 | 0.025235015 |
| AT4G14620 | 187.693 | -1.04 | 0.2785 | -3.7420 | 0.000182543 | 0.025463217 |
| AT5G41900 | 23.411 | -1.53 | 0.4086 | -3.7405 | 0.00018364 | 0.025463217 |
| AT5G59080 | 200.872 | -1.02 | 0.2735 | -3.7432 | 0.000181658 | 0.025463217 |
| AT5G22310 | 381.026 | 0.99 | 0.2678 | 3.6918 | 0.00022268 | 0.028830295 |
| AT5G66985 | 98.301 | 1.39 | 0.3759 | 3.6863 | 0.000227555 | 0.029110768 |
| AT2G44660 | 48.554 | -1.20 | 0.3251 | -3.6817 | 0.000231673 | 0.02928895 |
| AT4G30470 | 322.970 | -0.73 | 0.1988 | -3.6590 | 0.000253225 | 0.031458442 |
| AT5G48740 | 17.495 | -1.78 | 0.4866 | -3.6566 | 0.000255619 | 0.03153892 |
| AT2G15020 | 3.258 | -4.70 | 1.2906 | -3.6405 | 0.00027208 | 0.032851362 |
| AT4G35940 | 399.116 | 1.62 | 0.4452 | 3.6298 | 0.000283589 | 0.033488464 |
| AT1G13480 | 24.023 | 2.96 | 0.8161 | 3.6273 | 0.00028642 | 0.033635881 |
| AT1G15830 | 94.227 | -0.97 | 0.2669 | -3.6171 | 0.000297931 | 0.034027946 |
| AT1G29660 | 851.033 | -0.88 | 0.2462 | -3.5944 | 0.000325128 | 0.036584605 |
| AT2G01422 | 10.084 | -5.33 | 1.4838 | -3.5927 | 0.000327294 | 0.036636508 |
| AT1G05057 | 23.865 | 1.76 | 0.4930 | 3.5604 | 0.000370307 | 0.039993207 |
| AT3G54530 | 18.591 | 3.88 | 1.0952 | 3.5462 | 0.000390865 | 0.041381643 |
| AT3G14200 | 124.684 | -1.14 | 0.3233 | -3.5341 | 0.000409097 | 0.042889314 |
| AT4G17260 | 186.380 | 0.81 | 0.2281 | 3.5322 | 0.000412059 | 0.042990193 |
| AT4G38410 | 199.046 | 1.87 | 0.5302 | 3.5254 | 0.000422782 | 0.043475712 |
| AT2G44230 | 136.953 | -1.07 | 0.3028 | -3.5220 | 0.000428361 | 0.043839693 |
| AT5G28630 | 553.185 | 1.07 | 0.3048 | 3.5131 | 0.00044283 | 0.045105681 |
| AT1G13650 | 97.445 | -1.34 | 0.3819 | -3.5031 | 0.000459854 | 0.046618797 |
| AT3G28510 | 10.704 | 2.57 | 0.7331 | 3.4996 | 0.000465881 | 0.046869462 |

| | | | | | | |
|---|---|---|---|---|---|---|
| AT4G27900 | 248.019 | 0.81 | 0.2329 | 3.4956 | 0.000472946 | 0.047058084 |
| AT5G12900 | 129.672 | -0.85 | 0.2435 | -3.4930 | 0.000477541 | 0.04729635 |
| AT4G29905 | 1831.021 | -1.01 | 0.2894 | -3.4863 | 0.000489716 | 0.048279659 |
| AT1G07690 | 9.007 | 2.80 | 0.8049 | 3.4811 | 0.00049935 | 0.048781983 |
| AT1G47340 | 148.401 | 0.80 | 0.2306 | 3.4745 | 0.000511735 | 0.04976568 |
| AT1G32928 | 150.798 | -1.06 | 0.3043 | -3.4671 | 0.000526167 | 0.050710182 |
| AT1G53035 | 151.522 | 0.81 | 0.2341 | 3.4633 | 0.000533648 | 0.051201603 |
| AT4G13330 | 26.459 | -1.55 | 0.4469 | -3.4615 | 0.000537115 | 0.051305248 |
| AT5G61820 | 890.607 | -0.77 | 0.2241 | -3.4571 | 0.000545936 | 0.051917064 |
| AT3G46600 | 256.074 | -1.02 | 0.2968 | -3.4442 | 0.000572821 | 0.053760148 |
| AT5G60530 | 1146.987 | 2.20 | 0.6384 | 3.4415 | 0.000578592 | 0.054065621 |
| AT3G05400 | 76.251 | -1.28 | 0.3735 | -3.4401 | 0.000581516 | 0.054103664 |
| AT3G50840 | 210.025 | -1.02 | 0.2968 | -3.4319 | 0.000599378 | 0.055286862 |
| AT4G16140 | 143.142 | -0.84 | 0.2463 | -3.4031 | 0.000666299 | 0.059394515 |
| AT5G19890 | 193.685 | 1.78 | 0.5245 | 3.4021 | 0.000668782 | 0.059394515 |
| AT5G62730 | 88.885 | -1.53 | 0.4517 | -3.3909 | 0.000696761 | 0.0604706 |
| AT1G29640 | 29.513 | -1.36 | 0.4027 | -3.3799 | 0.000725203 | 0.061849441 |
| AT4G37530 | 185.695 | -0.80 | 0.2379 | -3.3727 | 0.000744472 | 0.0629929 |
| AT1G21050 | 356.255 | 0.68 | 0.2032 | 3.3583 | 0.000784298 | 0.06524344 |
| AT5G02830 | 224.155 | -0.83 | 0.2474 | -3.3579 | 0.000785475 | 0.06524344 |
| AT1G80930 | 3304.286 | 1.47 | 0.4404 | 3.3470 | 0.000816873 | 0.067265277 |
| AT5G24880 | 255.069 | 1.47 | 0.4405 | 3.3456 | 0.000820936 | 0.067341787 |
| AT5G62280 | 506.246 | 0.84 | 0.2519 | 3.3401 | 0.000837334 | 0.068166604 |
| AT1G68440 | 910.702 | -1.01 | 0.3016 | -3.3374 | 0.000845673 | 0.068585657 |
| AT4G02920 | 2011.010 | -0.57 | 0.1716 | -3.3316 | 0.000863476 | 0.069766268 |
| AT1G60060 | 140.860 | 1.06 | 0.3195 | 3.3272 | 0.000877095 | 0.070337802 |
| AT1G07160 | 18.455 | 3.13 | 0.9430 | 3.3223 | 0.000892681 | 0.070795211 |
| AT1G19000 | 1345.841 | -0.53 | 0.1597 | -3.3130 | 0.000922853 | 0.072651872 |
| AT1G80630 | 78.868 | -0.98 | 0.2973 | -3.2835 | 0.00102543 | 0.078912565 |
| AT5G45520 | 90.143 | 1.40 | 0.4270 | 3.2787 | 0.001042722 | 0.079468729 |
| AT2G40085 | 64.296 | 1.19 | 0.3637 | 3.2764 | 0.001051306 | 0.07983562 |
| AT2G07783 | 1342.320 | 1.99 | 0.6095 | 3.2631 | 0.001101968 | 0.081997214 |
| AT1G51080 | 432.343 | 1.69 | 0.5202 | 3.2487 | 0.001159268 | 0.083888875 |
| AT1G73120 | 161.897 | 1.00 | 0.3082 | 3.2488 | 0.001159054 | 0.083888875 |
| AT5G47060 | 248.728 | 0.73 | 0.2277 | 3.2204 | 0.001280275 | 0.08869972 |
| AT5G55040 | 1273.417 | 1.08 | 0.3342 | 3.2206 | 0.001279086 | 0.08869972 |
| AT5G40590 | 80.167 | 1.36 | 0.4224 | 3.2133 | 0.001312048 | 0.08954532 |
| AT1G48770 | 123.722 | 0.75 | 0.2347 | 3.2092 | 0.001331067 | 0.08996005 |
| AT2G25720 | 567.266 | 1.44 | 0.4501 | 3.2037 | 0.001356652 | 0.091350571 |
| AT3G57020 | 432.152 | -0.68 | 0.2128 | -3.2014 | 0.001367716 | 0.091573028 |
| AT5G23950 | 13.666 | -1.83 | 0.5721 | -3.1922 | 0.001411977 | 0.093951137 |
| AT5G22530 | 6.476 | 3.26 | 1.0264 | 3.1807 | 0.001468953 | 0.096842731 |
| AT2G29670 | 810.164 | -1.08 | 0.3407 | -3.1684 | 0.001532787 | 0.09899103 |
| AT5G10340 | 9.603 | 2.07 | 0.6543 | 3.1678 | 0.001535709 | 0.09899103 |
| AT2G19160 | 91.086 | -0.93 | 0.2925 | -3.1663 | 0.001543824 | 0.099044365 |
| AT1G68945 | 199.221 | 1.32 | 0.4181 | 3.1654 | 0.001548913 | 0.099075098 |
| AT5G57785 | 252.629 | -1.12 | 0.3553 | -3.1617 | 0.001568595 | 0.099740354 |

**Supplemental Table 4.** List of the 219 putative WOX4 downstream targets based on the RNA-seq data using the *pWOX4:WOX4-GR* line with subtraction of genes also identified in the *wox4-1* control line. Padj value threshold = 0.1, log2FC threshold = >0.5/ <-0.5.

| Gene | BaseMean | log2FC | LfcSE | Stat | Pvalue | Padj value |
|---|---|---|---|---|---|---|
| AT2G01422 | 10.0839087 | -5.33 | 1.4838 | -3.5927 | 0.00032729 | 0.03663651 |
| AT2G15020 | 3.25845887 | -4.70 | 1.2906 | -3.6405 | 0.00027208 | 0.03285136 |
| AT3G30725 | 2.25868047 | -4.20 | 1.2879 | -3.2594 | 0.00111656 | 0.08246397 |
| AT3G52310 | 8.98328095 | -3.64 | 0.9671 | -3.7676 | 0.00016484 | 0.0240532 |
| AT2G20880 | 13.9045465 | -2.96 | 0.6850 | -4.3204 | 1.5577E-05 | 0.00429214 |
| AT3G08870 | 8.57249671 | -2.76 | 0.7621 | -3.6163 | 0.00029885 | 0.03402795 |
| AT1G60590 | 26.949641 | -2.01 | 0.4248 | -4.7318 | 2.2258E-06 | 0.00087797 |
| AT3G15500 | 453.037415 | -1.97 | 0.3684 | -5.3600 | 8.3245E-08 | 5.7713E-05 |
| AT5G59310 | 238.404357 | -1.96 | 0.5775 | -3.3941 | 0.00068844 | 0.06039147 |
| AT3G55130 | 111.051192 | -1.96 | 0.3624 | -5.4080 | 6.3718E-08 | 4.7222E-05 |
| AT2G02990 | 31.5868095 | -1.83 | 0.5532 | -3.3065 | 0.00094461 | 0.07355639 |
| AT5G23950 | 13.665952 | -1.83 | 0.5721 | -3.1922 | 0.00141198 | 0.09395114 |
| AT4G17920 | 12.9348021 | -1.82 | 0.5489 | -3.3199 | 0.00090054 | 0.07115598 |
| AT3G49760 | 13.1269175 | -1.81 | 0.5306 | -3.4085 | 0.00065331 | 0.05850412 |
| AT5G48740 | 17.4949439 | -1.78 | 0.4866 | -3.6566 | 0.00025562 | 0.03153892 |
| AT5G57560 | 436.55038 | -1.76 | 0.3603 | -4.8710 | 1.1103E-06 | 0.0005077 |
| AT5G59845 | 17.1711564 | -1.75 | 0.5152 | -3.3998 | 0.00067431 | 0.05963874 |
| AT2G37770 | 133.263307 | -1.66 | 0.4349 | -3.8093 | 0.00013936 | 0.02186273 |
| AT5G03230 | 616.335237 | -1.64 | 0.2546 | -6.4358 | 1.2282E-10 | 2.1997E-07 |
| AT2G33750 | 16.1311704 | -1.63 | 0.4916 | -3.3224 | 0.00089257 | 0.07079521 |
| AT4G13330 | 26.4585298 | -1.55 | 0.4469 | -3.4615 | 0.00053712 | 0.05130525 |
| AT5G62730 | 88.8854639 | -1.53 | 0.4517 | -3.3909 | 0.00069676 | 0.0604706 |
| AT1G01060 | 119.791412 | -1.51 | 0.2923 | -5.1611 | 2.455E-07 | 0.00013885 |
| AT1G66230 | 69.2533998 | -1.49 | 0.4033 | -3.6937 | 0.00022103 | 0.02883021 |
| AT3G44300 | 71.3534236 | -1.43 | 0.4009 | -3.5558 | 0.00037683 | 0.04049457 |
| AT1G26800 | 171.925323 | -1.40 | 0.4161 | -3.3607 | 0.0007775 | 0.06524344 |
| AT1G29640 | 29.5125291 | -1.36 | 0.4027 | -3.3799 | 0.0007252 | 0.06184944 |
| AT3G29030 | 161.242154 | -1.35 | 0.3721 | -3.6316 | 0.00028164 | 0.03344211 |
| AT5G04950 | 777.072126 | -1.35 | 0.3453 | -3.9121 | 9.1478E-05 | 0.01624835 |
| AT4G27410 | 311.661235 | -1.35 | 0.2483 | -5.4295 | 5.652E-08 | 4.499E-05 |
| AT1G13650 | 97.4453187 | -1.34 | 0.3819 | -3.5031 | 0.00045985 | 0.0466188 |
| AT1G78450 | 76.6601067 | -1.31 | 0.3484 | -3.7647 | 0.00016676 | 0.0240532 |
| AT5G54230 | 48.7257738 | -1.30 | 0.4097 | -3.1636 | 0.0015583 | 0.09937985 |
| AT5G40460 | 45.4147774 | -1.29 | 0.3973 | -3.2552 | 0.0011332 | 0.08312209 |
| AT1G22500 | 323.420087 | -1.29 | 0.3527 | -3.6455 | 0.00026689 | 0.03240729 |
| AT2G28120 | 218.48433 | -1.29 | 0.2252 | -5.7053 | 1.1614E-08 | 1.1412E-05 |
| AT3G05400 | 76.2513201 | -1.28 | 0.3735 | -3.4401 | 0.00058152 | 0.05410366 |
| AT3G02380 | 43.4257915 | -1.26 | 0.3850 | -3.2824 | 0.00102924 | 0.07891256 |
| AT3G11110 | 48.9430437 | -1.26 | 0.3446 | -3.6554 | 0.00025681 | 0.03153892 |
| AT2G25090 | 55.1662231 | -1.25 | 0.3395 | -3.6774 | 0.00023566 | 0.02961876 |
| AT2G46790 | 45.5882521 | -1.25 | 0.3366 | -3.7026 | 0.0002134 | 0.02813736 |
| AT4G17090 | 383.724766 | -1.22 | 0.3715 | -3.2707 | 0.00107267 | 0.08089029 |
| AT1G22190 | 575.335419 | -1.20 | 0.3034 | -3.9703 | 7.1781E-05 | 0.01365237 |
| AT2G44660 | 48.5535984 | -1.20 | 0.3251 | -3.6817 | 0.00023167 | 0.02928895 |

| | | | | | | |
|---|---|---|---|---|---|---|
| AT4G01950 | 113.724773 | -1.19 | 0.2831 | -4.1875 | 2.8206E-05 | 0.0065891 |
| AT2G46510 | 64.3732013 | -1.17 | 0.3275 | -3.5633 | 0.0003662 | 0.03974913 |
| AT5G62020 | 99.3770466 | -1.17 | 0.2858 | -4.0828 | 4.4498E-05 | 0.00937589 |
| AT3G14200 | 124.683965 | -1.14 | 0.3233 | -3.5341 | 0.0004091 | 0.04288931 |
| AT2G34500 | 73.8701344 | -1.14 | 0.2766 | -4.1251 | 3.7059E-05 | 0.00829664 |
| AT3G21870 | 66.8861537 | -1.14 | 0.3343 | -3.4116 | 0.00064594 | 0.0580879 |
| AT1G70830 | 3165.1252 | -1.14 | 0.3042 | -3.7324 | 0.00018968 | 0.02563837 |
| AT5G57785 | 252.628628 | -1.12 | 0.3553 | -3.1617 | 0.00156859 | 0.09974035 |
| AT1G64740 | 62.3413821 | -1.11 | 0.3272 | -3.3899 | 0.00069909 | 0.0604706 |
| AT3G11660 | 341.327449 | -1.10 | 0.2980 | -3.7053 | 0.00021116 | 0.02801348 |
| AT4G35440 | 77.2075985 | -1.10 | 0.2761 | -3.9777 | 6.9598E-05 | 0.01335542 |
| AT3G14620 | 474.524432 | -1.09 | 0.3069 | -3.5656 | 0.00036297 | 0.03959837 |
| AT2G44230 | 136.952662 | -1.07 | 0.3028 | -3.5220 | 0.00042836 | 0.04383969 |
| AT2G46830 | 265.411952 | -1.04 | 0.1998 | -5.2221 | 1.7689E-07 | 0.0001056 |
| AT1G76590 | 146.61595 | -1.04 | 0.3229 | -3.2262 | 0.00125446 | 0.08791942 |
| AT1G23205 | 103.274048 | -1.03 | 0.2560 | -4.0184 | 5.8584E-05 | 0.01176715 |
| AT5G25140 | 98.1852928 | -1.03 | 0.2784 | -3.6866 | 0.00022729 | 0.02911077 |
| AT1G17840 | 283.394374 | -1.03 | 0.3099 | -3.3102 | 0.00093237 | 0.07313295 |
| AT3G50840 | 210.024867 | -1.02 | 0.2968 | -3.4319 | 0.00059938 | 0.05528686 |
| AT5G24160 | 198.219248 | -1.01 | 0.2404 | -4.2151 | 2.4969E-05 | 0.00589714 |
| AT4G29905 | 1831.02056 | -1.01 | 0.2894 | -3.4863 | 0.00048972 | 0.04827966 |
| AT1G68440 | 910.701534 | -1.01 | 0.3016 | -3.3374 | 0.00084567 | 0.06858566 |
| AT4G09630 | 142.083806 | -1.01 | 0.2284 | -4.4045 | 1.0604E-05 | 0.003122 |
| AT1G09575 | 70.5457127 | -0.98 | 0.2999 | -3.2665 | 0.00108904 | 0.08155923 |
| AT1G68670 | 460.149862 | -0.98 | 0.2698 | -3.6229 | 0.00029137 | 0.03384919 |
| AT1G80630 | 78.867897 | -0.98 | 0.2973 | -3.2835 | 0.00102543 | 0.07891256 |
| AT3G19480 | 174.719742 | -0.97 | 0.2688 | -3.6259 | 0.00028797 | 0.03363588 |
| AT1G22370 | 111.373741 | -0.97 | 0.2990 | -3.2387 | 0.00120095 | 0.08569333 |
| AT1G15830 | 94.2266533 | -0.97 | 0.2669 | -3.6171 | 0.00029793 | 0.03402795 |
| AT3G14770 | 219.866626 | -0.96 | 0.2234 | -4.2767 | 1.8964E-05 | 0.00488297 |
| AT3G48350 | 143.575288 | -0.95 | 0.2504 | -3.7950 | 0.00014763 | 0.02282691 |
| AT4G20820 | 211.746292 | -0.94 | 0.2936 | -3.2123 | 0.0013166 | 0.08954532 |
| AT3G27170 | 74.9565024 | -0.94 | 0.2655 | -3.5462 | 0.00039081 | 0.04138164 |
| AT3G15510 | 420.621697 | -0.94 | 0.2930 | -3.2123 | 0.00131659 | 0.08954532 |
| AT2G19160 | 91.0862752 | -0.93 | 0.2925 | -3.1663 | 0.00154382 | 0.09904437 |
| AT2G03750 | 346.023241 | -0.92 | 0.2404 | -3.8469 | 0.00011964 | 0.01990215 |
| AT3G44450 | 126.854187 | -0.92 | 0.2512 | -3.6819 | 0.00023148 | 0.02928895 |
| AT1G64500 | 429.71761 | -0.91 | 0.2216 | -4.1117 | 3.9268E-05 | 0.00861175 |
| AT5G47610 | 112.863738 | -0.91 | 0.2430 | -3.7374 | 0.00018596 | 0.02561925 |
| AT4G14500 | 167.817934 | -0.91 | 0.2358 | -3.8505 | 0.00011788 | 0.01990215 |
| AT5G37770 | 282.564617 | -0.90 | 0.2506 | -3.6074 | 0.00030923 | 0.03497885 |
| AT1G07720 | 320.177663 | -0.90 | 0.2802 | -3.2187 | 0.00128766 | 0.08869972 |
| AT1G26770 | 197.444983 | -0.89 | 0.2630 | -3.3876 | 0.00070497 | 0.0604706 |
| AT1G29660 | 851.032911 | -0.88 | 0.2462 | -3.5944 | 0.00032513 | 0.03658461 |
| AT4G13575 | 269.446948 | -0.88 | 0.2006 | -4.3807 | 1.1828E-05 | 0.00338929 |
| AT1G07350 | 437.862547 | -0.87 | 0.2161 | -4.0212 | 5.7892E-05 | 0.01173791 |
| AT1G55960 | 333.771431 | -0.87 | 0.2316 | -3.7477 | 0.00017847 | 0.02523502 |

| | | | | | | |
|---|---|---|---|---|---|---|
| AT3G19030 | 919.6538 | -0.86 | 0.1865 | -4.5935 | 4.3597E-06 | 0.00153603 |
| AT5G12900 | 129.671705 | -0.85 | 0.2435 | -3.4930 | 0.00047754 | 0.04729635 |
| AT2G01850 | 2286.32983 | -0.84 | 0.2004 | -4.2167 | 2.4785E-05 | 0.00589714 |
| AT4G16140 | 143.141517 | -0.84 | 0.2463 | -3.4031 | 0.0006663 | 0.05939452 |
| AT3G09600 | 121.422082 | -0.83 | 0.2364 | -3.5298 | 0.00041583 | 0.0430877 |
| AT5G02830 | 224.154883 | -0.83 | 0.2474 | -3.3579 | 0.00078547 | 0.06524344 |
| AT3G61890 | 242.513925 | -0.83 | 0.2322 | -3.5714 | 0.00035512 | 0.03934105 |
| AT3G55830 | 112.0198 | -0.82 | 0.2575 | -3.1992 | 0.00137793 | 0.09197072 |
| AT3G12320 | 298.736583 | -0.82 | 0.1918 | -4.2830 | 1.8439E-05 | 0.00483274 |
| AT3G26290 | 907.518858 | -0.81 | 0.2553 | -3.1810 | 0.00146783 | 0.09684273 |
| AT4G37530 | 185.695188 | -0.80 | 0.2379 | -3.3727 | 0.00074447 | 0.0629929 |
| AT2G23130 | 362.493146 | -0.79 | 0.2341 | -3.3922 | 0.00069329 | 0.0604706 |
| AT5G49480 | 767.787876 | -0.78 | 0.2286 | -3.3947 | 0.00068693 | 0.06039147 |
| AT5G61820 | 890.606658 | -0.77 | 0.2241 | -3.4571 | 0.00054594 | 0.05191706 |
| AT3G53420 | 8153.95303 | -0.77 | 0.2307 | -3.3416 | 0.00083285 | 0.06805937 |
| AT2G41250 | 495.392394 | -0.76 | 0.1903 | -3.9933 | 6.5172E-05 | 0.01285017 |
| AT3G10525 | 140.208605 | -0.75 | 0.2200 | -3.4140 | 0.00064006 | 0.0580879 |
| AT4G30470 | 322.970376 | -0.73 | 0.1988 | -3.6590 | 0.00025322 | 0.03145844 |
| AT3G57020 | 432.151925 | -0.68 | 0.2128 | -3.2014 | 0.00136772 | 0.09157303 |
| AT4G26690 | 335.656697 | -0.67 | 0.2052 | -3.2459 | 0.00117065 | 0.08442822 |
| AT5G25610 | 2312.32349 | -0.66 | 0.1813 | -3.6186 | 0.00029621 | 0.03402795 |
| AT2G24762 | 493.034625 | -0.65 | 0.1866 | -3.4969 | 0.00047063 | 0.04704511 |
| AT2G46340 | 576.175535 | -0.61 | 0.1730 | -3.5291 | 0.000417 | 0.0430877 |
| AT3G04290 | 948.418904 | -0.60 | 0.1871 | -3.2231 | 0.00126805 | 0.08848359 |
| AT4G28300 | 611.188624 | -0.60 | 0.1829 | -3.2754 | 0.00105497 | 0.07983562 |
| AT4G02920 | 2011.00984 | -0.57 | 0.1716 | -3.3316 | 0.00086348 | 0.06976627 |
| AT2G30490 | 1547.03075 | -0.55 | 0.1552 | -3.5681 | 0.00035955 | 0.0394838 |
| AT3G53260 | 1339.59973 | -0.54 | 0.1605 | -3.3787 | 0.0007283 | 0.06186828 |
| AT1G19000 | 1345.84075 | -0.53 | 0.1597 | -3.3130 | 0.00092285 | 0.07265187 |
| AT1G21050 | 356.254713 | 0.68 | 0.2032 | 3.3583 | 0.0007843 | 0.06524344 |
| AT2G02100 | 2040.26369 | 0.73 | 0.1661 | 4.4145 | 1.0123E-05 | 0.00302157 |
| AT5G47060 | 248.728409 | 0.73 | 0.2277 | 3.2204 | 0.00128028 | 0.08869972 |
| AT1G48770 | 123.721642 | 0.75 | 0.2347 | 3.2092 | 0.00133107 | 0.08996005 |
| AT1G09530 | 534.780696 | 0.78 | 0.2105 | 3.6933 | 0.00022134 | 0.02883021 |
| AT4G26670 | 886.130182 | 0.78 | 0.2342 | 3.3244 | 0.00088606 | 0.07079276 |
| AT5G53420 | 513.766544 | 0.79 | 0.2430 | 3.2664 | 0.00108913 | 0.08155923 |
| AT1G47340 | 148.400802 | 0.80 | 0.2306 | 3.4745 | 0.00051174 | 0.04976568 |
| AT4G17260 | 186.379861 | 0.81 | 0.2281 | 3.5322 | 0.00041206 | 0.04299019 |
| AT1G53035 | 151.521588 | 0.81 | 0.2341 | 3.4633 | 0.00053365 | 0.0512016 |
| AT1G04620 | 193.177717 | 0.83 | 0.2393 | 3.4706 | 0.00051921 | 0.05026521 |
| AT1G73830 | 488.125884 | 0.84 | 0.1902 | 4.4169 | 1.0012E-05 | 0.00302157 |
| AT5G62280 | 506.2463 | 0.84 | 0.2519 | 3.3401 | 0.00083733 | 0.0681666 |
| AT2G30424 | 143.389049 | 0.87 | 0.2520 | 3.4348 | 0.00059296 | 0.05493024 |
| AT5G22310 | 381.025714 | 0.99 | 0.2678 | 3.6918 | 0.00022268 | 0.0288303 |
| AT4G30570 | 86.5623467 | 1.00 | 0.2598 | 3.8387 | 0.00012369 | 0.01999142 |
| AT1G73120 | 161.897409 | 1.00 | 0.3082 | 3.2488 | 0.00115905 | 0.08388887 |
| AT2G33793 | 120.272112 | 1.02 | 0.3212 | 3.1741 | 0.00150279 | 0.09817033 |

| | | | | | | |
|---|---|---|---|---|---|---|
| AT3G59530 | 53.1345939 | 1.04 | 0.3154 | 3.2840 | 0.00102346 | 0.07891256 |
| AT1G11185 | 164.999381 | 1.05 | 0.3039 | 3.4491 | 0.00056248 | 0.05302084 |
| AT5G62920 | 297.698499 | 1.06 | 0.2648 | 3.9877 | 6.6729E-05 | 0.01303757 |
| AT5G63660 | 155.788657 | 1.07 | 0.2346 | 4.5622 | 5.0614E-06 | 0.00169969 |
| AT5G28630 | 553.184961 | 1.07 | 0.3048 | 3.5131 | 0.00044283 | 0.04510568 |
| AT5G55040 | 1273.41744 | 1.08 | 0.3342 | 3.2206 | 0.00127909 | 0.08869972 |
| AT5G60800 | 325.437126 | 1.10 | 0.3215 | 3.4137 | 0.00064092 | 0.0580879 |
| AT2G43140 | 234.692564 | 1.10 | 0.2884 | 3.8136 | 0.00013694 | 0.02164058 |
| AT4G12770 | 1101.63451 | 1.19 | 0.3740 | 3.1695 | 0.00152681 | 0.09899103 |
| AT2G40085 | 64.2962485 | 1.19 | 0.3637 | 3.2764 | 0.00105131 | 0.07983562 |
| AT4G34810 | 169.669564 | 1.19 | 0.2792 | 4.2691 | 1.963E-05 | 0.00488297 |
| AT1G06420 | 90.6866823 | 1.20 | 0.2758 | 4.3453 | 1.391E-05 | 0.0038933 |
| AT3G51340 | 41.4079356 | 1.24 | 0.3286 | 3.7727 | 0.00016148 | 0.02393459 |
| AT4G16146 | 196.689141 | 1.25 | 0.2586 | 4.8458 | 1.2612E-06 | 0.0005532 |
| AT1G74650 | 88.8410743 | 1.26 | 0.3739 | 3.3645 | 0.00076675 | 0.06462326 |
| AT3G05370 | 134.039211 | 1.29 | 0.2651 | 4.8480 | 1.2473E-06 | 0.0005532 |
| AT1G68945 | 199.221341 | 1.32 | 0.4181 | 3.1654 | 0.00154891 | 0.0990751 |
| AT5G28610 | 113.26537 | 1.34 | 0.2470 | 5.4132 | 6.1901E-08 | 4.7222E-05 |
| AT1G72150 | 13168.3329 | 1.34 | 0.3923 | 3.4180 | 0.00063089 | 0.05769852 |
| AT3G22380 | 5723.57296 | 1.35 | 0.4082 | 3.2957 | 0.00098175 | 0.07617232 |
| AT5G04890 | 284.635887 | 1.35 | 0.4129 | 3.2605 | 0.00111222 | 0.08242698 |
| AT1G62580 | 45.650212 | 1.37 | 0.4266 | 3.2190 | 0.00128633 | 0.08869972 |
| AT5G45520 | 90.1427617 | 1.40 | 0.4270 | 3.2787 | 0.00104272 | 0.07946873 |
| AT5G24655 | 87.371709 | 1.40 | 0.4386 | 3.2030 | 0.00136014 | 0.09135057 |
| AT2G25720 | 567.266098 | 1.44 | 0.4501 | 3.2037 | 0.00135665 | 0.09135057 |
| AT5G17890 | 1595.61193 | 1.47 | 0.4492 | 3.2629 | 0.00110261 | 0.08199721 |
| AT5G24880 | 255.069175 | 1.47 | 0.4405 | 3.3456 | 0.00082094 | 0.06734179 |
| AT1G80930 | 3304.28583 | 1.47 | 0.4404 | 3.3470 | 0.00081687 | 0.06726528 |
| AT5G50740 | 1582.0277 | 1.52 | 0.4768 | 3.1875 | 0.00143506 | 0.09519251 |
| AT2G15830 | 191.409982 | 1.53 | 0.2934 | 5.2124 | 1.8642E-07 | 0.00010828 |
| AT5G53980 | 83.9429076 | 1.54 | 0.4087 | 3.7590 | 0.00017056 | 0.02443829 |
| AT5G62390 | 11025.9075 | 1.58 | 0.4697 | 3.3576 | 0.00078625 | 0.06524344 |
| AT4G35940 | 399.116475 | 1.62 | 0.4452 | 3.6298 | 0.00028359 | 0.03348846 |
| AT5G66640 | 24.5249454 | 1.62 | 0.4951 | 3.2817 | 0.00103175 | 0.07891256 |
| AT5G44280 | 569.504658 | 1.64 | 0.5055 | 3.2370 | 0.00120813 | 0.08569333 |
| AT4G09820 | 17.1060705 | 1.65 | 0.5107 | 3.2373 | 0.00120667 | 0.08569333 |
| AT2G28815 | 57.4593205 | 1.66 | 0.3524 | 4.6991 | 2.6131E-06 | 0.00100286 |
| AT4G02800 | 363.321436 | 1.67 | 0.5017 | 3.3281 | 0.00087431 | 0.0703378 |
| AT4G11080 | 774.698537 | 1.68 | 0.4704 | 3.5677 | 0.00036008 | 0.0394838 |
| AT1G51080 | 432.342886 | 1.69 | 0.5202 | 3.2487 | 0.00115927 | 0.08388887 |
| AT2G17036 | 70.7520906 | 1.69 | 0.3169 | 5.3433 | 9.1287E-08 | 6.1311E-05 |
| AT4G14140 | 12.1289831 | 1.70 | 0.4739 | 3.5897 | 0.00033111 | 0.03687195 |
| AT1G05057 | 23.8646949 | 1.76 | 0.4930 | 3.5604 | 0.00037031 | 0.03999321 |
| AT5G19890 | 193.685075 | 1.78 | 0.5245 | 3.4021 | 0.00066878 | 0.05939452 |
| AT5G56300 | 28.0416252 | 1.83 | 0.4760 | 3.8453 | 0.00012038 | 0.01990215 |
| AT4G32280 | 15.2721601 | 1.86 | 0.5734 | 3.2427 | 0.00118413 | 0.08511512 |
| AT4G38410 | 199.046137 | 1.87 | 0.5302 | 3.5254 | 0.00042278 | 0.04347571 |

| | | | | | | |
|---|---|---|---|---|---|---|
| AT5G28300 | 2010.69437 | 1.88 | 0.4641 | 4.0423 | 5.2929E-05 | 0.01093808 |
| AT5G67060 | 95.1142213 | 1.97 | 0.2998 | 6.5773 | 4.7902E-11 | 1.1439E-07 |
| AT2G07783 | 1342.32021 | 1.99 | 0.6095 | 3.2631 | 0.00110197 | 0.08199721 |
| AT1G01480 | 24.7596846 | 2.00 | 0.6195 | 3.2259 | 0.00125587 | 0.08791942 |
| AT2G25650 | 77.8391203 | 2.00 | 0.6221 | 3.2161 | 0.00129926 | 0.08921314 |
| AT1G05035 | 67.936052 | 2.02 | 0.5125 | 3.9421 | 8.0783E-05 | 0.01509737 |
| AT1G49570 | 103.165801 | 2.03 | 0.4162 | 4.8749 | 1.0884E-06 | 0.0005077 |
| AT5G10340 | 9.60339085 | 2.07 | 0.6543 | 3.1678 | 0.00153571 | 0.09899103 |
| AT5G60530 | 1146.98679 | 2.20 | 0.6384 | 3.4415 | 0.00057859 | 0.05406562 |
| AT1G06450 | 87.444191 | 2.20 | 0.5813 | 3.7839 | 0.00015436 | 0.02324546 |
| AT3G28510 | 10.7039714 | 2.57 | 0.7331 | 3.4996 | 0.00046588 | 0.04686946 |
| AT1G08643 | 164.751167 | 2.70 | 0.6743 | 3.9975 | 6.4026E-05 | 0.01274126 |
| AT1G07690 | 9.00655679 | 2.80 | 0.8049 | 3.4811 | 0.00049935 | 0.04878198 |
| AT2G14610 | 9.20324145 | 2.82 | 0.7256 | 3.8873 | 0.00010137 | 0.01742964 |
| AT3G54520 | 15.0761854 | 2.84 | 0.7218 | 3.9363 | 8.2761E-05 | 0.0153336 |
| AT1G13480 | 24.0231352 | 2.96 | 0.8161 | 3.6273 | 0.00028642 | 0.03363588 |
| AT3G28580 | 69.3119943 | 2.96 | 0.6403 | 4.6242 | 3.7609E-06 | 0.00137057 |
| AT4G11470 | 5.02401717 | 2.98 | 0.8560 | 3.4845 | 0.00049301 | 0.04838293 |
| AT1G13470 | 9.74656458 | 3.03 | 0.7024 | 4.3103 | 1.6306E-05 | 0.00438939 |
| AT1G07160 | 18.4548052 | 3.13 | 0.9430 | 3.3223 | 0.00089268 | 0.07079521 |
| AT5G22530 | 6.47623592 | 3.26 | 1.0264 | 3.1807 | 0.00146895 | 0.09684273 |
| AT5G24110 | 22.1289979 | 3.52 | 1.1086 | 3.1785 | 0.00148045 | 0.09700576 |
| AT1G21850 | 9.18927453 | 3.74 | 1.1755 | 3.1788 | 0.00147863 | 0.09700576 |
| AT3G47720 | 3.44145202 | 3.74 | 1.1665 | 3.2104 | 0.0013253 | 0.08985303 |
| AT5G57510 | 6.70181781 | 3.78 | 0.9902 | 3.8156 | 0.00013586 | 0.02162841 |
| AT2G14247 | 22.6267254 | 3.81 | 0.9200 | 4.1401 | 3.4719E-05 | 0.00785457 |
| AT4G28460 | 17.2081072 | 3.88 | 0.8703 | 4.4568 | 8.3198E-06 | 0.00259143 |
| AT3G54530 | 18.5905691 | 3.88 | 1.0952 | 3.5462 | 0.00039087 | 0.04138164 |
| AT1G79680 | 7.2446124 | 3.95 | 1.0661 | 3.7082 | 0.00020875 | 0.02786615 |
| AT5G55150 | 8.00775088 | 3.98 | 1.2319 | 3.2279 | 0.001247 | 0.08787035 |
| AT2G04495 | 7.35959756 | 4.93 | 1.2817 | 3.8476 | 0.0001193 | 0.01990215 |
| AT2G17845 | 7.41946057 | 5.80 | 1.4093 | 4.1178 | 3.8251E-05 | 0.00847509 |
| AT4G31950 | 9.29508811 | 6.17 | 1.5692 | 3.9289 | 8.5352E-05 | 0.01554573 |
| AT3G12910 | 5.44843425 | 6.38 | 1.4337 | 4.4486 | 8.6426E-06 | 0.00265353 |

**Supplemental Table 5.** List of overlapping genes identified as WOX4 targets in both the *pWOX4:WOX4-GR* RNA-seq and the *pRPS5A:WOX4-GR* RNA-seq. The *pWOX4:WOX4-GR* RNA-seq and analysis was conducted by me. The *pRPS5A:WOX4-GR* RNA-seq was conducted by Dr. Eliana Mor, its re-analysis was conducted by me.

| Gene | Primary Gene Symbol |
|---|---|
| AT5G19120 | |
| AT1G68440 | |
| AT2G20670 | |
| AT5G40590 | |
| AT5G21940 | |
| AT3G26290 | |
| AT3G54530 | |
| AT4G32480 | |
| AT2G43140 | BHLH129 |
| AT4G17460 | HAT1 |
| AT1G76590 | PLATZ2 |
| AT2G23130 | ARABINOGALACTAN PROTEIN 17 (AGP17) |
| AT3G59900 | AUXIN-REGULATED GENE INVOLVED IN ORGAN SIZE (ARGOS) |
| AT5G18670 | BETA-AMYLASE 3 (BMY3) |
| AT4G37610 | BTB AND TAZ DOMAIN PROTEIN 5 (bt5) |
| AT4G17090 | CHLOROPLAST BETA-AMYLASE (CT-BMY) |
| AT2G20880 | ERF DOMAIN 53 (ERF53) |
| AT1G26770 | EXPANSIN A10 (EXPA10) |
| AT5G46330 | FLAGELLIN-SENSITIVE 2 (FLS2) |
| AT1G43800 | FLORAL TRANSITION AT THE MERISTEM1 (FTM1) |
| AT3G30725 | GLUTAMINE DUMPER 6 (GDU6) |
| AT5G41080 | GLYCEROPHOSPHODIESTER PHOSPHODIESTERASE 2 (GDPD2) |
| AT3G10525 | LOSS OF GIANT CELLS FROM ORGANS (LGO) |
| AT2G02100 | LOW-MOLECULAR-WEIGHT CYSTEINE-RICH 69 (LCR69) |
| AT1G74650 | MYB DOMAIN PROTEIN 31 (MYB31) |
| AT3G15500 | NAC DOMAIN CONTAINING PROTEIN 3 (NAC3) |
| AT5G64170 | NIGHT LIGHT-INDUCIBLE AND CLOCK-REGULATED GENE 1 (LNK1) |
| AT5G56550 | OXIDATIVE STRESS 3 (OXS3) |
| AT3G61060 | PHLOEM PROTEIN 2-A13 (PP2-A13) |
| AT2G46790 | PSEUDO-RESPONSE REGULATOR 9 (PRR9) |
| AT4G33070 | PYRUVATE DECARBOXYLASE 1 (PDC1) |
| AT5G22920 | RING ZINC-FINGER PROTEIN 34 (RZPF34) |
| AT1G13245 | ROTUNDIFOLIA LIKE 17 (RTFL17) |

**Supplemental Table 6.** List of cytokinin and auxin regulated genes in the *pRPS5A:WOX4-GR* RNA-seq dataset. The *pRPS5A:WOX4-GR* RNA-Seq was conducted by Dr. Eliana Mor, re-analysis was conducted by me.

| gene | Hormone | log2FC | Padj value |
|---|---|---|---|
| AT3G48360 | Auxin | -2.02 | 0.09176603 |
| AT4G12410 | Auxin | -1.43 | 0.03108701 |
| AT5G63160 | Auxin | -1.33 | 0.05590004 |

| | | | |
|---|---|---|---|
| AT3G59900 | Auxin | -1.26 | 0.00068318 |
| AT4G37610 | Auxin | -1.23 | 0.08435165 |
| AT4G37540 | Auxin | -0.99 | 0.00731796 |
| AT5G54490 | Auxin | -0.98 | 0.05925917 |
| AT1G19220 | Auxin | -0.93 | 0.00937186 |
| AT1G26870 | Auxin | -0.86 | 0.01781874 |
| AT5G47370 | Auxin | -0.84 | 7.9721E-08 |
| AT3G15540 | Auxin | -0.72 | 0.01367303 |
| AT3G14370 | Auxin | -0.66 | 0.04011182 |
| AT5G43700 | Auxin | -0.60 | 0.00365588 |
| AT3G23050 | Auxin | -0.60 | 4.7026E-06 |
| AT1G68130 | Auxin | -0.48 | 0.09477052 |
| AT2G26170 | Auxin | 0.39 | 0.09942207 |
| AT1G30690 | Auxin | 0.48 | 0.01096136 |
| AT1G55320 | Auxin | 0.51 | 0.00298076 |
| AT1G28130 | Auxin | 0.55 | 0.0710425 |
| AT5G08640 | Auxin | 0.56 | 0.01900436 |
| AT5G38030 | Auxin | 0.58 | 0.03691987 |
| AT2G33860 | Auxin | 0.75 | 0.00023509 |
| AT5G13930 | Auxin | 0.84 | 4.1083E-07 |
| AT3G55120 | Auxin | 0.84 | 0.00365588 |
| AT4G24670 | Auxin | 0.85 | 0.03850778 |
| AT4G29080 | Auxin | 0.88 | 0.09640699 |
| AT4G31910 | Auxin | 0.90 | 0.01424063 |
| AT5G07990 | Auxin | 0.93 | 0.00036674 |
| AT1G34670 | Auxin | 1.12 | 0.0757424 |
| AT4G37750 | Auxin | 1.17 | 0.09782628 |
| AT1G14120 | Auxin | 1.30 | 0.0001282 |
| AT1G64625 | Auxin | 1.59 | 0.07528585 |
| AT1G74650 | Auxin | 1.62 | 0.0210148 |
| AT1G80100 | Cytokinin | -1.08 | 0.00596106 |
| AT1G74890 | Cytokinin | -1.04 | 0.04011182 |
| AT3G48100 | Cytokinin | -0.69 | 0.03305714 |
| AT5G06300 | Cytokinin | -0.69 | 0.00791113 |
| AT1G69040 | Cytokinin | -0.52 | 0.00669226 |
| AT4G34160 | Cytokinin | 0.45 | 0.09074636 |
| AT1G13420 | Cytokinin | 0.48 | 0.01695676 |
| AT1G31770 | Cytokinin | 0.82 | 0.02480932 |
| AT5G02810 | Cytokinin | 0.97 | 0.0002162 |
| AT3G23630 | Cytokinin | 1.01 | 0.00559746 |
| AT5G21482 | Cytokinin | 1.27 | 0.01134692 |
| AT2G46790 | Cytokinin | 1.79 | 0.00166409 |

**Supplemental Table 7.** Cambium domain-specific expression of *WOX4*, *PXY* and *SMXL5*. The relative mean across all cambium domains or mean of the normalized count values are given. LRT = Likelihood ratio test. LRT=1 indicates significance difference of expression levels across cambium domains. A mean value of all domains lower than 10 was interpreted as no expression within the cambium. The RNA-seq data and analysis was produced by Dr. Dongbo Shi. The analysis of *WOX4*, *PXY* and *SMXL5* was conducted by myself.

| | Realtive mean | | | | Mean normalized count values | | | Mean |
|---|---|---|---|---|---|---|---|---|
| Gene | proximal | central | distal | LRT | proximal | central | distal | All domains |
| AT5G61480 | 0.37 | 0.52 | 0.11 | 1 | 775.22 | 1122.60 | 232.06 | 709.96 |
| AT5G57130 | 0.09 | 0.55 | 0.36 | 1 | 127.60 | 792.91 | 524.28 | 481.60 |
| AT1G46480 | 0.19 | 0.66 | 0.15 | 1 | 426.09 | 1520.26 | 347.84 | 764.73 |

**Supplemental Table 8.** Cambium domain-specific expression of the 338 putative WOX4 targets identified in the *pWOX4:WOX4-GR* RNA-seq. The relative mean across all cambium domains or mean of the normalized count values are given. LRT = Likelihood ratio test. LRT=1 indicates significance difference of expression levels across cambium domains. A mean value of all domains lower 10 was interpreted as no expression within the cambium. The RNA-seq data and analysis was produced by Dr. Dongbo Shi. The analysis of WOX4 targets was conducted by myself.

| | Relative mean | | | | Mean normalized count values | | | Mean |
|---|---|---|---|---|---|---|---|---|
| Gene | proximal | central | distal | LRT | proximal | central | distal | All domains |
| AT3G19480 | 0.25 | 0.33 | 0.42 | | 146.14 | 195.65 | 245.24 | 195.68 |
| AT4G20820 | 0.14 | 0.35 | 0.51 | | 12.02 | 29.11 | 41.47 | 27.53 |
| AT2G43140 | 0.58 | 0.19 | 0.23 | 1 | 266.06 | 88.74 | 106.80 | 153.87 |
| AT3G62950 | 0.00 | 0.47 | 0.53 | | 0.00 | 6.39 | 6.14 | 4.18 |
| AT4G17460 | 0.35 | 0.39 | 0.26 | | 32.70 | 32.86 | 24.28 | 29.94 |
| AT1G68670 | 0.42 | 0.30 | 0.28 | | 503.54 | 361.06 | 339.79 | 401.46 |
| AT3G48870 | 0.34 | 0.32 | 0.34 | | 633.29 | 608.99 | 642.53 | 628.27 |
| AT4G02800 | 0.06 | 0.65 | 0.28 | 1 | 21.40 | 215.16 | 95.63 | 110.73 |
| AT1G74930 | 0.36 | 0.32 | 0.32 | | 851.00 | 746.18 | 744.80 | 780.66 |
| AT5G63660 | 0.15 | 0.34 | 0.50 | | 0.93 | 4.08 | 6.71 | 3.91 |
| AT1G76590 | 0.13 | 0.32 | 0.55 | 1 | 36.21 | 92.02 | 161.65 | 96.63 |
| AT5G40460 | 0.32 | 0.47 | 0.20 | | 78.90 | 113.89 | 47.44 | 80.08 |
| AT5G24150 | 0.23 | 0.25 | 0.52 | | 40.28 | 46.86 | 91.35 | 59.50 |
| AT3G14770 | 0.26 | 0.17 | 0.57 | | 51.04 | 36.21 | 122.12 | 69.79 |
| AT1G01480 | 0.39 | 0.27 | 0.34 | | 127.90 | 88.46 | 114.80 | 110.39 |
| AT1G01120 | 0.13 | 0.40 | 0.47 | | 15.30 | 53.90 | 59.63 | 42.94 |
| AT1G07720 | 0.14 | 0.33 | 0.53 | 1 | 39.35 | 88.25 | 147.97 | 91.85 |
| AT4G11080 | 0.25 | 0.47 | 0.28 | 1 | 1031.09 | 1939.70 | 1154.94 | 1375.24 |
| AT1G13700 | 0.27 | 0.37 | 0.37 | | 197.81 | 273.50 | 272.98 | 248.10 |
| AT1G04620 | 0.24 | 0.59 | 0.18 | | 19.83 | 40.84 | 14.75 | 25.14 |
| AT2G46510 | 0.17 | 0.33 | 0.49 | 1 | 53.90 | 104.13 | 154.79 | 104.27 |
| AT4G22780 | 0.55 | 0.23 | 0.23 | 1 | 1831.46 | 769.64 | 757.68 | 1119.59 |
| AT1G64740 | 0.33 | 0.44 | 0.23 | 1 | 213.55 | 278.07 | 145.67 | 212.43 |
| AT4G17920 | 0.25 | 0.26 | 0.48 | | 28.52 | 17.31 | 44.58 | 30.14 |
| AT3G11110 | 0.42 | 0.32 | 0.25 | | 43.51 | 32.08 | 25.38 | 33.66 |
| AT5G47610 | 0.50 | 0.27 | 0.23 | | 83.84 | 43.51 | 38.44 | 55.27 |
| AT3G20395 | 0.19 | 0.29 | 0.52 | | 5.80 | 17.30 | 15.06 | 12.72 |

| | | | | | | | | |
|---|---|---|---|---|---|---|---|---|
| AT1G22500 | 0.13 | 0.41 | 0.46 | | 13.49 | 40.57 | 46.28 | 33.45 |
| AT2G23130 | 0.33 | 0.33 | 0.34 | | 101.36 | 108.08 | 105.20 | 104.88 |
| AT2G44080 | 0.30 | 0.31 | 0.39 | | 585.30 | 629.07 | 767.17 | 660.51 |
| AT2G33793 | 0.09 | 0.62 | 0.29 | 1 | 13.77 | 92.70 | 45.12 | 50.53 |
| AT3G28270 | 0.21 | 0.75 | 0.04 | | 8.84 | 18.54 | 1.83 | 9.74 |
| AT1G17840 | 0.31 | 0.38 | 0.31 | | 142.42 | 177.42 | 139.83 | 153.22 |
| AT3G55130 | 0.20 | 0.50 | 0.30 | | 34.66 | 90.55 | 48.43 | 57.88 |
| AT3G52310 | 0.47 | 0.26 | 0.27 | | 107.74 | 61.57 | 68.27 | 79.19 |
| AT1G08570 | 0.29 | 0.36 | 0.35 | | 359.42 | 444.18 | 439.50 | 414.37 |
| AT5G61440 | 0.50 | 0.30 | 0.20 | 1 | 369.14 | 222.73 | 149.87 | 247.25 |
| AT4G12770 | 0.37 | 0.29 | 0.33 | | 937.65 | 730.26 | 838.96 | 835.62 |
| AT3G59900 | 0.30 | 0.28 | 0.42 | | 92.39 | 83.90 | 128.73 | 101.67 |
| AT5G15830 | 0.16 | 0.25 | 0.59 | 1 | 29.63 | 48.19 | 116.22 | 64.68 |
| AT3G49760 | 0.23 | 0.42 | 0.35 | | 6.66 | 3.56 | 0.75 | 3.66 |
| AT1G68520 | 0.10 | 0.19 | 0.71 | 1 | 39.28 | 77.91 | 296.58 | 137.92 |
| AT5G62390 | 0.25 | 0.41 | 0.34 | 1 | 2592.22 | 4225.11 | 3530.44 | 3449.26 |
| AT5G18670 | 0.24 | 0.29 | 0.47 | 1 | 181.67 | 219.82 | 352.52 | 251.33 |
| AT3G44450 | 0.40 | 0.38 | 0.22 | | 44.31 | 42.95 | 24.77 | 37.35 |
| AT3G12920 | 0.37 | 0.38 | 0.25 | 1 | 672.51 | 688.92 | 448.41 | 603.28 |
| AT1G18400 | 0.28 | 0.29 | 0.42 | | 50.07 | 52.10 | 72.50 | 58.22 |
| AT1G73830 | 0.27 | 0.34 | 0.39 | | 22.17 | 23.21 | 34.61 | 26.66 |
| AT4G37610 | 0.47 | 0.29 | 0.24 | 1 | 1293.29 | 794.17 | 648.38 | 911.95 |
| AT5G49480 | 0.24 | 0.26 | 0.51 | 1 | 155.47 | 166.66 | 331.81 | 217.98 |
| AT1G49660 | 0.30 | 0.34 | 0.36 | | 47.20 | 50.32 | 54.86 | 50.79 |
| AT2G25090 | 0.19 | 0.24 | 0.57 | 1 | 66.71 | 85.24 | 195.28 | 115.74 |
| AT1G06450 | 0.28 | 0.41 | 0.31 | | 29.81 | 43.46 | 33.02 | 35.43 |
| AT3G27170 | 0.43 | 0.34 | 0.23 | | 86.39 | 61.20 | 42.94 | 63.51 |
| AT4G35440 | 0.30 | 0.36 | 0.34 | | 174.30 | 202.67 | 195.80 | 190.92 |
| AT4G17090 | 0.22 | 0.34 | 0.44 | 1 | 2719.39 | 4141.09 | 5371.87 | 4077.45 |
| AT2G37770 | 0.44 | 0.37 | 0.19 | | 69.42 | 60.22 | 31.33 | 53.66 |
| AT2G30490 | 0.47 | 0.28 | 0.26 | 1 | 1767.84 | 1059.22 | 975.31 | 1267.46 |
| AT1G15950 | 0.33 | 0.34 | 0.34 | | 122.45 | 126.64 | 126.66 | 125.25 |
| AT2G46830 | 0.35 | 0.25 | 0.40 | 1 | 1099.68 | 785.59 | 1278.16 | 1054.48 |
| AT2G21660 | 0.27 | 0.44 | 0.29 | 1 | 586.28 | 952.22 | 618.46 | 718.99 |
| AT5G53420 | 0.21 | 0.26 | 0.52 | 1 | 195.03 | 246.25 | 480.15 | 307.14 |
| AT3G02380 | 0.44 | 0.33 | 0.23 | 1 | 184.21 | 141.25 | 95.10 | 140.19 |
| AT3G21870 | 0.05 | 0.62 | 0.33 | | 0.88 | 8.27 | 3.72 | 4.29 |
| AT5G62430 | 0.36 | 0.27 | 0.37 | | 240.20 | 179.28 | 253.11 | 224.20 |
| AT3G48350 | 0.22 | 0.24 | 0.54 | | 33.38 | 37.50 | 75.92 | 48.93 |
| AT4G11470 | 0.65 | 0.24 | 0.10 | 1 | 87.40 | 36.57 | 12.36 | 45.44 |
| AT5G40380 | 0.10 | 0.44 | 0.46 | 1 | 13.90 | 62.64 | 63.70 | 46.75 |
| AT5G25140 | 0.20 | 0.22 | 0.58 | 1 | 89.73 | 106.45 | 269.75 | 155.31 |
| AT1G13080 | 0.12 | 0.23 | 0.65 | 1 | 29.16 | 50.07 | 145.79 | 75.01 |
| AT3G26290 | 0.13 | 0.18 | 0.69 | 1 | 61.40 | 80.71 | 315.84 | 152.65 |
| AT2G34500 | 0.20 | 0.25 | 0.55 | 1 | 57.27 | 74.64 | 160.47 | 97.46 |
| AT3G14620 | 0.27 | 0.29 | 0.44 | 1 | 341.54 | 376.39 | 555.30 | 424.41 |
| AT4G31950 | 0.39 | 0.28 | 0.33 | | 1.57 | 1.86 | 10.32 | 4.58 |

| | | | | | | | | |
|---|---|---|---|---|---|---|---|---|
| AT4G00360 | 0.20 | 0.40 | 0.40 | | 27.47 | 47.65 | 49.65 | 41.59 |
| AT5G66640 | 0.37 | 0.40 | 0.23 | 1 | 849.68 | 906.09 | 530.00 | 761.92 |
| AT5G17890 | 0.27 | 0.35 | 0.38 | 1 | 1400.76 | 1765.44 | 1923.15 | 1696.45 |
| AT4G14140 | 0.33 | 0.37 | 0.30 | | 78.12 | 86.07 | 68.69 | 77.63 |
| AT5G55970 | 0.64 | 0.15 | 0.21 | 1 | 379.43 | 88.88 | 130.33 | 199.55 |
| AT5G60800 | 0.35 | 0.42 | 0.24 | 1 | 2354.13 | 2840.98 | 1600.25 | 2265.12 |
| AT3G55830 | 0.46 | 0.31 | 0.22 | 1 | 161.24 | 108.61 | 77.47 | 115.77 |
| AT2G01850 | 0.33 | 0.31 | 0.36 | | 1115.89 | 1037.18 | 1226.39 | 1126.49 |
| AT2G20880 | 0.48 | 0.26 | 0.26 | | 46.04 | 23.50 | 24.49 | 31.35 |
| AT5G44210 | 0.35 | 0.50 | 0.15 | | 19.69 | 18.75 | 8.98 | 15.81 |
| AT3G23150 | 0.33 | 0.26 | 0.42 | | 34.73 | 33.36 | 60.63 | 42.91 |
| AT2G47520 | 0.48 | 0.24 | 0.27 | | 63.57 | 32.56 | 33.33 | 43.15 |
| AT2G31230 | 0.16 | 0.27 | 0.57 | | 11.42 | 17.50 | 34.34 | 21.09 |
| AT1G26770 | 0.11 | 0.43 | 0.46 | | 2.41 | 7.54 | 8.89 | 6.28 |
| AT3G29030 | 0.24 | 0.30 | 0.47 | | 24.24 | 30.52 | 43.64 | 32.80 |
| AT2G40610 | 0.05 | 0.42 | 0.53 | | 0.78 | 4.03 | 10.26 | 5.03 |
| AT2G17036 | 0.35 | 0.35 | 0.30 | | 128.97 | 129.93 | 111.92 | 123.61 |
| AT5G55150 | 0.43 | 0.33 | 0.24 | | 40.00 | 30.44 | 23.22 | 31.22 |
| AT5G49730 | 0.42 | 0.19 | 0.39 | | 50.13 | 22.83 | 41.74 | 38.23 |
| AT5G49740 | 0.15 | 0.33 | 0.52 | | 5.11 | 13.59 | 21.14 | 13.28 |
| AT1G07050 | 0.47 | 0.33 | 0.20 | | 45.34 | 34.03 | 21.57 | 33.65 |
| AT5G46330 | 0.45 | 0.23 | 0.32 | 1 | 536.69 | 273.06 | 380.52 | 396.76 |
| AT4G28300 | 0.40 | 0.28 | 0.32 | 1 | 1532.31 | 1066.91 | 1245.92 | 1281.71 |
| AT1G43800 | 0.39 | 0.17 | 0.44 | | 7.94 | 6.76 | 20.59 | 11.76 |
| AT2G25650 | 0.35 | 0.34 | 0.31 | | 220.66 | 219.31 | 193.10 | 211.02 |
| AT5G56300 | 0.50 | 0.49 | 0.01 | | 20.26 | 17.04 | 0.93 | 12.74 |
| AT5G59845 | 0.57 | 0.22 | 0.20 | 1 | 104.44 | 38.68 | 33.95 | 59.02 |
| AT2G24762 | 0.48 | 0.40 | 0.13 | 1 | 1510.29 | 1274.96 | 410.02 | 1065.09 |
| AT3G30725 | 0.47 | 0.22 | 0.31 | | 4.19 | 2.02 | 4.89 | 3.70 |
| AT2G29450 | 0.20 | 0.28 | 0.52 | 1 | 300.54 | 402.77 | 761.43 | 488.25 |
| AT4G01950 | 0.29 | 0.24 | 0.47 | | 102.52 | 87.05 | 165.82 | 118.46 |
| AT5G41080 | 0.39 | 0.20 | 0.41 | 1 | 230.53 | 115.06 | 240.51 | 195.36 |
| AT5G44190 | 0.18 | 0.26 | 0.56 | 1 | 129.03 | 184.16 | 383.98 | 232.39 |
| AT5G28300 | 0.16 | 0.28 | 0.56 | 1 | 143.87 | 257.19 | 515.28 | 305.44 |
| AT5G62020 | 0.49 | 0.28 | 0.23 | 1 | 348.40 | 195.23 | 166.44 | 236.69 |
| AT5G50740 | 0.21 | 0.57 | 0.22 | | 4.31 | 14.61 | 6.26 | 8.40 |
| AT5G67060 | 0.56 | 0.14 | 0.30 | | 22.18 | 1.11 | 18.32 | 13.87 |
| AT2G16060 | 0.32 | 0.37 | 0.31 | | 104.87 | 119.04 | 107.69 | 110.53 |
| AT5G14570 | 0.65 | 0.18 | 0.17 | 1 | 869.36 | 240.47 | 220.99 | 443.61 |
| AT3G61890 | 0.13 | 0.32 | 0.55 | 1 | 184.20 | 465.23 | 784.82 | 478.08 |
| AT5G53980 | 0.21 | 0.47 | 0.32 | | 11.22 | 23.32 | 11.18 | 15.24 |
| AT1G25550 | 0.37 | 0.28 | 0.35 | | 925.00 | 690.74 | 872.25 | 829.33 |
| AT3G24715 | 0.41 | 0.35 | 0.24 | | 234.45 | 199.78 | 130.46 | 188.23 |
| AT4G26670 | 0.23 | 0.32 | 0.45 | 1 | 166.54 | 233.47 | 326.52 | 242.18 |
| AT3G10040 | 0.29 | 0.42 | 0.29 | 1 | 265.48 | 384.28 | 260.58 | 303.45 |
| AT4G32280 | 0.60 | 0.24 | 0.16 | 1 | 108.98 | 42.62 | 29.18 | 60.26 |
| AT2G34600 | 0.14 | 0.25 | 0.61 | 1 | 205.60 | 354.86 | 874.20 | 478.22 |

| | | | | | | | | |
|---|---|---|---|---|---|---|---|---|
| AT1G23390 | 0.31 | 0.29 | 0.40 | | 151.47 | 141.88 | 197.76 | 163.70 |
| AT1G80440 | 0.20 | 0.27 | 0.52 | 1 | 373.30 | 502.46 | 961.79 | 612.52 |
| AT1G01060 | 0.36 | 0.29 | 0.35 | | 753.07 | 600.11 | 735.47 | 696.22 |
| AT3G59530 | 0.36 | 0.36 | 0.28 | | 433.34 | 434.05 | 340.17 | 402.52 |
| AT5G59310 | 0.42 | 0.41 | 0.16 | | 9.36 | 3.90 | 0.61 | 4.62 |
| AT3G04290 | 0.28 | 0.24 | 0.48 | | 16.86 | 10.53 | 30.77 | 19.39 |
| AT3G10525 | 0.58 | 0.06 | 0.35 | | 15.65 | 2.06 | 10.67 | 9.46 |
| AT2G02100 | 0.14 | 0.46 | 0.40 | 1 | 466.50 | 1543.46 | 1321.62 | 1110.52 |
| AT3G08870 | 0.15 | 0.63 | 0.22 | | 4.61 | 17.21 | 5.76 | 9.19 |
| AT1G26800 | 0.27 | 0.26 | 0.47 | 1 | 132.04 | 124.61 | 231.76 | 162.81 |
| AT1G09575 | 0.40 | 0.32 | 0.28 | | 279.12 | 220.41 | 189.33 | 229.62 |
| AT1G70830 | 0.18 | 0.25 | 0.57 | 1 | 77.34 | 112.37 | 249.26 | 146.33 |
| AT3G24500 | 0.35 | 0.31 | 0.34 | | 54.24 | 44.01 | 47.42 | 48.55 |
| AT1G66230 | 0.64 | 0.17 | 0.19 | | 43.86 | 11.95 | 13.20 | 23.00 |
| AT3G53200 | 0.43 | 0.42 | 0.15 | 1 | 268.44 | 260.16 | 96.01 | 208.20 |
| AT1G74650 | 0.37 | 0.27 | 0.37 | | 46.47 | 37.77 | 50.94 | 45.06 |
| AT5G54230 | 0.29 | 0.29 | 0.42 | | 19.01 | 20.37 | 29.34 | 22.91 |
| AT3G15510 | 0.24 | 0.24 | 0.52 | 1 | 163.58 | 153.33 | 337.28 | 218.06 |
| AT3G15500 | 0.21 | 0.37 | 0.42 | | 11.10 | 29.47 | 31.94 | 24.17 |
| AT3G11660 | 0.31 | 0.21 | 0.48 | 1 | 133.41 | 92.81 | 213.02 | 146.41 |
| AT4G14760 | 0.36 | 0.30 | 0.34 | | 1177.39 | 992.80 | 1118.45 | 1096.21 |
| AT5G04950 | 0.28 | 0.27 | 0.45 | 1 | 160.12 | 154.96 | 256.91 | 190.66 |
| AT5G64170 | 0.25 | 0.35 | 0.40 | | 186.13 | 251.01 | 290.34 | 242.49 |
| AT3G12320 | 0.38 | 0.32 | 0.31 | | 899.72 | 753.89 | 737.14 | 796.92 |
| AT4G19170 | 0.33 | 0.28 | 0.39 | | 126.74 | 109.87 | 151.83 | 129.48 |
| AT1G62580 | 0.26 | 0.33 | 0.42 | | 35.92 | 45.97 | 58.22 | 46.70 |
| AT3G44300 | 0.12 | 0.20 | 0.68 | 1 | 186.40 | 303.86 | 1055.86 | 515.37 |
| AT4G10380 | 0.13 | 0.18 | 0.69 | 1 | 186.59 | 262.38 | 1020.74 | 489.90 |
| AT3G21670 | 0.21 | 0.39 | 0.40 | | 10.84 | 28.33 | 24.65 | 21.28 |
| AT2G41230 | 0.66 | 0.16 | 0.18 | | 27.97 | 8.40 | 4.51 | 13.63 |
| AT2G40000 | 0.35 | 0.34 | 0.30 | | 2301.67 | 2251.16 | 2015.74 | 2189.52 |
| AT2G28120 | 0.19 | 0.33 | 0.49 | | 7.84 | 12.79 | 20.31 | 13.65 |
| AT5G56550 | 0.27 | 0.39 | 0.34 | | 130.05 | 185.46 | 162.05 | 159.19 |
| AT1G72150 | 0.30 | 0.31 | 0.39 | 1 | 4913.95 | 5057.30 | 6334.38 | 5435.21 |
| AT2G14610 | 0.31 | 0.37 | 0.33 | | 16.50 | 14.11 | 20.39 | 17.00 |
| AT4G19420 | 0.29 | 0.24 | 0.47 | 1 | 2279.35 | 1942.91 | 3767.19 | 2663.15 |
| AT3G53260 | 0.42 | 0.27 | 0.30 | | 542.22 | 353.92 | 393.93 | 430.02 |
| AT3G61060 | 0.37 | 0.22 | 0.40 | | 127.89 | 74.84 | 131.89 | 111.54 |
| AT1G09530 | 0.26 | 0.27 | 0.47 | | 71.12 | 73.20 | 127.64 | 90.65 |
| AT4G02075 | 0.18 | 0.19 | 0.63 | 1 | 197.46 | 210.32 | 704.81 | 370.86 |
| AT5G15120 | 0.13 | 0.29 | 0.58 | 1 | 64.82 | 145.59 | 298.40 | 169.60 |
| AT5G39890 | 0.31 | 0.35 | 0.33 | | 72.16 | 81.74 | 77.14 | 77.01 |
| AT3G53420 | 0.18 | 0.29 | 0.53 | 1 | 536.15 | 859.90 | 1570.30 | 988.78 |
| AT4G28460 | 0.58 | 0.24 | 0.18 | 1 | 309.71 | 127.88 | 97.90 | 178.50 |
| AT2G46790 | 0.28 | 0.31 | 0.42 | 1 | 321.81 | 357.42 | 485.62 | 388.28 |
| AT2G33750 | 0.36 | 0.34 | 0.30 | | 52.06 | 46.38 | 41.56 | 46.67 |
| AT4G33070 | 0.36 | 0.37 | 0.26 | | 119.40 | 121.97 | 84.82 | 108.73 |

| | | | | | | | | |
|---|---|---|---|---|---|---|---|---|
| AT3G05370 | 0.16 | 0.28 | 0.56 | | 9.51 | 22.06 | 34.95 | 22.17 |
| AT1G13260 | 0.14 | 0.39 | 0.47 | 1 | 118.83 | 315.75 | 375.03 | 269.87 |
| AT1G68840 | 0.16 | 0.27 | 0.56 | 1 | 118.55 | 198.87 | 404.01 | 240.48 |
| AT1G22190 | 0.23 | 0.32 | 0.44 | 1 | 872.50 | 1199.14 | 1672.24 | 1247.96 |
| AT5G62920 | 0.25 | 0.32 | 0.44 | 1 | 224.68 | 287.70 | 396.62 | 303.00 |
| AT1G19050 | 0.27 | 0.26 | 0.47 | 1 | 853.62 | 807.26 | 1466.56 | 1042.48 |
| AT5G24655 | 0.47 | 0.31 | 0.23 | 1 | 173.02 | 114.01 | 84.99 | 124.01 |
| AT5G25610 | 0.29 | 0.36 | 0.35 | | 38.69 | 48.82 | 40.81 | 42.77 |
| AT4G27410 | 0.19 | 0.25 | 0.57 | 1 | 189.34 | 248.04 | 576.67 | 338.02 |
| AT2G37180 | 0.21 | 0.31 | 0.49 | 1 | 75.49 | 109.54 | 175.09 | 120.04 |
| AT5G04890 | 0.45 | 0.35 | 0.20 | 1 | 1312.75 | 1027.37 | 572.64 | 970.92 |
| AT5G17300 | 0.34 | 0.31 | 0.35 | | 268.66 | 243.10 | 283.00 | 264.92 |
| AT3G09600 | 0.24 | 0.30 | 0.47 | 1 | 378.00 | 475.65 | 747.35 | 533.67 |
| AT2G02990 | 0.10 | 0.84 | 0.06 | | 1.57 | 12.50 | 0.84 | 4.97 |
| AT5G44280 | 0.36 | 0.38 | 0.26 | 1 | 1007.95 | 1074.03 | 749.32 | 943.77 |
| AT4G03510 | 0.47 | 0.22 | 0.31 | | 67.38 | 32.54 | 43.77 | 47.89 |
| AT5G22920 | 0.31 | 0.33 | 0.37 | | 786.59 | 848.12 | 939.35 | 858.02 |
| AT2G17450 | 0.17 | 0.17 | 0.66 | | 9.55 | 9.44 | 36.42 | 18.47 |
| AT1G13245 | 0.19 | 0.21 | 0.60 | 1 | 64.55 | 70.19 | 205.31 | 113.35 |
| AT1G67265 | 0.36 | 0.38 | 0.26 | | 6.05 | 7.62 | 5.72 | 6.46 |
| AT1G07350 | 0.36 | 0.28 | 0.36 | | 1120.05 | 883.44 | 1122.55 | 1042.01 |
| AT4G26690 | 0.27 | 0.30 | 0.43 | 1 | 369.30 | 406.49 | 591.20 | 455.66 |
| AT1G11185 | 0.32 | 0.31 | 0.37 | | 252.39 | 248.23 | 295.06 | 265.22 |
| AT3G47720 | 0.40 | 0.29 | 0.31 | | 121.74 | 89.05 | 99.45 | 103.41 |
| AT1G21850 | 0.26 | 0.41 | 0.33 | | 42.65 | 74.64 | 52.30 | 56.53 |
| AT4G34770 | 0.00 | 0.00 | 1.00 | | 0.00 | 0.00 | 4.20 | 1.40 |
| AT4G34810 | 0.15 | 0.34 | 0.50 | | 7.08 | 13.06 | 18.57 | 12.91 |
| AT2G21200 | 0.30 | 0.31 | 0.39 | | 53.78 | 56.64 | 70.15 | 60.19 |
| AT5G24160 | 0.12 | 0.16 | 0.73 | 1 | 313.25 | 430.86 | 1988.25 | 910.79 |
| AT2G46340 | 0.20 | 0.30 | 0.51 | 1 | 450.20 | 687.73 | 1166.20 | 768.04 |
| AT3G22380 | 0.30 | 0.32 | 0.38 | 1 | 8066.75 | 8865.13 | 10421.48 | 9117.79 |
| AT5G37770 | 0.30 | 0.36 | 0.34 | | 393.81 | 470.20 | 436.60 | 433.53 |
| AT5G57560 | 0.45 | 0.26 | 0.29 | 1 | 4347.31 | 2441.84 | 2788.51 | 3192.55 |
| AT4G09820 | 0.43 | 0.18 | 0.40 | | 18.47 | 11.51 | 9.80 | 13.26 |
| AT2G18700 | 0.35 | 0.35 | 0.30 | | 518.11 | 509.33 | 437.12 | 488.19 |
| AT1G70290 | 0.30 | 0.28 | 0.42 | | 277.26 | 263.16 | 390.32 | 310.25 |
| AT2G30424 | 0.75 | 0.23 | 0.02 | | 32.33 | 13.43 | 1.21 | 15.66 |
| AT4G34138 | 0.24 | 0.25 | 0.52 | | 27.91 | 30.61 | 63.47 | 40.66 |
| AT1G22370 | 0.25 | 0.21 | 0.55 | | 37.57 | 26.71 | 80.35 | 48.21 |
| AT1G79680 | 0.47 | 0.25 | 0.27 | 1 | 561.24 | 296.06 | 328.82 | 395.37 |
| AT4G33560 | 0.36 | 0.37 | 0.27 | | 22.16 | 16.80 | 14.62 | 17.86 |
| AT5G24110 | 0.60 | 0.20 | 0.21 | 1 | 495.07 | 163.47 | 168.92 | 275.82 |
| AT1G80930 | 0.34 | 0.32 | 0.34 | | 6587.54 | 6073.86 | 6525.73 | 6395.71 |
| AT5G55040 | 0.32 | 0.34 | 0.34 | | 5730.02 | 6042.25 | 6146.44 | 5972.90 |
| AT2G24550 | 0.43 | 0.29 | 0.28 | 1 | 2824.85 | 1894.09 | 1873.69 | 2197.54 |
| AT4G35940 | 0.32 | 0.36 | 0.32 | | 1976.21 | 2222.46 | 1994.74 | 2064.47 |
| AT1G06420 | 0.37 | 0.34 | 0.29 | | 2159.66 | 1977.14 | 1706.93 | 1947.91 |

| | | | | | | | | |
|---|---|---|---|---|---|---|---|---|
| AT3G28580 | 0.24 | 0.46 | 0.29 | 1 | 1144.10 | 2162.28 | 1379.21 | 1561.86 |
| AT3G19030 | 0.16 | 0.37 | 0.48 | 1 | 545.72 | 1265.19 | 1682.16 | 1164.36 |
| AT5G21940 | 0.35 | 0.34 | 0.31 | | 1043.75 | 1032.89 | 932.80 | 1003.15 |
| AT5G54170 | 0.37 | 0.32 | 0.32 | | 996.02 | 856.64 | 852.78 | 901.81 |
| AT3G06435 | 0.26 | 0.40 | 0.34 | 1 | 627.60 | 956.38 | 827.04 | 803.67 |
| AT3G22970 | 0.25 | 0.32 | 0.43 | 1 | 605.50 | 768.90 | 1010.96 | 795.12 |
| AT4G30470 | 0.23 | 0.30 | 0.47 | 1 | 507.52 | 682.78 | 1048.48 | 746.26 |
| AT2G41250 | 0.23 | 0.33 | 0.44 | 1 | 505.29 | 748.20 | 973.59 | 742.36 |
| AT1G28190 | 0.18 | 0.31 | 0.51 | 1 | 385.43 | 680.40 | 1126.82 | 730.88 |
| AT1G19000 | 0.29 | 0.33 | 0.38 | | 570.29 | 661.78 | 770.23 | 667.43 |
| AT1G68945 | 0.35 | 0.35 | 0.31 | | 673.75 | 678.64 | 593.82 | 648.74 |
| AT5G45520 | 0.34 | 0.34 | 0.32 | | 616.43 | 606.23 | 566.91 | 596.52 |
| AT5G48740 | 0.90 | 0.08 | 0.02 | 1 | 1514.12 | 142.69 | 32.18 | 563.00 |
| AT5G28630 | 0.39 | 0.27 | 0.35 | 1 | 614.49 | 421.61 | 550.17 | 528.76 |
| AT1G32928 | 0.35 | 0.31 | 0.34 | | 489.37 | 446.22 | 478.55 | 471.38 |
| AT5G03230 | 0.25 | 0.26 | 0.49 | 1 | 337.52 | 359.93 | 670.08 | 455.85 |
| AT5G19120 | 0.32 | 0.32 | 0.36 | | 434.58 | 433.77 | 479.34 | 449.23 |
| AT2G28815 | 0.36 | 0.32 | 0.32 | | 468.27 | 422.32 | 412.18 | 434.25 |
| AT4G09630 | 0.30 | 0.32 | 0.38 | | 385.23 | 415.27 | 493.66 | 431.39 |
| AT1G47340 | 0.28 | 0.32 | 0.40 | | 336.73 | 393.25 | 486.43 | 405.47 |
| AT5G47060 | 0.42 | 0.31 | 0.28 | | 500.63 | 371.57 | 329.43 | 400.54 |
| AT4G29905 | 0.19 | 0.25 | 0.56 | 1 | 227.36 | 297.62 | 659.01 | 394.66 |
| AT2G20670 | 0.20 | 0.22 | 0.59 | 1 | 214.19 | 235.53 | 637.77 | 362.50 |
| AT1G68440 | 0.45 | 0.24 | 0.30 | 1 | 473.13 | 255.15 | 316.73 | 348.34 |
| AT1G08643 | 0.30 | 0.47 | 0.23 | 1 | 259.78 | 410.77 | 192.44 | 287.66 |
| AT3G28510 | 0.11 | 0.31 | 0.58 | 1 | 91.36 | 268.17 | 494.43 | 284.65 |
| AT4G14620 | 0.21 | 0.39 | 0.40 | 1 | 172.82 | 324.92 | 327.05 | 274.93 |
| AT4G02920 | 0.21 | 0.32 | 0.48 | 1 | 163.77 | 250.21 | 387.50 | 267.16 |
| AT1G02610 | 0.29 | 0.23 | 0.48 | 1 | 227.34 | 178.89 | 375.85 | 260.69 |
| AT2G29670 | 0.25 | 0.38 | 0.37 | | 190.16 | 285.00 | 275.71 | 250.29 |
| AT5G22530 | 0.27 | 0.30 | 0.43 | | 195.57 | 210.67 | 314.83 | 240.36 |
| AT4G17260 | 0.29 | 0.47 | 0.24 | 1 | 202.98 | 323.30 | 173.14 | 233.14 |
| AT5G60680 | 0.38 | 0.30 | 0.32 | | 260.90 | 208.69 | 224.57 | 231.39 |
| AT3G46600 | 0.23 | 0.36 | 0.40 | | 155.91 | 243.38 | 265.94 | 221.74 |
| AT2G25720 | 0.29 | 0.35 | 0.36 | | 190.45 | 226.89 | 239.92 | 219.09 |
| AT3G49790 | 0.20 | 0.29 | 0.51 | 1 | 131.41 | 191.09 | 323.65 | 215.39 |
| AT5G61820 | 0.18 | 0.28 | 0.53 | 1 | 114.44 | 173.56 | 327.00 | 205.00 |
| AT1G21050 | 0.33 | 0.34 | 0.33 | | 199.43 | 202.74 | 195.07 | 199.08 |
| AT5G28610 | 0.28 | 0.26 | 0.46 | 1 | 162.01 | 150.18 | 259.52 | 190.57 |
| AT3G14200 | 0.19 | 0.40 | 0.42 | 1 | 102.36 | 217.96 | 228.70 | 183.01 |
| AT3G27220 | 0.32 | 0.30 | 0.38 | | 174.69 | 165.65 | 207.27 | 182.54 |
| AT5G60530 | 0.24 | 0.29 | 0.47 | 1 | 131.04 | 155.47 | 250.83 | 179.11 |
| AT4G32480 | 0.19 | 0.35 | 0.46 | 1 | 95.27 | 186.96 | 254.31 | 178.85 |
| AT4G14500 | 0.29 | 0.33 | 0.38 | | 151.86 | 166.60 | 200.94 | 173.13 |
| AT5G59000 | 0.29 | 0.38 | 0.33 | | 144.44 | 186.39 | 161.56 | 164.13 |
| AT3G05400 | 0.14 | 0.23 | 0.63 | 1 | 66.56 | 114.18 | 303.75 | 161.50 |
| AT5G02830 | 0.32 | 0.36 | 0.32 | | 139.46 | 163.55 | 144.83 | 149.28 |

| | | | | | | | | |
|---|---|---|---|---|---|---|---|---|
| AT3G07350 | 0.24 | 0.33 | 0.44 | | 103.80 | 135.34 | 190.00 | 143.05 |
| AT5G54300 | 0.20 | 0.28 | 0.52 | 1 | 85.36 | 115.99 | 214.82 | 138.72 |
| AT1G13470 | 0.40 | 0.30 | 0.30 | | 165.46 | 123.99 | 124.99 | 138.14 |
| AT1G55960 | 0.29 | 0.34 | 0.37 | | 126.34 | 147.14 | 140.75 | 138.08 |
| AT4G24110 | 0.22 | 0.34 | 0.45 | | 83.42 | 131.35 | 177.46 | 130.74 |
| AT5G19190 | 0.31 | 0.30 | 0.39 | | 108.94 | 108.12 | 144.91 | 120.66 |
| AT4G16140 | 0.33 | 0.43 | 0.24 | | 119.07 | 151.08 | 85.95 | 118.70 |
| AT1G60060 | 0.45 | 0.31 | 0.24 | | 155.91 | 107.09 | 80.53 | 114.51 |
| AT2G19160 | 0.41 | 0.31 | 0.29 | | 138.32 | 93.96 | 92.71 | 108.33 |
| AT5G12900 | 0.16 | 0.31 | 0.53 | 1 | 52.18 | 100.15 | 172.33 | 108.22 |
| AT2G38820 | 0.46 | 0.25 | 0.30 | | 143.04 | 74.05 | 90.08 | 102.39 |
| AT2G04495 | 0.45 | 0.30 | 0.25 | | 142.82 | 91.15 | 72.62 | 102.20 |
| AT2G24240 | 0.40 | 0.35 | 0.25 | | 119.71 | 104.64 | 76.72 | 100.36 |
| AT5G10340 | 0.31 | 0.34 | 0.35 | | 89.86 | 100.86 | 108.16 | 99.63 |
| AT1G48770 | 0.39 | 0.28 | 0.33 | | 115.06 | 81.74 | 101.03 | 99.28 |
| AT5G57785 | 0.18 | 0.27 | 0.55 | 1 | 56.23 | 71.62 | 167.86 | 98.57 |
| AT3G57020 | 0.15 | 0.24 | 0.60 | 1 | 42.44 | 68.58 | 180.35 | 97.12 |
| AT4G13575 | 0.14 | 0.26 | 0.60 | 1 | 40.72 | 74.52 | 172.10 | 95.78 |
| AT1G78450 | 0.17 | 0.27 | 0.56 | 1 | 47.14 | 74.47 | 156.80 | 92.80 |
| AT3G63445 | 0.37 | 0.28 | 0.35 | | 92.72 | 68.41 | 90.01 | 83.71 |
| AT5G59080 | 0.15 | 0.32 | 0.53 | 1 | 37.47 | 81.75 | 128.49 | 82.57 |
| AT1G05035 | 0.43 | 0.29 | 0.28 | | 105.00 | 70.97 | 68.40 | 81.46 |
| AT1G51080 | 0.26 | 0.33 | 0.40 | | 60.96 | 81.29 | 95.05 | 79.10 |
| AT4G30570 | 0.33 | 0.40 | 0.26 | | 74.28 | 84.43 | 52.90 | 70.53 |
| AT3G50840 | 0.33 | 0.27 | 0.40 | | 62.24 | 54.54 | 80.72 | 65.83 |
| AT3G12910 | 0.63 | 0.19 | 0.18 | 1 | 122.06 | 35.46 | 35.77 | 64.43 |
| AT1G64500 | 0.19 | 0.22 | 0.59 | 1 | 35.53 | 41.13 | 112.82 | 63.16 |
| AT4G37530 | 0.19 | 0.25 | 0.56 | | 35.62 | 49.06 | 100.60 | 61.76 |
| AT5G03890 | 0.45 | 0.42 | 0.12 | 1 | 80.87 | 74.32 | 22.61 | 59.27 |
| AT2G25200 | 0.46 | 0.27 | 0.27 | | 67.91 | 41.21 | 41.16 | 50.10 |
| AT2G28200 | 0.33 | 0.23 | 0.45 | | 41.49 | 35.37 | 70.42 | 49.09 |
| AT4G27900 | 0.20 | 0.35 | 0.45 | | 29.28 | 49.95 | 66.39 | 48.54 |
| AT1G13650 | 0.60 | 0.18 | 0.22 | 1 | 88.71 | 23.91 | 31.80 | 48.14 |
| AT3G51340 | 0.37 | 0.36 | 0.27 | | 52.55 | 49.30 | 38.58 | 46.81 |
| AT1G80630 | 0.35 | 0.35 | 0.30 | | 48.21 | 48.55 | 42.23 | 46.33 |
| AT1G17665 | 0.35 | 0.25 | 0.40 | | 51.29 | 29.82 | 49.47 | 43.52 |
| AT1G15830 | 0.41 | 0.35 | 0.24 | | 44.47 | 37.60 | 25.05 | 35.71 |
| AT1G73120 | 0.32 | 0.31 | 0.36 | | 31.46 | 28.57 | 34.94 | 31.66 |
| AT1G60590 | 0.16 | 0.26 | 0.58 | | 14.71 | 20.37 | 54.72 | 29.94 |
| AT1G29640 | 0.30 | 0.37 | 0.33 | | 22.36 | 27.37 | 24.33 | 24.69 |
| AT2G03750 | 0.30 | 0.36 | 0.34 | | 15.96 | 28.41 | 28.48 | 24.28 |
| AT5G22310 | 0.15 | 0.35 | 0.50 | | 10.33 | 25.02 | 29.72 | 21.69 |
| AT1G13480 | 0.40 | 0.28 | 0.33 | | 25.72 | 17.10 | 20.04 | 20.95 |
| AT2G14247 | 0.45 | 0.22 | 0.34 | | 25.88 | 14.13 | 21.82 | 20.61 |
| AT4G13330 | 0.45 | 0.41 | 0.13 | | 26.08 | 24.57 | 7.92 | 19.52 |
| AT2G44230 | 0.20 | 0.28 | 0.51 | | 11.92 | 14.71 | 29.31 | 18.64 |
| AT1G29660 | 0.45 | 0.35 | 0.21 | | 21.99 | 20.59 | 9.76 | 17.45 |

| | | | | | | | | |
|---|---|---|---|---|---|---|---|---|
| AT5G23950 | 0.14 | 0.09 | 0.78 | | 9.00 | 3.78 | 36.56 | 16.45 |
| AT1G07690 | 0.49 | 0.10 | 0.41 | | 24.28 | 6.34 | 18.36 | 16.33 |
| AT4G16146 | 0.35 | 0.30 | 0.35 | | 16.36 | 15.85 | 16.71 | 16.31 |
| AT4G38410 | 0.02 | 0.35 | 0.63 | 1 | 0.98 | 16.50 | 26.50 | 14.66 |
| AT5G24880 | 0.10 | 0.30 | 0.60 | | 3.45 | 13.95 | 21.80 | 13.06 |
| AT2G15020 | 0.25 | 0.36 | 0.39 | | 9.28 | 11.84 | 14.67 | 11.93 |
| AT2G44660 | 0.41 | 0.45 | 0.14 | | 13.84 | 16.11 | 5.53 | 11.83 |
| AT5G40590 | 0.24 | 0.45 | 0.32 | | 7.22 | 15.25 | 12.94 | 11.80 |
| AT5G62730 | 0.01 | 0.84 | 0.16 | 1 | 0.39 | 30.82 | 3.49 | 11.57 |
| AT3G54520 | 0.13 | 0.44 | 0.43 | | 4.97 | 19.27 | 9.88 | 11.37 |
| AT1G53035 | 0.14 | 0.36 | 0.50 | | 9.41 | 10.82 | 13.87 | 11.37 |
| AT5G35777 | 0.12 | 0.56 | 0.31 | | 2.46 | 16.27 | 11.84 | 10.19 |
| AT5G57510 | 0.21 | 0.25 | 0.54 | | 5.40 | 7.68 | 16.57 | 9.88 |
| AT2G40085 | 0.25 | 0.34 | 0.41 | | 11.18 | 7.62 | 10.33 | 9.71 |
| AT2G01422 | 0.29 | 0.45 | 0.26 | | 8.90 | 11.83 | 8.25 | 9.66 |
| AT1G49570 | 0.15 | 0.15 | 0.69 | | 4.70 | 4.83 | 17.23 | 8.92 |
| AT1G23205 | 0.49 | 0.21 | 0.30 | | 13.42 | 5.98 | 5.69 | 8.36 |
| AT5G19890 | 0.33 | 0.67 | 0.00 | | 6.67 | 17.09 | 0.00 | 7.92 |
| AT5G62280 | 0.24 | 0.30 | 0.46 | | 5.44 | 6.87 | 11.15 | 7.82 |
| AT5G66985 | 0.38 | 0.33 | 0.29 | | 10.91 | 4.94 | 7.16 | 7.67 |
| AT5G41900 | 0.30 | 0.17 | 0.54 | | 12.67 | 2.59 | 7.56 | 7.61 |
| AT2G15830 | 0.16 | 0.39 | 0.45 | | 4.52 | 4.83 | 13.45 | 7.60 |
| AT2G17850 | 0.53 | 0.36 | 0.11 | | 7.49 | 10.64 | 2.80 | 6.98 |
| AT3G54530 | 0.40 | 0.18 | 0.42 | | 2.17 | 9.28 | 8.33 | 6.60 |
| AT1G07160 | 0.00 | 0.39 | 0.61 | | 0.00 | 9.22 | 10.36 | 6.53 |
| AT2G17845 | 0.47 | 0.46 | 0.06 | | 6.84 | 9.12 | 0.58 | 5.51 |
| AT2G07783 | 0.24 | 0.37 | 0.39 | | 3.85 | 5.95 | 5.42 | 5.08 |
| AT1G12805 | 0.16 | 0.43 | 0.41 | | 2.11 | 8.06 | 4.31 | 4.82 |
| AT1G05057 | 0.58 | 0.23 | 0.19 | | 6.93 | 2.63 | 2.10 | 3.89 |

**Supplemental Table 9.** Cambium domain-specific expression of the 620 auxin related or regulated genes. The relative mean across all cambium domains or mean of the normalized count values are given. LRT = Likelihood ratio test. LRT=1 indicates significance difference of expression levels across cambium domains. A mean value of all domains lower 10 was interpreted as no expression within the cambium. The RNA-seq data and analysis was produced by Dr. Dongbo Shi. The analysis of auxin related genes was conducted by myself.

| | Relative Mean | | | | Mean normalized count values | | | Mean |
|---|---|---|---|---|---|---|---|---|
| Gene | proximal | central | distal | LRT | proximal | central | distal | All domains |
| AT5G54500 | 0.55 | 0.26 | 0.18 | 1 | 7071.14 | 3362.91 | 2336.85 | 4256.97 |
| AT2G32700 | 0.41 | 0.30 | 0.29 | 1 | 4342.91 | 3180.57 | 3131.69 | 3551.72 |
| AT5G57560 | 0.45 | 0.26 | 0.29 | 1 | 4347.31 | 2441.84 | 2788.51 | 3192.55 |
| AT1G59870 | 0.42 | 0.25 | 0.33 | 1 | 3803.21 | 2314.73 | 2961.79 | 3026.58 |
| AT5G65670 | 0.34 | 0.33 | 0.33 | | 3093.90 | 2968.16 | 2981.84 | 3014.63 |
| AT4G24390 | 0.37 | 0.36 | 0.27 | 1 | 3278.72 | 3225.17 | 2451.22 | 2985.04 |
| AT3G02260 | 0.38 | 0.32 | 0.30 | 1 | 3340.65 | 2772.41 | 2663.88 | 2925.64 |
| AT4G11280 | 0.40 | 0.32 | 0.28 | 1 | 3453.42 | 2788.36 | 2362.44 | 2868.07 |
| AT3G23030 | 0.27 | 0.35 | 0.38 | 1 | 2247.07 | 2887.26 | 3212.15 | 2782.16 |
| AT4G32880 | 0.58 | 0.35 | 0.08 | 1 | 4813.06 | 2878.66 | 629.97 | 2773.89 |
| AT1G22530 | 0.23 | 0.22 | 0.54 | 1 | 1849.12 | 1753.45 | 4255.61 | 2619.40 |
| AT3G13300 | 0.31 | 0.32 | 0.37 | | 2365.22 | 2449.72 | 2825.36 | 2546.77 |
| AT1G18740 | 0.32 | 0.37 | 0.31 | | 2265.97 | 2646.33 | 2253.97 | 2388.76 |
| AT1G75500 | 0.39 | 0.50 | 0.10 | 1 | 2438.88 | 3174.47 | 645.17 | 2086.18 |
| AT5G67300 | 0.31 | 0.30 | 0.39 | 1 | 1885.67 | 1838.50 | 2390.38 | 2038.18 |
| AT4G34410 | 0.33 | 0.30 | 0.37 | | 1933.36 | 1813.96 | 2208.05 | 1985.12 |
| AT5G22220 | 0.41 | 0.27 | 0.32 | 1 | 2309.04 | 1544.22 | 1851.90 | 1901.72 |
| AT1G15750 | 0.31 | 0.31 | 0.38 | 1 | 1750.73 | 1730.12 | 2122.87 | 1867.91 |
| AT1G70940 | 0.29 | 0.40 | 0.31 | 1 | 1432.87 | 1981.70 | 1543.86 | 1652.81 |
| AT2G23810 | 0.37 | 0.26 | 0.37 | 1 | 1822.94 | 1241.63 | 1799.22 | 1621.26 |
| AT5G65940 | 0.31 | 0.35 | 0.34 | | 1521.24 | 1681.92 | 1629.47 | 1610.88 |
| AT4G14550 | 0.36 | 0.38 | 0.26 | 1 | 1649.97 | 1737.88 | 1208.26 | 1532.04 |
| AT3G62150 | 0.30 | 0.26 | 0.44 | 1 | 1365.44 | 1174.88 | 2012.19 | 1517.51 |
| AT4G29940 | 0.33 | 0.34 | 0.33 | | 1483.37 | 1506.46 | 1478.27 | 1489.37 |
| AT5G19530 | 0.75 | 0.24 | 0.02 | 1 | 3335.97 | 1062.00 | 69.15 | 1489.04 |
| AT3G43300 | 0.39 | 0.30 | 0.30 | | 1735.84 | 1341.91 | 1335.32 | 1471.02 |
| AT1G59750 | 0.46 | 0.32 | 0.23 | 1 | 1985.95 | 1365.33 | 982.09 | 1444.46 |
| AT3G04730 | 0.23 | 0.32 | 0.45 | 1 | 933.08 | 1328.50 | 1877.97 | 1379.85 |
| AT1G19220 | 0.43 | 0.30 | 0.27 | 1 | 1706.53 | 1217.44 | 1075.20 | 1333.05 |
| AT2G25170 | 0.37 | 0.32 | 0.30 | | 1441.33 | 1248.11 | 1164.88 | 1284.77 |
| AT3G53020 | 0.35 | 0.37 | 0.28 | 1 | 1284.62 | 1379.64 | 1035.29 | 1233.18 |
| AT4G14740 | 0.43 | 0.37 | 0.21 | 1 | 1581.68 | 1357.20 | 760.05 | 1232.98 |
| AT3G16500 | 0.39 | 0.33 | 0.28 | 1 | 1429.29 | 1219.65 | 1014.90 | 1221.28 |
| AT2G33310 | 0.37 | 0.36 | 0.26 | 1 | 1348.80 | 1312.96 | 951.89 | 1204.55 |
| AT3G44310 | 0.18 | 0.26 | 0.56 | 1 | 630.20 | 933.53 | 2004.33 | 1189.35 |
| AT4G14560 | 0.31 | 0.36 | 0.33 | | 1110.25 | 1269.82 | 1175.67 | 1185.25 |
| AT5G09410 | 0.36 | 0.34 | 0.30 | | 1268.83 | 1188.98 | 1070.92 | 1176.25 |
| AT1G25400 | 0.36 | 0.31 | 0.33 | | 1282.01 | 1088.74 | 1154.91 | 1175.22 |
| AT1G48410 | 0.37 | 0.31 | 0.32 | | 1289.57 | 1095.49 | 1105.23 | 1163.43 |
| AT2G47170 | 0.30 | 0.29 | 0.40 | 1 | 1060.40 | 1025.75 | 1402.18 | 1162.78 |

| | | | | | | | | |
|---|---|---|---|---|---|---|---|---|
| AT1G67900 | 0.25 | 0.30 | 0.45 | 1 | 816.31 | 989.67 | 1509.50 | 1105.16 |
| AT2G22670 | 0.48 | 0.37 | 0.15 | 1 | 1502.68 | 1179.01 | 478.21 | 1053.30 |
| AT1G72700 | 0.41 | 0.32 | 0.27 | 1 | 1271.91 | 995.49 | 839.78 | 1035.72 |
| AT1G59820 | 0.43 | 0.28 | 0.29 | 1 | 1298.79 | 839.92 | 890.37 | 1009.69 |
| AT4G27280 | 0.27 | 0.33 | 0.40 | 1 | 804.99 | 998.62 | 1201.00 | 1001.54 |
| AT4G18710 | 0.29 | 0.36 | 0.35 | | 850.07 | 1088.91 | 1047.51 | 995.50 |
| AT4G37260 | 0.30 | 0.42 | 0.28 | | 899.36 | 1240.35 | 839.41 | 993.04 |
| AT2G36910 | 0.34 | 0.35 | 0.31 | | 1014.59 | 1023.84 | 925.33 | 987.92 |
| AT1G44350 | 0.31 | 0.28 | 0.41 | 1 | 919.80 | 825.29 | 1212.97 | 986.02 |
| AT4G30960 | 0.21 | 0.34 | 0.46 | 1 | 615.67 | 990.16 | 1346.78 | 984.20 |
| AT1G63420 | 0.24 | 0.41 | 0.34 | 1 | 707.63 | 1216.19 | 1005.66 | 976.49 |
| AT4G39950 | 0.14 | 0.27 | 0.58 | 1 | 408.23 | 757.61 | 1654.73 | 940.19 |
| AT5G63160 | 0.30 | 0.44 | 0.26 | 1 | 855.22 | 1236.04 | 725.86 | 939.04 |
| AT5G09810 | 0.31 | 0.33 | 0.36 | | 859.04 | 919.53 | 985.89 | 921.48 |
| AT1G64625 | 0.46 | 0.48 | 0.07 | 1 | 1268.66 | 1314.84 | 180.80 | 921.43 |
| AT4G37610 | 0.47 | 0.29 | 0.24 | 1 | 1293.29 | 794.17 | 648.38 | 911.95 |
| AT2G34680 | 0.25 | 0.40 | 0.35 | 1 | 693.23 | 1083.97 | 957.77 | 911.66 |
| AT5G08560 | 0.44 | 0.28 | 0.28 | 1 | 1193.09 | 761.92 | 770.61 | 908.54 |
| AT5G62000 | 0.38 | 0.33 | 0.29 | | 1009.23 | 870.78 | 754.62 | 878.21 |
| AT5G56750 | 0.36 | 0.32 | 0.32 | | 937.15 | 825.20 | 825.28 | 862.54 |
| AT1G50030 | 0.31 | 0.38 | 0.31 | | 793.03 | 961.80 | 789.90 | 848.25 |
| AT5G47390 | 0.26 | 0.31 | 0.43 | 1 | 664.45 | 776.44 | 1087.83 | 842.91 |
| AT5G01990 | 0.36 | 0.33 | 0.31 | | 892.92 | 820.63 | 760.41 | 824.65 |
| AT2G42580 | 0.27 | 0.32 | 0.41 | 1 | 648.00 | 767.12 | 974.83 | 796.65 |
| AT2G47000 | 0.41 | 0.28 | 0.31 | 1 | 957.20 | 649.89 | 714.28 | 773.79 |
| AT3G25610 | 0.43 | 0.30 | 0.27 | 1 | 963.51 | 681.86 | 615.19 | 753.52 |
| AT1G24100 | 0.17 | 0.28 | 0.55 | 1 | 383.61 | 624.12 | 1235.57 | 747.77 |
| AT1G74840 | 0.32 | 0.35 | 0.33 | | 710.86 | 785.35 | 745.73 | 747.32 |
| AT2G02560 | 0.38 | 0.36 | 0.27 | 1 | 843.12 | 800.11 | 598.48 | 747.24 |
| AT5G20960 | 0.27 | 0.32 | 0.41 | 1 | 596.16 | 710.54 | 921.95 | 742.88 |
| AT1G15690 | 0.50 | 0.28 | 0.22 | 1 | 1102.03 | 621.61 | 478.46 | 734.03 |
| AT2G21050 | 0.55 | 0.41 | 0.04 | 1 | 1176.38 | 882.97 | 87.02 | 715.46 |
| AT2G38120 | 0.49 | 0.36 | 0.15 | 1 | 1051.59 | 762.61 | 321.39 | 711.86 |
| AT3G08510 | 0.30 | 0.31 | 0.38 | | 636.64 | 671.36 | 805.01 | 704.34 |
| AT4G33090 | 0.37 | 0.29 | 0.34 | | 783.23 | 608.03 | 715.81 | 702.36 |
| AT4G23570 | 0.34 | 0.40 | 0.26 | 1 | 713.12 | 843.99 | 531.58 | 696.23 |
| AT4G39080 | 0.32 | 0.31 | 0.38 | | 657.11 | 637.25 | 788.98 | 694.45 |
| AT4G37540 | 0.25 | 0.31 | 0.44 | 1 | 521.73 | 631.44 | 897.70 | 683.62 |
| AT1G19000 | 0.29 | 0.33 | 0.38 | | 570.29 | 661.78 | 770.23 | 667.43 |
| AT4G02570 | 0.36 | 0.33 | 0.31 | | 706.87 | 662.19 | 604.85 | 657.97 |
| AT4G31500 | 0.22 | 0.28 | 0.50 | 1 | 431.63 | 555.69 | 984.79 | 657.37 |
| AT3G12670 | 0.32 | 0.28 | 0.39 | | 630.36 | 557.98 | 767.14 | 651.83 |
| AT4G04920 | 0.37 | 0.32 | 0.32 | | 714.78 | 613.76 | 624.57 | 651.04 |
| AT5G05730 | 0.29 | 0.28 | 0.43 | 1 | 553.09 | 540.55 | 839.90 | 644.51 |
| AT4G16890 | 0.32 | 0.27 | 0.40 | 1 | 626.75 | 529.81 | 776.34 | 644.30 |
| AT4G16340 | 0.47 | 0.30 | 0.23 | 1 | 907.16 | 565.53 | 432.31 | 635.00 |
| AT3G22810 | 0.40 | 0.44 | 0.16 | 1 | 762.58 | 829.56 | 300.83 | 630.99 |

| | | | | | | | | |
|---|---|---|---|---|---|---|---|---|
| AT5G64260 | 0.36 | 0.33 | 0.32 | | 678.04 | 612.60 | 592.47 | 627.70 |
| AT1G19850 | 0.49 | 0.35 | 0.16 | 1 | 910.59 | 659.93 | 291.54 | 620.69 |
| AT1G24180 | 0.38 | 0.34 | 0.29 | | 699.52 | 622.09 | 529.40 | 617.01 |
| AT5G03280 | 0.35 | 0.31 | 0.34 | | 638.31 | 571.06 | 620.62 | 610.00 |
| AT4G37750 | 0.04 | 0.61 | 0.35 | 1 | 66.20 | 1102.91 | 643.95 | 604.35 |
| AT3G59060 | 0.12 | 0.24 | 0.63 | 1 | 222.33 | 440.42 | 1149.89 | 604.21 |
| AT5G60450 | 0.28 | 0.35 | 0.37 | | 498.65 | 632.09 | 678.14 | 602.96 |
| AT5G20990 | 0.35 | 0.30 | 0.36 | | 617.17 | 532.05 | 645.64 | 598.29 |
| AT5G13300 | 0.34 | 0.37 | 0.29 | | 599.63 | 652.74 | 517.56 | 589.98 |
| AT4G29080 | 0.35 | 0.35 | 0.30 | | 618.70 | 617.44 | 523.75 | 586.63 |
| AT3G23050 | 0.18 | 0.26 | 0.56 | 1 | 317.05 | 450.59 | 972.17 | 579.94 |
| AT2G17800 | 0.52 | 0.24 | 0.24 | 1 | 899.24 | 422.04 | 406.36 | 575.88 |
| AT2G26170 | 0.47 | 0.31 | 0.22 | 1 | 811.05 | 539.19 | 370.64 | 573.63 |
| AT1G54200 | 0.21 | 0.38 | 0.42 | 1 | 354.95 | 648.69 | 715.67 | 573.10 |
| AT4G07410 | 0.34 | 0.35 | 0.30 | | 588.98 | 605.98 | 518.02 | 571.00 |
| AT5G54490 | 0.33 | 0.40 | 0.27 | 1 | 554.05 | 666.55 | 452.82 | 557.81 |
| AT5G11790 | 0.36 | 0.28 | 0.36 | | 603.68 | 471.61 | 592.13 | 555.81 |
| AT1G06400 | 0.37 | 0.28 | 0.34 | | 610.05 | 474.45 | 574.75 | 553.09 |
| AT5G13680 | 0.38 | 0.38 | 0.24 | 1 | 623.77 | 635.35 | 389.05 | 549.39 |
| AT1G18460 | 0.35 | 0.33 | 0.33 | | 562.38 | 535.64 | 529.60 | 542.54 |
| AT4G32810 | 0.62 | 0.26 | 0.12 | 1 | 1000.18 | 409.90 | 192.94 | 534.34 |
| AT1G25220 | 0.33 | 0.31 | 0.36 | | 520.31 | 484.16 | 554.17 | 519.54 |
| AT1G68710 | 0.44 | 0.27 | 0.29 | 1 | 689.45 | 418.74 | 444.08 | 517.42 |
| AT3G44300 | 0.12 | 0.20 | 0.68 | 1 | 186.40 | 303.86 | 1055.86 | 515.37 |
| AT5G01240 | 0.35 | 0.39 | 0.26 | 1 | 532.08 | 599.83 | 395.08 | 509.00 |
| AT3G51670 | 0.31 | 0.47 | 0.22 | 1 | 471.63 | 717.73 | 330.35 | 506.57 |
| AT4G23980 | 0.36 | 0.36 | 0.28 | | 541.17 | 539.40 | 413.44 | 498.00 |
| AT1G27370 | 0.44 | 0.31 | 0.25 | 1 | 662.75 | 462.58 | 366.61 | 497.31 |
| AT5G55540 | 0.25 | 0.37 | 0.38 | 1 | 376.36 | 549.12 | 556.66 | 494.05 |
| AT2G42620 | 0.34 | 0.36 | 0.30 | | 504.92 | 527.96 | 446.08 | 492.99 |
| AT1G13210 | 0.38 | 0.30 | 0.31 | | 567.00 | 449.83 | 461.16 | 492.66 |
| AT3G63300 | 0.36 | 0.31 | 0.33 | | 523.61 | 442.83 | 488.97 | 485.13 |
| AT3G15540 | 0.50 | 0.27 | 0.23 | 1 | 709.23 | 390.23 | 334.26 | 477.90 |
| AT2G47260 | 0.31 | 0.42 | 0.27 | 1 | 430.51 | 582.25 | 366.41 | 459.72 |
| AT4G02450 | 0.31 | 0.33 | 0.36 | | 427.30 | 452.51 | 490.49 | 456.76 |
| AT5G56650 | 0.36 | 0.35 | 0.29 | | 489.41 | 479.45 | 396.20 | 455.02 |
| AT1G30690 | 0.12 | 0.50 | 0.38 | 1 | 165.80 | 678.04 | 520.65 | 454.83 |
| AT5G20730 | 0.32 | 0.32 | 0.36 | | 438.65 | 431.62 | 492.95 | 454.41 |
| AT2G01950 | 0.34 | 0.51 | 0.15 | 1 | 464.65 | 694.62 | 196.59 | 451.95 |
| AT3G48360 | 0.15 | 0.21 | 0.65 | 1 | 198.03 | 275.84 | 863.63 | 445.83 |
| AT2G46370 | 0.29 | 0.28 | 0.43 | 1 | 384.51 | 370.95 | 577.04 | 444.17 |
| AT1G04550 | 0.50 | 0.33 | 0.16 | 1 | 670.71 | 440.32 | 212.18 | 441.07 |
| AT5G01270 | 0.32 | 0.32 | 0.36 | | 429.61 | 414.83 | 475.98 | 440.14 |
| AT5G37770 | 0.30 | 0.36 | 0.34 | | 393.81 | 470.20 | 436.60 | 433.53 |
| AT5G10200 | 0.29 | 0.35 | 0.37 | | 370.08 | 448.56 | 474.02 | 430.89 |
| AT1G73590 | 0.44 | 0.41 | 0.15 | 1 | 565.17 | 521.41 | 198.62 | 428.40 |
| AT4G26610 | 0.37 | 0.33 | 0.30 | | 474.54 | 426.23 | 382.03 | 427.60 |

| | | | | | | | | |
|---|---|---|---|---|---|---|---|---|
| AT2G35600 | 0.72 | 0.24 | 0.04 | 1 | 910.25 | 307.47 | 49.66 | 422.46 |
| AT4G16780 | 0.38 | 0.32 | 0.30 | | 475.83 | 403.31 | 382.63 | 420.59 |
| AT4G31820 | 0.24 | 0.33 | 0.43 | 1 | 300.36 | 414.53 | 539.37 | 418.08 |
| AT1G14000 | 0.32 | 0.32 | 0.36 | | 402.16 | 403.69 | 442.13 | 415.99 |
| AT4G32551 | 0.34 | 0.33 | 0.33 | | 419.18 | 410.12 | 409.98 | 413.09 |
| AT5G03540 | 0.45 | 0.30 | 0.25 | 1 | 556.74 | 365.83 | 307.95 | 410.17 |
| AT3G51800 | 0.35 | 0.34 | 0.31 | | 424.78 | 416.60 | 369.87 | 403.75 |
| AT3G08760 | 0.31 | 0.34 | 0.35 | | 379.06 | 410.78 | 420.68 | 403.51 |
| AT1G33410 | 0.37 | 0.38 | 0.25 | | 442.23 | 451.07 | 299.13 | 397.48 |
| AT1G62810 | 0.18 | 0.35 | 0.47 | 1 | 205.08 | 413.15 | 547.97 | 388.73 |
| AT2G20610 | 0.18 | 0.28 | 0.54 | 1 | 211.57 | 325.22 | 626.87 | 387.89 |
| AT4G36760 | 0.33 | 0.31 | 0.36 | | 384.04 | 351.84 | 422.59 | 386.16 |
| AT1G51760 | 0.36 | 0.32 | 0.33 | | 415.69 | 365.83 | 373.06 | 384.86 |
| AT3G22942 | 0.34 | 0.29 | 0.38 | | 389.67 | 331.62 | 430.25 | 383.84 |
| AT1G30330 | 0.19 | 0.32 | 0.49 | 1 | 218.63 | 362.01 | 567.18 | 382.61 |
| AT4G36800 | 0.30 | 0.33 | 0.38 | | 338.73 | 376.63 | 427.50 | 380.95 |
| AT1G14350 | 0.37 | 0.29 | 0.34 | | 426.73 | 334.18 | 377.58 | 379.49 |
| AT3G28860 | 0.53 | 0.27 | 0.20 | 1 | 599.30 | 307.61 | 222.23 | 376.38 |
| AT1G53500 | 0.32 | 0.36 | 0.33 | | 351.52 | 401.63 | 373.18 | 375.44 |
| AT5G13750 | 0.22 | 0.43 | 0.36 | 1 | 245.61 | 477.08 | 397.79 | 373.49 |
| AT1G31710 | 0.22 | 0.38 | 0.39 | 1 | 250.55 | 425.88 | 443.57 | 373.33 |
| AT5G45800 | 0.22 | 0.33 | 0.45 | 1 | 245.40 | 367.86 | 503.60 | 372.29 |
| AT1G12110 | 0.11 | 0.21 | 0.68 | 1 | 121.63 | 231.58 | 759.92 | 371.04 |
| AT5G23850 | 0.39 | 0.35 | 0.26 | 1 | 438.54 | 383.55 | 285.67 | 369.25 |
| AT5G60440 | 0.42 | 0.30 | 0.28 | 1 | 470.03 | 331.68 | 305.46 | 369.05 |
| AT3G16350 | 0.23 | 0.27 | 0.50 | 1 | 251.28 | 298.48 | 553.70 | 367.82 |
| AT4G11260 | 0.36 | 0.33 | 0.31 | | 395.97 | 356.17 | 329.99 | 360.71 |
| AT2G22330 | 0.09 | 0.26 | 0.64 | 1 | 93.07 | 281.62 | 693.97 | 356.22 |
| AT3G53970 | 0.38 | 0.32 | 0.30 | | 407.69 | 339.94 | 313.19 | 353.61 |
| AT1G25490 | 0.40 | 0.33 | 0.27 | | 419.63 | 351.23 | 285.23 | 352.03 |
| AT1G56010 | 0.23 | 0.26 | 0.51 | 1 | 246.26 | 274.83 | 534.98 | 352.02 |
| AT5G37020 | 0.24 | 0.33 | 0.42 | 1 | 250.52 | 340.27 | 450.77 | 347.18 |
| AT4G38630 | 0.38 | 0.29 | 0.33 | | 391.63 | 296.40 | 342.24 | 343.43 |
| AT5G26600 | 0.28 | 0.32 | 0.40 | | 284.78 | 328.43 | 412.67 | 341.96 |
| AT1G80360 | 0.28 | 0.38 | 0.34 | | 283.39 | 389.41 | 349.44 | 340.74 |
| AT1G71930 | 0.86 | 0.12 | 0.02 | 1 | 864.84 | 119.83 | 23.49 | 336.05 |
| AT5G10510 | 0.29 | 0.40 | 0.31 | | 299.76 | 395.76 | 311.74 | 335.75 |
| AT1G07135 | 0.30 | 0.40 | 0.31 | | 287.41 | 391.20 | 294.02 | 324.21 |
| AT1G27340 | 0.47 | 0.28 | 0.25 | 1 | 456.10 | 270.55 | 236.24 | 320.96 |
| AT1G51950 | 0.35 | 0.26 | 0.39 | 1 | 338.61 | 248.44 | 375.69 | 320.91 |
| AT1G12990 | 0.36 | 0.34 | 0.30 | | 341.50 | 323.45 | 290.74 | 318.56 |
| AT3G43600 | 0.23 | 0.36 | 0.41 | 1 | 224.44 | 340.66 | 388.49 | 317.86 |
| AT1G77110 | 0.60 | 0.38 | 0.01 | 1 | 574.58 | 363.29 | 13.49 | 317.12 |
| AT3G05630 | 0.43 | 0.41 | 0.16 | | 406.90 | 385.68 | 151.28 | 314.62 |
| AT1G17500 | 0.32 | 0.37 | 0.30 | | 300.88 | 350.37 | 284.60 | 311.95 |
| AT1G07910 | 0.37 | 0.33 | 0.30 | | 339.84 | 304.61 | 279.56 | 308.00 |
| AT5G25890 | 0.59 | 0.31 | 0.10 | 1 | 538.31 | 287.02 | 91.89 | 305.74 |

| | | | | | | | | |
|---|---|---|---|---|---|---|---|---|
| AT1G17140 | 0.20 | 0.56 | 0.24 | 1 | 173.81 | 504.24 | 219.20 | 299.09 |
| AT1G76530 | 0.18 | 0.58 | 0.24 | 1 | 155.19 | 522.73 | 218.63 | 298.85 |
| AT3G23750 | 0.34 | 0.44 | 0.22 | 1 | 306.45 | 390.40 | 199.31 | 298.72 |
| AT3G28345 | 0.50 | 0.16 | 0.34 | 1 | 446.94 | 145.62 | 303.46 | 298.67 |
| AT5G56660 | 0.31 | 0.33 | 0.35 | | 277.92 | 298.55 | 315.70 | 297.39 |
| AT1G04250 | 0.17 | 0.37 | 0.47 | 1 | 148.47 | 324.30 | 419.23 | 297.33 |
| AT3G25540 | 0.23 | 0.32 | 0.46 | 1 | 201.79 | 278.34 | 408.99 | 296.37 |
| AT1G14120 | 0.15 | 0.28 | 0.57 | 1 | 134.02 | 229.32 | 521.11 | 294.82 |
| AT2G23170 | 0.18 | 0.27 | 0.55 | 1 | 150.09 | 242.28 | 491.79 | 294.72 |
| AT2G20000 | 0.34 | 0.33 | 0.33 | | 299.21 | 294.57 | 289.50 | 294.43 |
| AT5G45710 | 0.39 | 0.30 | 0.30 | | 341.78 | 264.99 | 272.35 | 293.04 |
| AT2G06850 | 0.17 | 0.52 | 0.32 | 1 | 145.56 | 459.08 | 272.98 | 292.54 |
| AT4G13750 | 0.39 | 0.34 | 0.26 | | 341.99 | 304.52 | 230.49 | 292.33 |
| AT4G08920 | 0.33 | 0.27 | 0.40 | | 291.52 | 231.55 | 352.23 | 291.77 |
| AT1G28560 | 0.28 | 0.32 | 0.39 | | 252.71 | 284.49 | 331.47 | 289.56 |
| AT5G40770 | 0.38 | 0.32 | 0.31 | | 325.54 | 272.83 | 263.84 | 287.40 |
| AT3G06810 | 0.28 | 0.31 | 0.41 | | 238.95 | 264.85 | 354.89 | 286.23 |
| AT5G67480 | 0.17 | 0.34 | 0.49 | 1 | 151.19 | 284.76 | 417.74 | 284.57 |
| AT1G79200 | 0.37 | 0.32 | 0.31 | | 305.11 | 272.77 | 269.35 | 282.41 |
| AT5G47370 | 0.10 | 0.40 | 0.49 | 1 | 87.10 | 338.07 | 415.27 | 280.15 |
| AT5G43270 | 0.35 | 0.27 | 0.38 | | 289.15 | 231.11 | 317.86 | 279.37 |
| AT3G53480 | 0.15 | 0.19 | 0.65 | 1 | 130.07 | 157.99 | 545.00 | 277.69 |
| AT3G42660 | 0.27 | 0.49 | 0.24 | 1 | 222.33 | 409.32 | 196.53 | 276.06 |
| AT5G48880 | 0.30 | 0.36 | 0.34 | | 245.57 | 296.51 | 277.57 | 273.22 |
| AT1G77140 | 0.42 | 0.31 | 0.27 | 1 | 340.90 | 250.07 | 219.48 | 270.15 |
| AT1G16540 | 0.38 | 0.28 | 0.34 | | 304.54 | 223.31 | 282.51 | 270.12 |
| AT5G17300 | 0.34 | 0.31 | 0.35 | | 268.66 | 243.10 | 283.00 | 264.92 |
| AT1G78100 | 0.23 | 0.34 | 0.43 | 1 | 179.86 | 267.30 | 344.99 | 264.05 |
| AT2G43010 | 0.16 | 0.27 | 0.56 | 1 | 129.32 | 214.54 | 447.75 | 263.87 |
| AT5G57390 | 0.08 | 0.68 | 0.24 | 1 | 65.59 | 533.28 | 188.70 | 262.52 |
| AT1G74660 | 0.32 | 0.42 | 0.26 | 1 | 251.40 | 329.50 | 206.36 | 262.42 |
| AT1G27360 | 0.34 | 0.33 | 0.33 | | 268.92 | 261.91 | 256.25 | 262.36 |
| AT1G76520 | 0.11 | 0.31 | 0.58 | 1 | 85.54 | 238.43 | 461.57 | 261.85 |
| AT1G66340 | 0.33 | 0.29 | 0.38 | | 256.47 | 224.38 | 293.25 | 258.03 |
| AT1G15810 | 0.22 | 0.37 | 0.42 | 1 | 167.13 | 285.45 | 318.10 | 256.89 |
| AT3G50410 | 0.32 | 0.47 | 0.21 | 1 | 241.36 | 359.20 | 153.14 | 251.23 |
| AT1G08030 | 0.38 | 0.27 | 0.34 | | 286.75 | 204.11 | 257.93 | 249.60 |
| AT3G01130 | 0.32 | 0.35 | 0.33 | | 236.38 | 268.57 | 241.96 | 248.97 |
| AT2G17500 | 0.25 | 0.26 | 0.49 | 1 | 185.24 | 191.09 | 365.06 | 247.13 |
| AT3G14790 | 0.28 | 0.31 | 0.40 | | 208.12 | 231.51 | 299.59 | 246.41 |
| AT3G21110 | 0.27 | 0.44 | 0.28 | 1 | 202.54 | 326.22 | 206.43 | 245.07 |
| AT5G43700 | 0.29 | 0.31 | 0.40 | | 212.40 | 223.07 | 291.66 | 242.38 |
| AT5G49980 | 0.29 | 0.29 | 0.42 | | 209.82 | 208.10 | 306.51 | 241.48 |
| AT5G06930 | 0.78 | 0.16 | 0.06 | 1 | 562.15 | 117.08 | 41.64 | 240.29 |
| AT4G21740 | 0.29 | 0.28 | 0.43 | | 207.86 | 202.07 | 309.81 | 239.91 |
| AT5G14420 | 0.39 | 0.35 | 0.25 | | 277.37 | 251.32 | 178.72 | 235.80 |
| AT4G35020 | 0.28 | 0.36 | 0.36 | | 198.82 | 254.02 | 250.22 | 234.35 |

| | | | | | | | | |
|---|---|---|---|---|---|---|---|---|
| AT3G63420 | 0.38 | 0.34 | 0.28 | | 266.63 | 241.00 | 194.75 | 234.13 |
| AT1G13980 | 0.35 | 0.33 | 0.32 | | 243.44 | 234.76 | 223.64 | 233.95 |
| AT5G55910 | 0.36 | 0.35 | 0.29 | | 251.18 | 245.95 | 198.78 | 231.97 |
| AT2G25930 | 0.45 | 0.24 | 0.31 | 1 | 312.39 | 168.49 | 214.26 | 231.71 |
| AT1G10840 | 0.35 | 0.34 | 0.32 | | 238.96 | 229.46 | 215.89 | 228.10 |
| AT3G15380 | 0.26 | 0.46 | 0.28 | 1 | 174.69 | 317.87 | 190.61 | 227.72 |
| AT3G26810 | 0.26 | 0.25 | 0.49 | 1 | 178.05 | 166.68 | 334.80 | 226.51 |
| AT2G33860 | 0.30 | 0.47 | 0.24 | | 200.18 | 302.19 | 170.37 | 224.25 |
| AT3G28970 | 0.35 | 0.34 | 0.31 | | 230.42 | 228.31 | 211.00 | 223.24 |
| AT3G50060 | 0.47 | 0.33 | 0.20 | 1 | 310.81 | 221.48 | 129.53 | 220.61 |
| AT3G01650 | 0.47 | 0.27 | 0.26 | 1 | 312.07 | 174.99 | 171.00 | 219.35 |
| AT5G54510 | 0.21 | 0.32 | 0.47 | 1 | 135.68 | 209.31 | 307.95 | 217.65 |
| AT2G39550 | 0.32 | 0.36 | 0.32 | | 209.03 | 230.70 | 206.71 | 215.48 |
| AT3G20630 | 0.35 | 0.34 | 0.31 | | 222.75 | 221.57 | 201.91 | 215.41 |
| AT4G16420 | 0.34 | 0.31 | 0.35 | | 213.52 | 197.47 | 225.49 | 212.16 |
| AT1G78570 | 0.24 | 0.35 | 0.41 | | 150.62 | 224.39 | 255.72 | 210.24 |
| AT4G29810 | 0.37 | 0.32 | 0.31 | | 231.33 | 200.05 | 193.85 | 208.41 |
| AT1G05180 | 0.28 | 0.37 | 0.35 | | 180.99 | 223.79 | 218.40 | 207.73 |
| AT2G47750 | 0.54 | 0.26 | 0.20 | 1 | 332.41 | 159.63 | 125.25 | 205.77 |
| AT3G42950 | 0.68 | 0.16 | 0.16 | 1 | 420.46 | 96.09 | 100.29 | 205.61 |
| AT5G24520 | 0.33 | 0.30 | 0.37 | | 199.84 | 186.24 | 220.75 | 202.28 |
| AT5G62380 | 0.81 | 0.16 | 0.03 | 1 | 472.21 | 91.49 | 17.36 | 193.69 |
| AT3G11220 | 0.31 | 0.36 | 0.33 | | 182.71 | 202.08 | 194.29 | 193.03 |
| AT5G47750 | 0.34 | 0.41 | 0.25 | | 194.70 | 237.33 | 144.55 | 192.19 |
| AT4G05530 | 0.35 | 0.32 | 0.32 | | 203.77 | 185.21 | 186.27 | 191.75 |
| AT1G28130 | 0.14 | 0.21 | 0.64 | 1 | 81.69 | 120.26 | 362.34 | 188.10 |
| AT4G09890 | 0.42 | 0.38 | 0.20 | 1 | 230.11 | 210.29 | 111.63 | 184.01 |
| AT2G34510 | 0.27 | 0.44 | 0.29 | | 149.21 | 246.39 | 154.56 | 183.39 |
| AT5G02130 | 0.22 | 0.40 | 0.38 | | 126.41 | 207.38 | 213.11 | 182.30 |
| AT5G45550 | 0.33 | 0.37 | 0.30 | | 178.14 | 203.46 | 164.16 | 181.92 |
| AT3G46110 | 0.32 | 0.43 | 0.25 | | 171.77 | 233.36 | 134.29 | 179.80 |
| AT5G60840 | 0.31 | 0.35 | 0.34 | | 161.41 | 186.72 | 185.97 | 178.03 |
| AT1G80680 | 0.31 | 0.36 | 0.32 | | 166.68 | 191.77 | 173.52 | 177.32 |
| AT4G03190 | 0.32 | 0.34 | 0.34 | | 166.72 | 182.44 | 181.75 | 176.97 |
| AT3G02875 | 0.24 | 0.39 | 0.36 | | 127.60 | 207.67 | 190.62 | 175.30 |
| AT4G12980 | 0.61 | 0.26 | 0.13 | 1 | 317.28 | 136.88 | 68.14 | 174.10 |
| AT5G53590 | 0.75 | 0.12 | 0.12 | 1 | 389.74 | 62.78 | 63.56 | 172.02 |
| AT5G13790 | 0.21 | 0.42 | 0.37 | 1 | 105.21 | 212.76 | 187.86 | 168.61 |
| AT5G63310 | 0.32 | 0.40 | 0.28 | | 160.50 | 201.79 | 143.51 | 168.60 |
| AT2G04550 | 0.31 | 0.30 | 0.39 | | 156.13 | 151.06 | 196.83 | 168.01 |
| AT5G55250 | 0.37 | 0.47 | 0.16 | 1 | 181.23 | 235.72 | 83.76 | 166.91 |
| AT3G12955 | 0.43 | 0.37 | 0.19 | 1 | 214.06 | 184.39 | 98.94 | 165.80 |
| AT1G55320 | 0.36 | 0.38 | 0.26 | | 178.97 | 190.33 | 127.11 | 165.47 |
| AT5G12210 | 0.37 | 0.32 | 0.31 | | 184.40 | 155.04 | 154.38 | 164.61 |
| AT2G26260 | 0.34 | 0.38 | 0.28 | | 166.18 | 186.71 | 139.90 | 164.26 |
| AT1G69960 | 0.38 | 0.29 | 0.33 | | 188.82 | 141.48 | 160.17 | 163.49 |
| AT5G57740 | 0.22 | 0.47 | 0.31 | | 108.13 | 227.93 | 150.81 | 162.29 |

| | | | | | | | | |
|---|---|---|---|---|---|---|---|---|
| AT5G63420 | 0.28 | 0.50 | 0.22 | 1 | 136.10 | 243.63 | 106.72 | 162.15 |
| AT1G04240 | 0.39 | 0.30 | 0.31 | | 184.55 | 151.09 | 150.38 | 162.01 |
| AT2G01200 | 0.30 | 0.34 | 0.36 | | 144.72 | 163.27 | 176.35 | 161.45 |
| AT5G13370 | 0.10 | 0.29 | 0.61 | 1 | 49.70 | 136.60 | 290.11 | 158.80 |
| AT1G58220 | 0.40 | 0.35 | 0.25 | | 188.56 | 164.49 | 119.71 | 157.59 |
| AT4G17350 | 0.28 | 0.38 | 0.34 | | 127.06 | 179.30 | 164.38 | 156.91 |
| AT1G43850 | 0.31 | 0.32 | 0.38 | | 140.56 | 147.20 | 175.83 | 154.53 |
| AT1G77690 | 0.15 | 0.35 | 0.50 | 1 | 69.80 | 163.55 | 229.71 | 154.35 |
| AT4G37900 | 0.39 | 0.39 | 0.22 | 1 | 181.83 | 179.65 | 100.81 | 154.10 |
| AT2G26740 | 0.24 | 0.25 | 0.51 | 1 | 106.43 | 115.36 | 234.59 | 152.13 |
| AT3G62070 | 0.24 | 0.56 | 0.20 | 1 | 108.18 | 255.88 | 89.54 | 151.20 |
| AT4G38430 | 0.31 | 0.36 | 0.33 | | 138.70 | 165.22 | 148.48 | 150.80 |
| AT3G07390 | 0.44 | 0.35 | 0.20 | 1 | 199.22 | 158.91 | 90.01 | 149.38 |
| AT1G26870 | 0.35 | 0.40 | 0.25 | | 154.98 | 174.39 | 108.96 | 146.11 |
| AT2G01940 | 0.50 | 0.29 | 0.20 | 1 | 217.41 | 129.21 | 88.15 | 144.93 |
| AT1G77850 | 0.40 | 0.38 | 0.22 | | 170.95 | 163.66 | 97.63 | 144.08 |
| AT4G23410 | 0.05 | 0.38 | 0.57 | 1 | 20.26 | 163.79 | 244.32 | 142.79 |
| AT3G13980 | 0.21 | 0.42 | 0.37 | | 89.43 | 177.92 | 159.72 | 142.36 |
| AT5G08530 | 0.30 | 0.28 | 0.42 | | 125.79 | 122.86 | 176.56 | 141.74 |
| AT2G24400 | 0.43 | 0.29 | 0.28 | | 179.97 | 120.50 | 113.75 | 138.07 |
| AT4G18670 | 0.20 | 0.31 | 0.49 | 1 | 83.77 | 124.89 | 201.11 | 136.59 |
| AT1G64520 | 0.32 | 0.36 | 0.32 | | 133.75 | 146.11 | 129.19 | 136.35 |
| AT3G47810 | 0.41 | 0.28 | 0.31 | | 167.08 | 113.41 | 124.52 | 135.00 |
| AT3G03773 | 0.51 | 0.30 | 0.19 | 1 | 210.45 | 116.33 | 77.89 | 134.89 |
| AT5G56290 | 0.40 | 0.24 | 0.36 | | 161.75 | 96.48 | 143.38 | 133.87 |
| AT4G10090 | 0.36 | 0.38 | 0.26 | | 143.32 | 153.39 | 100.21 | 132.30 |
| AT4G30080 | 0.36 | 0.32 | 0.32 | | 142.41 | 126.78 | 124.27 | 131.15 |
| AT2G21410 | 0.19 | 0.42 | 0.39 | 1 | 74.59 | 163.10 | 153.77 | 130.49 |
| AT4G29140 | 0.17 | 0.25 | 0.59 | 1 | 63.43 | 88.70 | 237.68 | 129.94 |
| AT2G01420 | 0.09 | 0.41 | 0.50 | 1 | 37.61 | 158.30 | 192.05 | 129.32 |
| AT1G47510 | 0.27 | 0.34 | 0.39 | | 103.35 | 129.28 | 153.14 | 128.59 |
| AT4G30430 | 0.51 | 0.29 | 0.20 | 1 | 195.88 | 110.91 | 78.03 | 128.28 |
| AT1G67050 | 0.30 | 0.28 | 0.41 | | 116.62 | 106.89 | 158.22 | 127.24 |
| AT2G31190 | 0.27 | 0.42 | 0.31 | | 103.45 | 158.02 | 119.42 | 126.96 |
| AT2G32760 | 0.31 | 0.32 | 0.36 | | 119.35 | 120.40 | 140.26 | 126.67 |
| AT1G08410 | 0.41 | 0.32 | 0.27 | | 156.30 | 120.86 | 102.57 | 126.58 |
| AT4G35060 | 0.18 | 0.30 | 0.52 | 1 | 67.99 | 111.82 | 194.77 | 124.86 |
| AT3G18485 | 0.48 | 0.33 | 0.19 | 1 | 178.10 | 122.75 | 72.93 | 124.59 |
| AT3G62100 | 0.42 | 0.46 | 0.12 | 1 | 154.36 | 171.40 | 43.76 | 123.17 |
| AT1G61255 | 0.36 | 0.33 | 0.31 | | 134.17 | 122.36 | 112.85 | 123.12 |
| AT1G52565 | 0.40 | 0.24 | 0.36 | | 136.42 | 77.15 | 154.60 | 122.72 |
| AT5G50320 | 0.28 | 0.34 | 0.38 | | 100.57 | 125.59 | 138.11 | 121.42 |
| AT3G10870 | 0.56 | 0.19 | 0.25 | 1 | 198.66 | 68.34 | 92.19 | 119.73 |
| AT3G01220 | 0.30 | 0.33 | 0.37 | | 107.20 | 106.40 | 138.10 | 117.23 |
| AT3G62980 | 0.16 | 0.32 | 0.52 | 1 | 56.60 | 113.82 | 180.07 | 116.83 |
| AT1G23080 | 0.25 | 0.25 | 0.51 | 1 | 86.26 | 86.99 | 175.68 | 116.31 |
| AT3G01490 | 0.18 | 0.29 | 0.52 | 1 | 64.68 | 98.79 | 180.50 | 114.66 |

| | | | | | | | | |
|---|---|---|---|---|---|---|---|---|
| AT2G46070 | 0.40 | 0.28 | 0.32 | | 138.68 | 95.96 | 108.24 | 114.29 |
| AT4G11880 | 0.34 | 0.26 | 0.40 | | 116.32 | 89.31 | 137.22 | 114.28 |
| AT3G45600 | 0.15 | 0.34 | 0.50 | 1 | 51.89 | 116.45 | 169.56 | 112.63 |
| AT3G27580 | 0.23 | 0.35 | 0.42 | | 76.94 | 117.78 | 142.57 | 112.43 |
| AT3G43670 | 0.17 | 0.24 | 0.59 | 1 | 57.72 | 75.03 | 195.51 | 109.42 |
| AT4G22560 | 0.43 | 0.35 | 0.22 | | 143.79 | 112.86 | 68.47 | 108.37 |
| AT5G47230 | 0.25 | 0.27 | 0.48 | | 80.53 | 87.83 | 152.97 | 107.11 |
| AT1G22920 | 0.25 | 0.31 | 0.44 | | 76.35 | 97.96 | 144.06 | 106.13 |
| AT3G50340 | 0.44 | 0.27 | 0.30 | | 140.20 | 82.86 | 94.17 | 105.75 |
| AT5G65510 | 0.24 | 0.26 | 0.50 | | 78.06 | 83.03 | 156.08 | 105.72 |
| AT2G39650 | 0.43 | 0.34 | 0.23 | | 139.64 | 102.89 | 71.72 | 104.75 |
| AT3G59280 | 0.35 | 0.33 | 0.32 | | 110.53 | 100.42 | 102.48 | 104.47 |
| AT1G63260 | 0.44 | 0.30 | 0.26 | | 137.57 | 95.79 | 78.60 | 103.99 |
| AT2G19620 | 0.35 | 0.35 | 0.29 | | 109.11 | 110.52 | 90.66 | 103.43 |
| AT4G32690 | 0.30 | 0.29 | 0.41 | | 91.75 | 83.76 | 131.19 | 102.23 |
| AT3G59900 | 0.30 | 0.28 | 0.42 | | 92.39 | 83.90 | 128.73 | 101.67 |
| AT5G57090 | 0.33 | 0.36 | 0.31 | | 101.02 | 107.94 | 95.09 | 101.35 |
| AT4G14430 | 0.30 | 0.47 | 0.23 | | 88.34 | 143.78 | 68.97 | 100.36 |
| AT1G12820 | 0.35 | 0.27 | 0.38 | | 103.59 | 82.49 | 111.76 | 99.28 |
| AT1G14130 | 0.21 | 0.28 | 0.51 | 1 | 59.41 | 81.10 | 156.85 | 99.12 |
| AT3G12090 | 0.31 | 0.35 | 0.33 | | 91.26 | 105.75 | 97.43 | 98.15 |
| AT1G31340 | 0.39 | 0.30 | 0.31 | | 116.46 | 86.12 | 91.50 | 98.03 |
| AT2G28350 | 0.32 | 0.30 | 0.38 | | 98.17 | 85.49 | 110.00 | 97.89 |
| AT2G19580 | 0.26 | 0.32 | 0.41 | | 76.19 | 93.14 | 122.59 | 97.30 |
| AT2G22240 | 0.18 | 0.34 | 0.48 | 1 | 52.16 | 100.60 | 138.94 | 97.23 |
| AT5G58090 | 0.31 | 0.31 | 0.38 | | 88.62 | 90.30 | 110.56 | 96.49 |
| AT4G34750 | 0.43 | 0.35 | 0.21 | | 124.80 | 101.67 | 62.32 | 96.26 |
| AT5G16760 | 0.44 | 0.30 | 0.26 | | 125.44 | 87.27 | 75.69 | 96.14 |
| AT1G54060 | 0.30 | 0.33 | 0.38 | | 85.81 | 94.25 | 107.82 | 95.96 |
| AT1G35240 | 0.26 | 0.30 | 0.44 | | 74.61 | 87.76 | 122.50 | 94.95 |
| AT4G35987 | 0.38 | 0.37 | 0.25 | | 105.27 | 101.25 | 69.08 | 91.87 |
| AT1G54990 | 0.37 | 0.34 | 0.29 | | 98.12 | 90.40 | 80.11 | 89.54 |
| AT4G33770 | 0.23 | 0.30 | 0.46 | | 62.37 | 81.70 | 123.08 | 89.05 |
| **AT5G25620 *YUCCA6*** | **0.72** | **0.22** | **0.06** | **1** | **192.24** | **55.99** | **15.46** | **87.90** |
| AT5G62470 | 0.32 | 0.19 | 0.49 | | 86.50 | 48.64 | 125.03 | 86.72 |
| AT3G09370 | 0.46 | 0.33 | 0.21 | | 123.71 | 79.44 | 51.76 | 84.97 |
| AT2G46530 | 0.40 | 0.27 | 0.33 | | 100.31 | 68.80 | 85.72 | 84.95 |
| AT5G20570 | 0.34 | 0.41 | 0.25 | | 86.52 | 103.69 | 63.09 | 84.43 |
| AT3G25717 | 0.31 | 0.24 | 0.45 | | 72.79 | 62.17 | 117.48 | 84.14 |
| AT5G14090 | 0.28 | 0.38 | 0.35 | | 68.93 | 94.92 | 88.43 | 84.09 |
| AT1G15050 | 0.27 | 0.36 | 0.37 | | 68.04 | 89.73 | 92.02 | 83.26 |
| AT1G34060 | 0.45 | 0.29 | 0.25 | | 111.95 | 75.07 | 62.58 | 83.20 |
| AT1G69160 | 0.40 | 0.39 | 0.20 | | 99.84 | 98.16 | 48.55 | 82.18 |
| AT3G27025 | 0.32 | 0.42 | 0.26 | | 74.41 | 106.79 | 65.02 | 82.08 |
| AT4G35550 | 0.36 | 0.30 | 0.34 | | 88.36 | 76.31 | 79.77 | 81.48 |
| AT1G10030 | 0.30 | 0.40 | 0.30 | | 73.28 | 96.32 | 72.68 | 80.76 |
| AT1G68130 | 0.21 | 0.29 | 0.51 | | 45.96 | 54.73 | 141.10 | 80.60 |

| | | | | | | | | |
|---|---|---|---|---|---|---|---|---|
| AT4G13520 | 0.25 | 0.41 | 0.33 | | 62.63 | 97.41 | 78.13 | 79.39 |
| AT1G31880 | 0.18 | 0.32 | 0.50 | | 42.57 | 77.09 | 117.82 | 79.16 |
| AT1G34040 | 0.11 | 0.53 | 0.36 | | 30.85 | 113.27 | 90.96 | 78.36 |
| AT1G21410 | 0.14 | 0.45 | 0.41 | 1 | 30.00 | 109.05 | 87.47 | 75.51 |
| AT1G15580 | 0.21 | 0.46 | 0.32 | | 47.58 | 104.38 | 74.46 | 75.48 |
| AT2G16580 | 0.37 | 0.54 | 0.09 | 1 | 82.67 | 117.71 | 20.11 | 73.50 |
| AT2G45000 | 0.31 | 0.32 | 0.37 | | 76.84 | 64.45 | 78.41 | 73.23 |
| AT3G59790 | 0.33 | 0.29 | 0.38 | | 74.13 | 63.77 | 81.74 | 73.21 |
| AT4G17980 | 0.19 | 0.57 | 0.24 | | 41.11 | 120.17 | 51.54 | 70.94 |
| AT3G51400 | 0.27 | 0.37 | 0.37 | | 60.70 | 74.73 | 75.82 | 70.42 |
| AT1G71230 | 0.38 | 0.30 | 0.32 | | 77.94 | 61.63 | 67.31 | 68.96 |
| AT4G32295 | 0.22 | 0.43 | 0.34 | | 46.80 | 85.83 | 71.20 | 67.94 |
| AT4G24500 | 0.28 | 0.32 | 0.40 | | 56.18 | 65.77 | 81.34 | 67.76 |
| AT5G49800 | 0.86 | 0.11 | 0.03 | 1 | 174.74 | 21.54 | 6.64 | 67.64 |
| AT2G01960 | 0.35 | 0.40 | 0.24 | | 68.97 | 79.60 | 52.46 | 67.01 |
| AT3G61830 | 0.29 | 0.47 | 0.24 | | 56.98 | 94.55 | 47.24 | 66.25 |
| AT4G39403 | 0.30 | 0.27 | 0.43 | | 56.34 | 54.42 | 81.91 | 64.22 |
| AT1G72430 | 0.39 | 0.23 | 0.38 | | 79.25 | 44.55 | 68.77 | 64.19 |
| AT4G28640 | 0.56 | 0.22 | 0.22 | | 108.15 | 42.71 | 41.38 | 64.08 |
| AT2G21210 | 0.27 | 0.26 | 0.48 | | 50.82 | 47.62 | 91.78 | 63.41 |
| AT3G52520 | 0.27 | 0.45 | 0.27 | | 51.40 | 85.87 | 51.81 | 63.03 |
| AT1G20925 | 0.13 | 0.63 | 0.23 | 1 | 25.91 | 118.02 | 44.32 | 62.75 |
| AT4G27260 | 0.21 | 0.18 | 0.61 | 1 | 39.37 | 35.50 | 113.04 | 62.63 |
| AT2G30770 | 0.38 | 0.37 | 0.24 | | 70.56 | 70.23 | 45.85 | 62.21 |
| AT5G22360 | 0.37 | 0.36 | 0.27 | | 70.77 | 67.25 | 48.19 | 62.07 |
| AT1G08810 | 0.50 | 0.29 | 0.21 | | 88.84 | 55.55 | 40.81 | 61.73 |
| AT3G30350 | 0.56 | 0.36 | 0.08 | 1 | 105.95 | 64.02 | 14.67 | 61.55 |
| AT4G32280 | 0.60 | 0.24 | 0.16 | 1 | 108.98 | 42.62 | 29.18 | 60.26 |
| AT2G21200 | 0.30 | 0.31 | 0.39 | | 53.78 | 56.64 | 70.15 | 60.19 |
| AT1G65920 | 0.17 | 0.37 | 0.46 | | 29.48 | 69.82 | 77.33 | 58.87 |
| AT3G22650 | 0.42 | 0.34 | 0.24 | | 69.43 | 58.69 | 43.02 | 57.05 |
| AT1G04580 | 0.33 | 0.41 | 0.25 | | 55.16 | 71.12 | 43.39 | 56.56 |
| AT1G02350 | 0.30 | 0.29 | 0.42 | | 51.38 | 46.03 | 72.24 | 56.55 |
| AT4G09160 | 0.17 | 0.37 | 0.46 | | 28.11 | 61.64 | 78.10 | 55.95 |
| AT5G54585 | 0.35 | 0.23 | 0.43 | | 57.25 | 39.60 | 69.94 | 55.60 |
| AT2G19690 | 0.42 | 0.41 | 0.17 | | 70.38 | 63.66 | 28.13 | 54.06 |
| AT1G04100 | 0.34 | 0.36 | 0.30 | | 53.79 | 57.99 | 46.37 | 52.72 |
| AT4G16670 | 0.30 | 0.23 | 0.47 | | 44.24 | 36.48 | 73.81 | 51.51 |
| AT3G60690 | 0.31 | 0.31 | 0.38 | | 45.93 | 47.43 | 60.47 | 51.28 |
| AT5G65980 | 0.25 | 0.29 | 0.46 | | 38.21 | 44.78 | 70.03 | 51.01 |
| AT4G02980 | 0.26 | 0.34 | 0.39 | | 39.55 | 52.05 | 59.84 | 50.48 |
| AT5G54140 | 0.25 | 0.35 | 0.40 | | 37.64 | 53.81 | 58.55 | 50.00 |
| AT1G13580 | 0.31 | 0.35 | 0.35 | | 46.01 | 51.99 | 51.54 | 49.84 |
| AT5G66260 | 0.34 | 0.30 | 0.35 | | 44.80 | 46.28 | 57.81 | 49.63 |
| AT4G34760 | 0.27 | 0.51 | 0.22 | | 39.24 | 73.40 | 32.34 | 48.32 |
| AT5G02440 | 0.53 | 0.29 | 0.19 | | 75.65 | 41.75 | 26.63 | 48.01 |
| AT1G10210 | 0.26 | 0.33 | 0.41 | | 34.87 | 45.41 | 60.70 | 46.99 |

| | | | | | | | | |
|---|---|---|---|---|---|---|---|---|
| AT1G08980 | 0.31 | 0.35 | 0.34 | | 38.60 | 51.29 | 49.46 | 46.45 |
| AT1G74650 | 0.37 | 0.27 | 0.37 | | 46.47 | 37.77 | 50.94 | 45.06 |
| AT4G12410 | 0.73 | 0.19 | 0.08 | 1 | 99.96 | 23.45 | 10.43 | 44.61 |
| AT3G44320 | 0.16 | 0.25 | 0.59 | | 21.90 | 34.75 | 76.59 | 44.41 |
| AT1G19840 | 0.23 | 0.43 | 0.34 | | 30.67 | 55.28 | 44.40 | 43.45 |
| AT3G07010 | 0.36 | 0.35 | 0.29 | | 48.41 | 43.71 | 33.80 | 41.97 |
| AT5G43870 | 0.30 | 0.27 | 0.42 | | 34.95 | 42.77 | 47.13 | 41.62 |
| AT3G47600 | 0.14 | 0.17 | 0.69 | 1 | 17.57 | 18.91 | 87.38 | 41.29 |
| AT4G37580 | 0.35 | 0.31 | 0.33 | | 46.19 | 41.02 | 36.64 | 41.28 |
| AT4G31320 | 0.34 | 0.33 | 0.33 | | 38.19 | 40.52 | 42.72 | 40.48 |
| AT2G14960 | 0.30 | 0.48 | 0.23 | | 34.90 | 54.28 | 24.73 | 37.97 |
| AT5G12330 | 0.29 | 0.21 | 0.50 | | 45.75 | 17.52 | 50.51 | 37.93 |
| AT1G71090 | 0.32 | 0.31 | 0.36 | | 35.15 | 35.02 | 42.39 | 37.52 |
| AT2G34650 | 0.30 | 0.32 | 0.38 | | 35.06 | 35.76 | 41.15 | 37.32 |
| AT4G28050 | 0.34 | 0.21 | 0.45 | | 37.74 | 21.74 | 51.18 | 36.89 |
| AT4G04950 | 0.20 | 0.45 | 0.35 | | 22.74 | 50.65 | 36.16 | 36.51 |
| AT4G00260 | 0.36 | 0.21 | 0.43 | | 39.07 | 22.86 | 47.00 | 36.31 |
| AT2G46990 | 0.46 | 0.43 | 0.11 | 1 | 52.27 | 44.02 | 10.62 | 35.64 |
| AT3G28857 | 0.85 | 0.12 | 0.03 | 1 | 89.12 | 10.76 | 3.45 | 34.44 |
| AT5G39610 | 0.13 | 0.26 | 0.61 | 1 | 11.35 | 22.08 | 68.57 | 34.00 |
| AT4G10100 | 0.39 | 0.35 | 0.26 | | 38.51 | 36.24 | 26.81 | 33.86 |
| AT5G14960 | 0.48 | 0.33 | 0.19 | | 48.70 | 30.43 | 19.89 | 33.00 |
| AT5G60220 | 0.11 | 0.44 | 0.45 | | 13.03 | 40.23 | 45.39 | 32.88 |
| AT5G47440 | 0.31 | 0.36 | 0.33 | | 35.62 | 32.33 | 30.05 | 32.67 |
| AT4G23820 | 0.40 | 0.38 | 0.22 | | 41.41 | 33.94 | 20.17 | 31.84 |
| AT1G18520 | 0.55 | 0.23 | 0.22 | | 50.71 | 21.64 | 20.85 | 31.07 |
| AT1G09700 | 0.31 | 0.29 | 0.39 | | 29.31 | 27.20 | 36.54 | 31.02 |
| AT5G12050 | 0.22 | 0.36 | 0.42 | | 20.65 | 33.38 | 38.24 | 30.76 |
| AT1G25250 | 0.48 | 0.32 | 0.20 | | 50.56 | 24.09 | 16.78 | 30.48 |
| AT3G53250 | 0.34 | 0.34 | 0.31 | | 30.36 | 28.75 | 27.62 | 28.91 |
| AT5G23030 | 0.25 | 0.37 | 0.38 | | 21.80 | 29.18 | 33.30 | 28.09 |
| AT3G09870 | 0.24 | 0.43 | 0.33 | | 21.47 | 34.28 | 28.46 | 28.07 |
| AT1G14185 | 0.46 | 0.31 | 0.23 | | 41.79 | 23.94 | 18.31 | 28.01 |
| AT3G28910 | 0.15 | 0.43 | 0.42 | | 12.47 | 36.08 | 35.21 | 27.92 |
| AT1G80390 | 0.17 | 0.40 | 0.43 | | 14.79 | 32.31 | 32.37 | 26.49 |
| AT5G56840 | 0.48 | 0.32 | 0.20 | | 39.07 | 24.60 | 15.11 | 26.26 |
| AT5G20810 | 0.35 | 0.33 | 0.32 | | 19.08 | 32.83 | 26.71 | 26.21 |
| AT3G03660 | 0.23 | 0.56 | 0.22 | | 25.02 | 32.92 | 20.32 | 26.08 |
| AT5G08640 | 0.23 | 0.36 | 0.41 | | 16.38 | 28.40 | 33.25 | 26.01 |
| AT5G20820 | 0.25 | 0.29 | 0.46 | | 13.69 | 21.85 | 39.47 | 25.00 |
| AT2G41170 | 0.29 | 0.28 | 0.42 | | 23.74 | 21.81 | 28.45 | 24.67 |
| AT1G21430 | 0.07 | 0.32 | 0.61 | | 5.86 | 25.43 | 42.64 | 24.64 |
| AT5G02540 | 0.35 | 0.35 | 0.30 | | 16.51 | 34.96 | 20.36 | 23.94 |
| AT4G31910 | 0.53 | 0.15 | 0.32 | | 31.42 | 13.23 | 24.33 | 23.00 |
| AT1G56650 | 0.02 | 0.32 | 0.66 | 1 | 1.57 | 22.42 | 44.24 | 22.74 |
| AT4G38840 | 0.40 | 0.18 | 0.42 | | 25.66 | 11.68 | 29.89 | 22.41 |
| AT4G36110 | 0.28 | 0.39 | 0.33 | | 18.00 | 25.89 | 22.96 | 22.28 |

| | | | | | | | | |
|---|---|---|---|---|---|---|---|---|
| AT3G55120 | 0.14 | 0.28 | 0.58 | | 11.97 | 18.89 | 32.84 | 21.24 |
| AT1G70560 | 0.44 | 0.34 | 0.22 | | 26.64 | 21.41 | 14.60 | 20.89 |
| AT5G07990 | 0.01 | 0.33 | 0.67 | 1 | 0.31 | 21.71 | 39.16 | 20.39 |
| AT1G51780 | 0.29 | 0.07 | 0.64 | 1 | 11.43 | 2.96 | 44.73 | 19.71 |
| AT5G66700 | 0.29 | 0.42 | 0.29 | | 20.72 | 19.61 | 18.70 | 19.68 |
| AT5G57810 | 0.29 | 0.19 | 0.51 | | 15.93 | 9.98 | 33.12 | 19.67 |
| AT1G13670 | 0.17 | 0.19 | 0.63 | | 10.21 | 11.41 | 36.85 | 19.49 |
| AT5G57420 | 0.39 | 0.39 | 0.22 | | 22.82 | 25.18 | 9.84 | 19.28 |
| AT5G56860 | 0.27 | 0.31 | 0.42 | | 13.12 | 23.70 | 20.90 | 19.24 |
| AT5G15100 | 0.14 | 0.22 | 0.64 | 1 | 4.47 | 8.30 | 43.88 | 18.88 |
| AT5G18080 | 0.28 | 0.36 | 0.36 | | 14.05 | 20.50 | 21.18 | 18.58 |
| AT3G26790 | 0.42 | 0.24 | 0.34 | | 23.23 | 13.56 | 16.51 | 17.77 |
| AT1G18510 | 0.31 | 0.30 | 0.39 | | 16.72 | 15.75 | 20.58 | 17.68 |
| AT1G74045 | 0.20 | 0.44 | 0.36 | | 11.44 | 22.86 | 18.67 | 17.66 |
| AT3G24650 | 0.28 | 0.37 | 0.35 | | 13.15 | 25.21 | 14.44 | 17.60 |
| AT4G30290 | 0.12 | 0.28 | 0.60 | | 7.14 | 17.97 | 27.09 | 17.40 |
| AT1G05530 | 0.37 | 0.23 | 0.40 | | 15.17 | 7.43 | 29.15 | 17.25 |
| AT4G19430 | 0.38 | 0.42 | 0.20 | | 20.09 | 21.98 | 9.55 | 17.21 |
| AT5G66580 | 0.16 | 0.19 | 0.66 | | 7.92 | 10.74 | 31.53 | 16.73 |
| AT4G37390 | 0.17 | 0.21 | 0.62 | | 7.12 | 10.53 | 32.01 | 16.55 |
| AT1G34310 | 0.29 | 0.38 | 0.33 | | 12.67 | 27.91 | 8.93 | 16.50 |
| AT5G66590 | 0.27 | 0.54 | 0.19 | | 14.09 | 24.83 | 10.51 | 16.48 |
| AT1G04180 | 0.38 | 0.41 | 0.21 | | 18.71 | 19.87 | 10.50 | 16.36 |
| AT5G50760 | 0.05 | 0.26 | 0.68 | | 2.29 | 11.83 | 34.60 | 16.24 |
| AT5G43890 | 0.18 | 0.42 | 0.40 | | 8.58 | 20.18 | 19.20 | 15.99 |
| AT1G17345 | 0.36 | 0.13 | 0.52 | | 13.20 | 4.74 | 29.26 | 15.73 |
| AT1G76190 | 0.38 | 0.26 | 0.36 | | 19.58 | 12.01 | 14.21 | 15.27 |
| AT1G18350 | 0.12 | 0.75 | 0.13 | | 5.68 | 32.19 | 6.38 | 14.75 |
| AT1G34170 | 0.70 | 0.18 | 0.12 | | 30.53 | 7.88 | 4.20 | 14.20 |
| AT5G67060 | 0.56 | 0.14 | 0.30 | | 22.18 | 1.11 | 18.32 | 13.87 |
| AT4G13790 | 0.39 | 0.13 | 0.48 | | 19.42 | 5.06 | 17.13 | 13.87 |
| AT4G25433 | 0.09 | 0.12 | 0.80 | 1 | 2.87 | 3.74 | 34.96 | 13.86 |
| AT5G16530 | 0.05 | 0.40 | 0.55 | | 1.57 | 16.64 | 22.83 | 13.68 |
| AT4G34810 | 0.15 | 0.34 | 0.50 | | 7.08 | 13.06 | 18.57 | 12.91 |
| AT4G24670 | 0.28 | 0.62 | 0.11 | | 14.91 | 14.75 | 8.41 | 12.69 |
| AT5G10990 | 0.43 | 0.42 | 0.15 | | 16.04 | 15.34 | 5.92 | 12.43 |
| AT5G64780 | 0.45 | 0.18 | 0.37 | | 13.97 | 7.05 | 15.76 | 12.26 |
| AT2G22810 | 0.00 | 0.36 | 0.64 | 1 | 0.29 | 7.36 | 28.92 | 12.19 |
| AT2G47460 | 0.13 | 0.49 | 0.37 | | 4.46 | 18.52 | 12.82 | 11.93 |
| AT2G37030 | 0.38 | 0.50 | 0.11 | | 8.44 | 21.64 | 5.69 | 11.92 |
| AT1G34670 | 0.42 | 0.44 | 0.14 | | 17.43 | 12.83 | 5.50 | 11.92 |
| AT1G28300 | 0.36 | 0.29 | 0.35 | | 14.81 | 7.05 | 13.68 | 11.85 |
| AT2G18010 | 0.34 | 0.18 | 0.48 | | 9.94 | 6.01 | 19.47 | 11.81 |
| AT1G52830 | 0.83 | 0.09 | 0.08 | | 29.16 | 1.90 | 3.25 | 11.43 |
| AT1G19830 | 0.40 | 0.36 | 0.24 | | 11.10 | 12.71 | 10.29 | 11.37 |
| AT3G29370 | 0.22 | 0.63 | 0.14 | | 14.14 | 17.07 | 2.79 | 11.34 |
| AT1G29460 | 0.34 | 0.18 | 0.48 | | 12.08 | 5.48 | 16.09 | 11.21 |

| | | | | | | | | |
|---|---|---|---|---|---|---|---|---|
| AT5G01490 | 0.42 | 0.26 | 0.32 | | 11.12 | 10.92 | 10.37 | 10.81 |
| AT1G16510 | 0.54 | 0.19 | 0.27 | | 16.36 | 6.46 | 9.14 | 10.65 |
| AT3G50610 | 0.34 | 0.66 | 0.00 | | 20.43 | 11.51 | 0.00 | 10.65 |
| AT1G31690 | 0.09 | 0.29 | 0.62 | | 3.03 | 7.92 | 20.80 | 10.58 |
| AT4G26150 | 0.48 | 0.42 | 0.10 | | 12.30 | 16.44 | 2.43 | 10.39 |
| AT1G34390 | 0.53 | 0.33 | 0.14 | | 9.42 | 14.46 | 6.82 | 10.23 |
| AT2G04160 | 0.38 | 0.23 | 0.39 | | 11.70 | 8.75 | 10.23 | 10.22 |
| AT5G52900 | 0.65 | 0.20 | 0.15 | | 19.76 | 5.71 | 4.53 | 10.00 |
| AT1G47600 | | | | | 11.61 | 15.96 | 2.33 | 9.97 |
| AT1G35520 | 0.33 | 0.64 | 0.02 | | 6.48 | 22.54 | 0.75 | 9.92 |
| AT5G02580 | 0.14 | 0.32 | 0.54 | | 6.09 | 13.49 | 9.99 | 9.86 |
| AT3G61900 | 0.09 | 0.71 | 0.21 | | 2.64 | 20.38 | 5.91 | 9.64 |
| AT5G11320 | 0.67 | 0.14 | 0.19 | | 15.16 | 5.89 | 6.90 | 9.32 |
| AT1G43040 | 0.15 | 0.25 | 0.61 | | 5.20 | 7.42 | 15.17 | 9.26 |
| AT5G13930 | 0.55 | 0.25 | 0.20 | | 12.94 | 8.12 | 6.35 | 9.14 |
| AT1G34410 | 0.33 | 0.26 | 0.41 | | 0.29 | 17.45 | 9.32 | 9.02 |
| AT5G22300 | 0.13 | 0.60 | 0.27 | | 5.24 | 16.10 | 5.24 | 8.86 |
| AT3G43120 | 0.15 | 0.41 | 0.44 | | 3.53 | 7.34 | 15.44 | 8.77 |
| AT4G38860 | 0.31 | 0.46 | 0.23 | | 8.25 | 12.31 | 5.71 | 8.76 |
| AT5G48070 | 0.17 | 0.59 | 0.25 | | 3.55 | 15.30 | 7.28 | 8.71 |
| AT1G04610 | 0.15 | 0.25 | 0.60 | | 3.82 | 9.32 | 11.57 | 8.24 |
| AT3G20220 | 0.18 | 0.53 | 0.29 | | 4.16 | 13.69 | 6.60 | 8.15 |
| AT5G27780 | 0.42 | 0.30 | 0.28 | | 9.34 | 7.30 | 6.58 | 7.74 |
| AT2G33230 | 0.67 | 0.29 | 0.04 | | 13.68 | 7.88 | 1.40 | 7.66 |
| AT5G41900 | 0.30 | 0.17 | 0.54 | | 12.67 | 2.59 | 7.56 | 7.61 |
| AT1G76610 | 0.60 | 0.10 | 0.30 | | 16.15 | 1.43 | 5.14 | 7.57 |
| AT3G06868 | 0.45 | 0.32 | 0.23 | | 9.52 | 7.58 | 5.17 | 7.42 |
| AT1G48910 | 0.41 | 0.42 | 0.17 | | 7.95 | 8.98 | 3.97 | 6.97 |
| AT1G23320 | 0.08 | 0.68 | 0.23 | | 2.35 | 11.08 | 7.33 | 6.92 |
| AT3G14370 | 0.31 | 0.35 | 0.35 | | 7.26 | 6.59 | 6.90 | 6.92 |
| AT2G36210 | 0.16 | 0.35 | 0.49 | | 3.54 | 8.62 | 8.32 | 6.83 |
| AT1G29430 | 0.29 | 0.15 | 0.56 | | 5.29 | 3.96 | 10.60 | 6.62 |
| AT2G03840 | 0.00 | 0.46 | 0.54 | | 0.00 | 7.88 | 11.98 | 6.62 |
| AT2G44990 | 0.77 | 0.23 | 0.00 | | 16.17 | 3.64 | 0.00 | 6.60 |
| **AT4G32540 *YUCCA1*** | **0.01** | **0.99** | **0.00** | **1** | **0.29** | **19.51** | **0.00** | **6.60** |
| AT2G18970 | 0.30 | 0.39 | 0.31 | | 6.42 | 7.32 | 5.65 | 6.46 |
| AT1G29500 | 0.22 | 0.24 | 0.53 | | 2.58 | 5.89 | 10.46 | 6.31 |
| AT1G59500 | 0.80 | 0.00 | 0.20 | | 11.59 | 0.00 | 7.33 | 6.31 |
| AT1G51470 | 0.00 | 0.50 | 0.50 | | 0.00 | 14.43 | 4.45 | 6.29 |
| AT2G23260 | 0.14 | 0.33 | 0.53 | | 1.96 | 4.83 | 12.07 | 6.29 |
| AT5G18060 | 0.35 | 0.16 | 0.48 | | 3.27 | 4.64 | 10.88 | 6.26 |
| AT1G27740 | 0.01 | 0.72 | 0.27 | | 0.31 | 9.61 | 8.37 | 6.10 |
| AT1G05680 | 0.17 | 0.31 | 0.52 | | 3.75 | 6.44 | 7.92 | 6.04 |
| AT1G75590 | 0.23 | 0.28 | 0.49 | | 2.48 | 2.68 | 12.08 | 5.75 |
| AT3G60650 | 0.26 | 0.58 | 0.16 | | 2.96 | 8.71 | 4.13 | 5.27 |
| AT4G00880 | 0.48 | 0.26 | 0.26 | | 7.80 | 4.22 | 3.54 | 5.19 |
| AT4G36740 | 0.36 | 0.26 | 0.38 | | 5.17 | 3.78 | 6.02 | 4.99 |

| | | | | | | | | |
|---|---|---|---|---|---|---|---|---|
| AT1G75580 | 0.22 | 0.36 | 0.41 | | 3.39 | 8.01 | 3.41 | 4.93 |
| AT1G28010 | 0.08 | 0.46 | 0.46 | | 1.77 | 6.41 | 6.15 | 4.78 |
| AT1G29420 | 0.55 | 0.18 | 0.27 | | 8.03 | 2.26 | 3.26 | 4.52 |
| AT3G47295 | 0.56 | 0.23 | 0.21 | | 6.47 | 3.99 | 3.07 | 4.51 |
| AT1G53230 | 0.11 | 0.54 | 0.36 | | 1.00 | 7.28 | 5.04 | 4.44 |
| AT5G18050 | 0.38 | 0.26 | 0.36 | | 3.27 | 2.02 | 7.91 | 4.40 |
| AT1G31040 | 0.02 | 0.49 | 0.49 | | 0.39 | 7.10 | 5.63 | 4.37 |
| AT1G20470 | 0.32 | 0.26 | 0.42 | | 3.87 | 4.25 | 4.49 | 4.20 |
| AT3G62680 | 0.54 | 0.02 | 0.44 | | 8.54 | 0.37 | 2.98 | 3.96 |
| AT1G43950 | 0.02 | 0.85 | 0.13 | | 0.29 | 9.33 | 1.38 | 3.67 |
| AT1G24590 | 0.00 | 1.00 | 0.00 | | 0.00 | 10.80 | 0.00 | 3.60 |
| AT1G53700 | 0.65 | 0.31 | 0.03 | | 5.77 | 4.21 | 0.56 | 3.51 |
| AT4G33880 | 0.00 | 0.50 | 0.50 | | 0.00 | 6.31 | 3.97 | 3.43 |
| AT4G34800 | 0.26 | 0.04 | 0.69 | | 2.47 | 0.41 | 7.00 | 3.29 |
| AT5G61620 | 0.00 | 0.69 | 0.31 | | 0.00 | 7.56 | 1.82 | 3.13 |
| AT1G29490 | 0.00 | 0.52 | 0.48 | | 0.00 | 1.97 | 6.72 | 2.90 |
| AT4G13260 | 0.53 | 0.47 | 0.00 | | 2.75 | 5.57 | 0.00 | 2.77 |
| AT1G29510 | 0.00 | 0.26 | 0.74 | | 0.00 | 5.20 | 2.82 | 2.67 |
| AT1G53940 | 0.00 | 0.67 | 0.33 | | 0.00 | 7.10 | 0.84 | 2.64 |
| AT2G28085 | 0.00 | 0.44 | 0.56 | | 0.00 | 3.34 | 4.20 | 2.51 |
| AT5G64770 | 0.14 | 0.52 | 0.33 | | 1.96 | 4.25 | 0.31 | 2.17 |
| AT4G09530 | 0.00 | 0.33 | 0.67 | | 0.00 | 3.34 | 3.10 | 2.15 |
| AT3G17600 | 0.00 | 0.50 | 0.50 | | 0.00 | 1.11 | 4.27 | 1.80 |
| AT3G11260 | 0.16 | 0.33 | 0.50 | | 2.06 | 0.37 | 2.70 | 1.71 |
| AT4G22620 | 0.00 | 0.23 | 0.77 | | 0.00 | 1.11 | 3.74 | 1.62 |
| AT1G49200 | 0.24 | 0.45 | 0.31 | | 1.47 | 1.88 | 1.47 | 1.61 |
| AT2G23440 | 0.00 | 0.82 | 0.18 | | 0.00 | 3.24 | 1.40 | 1.55 |
| AT3G42800 | 0.55 | 0.40 | 0.06 | | 0.69 | 3.34 | 0.47 | 1.50 |
| AT1G35540 | 0.18 | 0.17 | 0.64 | | 1.18 | 1.11 | 2.05 | 1.45 |
| AT1G47485 | 0.00 | 1.00 | 0.00 | | 0.00 | 4.29 | 0.00 | 1.43 |
| AT4G34770 | 0.00 | 0.00 | 1.00 | | 0.00 | 0.00 | 4.20 | 1.40 |
| AT5G66815 | 0.22 | 0.72 | 0.07 | | 0.59 | 2.59 | 0.47 | 1.22 |
| AT1G29450 | 0.67 | 0.00 | 0.33 | | 3.04 | 0.00 | 0.56 | 1.20 |
| AT3G03820 | 0.36 | 0.15 | 0.49 | | 1.32 | 0.37 | 1.86 | 1.18 |
| AT5G45890 | 0.00 | 1.00 | 0.00 | | 0.00 | 3.34 | 0.00 | 1.11 |
| AT4G34790 | 0.24 | 0.64 | 0.12 | | 0.29 | 1.81 | 0.47 | 0.86 |
| AT4G37290 | 0.26 | 0.74 | 0.00 | | 0.39 | 2.02 | 0.00 | 0.80 |
| AT4G28720 | 0.00 | 0.38 | 0.62 | | 0.00 | 1.49 | 0.77 | 0.75 |
| AT4G38850 | 0.38 | 0.12 | 0.50 | | 1.18 | 0.37 | 0.56 | 0.70 |
| AT2G21220 | 0.16 | 0.15 | 0.69 | | 0.39 | 0.37 | 1.30 | 0.69 |
| AT3G24280 | 0.00 | 1.00 | 0.00 | | 0.00 | 1.86 | 0.00 | 0.62 |
| AT4G31380 | 0.00 | 1.00 | 0.00 | | 0.00 | 1.28 | 0.00 | 0.43 |
| AT4G12550 | 0.50 | 0.22 | 0.28 | | 0.29 | 0.37 | 0.47 | 0.38 |
| AT2G23250 | 0.50 | 0.50 | 0.00 | | 0.31 | 0.74 | 0.00 | 0.35 |
| AT4G16515 | 0.00 | 0.50 | 0.50 | | 0.00 | 0.41 | 0.31 | 0.24 |
| AT4G14819 | 0.00 | 0.50 | 0.50 | | 0.00 | 0.41 | 0.31 | 0.24 |
| AT4G38825 | 0.00 | 0.00 | 1.00 | | 0.00 | 0.00 | 0.61 | 0.20 |

| | | | | | | | | |
|---|---|---|---|---|---|---|---|---|
| AT3G51200 | 0.00 | 0.00 | 1.00 | | 0.00 | 0.00 | 0.47 | 0.16 |
| AT5G42410 | 0.00 | 1.00 | 0.00 | | 0.00 | 0.37 | 0.00 | 0.12 |
| AT3G03847 | 0.00 | 1.00 | 0.00 | | 0.00 | 0.37 | 0.00 | 0.12 |
| AT1G69588 | | | | | 0.00 | 0.00 | 0.00 | 0.00 |
| AT5G18010 | | | | | 0.00 | 0.00 | 0.00 | 0.00 |
| AT5G18020 | | | | | 0.00 | 0.00 | 0.00 | 0.00 |
| AT5G18030 | | | | | 0.00 | 0.00 | 0.00 | 0.00 |
| AT3G03840 | | | | | 0.00 | 0.00 | 0.00 | 0.00 |
| AT3G03830 | | | | | 0.00 | 0.00 | 0.00 | 0.00 |
| AT1G29440 | | | | | 0.00 | 0.00 | 0.00 | 0.00 |
| AT4G34780 | | | | | 0.00 | 0.00 | 0.00 | 0.00 |
| AT5G03310 | | | | | 0.00 | 0.00 | 0.00 | 0.00 |
| AT2G31750 | | | | | 0.00 | 0.00 | 0.00 | 0.00 |
| AT1G05560 | | | | | 0.00 | 0.00 | 0.00 | 0.00 |
| AT4G20420 | | | | | 0.00 | 0.00 | 0.00 | 0.00 |
| AT4G38820 | | | | | 0.00 | 0.00 | 0.00 | 0.00 |

**Supplemental Table 10.** Cambium domain-specific expression of the 198 cytokinin related or regulated genes. The relative mean across all cambium domains or mean of the normalized count values are given. LRT = Likelihood ratio test. LRT=1 indicates significance difference of expression levels across cambium domains. A mean value of all domains lower 10 was interpreted as no expression within the cambium. The RNA-seq data and analysis was produced by Dr. Dongbo Shi. The analysis of cytokinin related genes was conducted by myself.

| | **Relative mean** | | | | **Mean normalized count values** | | | **Mean** |
|---|---|---|---|---|---|---|---|---|
| **Gene** | **proximal** | **central** | **distal** | **LRT** | **proximal** | **central** | **distal** | **All domains** |
| AT3G16770 *EBP* | 0.23 | 0.31 | 0.45 | 1 | 2756.63 | 3701.10 | 5377.28 | 3945.01 |
| AT5G02810 *PRR7* | 0.28 | 0.30 | 0.42 | 1 | 2402.34 | 2546.61 | 3647.82 | 2865.59 |
| AT1G78080 *RAP2.4* | 0.29 | 0.26 | 0.45 | 1 | 2051.49 | 1820.15 | 3119.07 | 2330.24 |
| **AT1G19770 *PUP14*** | **0.31** | **0.33** | **0.35** | | **1669.04** | **1779.93** | **1867.04** | **1772.00** |
| **AT3G48100 *ARR5*** | **0.34** | **0.30** | **0.35** | | **1795.55** | **1576.19** | **1834.43** | **1735.39** |
| AT4G34160 *CYCD3;1* | 0.30 | 0.37 | 0.33 | | 1527.53 | 1899.48 | 1664.60 | 1697.20 |
| **AT1G10470 *ARR4*** | **0.40** | **0.30** | **0.30** | **1** | **1924.60** | **1452.48** | **1481.78** | **1619.62** |
| AT2G25170 *PKL* | 0.37 | 0.32 | 0.30 | | 1441.33 | 1248.11 | 1164.88 | 1284.77 |
| **AT3G57040 *ARR9*** | **0.40** | **0.33** | **0.27** | **1** | **1504.81** | **1266.71** | **1022.19** | **1264.57** |
| AT5G61380 *TOC1* | 0.31 | 0.35 | 0.34 | | 1078.72 | 1209.13 | 1185.24 | 1157.70 |
| **AT2G01830 *WOL*** | **0.42** | **0.37** | **0.21** | **1** | **1399.07** | **1249.14** | **692.00** | **1113.40** |
| **AT3G16857 *ARR1*** | **0.30** | **0.31** | **0.39** | | **961.17** | **1000.67** | **1241.75** | **1067.86** |

| | | | | | | | | |
|---|---|---|---|---|---|---|---|---|
| **AT1G19050 *ARR7*** | **0.27** | **0.26** | **0.47** | **1** | **853.62** | **807.26** | **1466.56** | **1042.48** |
| AT3G54010 *PAS1* | 0.36 | 0.31 | 0.33 | | 1063.25 | 909.95 | 979.12 | 984.11 |
| AT4G00760 *PRR8* | 0.30 | 0.36 | 0.34 | | 869.87 | 1066.31 | 983.58 | 973.26 |
| **AT5G03270 *LOG6*** | **0.33** | **0.43** | **0.24** | **1** | **938.56** | **1235.69** | **685.11** | **953.12** |
| **AT2G29970 *SMXL7*** | **0.39** | **0.32** | **0.29** | | **989.33** | **820.55** | **752.86** | **854.25** |
| AT4G37790 | 0.38 | 0.33 | 0.29 | | 968.16 | 829.44 | 749.47 | 849.02 |
| AT1G05850 | 0.49 | 0.25 | 0.27 | 1 | 1225.34 | 617.98 | 666.04 | 836.45 |
| AT1G70510 | 0.47 | 0.30 | 0.23 | 1 | 1155.42 | 749.98 | 576.40 | 827.27 |
| AT1G27320 | 0.32 | 0.27 | 0.41 | 1 | 758.08 | 635.55 | 964.58 | 786.07 |
| AT2G47000 | 0.41 | 0.28 | 0.31 | 1 | 957.20 | 649.89 | 714.28 | 773.79 |
| AT2G28305 | 0.61 | 0.34 | 0.05 | 1 | 1414.52 | 781.18 | 115.16 | 770.28 |
| AT3G47620 | 0.21 | 0.38 | 0.40 | 1 | 481.24 | 859.60 | 909.83 | 750.22 |
| AT5G49720 | 0.45 | 0.26 | 0.29 | 1 | 940.32 | 551.96 | 611.32 | 701.20 |
| AT1G03850 | 0.27 | 0.18 | 0.55 | 1 | 569.67 | 380.03 | 1147.84 | 699.18 |
| **AT4G37540 *LBD39*** | **0.25** | **0.31** | **0.44** | **1** | **521.73** | **631.44** | **897.70** | **683.62** |
| AT2G26980 | 0.26 | 0.29 | 0.46 | 1 | 517.45 | 575.39 | 916.03 | 669.62 |
| AT1G36160 | 0.35 | 0.33 | 0.32 | | 699.07 | 656.94 | 620.90 | 658.97 |
| AT1G57990 | 0.44 | 0.26 | 0.31 | 1 | 869.03 | 501.15 | 599.70 | 656.63 |
| AT3G18780 | 0.27 | 0.28 | 0.45 | 1 | 486.32 | 522.38 | 830.86 | 613.19 |
| AT1G80440 | 0.20 | 0.27 | 0.52 | 1 | 373.30 | 502.46 | 961.79 | 612.52 |
| AT2G41310 | 0.41 | 0.28 | 0.30 | 1 | 754.54 | 519.93 | 553.05 | 609.17 |
| AT3G12380 | 0.31 | 0.34 | 0.35 | | 531.95 | 585.35 | 608.71 | 575.34 |
| AT2G17820 | 0.54 | 0.21 | 0.25 | 1 | 901.78 | 356.58 | 427.27 | 561.87 |
| AT1G78240 | 0.39 | 0.30 | 0.31 | | 626.36 | 472.95 | 498.19 | 532.50 |
| AT5G06100 | 0.31 | 0.32 | 0.36 | | 499.49 | 514.57 | 580.67 | 531.58 |
| AT1G80050 | 0.39 | 0.45 | 0.16 | 1 | 618.90 | 716.16 | 254.85 | 529.97 |
| AT4G22570 | 0.46 | 0.36 | 0.19 | 1 | 710.76 | 554.75 | 288.31 | 517.94 |
| AT1G75450 | 0.36 | 0.30 | 0.34 | | 517.01 | 431.78 | 490.04 | 479.61 |
| AT5G24470 | 0.31 | 0.31 | 0.37 | | 444.46 | 446.71 | 529.48 | 473.55 |
| AT4G02450 | 0.31 | 0.33 | 0.36 | | 427.30 | 452.51 | 490.49 | 456.76 |
| AT1G17440 | 0.39 | 0.29 | 0.33 | | 517.72 | 380.84 | 434.06 | 444.21 |
| AT1G10460 | 0.36 | 0.33 | 0.31 | | 460.99 | 411.63 | 391.57 | 421.40 |
| AT4G16780 | 0.38 | 0.32 | 0.30 | | 475.83 | 403.31 | 382.63 | 420.59 |
| AT2G46790 | 0.28 | 0.31 | 0.42 | 1 | 321.81 | 357.42 | 485.62 | 388.28 |
| **AT5G06300 *LOG7*** | **0.37** | **0.27** | **0.36** | | **420.62** | **314.67** | **412.14** | **382.48** |
| AT5G11950 | 0.51 | 0.35 | 0.15 | 1 | 580.48 | 396.58 | 167.50 | 381.52 |
| AT2G18300 | 0.18 | 0.20 | 0.63 | 1 | 205.64 | 218.52 | 720.10 | 381.42 |
| AT4G01540 | 0.39 | 0.38 | 0.23 | 1 | 454.68 | 425.24 | 263.79 | 381.24 |
| AT5G03300 | 0.31 | 0.34 | 0.35 | | 359.01 | 378.66 | 395.39 | 377.69 |
| AT3G11540 | 0.37 | 0.36 | 0.26 | | 424.59 | 407.54 | 296.67 | 376.27 |
| AT5G25220 | 0.23 | 0.39 | 0.38 | 1 | 246.81 | 420.80 | 411.55 | 359.72 |
| AT4G38630 | 0.38 | 0.29 | 0.33 | | 391.63 | 296.40 | 342.24 | 343.43 |
| AT1G71930 | 0.86 | 0.12 | 0.02 | 1 | 864.84 | 119.83 | 23.49 | 336.05 |

| | | | | | | | | |
|---|---|---|---|---|---|---|---|---|
| **AT1G67710 *ARR11*** | **0.27** | **0.38** | **0.36** | | **245.88** | **352.35** | **332.85** | **310.36** |
| AT5G62920 | 0.25 | 0.32 | 0.44 | 1 | 224.68 | 287.70 | 396.62 | 303.00 |
| AT1G28560 | 0.28 | 0.32 | 0.39 | | 252.71 | 284.49 | 331.47 | 289.56 |
| AT1G19200 | 0.20 | 0.24 | 0.56 | 1 | 167.48 | 198.94 | 452.32 | 272.91 |
| **AT3G29350 *AHP2*** | **0.28** | **0.32** | **0.40** | | **222.24** | **255.45** | **314.93** | **264.20** |
| AT1G78100 | 0.23 | 0.34 | 0.43 | 1 | 179.86 | 267.30 | 344.99 | 264.05 |
| **AT5G58080 *ARR18*** | **0.40** | **0.34** | **0.26** | | **317.85** | **265.17** | **207.71** | **263.58** |
| AT1G74660 | 0.32 | 0.42 | 0.26 | 1 | 251.40 | 329.50 | 206.36 | 262.42 |
| AT5G35750 | 0.33 | 0.27 | 0.40 | | 250.37 | 207.36 | 318.38 | 258.70 |
| AT1G66340 | 0.33 | 0.29 | 0.38 | | 256.47 | 224.38 | 293.25 | 258.03 |
| **AT1G03430 *AHP5*** | **0.29** | **0.35** | **0.36** | | **218.33** | **262.62** | **264.24** | **248.40** |
| **AT1G16530 *LBD3*** | **0.23** | **0.46** | **0.31** | **1** | **167.13** | **332.24** | **232.53** | **243.97** |
| AT1G10480 | 0.33 | 0.35 | 0.32 | | 241.04 | 247.46 | 225.32 | 237.94 |
| AT5G14420 | 0.39 | 0.35 | 0.25 | | 277.37 | 251.32 | 178.72 | 235.80 |
| **AT4G16110 *ARR2*** | **0.23** | **0.45** | **0.32** | **1** | **162.05** | **317.44** | **224.95** | **234.81** |
| AT5G21482 | 0.18 | 0.47 | 0.35 | 1 | 129.81 | 317.96 | 228.26 | 225.34 |
| AT3G01650 | 0.47 | 0.27 | 0.26 | 1 | 312.07 | 174.99 | 171.00 | 219.35 |
| AT4G16420 | 0.34 | 0.31 | 0.35 | | 213.52 | 197.47 | 225.49 | 212.16 |
| **AT2G01760 *ARR14*** | **0.27** | **0.35** | **0.38** | | **171.64** | **221.07** | **234.24** | **208.98** |
| AT1G05180 | 0.28 | 0.37 | 0.35 | | 180.99 | 223.79 | 218.40 | 207.73 |
| AT1G31320 | 0.26 | 0.35 | 0.38 | | 159.10 | 215.71 | 230.30 | 201.70 |
| AT1G69040 | 0.22 | 0.36 | 0.42 | | 131.35 | 206.47 | 252.68 | 196.83 |
| **AT2G25180 *ARR12*** | **0.41** | **0.25** | **0.34** | | **242.78** | **147.50** | **197.53** | **195.94** |
| AT5G62380 | 0.81 | 0.16 | 0.03 | 1 | 472.21 | 91.49 | 17.36 | 193.69 |
| AT1G31770 | 0.29 | 0.39 | 0.32 | | 170.56 | 223.65 | 186.29 | 193.50 |
| AT1G27210 | 0.25 | 0.28 | 0.47 | 1 | 139.08 | 155.88 | 262.15 | 185.70 |
| AT2G34510 | 0.27 | 0.44 | 0.29 | | 149.21 | 246.39 | 154.56 | 183.39 |
| AT1G27450 | 0.35 | 0.39 | 0.26 | | 188.37 | 213.66 | 143.30 | 181.78 |
| AT2G27760 | 0.55 | 0.26 | 0.19 | 1 | 281.20 | 130.49 | 96.61 | 169.43 |
| AT3G09820 | 0.42 | 0.28 | 0.30 | | 210.35 | 140.47 | 150.14 | 166.99 |
| **AT5G39340 *AHP3*** | **0.28** | **0.31** | **0.41** | | **139.24** | **149.74** | **205.19** | **164.72** |
| AT5G05860 | 0.12 | 0.33 | 0.56 | 1 | 58.91 | 160.80 | 272.89 | 164.20 |
| AT3G15353 | 0.17 | 0.34 | 0.49 | 1 | 82.78 | 163.79 | 243.12 | 163.23 |
| AT1G58220 | 0.40 | 0.35 | 0.25 | | 188.56 | 164.49 | 119.71 | 157.59 |
| AT2G37210 | 0.33 | 0.44 | 0.23 | 1 | 150.26 | 201.36 | 104.18 | 151.93 |
| AT1G33170 | 0.17 | 0.41 | 0.41 | 1 | 75.30 | 178.08 | 178.16 | 143.85 |
| **AT2G28500 *LBD11*** | **0.13** | **0.67** | **0.20** | **1** | **57.44** | **283.09** | **86.54** | **142.36** |
| AT2G01890 | 0.28 | 0.19 | 0.53 | 1 | 112.41 | 79.32 | 222.69 | 138.14 |
| AT1G13430 | 0.26 | 0.33 | 0.41 | | 106.69 | 135.96 | 169.12 | 137.26 |
| AT1G64520 | 0.32 | 0.36 | 0.32 | | 133.75 | 146.11 | 129.19 | 136.35 |
| AT3G03773 | 0.51 | 0.30 | 0.19 | 1 | 210.45 | 116.33 | 77.89 | 134.89 |

| | | | | | | | | |
|---|---|---|---|---|---|---|---|---|
| AT1G07900 | 0.30 | 0.33 | 0.37 | | 122.02 | 133.51 | 148.15 | 134.56 |
| AT1G07900 | 0.30 | 0.33 | 0.37 | | 122.02 | 133.51 | 148.15 | 134.56 |
| AT3G56380 | 0.29 | 0.37 | 0.34 | | 108.17 | 136.13 | 131.28 | 125.19 |
| AT1G15670 | 0.31 | 0.22 | 0.47 | 1 | 112.38 | 82.56 | 174.01 | 122.98 |
| AT5G20040 | 0.32 | 0.34 | 0.34 | | 112.59 | 123.92 | 132.00 | 122.84 |
| AT5G10720 | 0.38 | 0.28 | 0.34 | | 135.57 | 96.92 | 118.39 | 116.96 |
| AT3G21510 | 0.10 | 0.27 | 0.63 | 1 | 31.23 | 89.56 | 216.56 | 112.45 |
| AT5G53290 | 0.10 | 0.62 | 0.28 | 1 | 33.03 | 203.24 | 87.52 | 107.93 |
| **AT4G31920 *ARR10*** | **0.27** | **0.27** | **0.46** | | **85.16** | **87.67** | **142.64** | **105.16** |
| AT5G05870 | 0.25 | 0.32 | 0.43 | | 79.20 | 99.87 | 131.67 | 103.58 |
| AT1G71130 | 0.34 | 0.35 | 0.30 | | 106.49 | 107.97 | 93.90 | 102.78 |
| AT4G12440 | 0.70 | 0.16 | 0.14 | | 211.99 | 50.62 | 43.90 | 102.17 |
| **AT4G35190 *LOG5*** | **0.51** | **0.30** | **0.19** | | **142.88** | **89.44** | **61.25** | **97.86** |
| AT1G13250 | 0.30 | 0.47 | 0.24 | | 82.13 | 130.57 | 65.07 | 92.59 |
| **AT2G35990 *LOG2*** | **0.52** | **0.31** | **0.16** | | **137.81** | **88.56** | **46.30** | **90.89** |
| AT2G36800 | 0.24 | 0.29 | 0.47 | | 62.20 | 73.85 | 121.52 | 85.85 |
| AT4G18210 | 0.32 | 0.29 | 0.40 | | 79.31 | 71.24 | 99.47 | 83.34 |
| AT1G31880 | 0.18 | 0.32 | 0.50 | | 42.57 | 77.09 | 117.82 | 79.16 |
| AT1G68360 | 0.17 | 0.31 | 0.52 | 1 | 35.73 | 66.23 | 120.90 | 74.29 |
| AT3G53450 | 0.61 | 0.33 | 0.06 | 1 | 132.78 | 74.38 | 14.08 | 73.75 |
| AT3G63110 | 0.27 | 0.35 | 0.38 | | 58.54 | 73.24 | 78.12 | 69.96 |
| AT1G74890 | 0.51 | 0.30 | 0.19 | 1 | 101.74 | 56.64 | 35.75 | 64.71 |
| AT4G39403 | 0.30 | 0.27 | 0.43 | | 56.34 | 54.42 | 81.91 | 64.22 |
| AT1G30260 | 0.16 | 0.19 | 0.65 | 1 | 30.82 | 36.34 | 124.19 | 63.78 |
| AT2G47430 | 0.32 | 0.39 | 0.28 | | 54.97 | 83.04 | 52.86 | 63.62 |
| AT2G46310 | 0.34 | 0.47 | 0.18 | | 62.53 | 89.82 | 33.07 | 61.81 |
| AT2G21200 | 0.30 | 0.31 | 0.39 | | 53.78 | 56.64 | 70.15 | 60.19 |
| AT3G61630 | 0.31 | 0.31 | 0.37 | | 53.24 | 59.29 | 64.55 | 59.02 |
| AT1G13420 | 0.13 | 0.27 | 0.60 | 1 | 23.65 | 48.18 | 104.68 | 58.84 |
| AT1G66190 | 0.18 | 0.30 | 0.52 | | 26.49 | 41.93 | 77.46 | 48.63 |
| AT1G48270 | 0.33 | 0.34 | 0.33 | | 48.02 | 48.85 | 48.71 | 48.53 |
| AT2G33750 | 0.36 | 0.34 | 0.30 | | 52.06 | 46.38 | 41.56 | 46.67 |
| AT1G67030 | 0.18 | 0.47 | 0.35 | | 27.25 | 62.48 | 45.14 | 44.96 |
| AT1G69690 | 0.18 | 0.40 | 0.42 | | 24.20 | 51.61 | 57.79 | 44.53 |
| AT3G10520 | 0.56 | 0.20 | 0.24 | | 76.48 | 24.79 | 30.07 | 43.78 |
| AT1G62360 | 0.28 | 0.54 | 0.18 | | 31.33 | 68.73 | 19.18 | 39.75 |
| AT4G23750 | 0.17 | 0.27 | 0.55 | | 19.48 | 30.62 | 60.14 | 36.75 |
| AT3G29670 | 0.53 | 0.34 | 0.12 | | 56.11 | 39.81 | 12.39 | 36.10 |
| AT1G09250 | 0.25 | 0.25 | 0.51 | | 27.71 | 26.61 | 52.37 | 35.57 |
| AT3G15150 | 0.41 | 0.37 | 0.22 | | 42.43 | 39.38 | 22.59 | 34.80 |
| AT2G40670 | 0.27 | 0.49 | 0.24 | | 27.51 | 48.55 | 24.75 | 33.60 |
| AT5G25130 | 0.15 | 0.33 | 0.52 | | 13.87 | 33.08 | 51.03 | 32.66 |
| AT1G09700 | 0.31 | 0.29 | 0.39 | | 29.31 | 27.20 | 36.54 | 31.02 |
| AT2G19500 | 0.24 | 0.44 | 0.32 | | 17.20 | 36.01 | 27.40 | 26.87 |
| AT2G40230 | 0.23 | 0.40 | 0.37 | | 17.88 | 30.11 | 28.89 | 25.62 |

| | | | | | | | | |
|---|---|---|---|---|---|---|---|---|
| AT1G28220 | 0.53 | 0.39 | 0.07 | | 40.56 | 26.19 | 5.32 | 24.02 |
| AT5G60100 | 0.26 | 0.36 | 0.38 | | 19.48 | 29.04 | 22.12 | 23.55 |
| AT4G27950 | 0.14 | 0.56 | 0.30 | | 9.72 | 35.77 | 22.44 | 22.64 |
| AT1G12980 | 0.13 | 0.52 | 0.35 | | 12.76 | 26.17 | 28.84 | 22.59 |
| **AT3G62670 *ARR20*** | **0.70** | **0.19** | **0.10** | | **40.59** | **18.82** | **5.20** | **21.54** |
| AT1G67110 | 0.70 | 0.22 | 0.08 | | 39.92 | 18.16 | 4.68 | 20.92 |
| AT5G56860 | 0.27 | 0.31 | 0.42 | | 13.12 | 23.70 | 20.90 | 19.24 |
| AT5G19040 | 0.35 | 0.26 | 0.39 | | 19.98 | 15.24 | 22.13 | 19.12 |
| **AT1G49190 *ARR19*** | **0.41** | **0.51** | **0.08** | | **27.19** | **21.25** | **7.47** | **18.64** |
| AT2G41510 | 0.36 | 0.30 | 0.34 | | 25.23 | 14.59 | 15.69 | 18.50 |
| AT4G29740 | 0.19 | 0.18 | 0.63 | | 9.38 | 10.68 | 34.27 | 18.11 |
| AT5G38450 | 0.24 | 0.48 | 0.28 | | 14.24 | 17.23 | 21.46 | 17.64 |
| AT3G16360 | 0.30 | 0.34 | 0.36 | | 18.17 | 25.21 | 9.19 | 17.52 |
| AT1G22985 | 0.46 | 0.36 | 0.18 | | 23.92 | 13.90 | 9.94 | 15.92 |
| AT4G04402 | 0.09 | 0.47 | 0.45 | | 4.12 | 19.91 | 22.65 | 15.56 |
| AT5G08150 | 0.40 | 0.32 | 0.28 | | 18.63 | 15.21 | 12.39 | 15.41 |
| AT2G25625 | 0.22 | 0.20 | 0.57 | | 9.45 | 9.73 | 25.16 | 14.78 |
| AT3G19160 | 0.12 | 0.19 | 0.69 | | 4.93 | 7.43 | 30.37 | 14.24 |
| AT4G11140 | 0.01 | 0.34 | 0.65 | | 0.39 | 18.16 | 23.78 | 14.11 |
| AT3G63440 | 0.44 | 0.28 | 0.28 | | 15.76 | 9.53 | 9.87 | 11.72 |
| **AT2G27070 *ARR13*** | **0.23** | **0.50** | **0.27** | | **10.02** | **16.97** | **7.77** | **11.58** |
| AT4G33800 | 0.44 | 0.42 | 0.14 | | 13.26 | 8.33 | 10.69 | 10.76 |
| AT5G50915 | 0.02 | 0.51 | 0.47 | | 0.29 | 17.61 | 13.48 | 10.46 |
| AT4G26150 | 0.48 | 0.42 | 0.10 | | 12.30 | 16.44 | 2.43 | 10.39 |
| AT3G44326 | 0.32 | 0.15 | 0.53 | | 5.90 | 6.06 | 15.10 | 9.02 |
| AT5G56970 | 0.12 | 0.62 | 0.26 | | 2.57 | 12.03 | 7.93 | 7.51 |
| AT4G24650 | 0.07 | 0.27 | 0.67 | | 2.95 | 5.57 | 13.56 | 7.36 |
| AT5G11160 | 0.11 | 0.63 | 0.26 | | 2.48 | 12.58 | 5.92 | 6.99 |
| AT1G68870 | 0.33 | 0.42 | 0.26 | | 6.31 | 8.13 | 5.28 | 6.57 |
| AT2G14920 | 0.04 | 0.91 | 0.05 | | 0.70 | 17.61 | 1.12 | 6.48 |
| AT4G24080 | 0.33 | 0.49 | 0.18 | | 8.77 | 8.53 | 2.08 | 6.46 |
| AT5G46720 | 0.40 | 0.35 | 0.25 | | 6.59 | 4.83 | 6.68 | 6.03 |
| AT3G23630 | 0.00 | 0.30 | 0.70 | | 0.00 | 7.84 | 9.76 | 5.86 |
| AT1G59940 | 0.17 | 0.42 | 0.41 | | 3.34 | 9.53 | 3.53 | 5.47 |
| AT5G26140 | 0.02 | 0.43 | 0.55 | | 0.31 | 8.17 | 7.82 | 5.43 |
| AT1G28230 | 0.26 | 0.09 | 0.65 | | 6.33 | 2.60 | 5.80 | 4.91 |
| AT2G36750 | 0.33 | 0.63 | 0.04 | | 11.75 | 2.61 | 0.31 | 4.89 |
| AT5G62120 | 0.02 | 0.58 | 0.40 | | 0.39 | 12.29 | 1.67 | 4.79 |
| AT1G31040 | 0.02 | 0.49 | 0.49 | | 0.39 | 7.10 | 5.63 | 4.37 |
| AT5G49240 | 0.54 | 0.46 | 0.00 | | 7.06 | 5.94 | 0.00 | 4.33 |
| AT5G06650 | 0.56 | 0.40 | 0.03 | | 6.25 | 5.26 | 0.47 | 3.99 |
| AT1G80100 | 0.43 | 0.35 | 0.23 | | 5.60 | 3.84 | 2.14 | 3.86 |
| AT1G25410 | 0.27 | 0.16 | 0.57 | | 3.04 | 2.61 | 4.97 | 3.54 |
| AT1G68460 | 0.00 | 0.89 | 0.11 | | 0.00 | 7.51 | 1.87 | 3.13 |
| **AT5G07210 *ARR21*** | **0.35** | **0.00** | **0.65** | | **1.22** | **0.00** | **7.54** | **2.92** |

| | | | | | | | | |
|---|---|---|---|---|---|---|---|---|
| AT2G33880 | 0.27 | 0.65 | 0.07 | | 1.30 | 5.30 | 0.93 | 2.51 |
| AT3G04280 | 0.50 | 0.50 | 0.00 | | 3.24 | 4.08 | 0.00 | 2.44 |
| AT1G58460 | 0.08 | 0.92 | 0.00 | | 0.78 | 4.72 | 0.00 | 1.84 |
| AT2G07440 | 1.00 | 0.00 | 0.00 | | 5.01 | 0.00 | 0.00 | 1.67 |
| AT5G19710 | 0.17 | 0.77 | 0.07 | | 1.18 | 2.18 | 0.47 | 1.27 |
| AT5G45890 | 0.00 | 1.00 | 0.00 | | 0.00 | 3.34 | 0.00 | 1.11 |
| AT5G38790 | 0.50 | 0.27 | 0.23 | | 1.18 | 1.11 | 0.93 | 1.08 |
| AT5G54060 | 1.00 | 0.00 | 0.00 | | 2.33 | 0.00 | 0.00 | 0.78 |
| AT4G28720 | 0.00 | 0.38 | 0.62 | | 0.00 | 1.49 | 0.77 | 0.75 |
| AT5G65800 | 0.00 | 0.35 | 0.65 | | 0.00 | 1.11 | 0.75 | 0.62 |
| AT3G30580 | 0.00 | 0.00 | 1.00 | | 0.00 | 0.00 | 1.36 | 0.45 |
| AT1G06280 | 0.00 | 1.00 | 0.00 | | 0.00 | 0.37 | 0.00 | 0.12 |

# 7. Literature

**Adamowski M, Friml J**. **2015**. PIN-Dependent Auxin Transport: Action, Regulation, and Evolution. *The Plant Cell* **27**: 20–32.

**Agusti J, Herold S, Schwarz M, Sanchez P, Ljung K, Dun EA, Brewer PB, Beveridge CA, Sieberer T, Sehr EM, *et al.* 2011**. Strigolactone signaling is required for auxin-dependent stimulation of secondary growth in plants. *Proceedings of the National Academy of Sciences* **108**: 20242–20247.

**Andersen TG, Naseer S, Ursache R, Wybouw B, Smet W, De Rybel B, Vermeer JEM, Geldner N**. **2018**. Diffusible repression of cytokinin signalling produces endodermal symmetry and passage cells. *Nature* **555**: 529–533.

**Andrews S**. **2010**. FastQC: A Quality Control Tool for High Throughput Sequence Data. *Babraham Bioinformatics*.

**Bagdassarian KS, Etchells JP, Savage NS**. **2023**. A mathematical model integrates diverging PXY and MP interactions in cambium development. *In silico Plants* **5**: 1–15.

**Baima S, Possenti M, Matteucci A, Wisman E, Altamura MM, Ruberti I, Morelli G**. **2001**. The Arabidopsis ATHB-8 HD-Zip Protein Acts as a Differentiation-Promoting Transcription Factor of the Vascular Meristems. *Plant Physiology* **126**: 643–655.

**Ben-Targem M, Ripper D, Bayer M, Ragni L**. **2021**. Auxin and gibberellin signaling cross-talk promotes hypocotyl xylem expansion and cambium homeostasis. *Journal of Experimental Botany* **72**: 3647–3660.

**Bhalerao RP, Fischer U**. **2014**. Auxin gradients across wood - instructive or incidental? *Physiologia Plantarum* **151**: 43–51.

**Bhattacharya S, Zhang Q, Andersen ME**. **2011**. Double-negative feedback loops as a common design motif in the transcriptional networks regulating cell fate. *Int. J. Design Engineering* **4**: 41–57.

**Bishopp A, Benková E, Helariutta Y**. **2011a**. Sending mixed messages: Auxin-cytokinin crosstalk in roots. *Current Opinion in Plant Biology* **14**: 10–16.

**Bishopp A, Help H, El-Showk S, Weijers D, Scheres B, Friml J, Benkova E,**

**Mähönen AP, Helariutta Y**. **2011b**. A Mutually Inhibitory Interaction between Auxin and Cytokinin Specifies Vascular Pattern in Roots. *Current Biology* **21**: 917–926.

**Bossinger G, Spokevicius A V. 2018**. Sector analysis reveals patterns of cambium differentiation in poplar stems. *Journal of Experimental Botany* **69**: 4339–4348.

**Brackmann K, Qi J, Gebert M, Jouannet V, Schlamp T, Grünwald K, Wallner ES, Novikova DD, Levitsky VG, Agustí J, *et al.* 2018**. Spatial specificity of auxin responses coordinates wood formation. *Nature Communications* **9**: 875.

**Brenner WG, Romanov GA, Köllmer I, Bürkle L, Schmülling T**. **2005**. Immediate-early and delayed cytokinin response genes of Arabidopsis thaliana identified by genome-wide expression profiling reveal novel cytokinin-sensitive processes and suggest cytokinin action through transcriptional cascades. *The Plant Journal* **44**: 314–333.

**Bürkle L, Cedzich A, Döpke C, Stransky H, Okumoto S, Gillissen B, Kühn C, Frommer WB**. **2003**. Transport of cytokinins mediated by purine transporters of the PUP family expressed in phloem, hydathodes, and pollen of Arabidopsis. *The Plant Journal* **34**: 13–26.

**Busch W, Miotk A, Ariel FD, Zhao Z, Forner J, Daum G, Suzaki T, Schuster C, Schultheiss SJ, Leibfried A, *et al.* 2010**. Transcriptional control of a plant stem cell niche. *Developmental Cell* **18**: 841–853.

**Caumon H, Vernoux T**. **2023**. A matter of time: auxin signaling dynamics and the regulation of auxin responses during plant development. *Journal of Experimental Botany*: https://doi.org/10.1093/jxb/erad132.

**Chaffey N, Cholewa E, Regan S, Sundberg B**. **2002**. Secondary xylem development in Arabidopsis: A model for wood formation. *Physiologia Plantarum* **114**: 594–600.

**Charitos IA, Ballini A, Cantore S, Boccellino M, Di Domenico M, Borsani E, Nocini R, Di Cosola M, Santacroce L, Bottalico L**. **2021**. Stem Cells: A Historical Review about Biological, Religious, and Ethical Issues. *Stem Cells International* **2021**: Article ID 9978837.

**Cheng CY, Krishnakumar V, Chan AP, Thibaud-Nissen F, Schobel S, Town CD**. **2017**. Araport11: a complete reannotation of the Arabidopsis thaliana reference genome. *Plant Journal* **89**: 789–804.

**Chickarmane V, Troein C, Nuber UA, Sauro HM, Peterson C**. **2006**. Transcriptional

Dynamics of the Dmbryonic Stem Cell Switch. *PLoS Computational Biology* **2**: 1080–1092.

**Clough SJ, Bent AF**. **1998**. Floral dip: A simplified method for Agrobacterium-mediated transformation of Arabidopsis thaliana. *The Plant Journal* **16**: 735–743.

**Dang TVT, Lee S, Cho H, Choi K, Hwang I**. **2023**. The LBD11-ROS feedback regulatory loop modulates vascular cambium proliferation and secondary growth in Arabidopsis. *Molecular Plant* **16**: 1–15.

**Denis E, Kbiri N, Mary V, Claisse G, Conde e Silva N, Kreis M, Deveaux Y**. **2017**. WOX14 promotes bioactive gibberellin synthesis and vascular cell differentiation in Arabidopsis. *The Plant Journal* **90**: 560–572.

**Dobin A, Davis CA, Schlesinger F, Drenkow J, Zaleski C, Jha S, Batut P, Chaisson M, Gingeras TR**. **2013**. STAR: Ultrafast universal RNA-seq aligner. *Bioinformatics* **29**: 15–21.

**Dolzblasz A, Nardmann J, Clerici E, Causier B, van der Graaff E, Chen J, Davies B, Werr W, Laux T**. **2016**. Stem Cell Regulation by Arabidopsis WOX Genes. *Molecular Plant* **9**: 1028–1039.

**Durán-Medina Y, Díaz-Ramírez D, Marsch-Martínez N**. **2017**. Cytokinins on the move. *Frontiers in Plant Science* **8**: Article 146.

**el-Showk S, Help-Rinta-Rahko H, Blomster T, Siligato R, Marée AFM, Mähönen AP, Grieneisen VA**. **2015**. Parsimonious Model of Vascular Patterning Links Transverse Hormone Fluxes to Lateral Root Initiation: Auxin Leads the Way, while Cytokinin Levels Out. *PLoS Computational Biology* **11**: 1–40.

**Elahi FE, Hasan A**. **2018**. A method for estimating hill function-based dynamic models of gene regulatory networks. *Royal Society Open Science* **5**: 171226.

**Enver T, Pera M, Peterson C, Andrews PW**. **2009**. Stem Cell States, Fates, and the Rules of Attraction. *Cell Stem Cell* **4**: 387–397.

**Etchells JP, Provost CM, Mishr L, Turner SR**. **2013**. WOX4 and WOX14 act downstream of the PXY receptor kinase to regulate plant vascular proliferation independently of any role in vascular organisation. *Development (Cambridge)* **140**: 2224–2234.

**Etchells JP, Provost CM, Turner SR**. **2012**. Plant Vascular Cell Division Is Maintained by an Interaction between PXY and Ethylene Signalling. *PLoS Genetics* **8**.

**Ferrell JE**. **2012**. Bistability, bifurcations, and Waddington's epigenetic landscape. *Current Biology* **22**: R458–R466.

**Fischer U, Kucukoglu M, Helariutta Y, Bhalerao RP**. **2019**. The Dynamics of Cambial Stem Cell Activity. *Annual Review of Plant Biology* **70**: 293–319.

**Fisher K, Turner S**. **2007**. PXY, a Receptor-like Kinase Essential for Maintaining Polarity during Plant Vascular-Tissue Development. *Current Biology* **17**: 1061–1066.

**Friml J, Benkova E, Blilou I, Wisniewska J, Hamann T, Ljung K, Woody S, Sandberg G, Scheres B, Jürgens G, *et al.* 2002**. AtPIN4 Mediates Sink-Driven Auxin Gradients and Root Patterning in Arabidopsis. *Cell* **108**: 661–673.

**Fu X, Su H, Liu S, Du X, Xu C, Luo K**. **2021**. Cytokinin signaling localized in phloem noncell-autonomously regulates cambial activity during secondary growth of Populus stems. *New Phytologist* **230**: 1476–1488.

**Fujiwara M, Imamura M, Matsushita K, Roszak P, Yamashino T, Hosokawa Y, Nakajima K, Fujimoto K, Miyashima S**. **2023**. Patterned proliferation orients tissue-wide stress to control root vascular symmetry in Arabidopsis. *Current Biology* **33**: 886–898.

**Furuya T, Saito M, Uchimura H, Satake A, Nosaki S, Miyakawa T, Shimadzu S, Yamori W, Tanokura M, Fukuda H, *et al.* 2021**. Gene co-expression network analysis identifies BEH3 as a stabilizer of secondary vascular development in Arabidopsis. *Plant Cell* **33**: 2618–2636.

**Gaillochet C, Stiehl T, Wenzl C, Ripoll JJ, Bailey-Steinitz LJ, Li L, Pfeiffer A, Miotk A, Hakenjos JP, Forner J, *et al.* 2017**. Control of plant cell fate transitions by transcriptional and hormonal signals. *eLife* **6**: 1–30.

**Ge SX, Jung D, Yao R**. **2020**. ShinyGO: A graphical gene-set enrichment tool for animals and plants. *Bioinformatics* **36**: 2628–2629.

**Gillissen B, Bürkle L, André B, Kühn C, Rentsch D, Brandl B, Frommer WB**. **2000**. A New Family of High-Affinity Transporters for Adenine, Cytosine, and Purine Derivatives in Arabidopsis. *The Plant Cell* **12**: 291–300.

**Gordon SP, Chickarmane VS, Ohno C, Meyerowitz EM**. **2009**. Multiple feedback loops through cytokinin signaling control stem cell number within the *Arabidopsis* shoot meristem. *Proceedings of the National Academy of Sciences* **106**: 16529–16534.

**van der Graaff E, Laux T, Rensing SA**. **2009**. The WUS homeobox-containing (WOX)

protein family. *Genome Biology* **10**: 248.

**Greb T, Lohmann JU**. **2016**. Plant Stem Cells. *Current Biology* **26**: R816–R821.

**Guan C, Qiao L, Xiong Y, Zhang L, Jiao Y**. **2022**. Coactivation of antagonistic genes stabilizes polarity patterning during shoot organogenesis. *Science Advances* **8**.

**Guo Y, Qin G, Gu H, Qu LJ**. **2009**. Dof5.6/HCA2, a dof transcription factor gene, regulates interfascicular cambium formation and vascular tissue development in Arabidopsis. *Plant Cell* **21**: 3518–3534.

**Haas AS, Shi D, Greb T**. **2022**. Cell Fate Decisions Within the Vascular Cambium – Initiating Wood and Bast Formation. *Frontiers in Plant Science* **13**: Article 86442.

**Haas S, Trumpp A, Milsom MD**. **2018**. Causes and Consequences of Hematopoietic Stem Cell Heterogeneity. *Cell Stem Cell* **22**: 627–638.

**Haecker A, Groß-Hardt R, Geiges B, Sarkar A, Breuninger H, Herrmann M, Laux T**. **2004**. Expression dynamics of WOX genes mark cell fate decisions during early embryonic patterning in Arabidopsis thaliana. *Development* **131**: 657–668.

**Haghverdi L, Ludwig LS**. **2023**. Single-cell multi-omics and lineage tracing to dissect cell fate decision-making. *Stem Cell Reports* **18**: 13–25.

**Han S, Cho H, Noh J, Qi J, Jung HJ, Nam H, Lee S, Hwang D, Greb T, Hwang I**. **2018**. BIL1-mediated MP phosphorylation integrates PXY and cytokinin signalling in secondary growth. *Nature Plants* **4**: 605–614.

**Herud-Sikimić O, Stiel AC, Kolb M, Shanmugaratnam S, Berendzen KW, Feldhaus C, Höcker B, Jürgens G**. **2021**. A biosensor for the direct visualization of auxin. *Nature* **592**: 768–772.

**Hetherington AJ, Dubrovsky JG, Dolan L**. **2016**. Unique Cellular Organization in the Oldest Root Meristem. *Current Biology* **26**: 1629–1633.

**Hirakawa Y, Kondo Y, Fukuda H**. **2010**. TDIF peptide signaling regulates vascular stem cell proliferation via the WOX4 homeobox gene in Arabidopsis. *Plant Cell* **22**: 2618–2629.

**Horák J, Grefen C, Berendzen KW, Hahn A, Stierhof YD, Stadelhofer B, Stahl M, Koncz C, Harter K**. **2008**. The Arabidopsis thaliana response regulator ARR22 is a putative AHP phospho-histidine phosphatase expressed in the chalaza of developing seeds. *BMC Plant Biology* **8**: 1–18.

**Hwang I, Sheen J**. **2001**. Two-component circuitry in Arabidopsis cytokinin signal

transduction. *Nature* **413**: 383–389.

**Ikeda M, Mitsuda N, Ohme-Takagi M**. **2009**. Arabidopsis WUSCHEL Is a Bifunctional Transcription Factor That Acts as a Repressor in Stem Cell Regulation and as an Activator in Floral Patterning. *The Plant Cell* **21**: 3493–3505.

**Immanen J, Nieminen K, Smolander OP, Kojima M, Alonso Serra J, Koskinen P, Zhang J, Elo A, Mähönen AP, Street N, *et al.* 2016**. Cytokinin and Auxin Display Distinct but Interconnected Distribution and Signaling Profiles to Stimulate Cambial Activity. *Current Biology* **26**: 1990–1997.

**Ito Y, Nakanomyo I, Motse H, Iwamoto K, Sawa S, Dohmae N, Fukuda H**. **2006**. Dodeca-CLE Peptides as Suppressors of Plant Stem Cell Differentiation. *Science* **313**: 842–845.

**Jeon J, Kim NY, Kim S, Kang NY, Novák O, Ku SJ, Cho C, Lee DJ, Lee EJ, Strnad M, *et al.* 2010**. A subset of cytokinin two-component signaling system plays a role in cold temperature stress response in Arabidopsis. *Journal of Biological Chemistry* **285**: 23371–23386.

**Ji J, Strable J, Shimizu R, Koenig D, Sinha N, Scanlon MJ**. **2010**. Wox4 promotes procambial development. *Plant Physiology* **152**: 1346–1356.

**Kalmar T, Lim C, Hayward P, Muñoz-Descalzo S, Nichols J, Garcia-Ojalvo J, Arias AM**. **2009**. Regulated fluctuations in Nanog expression mediate cell fate decisions in embryonic stem cells. *PLoS Biology* **7**: e1000149.

**Kelsh RN, Sosa KC, Farjami S, Makeev V, Dawes JHP, Rocco A**. **2021**. Cyclical fate restriction: A new view of neural crest cell fate specification. *Development (Cambridge)* **148**: dev176057.

**Kiba T, Aoki K, Sakakibara H, Mizuno T**. **2004**. Arabidopsis response regulator, ARR22, ectopic expression of which results in phenotypes similar to the wol cytokinin-receptor mutant. *Plant Cell Physiology* **45**: 1063–1077.

**Kieber JJ, Schaller GE**. **2014**. Cytokinins. *The Arabidopsis Book*: e0168.

**Kieber JJ, Schaller GE**. **2018**. Cytokinin signaling in plant development. *Development (Cambridge)* **145**: 1–7.

**Kondo Y, Tamaki T, Fukuda H**. **2014**. Regulation of xylem cell fate. *Frontiers in Plant Science* **5**: Article 315.

**Kucukoglu M, Nilsson J, Zheng B, Chaabouni S, Nilsson O**. **2017**. WUSCHEL-

RELATED HOMEOBOX4 (WOX4)-like genes regulate cambial cell division activity and secondary growth in Populus trees. *New Phytologist* **215**: 642–657.

**Kunze C, Khalil AS**. **2022**. One cell, many fates. *Science* **375**: 262–263.

**Kuroha T, Tokunaga H, Kojima M, Ueda N, Ishida T, Nagawa S, Fukuda H, Sugimoto K, Sakakibara H**. **2009**. Functional Analyses of LONELY GUY Cytokinin-Activating Enzymes Reveal the Importance of the Direct Activation Pathway in Arabidopsis. *The Plant Cell* **21**: 3152–3169.

**Lackner A, Sehlke R, Garmhausen M, Stirparo GG, Huth M, Titz-teixeira F, Van Der Lelij P, Ramesmayer J, Thomas HF, Ralser M, *et al.* 2021**. Cooperative genetic networks drive embryonic stem cell transition from naïve to formative pluripotency. *The EMBO Journal* **40**: e105776.

**Lampropoulos A, Sutikovic Z, Wenzl C, Maegele I, Lohmann JU, Forner J**. **2013**. GreenGate - A novel, versatile, and efficient cloning system for plant transgenesis. *PLoS ONE* **8**: e83043.

**Laurenti E, Göttgens B**. **2018**. From haematopoietic stem cells to complex differentiation landscapes. *Nature* **553**: 418–426.

**Laux T, Mayer KFX, Berger J, Jürgens G**. **1996**. The WUSCHEL gene is required for shoot and floral meristem integrity in Arabidopsis. *Development* **122**: 87–96.

**Lavedrine C, Farcot E, Vernoux T**. **2015**. Modeling plant development: From signals to gene networks. *Current Opinion in Plant Biology* **27**: 148–153.

**Lawrence M, Huber W, Pagès H, Aboyoun P, Carlson M, Gentleman R, Morgan MT, Carey VJ**. **2013**. Software for Computing and Annotating Genomic Ranges. *PLoS Computational Biology* **9**: e1003118.

**Lebovka I, Hay Mele B, Liu X, Zakieva A, Schlamp T, Gursanscky NR, Merks RM, Großeholz R, Greb T**. **2023**. Computational modelling of cambium activity provides a regulatory framework for simulating radial plant growth. *eLife* **12**: e66627.

**Lee K, Kim JH, Park O-S, Jung YJ, Seo PJ**. **2022**. Ectopic expression of WOX5 promotes cytokinin signaling and de novo shoot regeneration. *Plant Cell Reports* **41**: 2415–2422.

**Lee DJ, Park JY, Ku SJ, Ha YM, Kim S, Kim MD, Oh MH, Kim J**. **2007**. Genome-wide expression profiling of Arabidopsis Response Regulator 7(ARR7) overexpression in cytokinin response. *Molecular Genetics and Genomics* **277**: 115–137.

**Leibfried A, To JPC, Busch W, Stehling S, Kehle A, Demar M, Kieber JJ, Lohmann JU**. **2005**. WUSCHEL controls meristem function by direct regulation of cytokinin-inducible response regulators. *Nature* **438**: 1172–1175.

**Leyser O**. **2018**. Auxin Signaling. *Plant Physiology* **176**: 465–479.

**Liao CY, Smet W, Brunoud G, Yoshida S, Vernoux T, Weijers D**. **2015**. Reporters for sensitive and quantitative measurement of auxin response. *Nature Methods* **12**: 207–210.

**Liebsch D, Sunaryo W, Holmlund M, Norberg M, Zhang J, Hall HC, Helizon H, Jin X, Helariutta Y, Nilsson O, *et al.* 2014**. Class I KNOX transcription factors promote differentiation of cambial derivatives into xylem fibers in the Arabidopsis hypocotyls. *Development (Cambridge)* **141**: 4311–4319.

**Lloyd AM, Schena M, Walbot V, Davis RW**. **1994**. Epidermal cell fate determination in Arabidopsis: Patterns defined by a steroid-inducible regulator. *Science* **266**: 436–439.

**López-Salmerón V, Schürholz A-K, Li Z, Schlamp T, Wenzl C, Lohmann JU, Greb T, Wolf S**. **2019**. Inducible, Cell Type-Specific Expression in Arabidopsis thaliana Through LhGR-Mediated Trans-Activation. *JoVE*: e59394.

**Love MI, Huber W, Anders S**. **2014**. Moderated estimation of fold change and dispersion for RNA-seq data with DESeq2. *Genome Biology* **15**: 550.

**Ma Y, Miotk A, Šutiković Z, Ermakova O, Wenzl C, Medzihradszky A, Gaillochet C, Forner J, Utan G, Brackmann K, *et al.* 2019**. WUSCHEL acts as an auxin response rheostat to maintain apical stem cells in Arabidopsis. *Nature Communications* **10**: 5093.

**Mähönen AP, Bishopp A, Higuchi M, Nieminen KM, Kinoshita K, Törmäkangas K, Ikeda Y, Oka A, Kakimoto T, Helariutta Y**. **2006a**. Cytokinin signaling and its inhibitor AHP6 regulate cell fate during vascular development. *Science* **311**: 94–98.

**Mähönen AP, Bonke M, Kauppinen L, Riikonen M, Benfey PN, Helariutta Y**. **2000**. A novel two-component hybrid molecule regulates vascular morphogenesis of the Arabidopsis root. *Genes and Development* **14**: 2938–2943.

**Mähönen AP, Higuchi M, Törmäkangas K, Miyawaki K, Pischke MS, Sussman MR, Helariutta Y, Kakimoto T**. **2006b**. Cytokinins Regulate a Bidirectional Phosphorelay Network in Arabidopsis. *Current Biology* **16**: 1116–1122.

**Mäkilä R, Wybouw B, Smetana O, Vainio L, Solé-Gil A, Lyu M, Ye L, Wang X, Siligato R, Jenness MK, *et al.* 2023**. Gibberellins promote polar auxin transport to regulate stem cell fate decisions in cambium. *Nature Plants* **9**: 631–644.

**Marhavý P, Bielach A, Abas L, Abuzeineh A, Duclercq J, Tanaka H, Pařezová M, Petrášek J, Friml J, Kleine-Vehn J, *et al.* 2011**. Cytokinin Modulates Endocytic Trafficking of PIN1 Auxin Efflux Carrier to Control Plant Organogenesis. *Developmental Cell* **21**: 796–804.

**Martin-Arevalillo R, Vernoux T**. **2023**. Decoding the Auxin Matrix: Auxin Biology Through the Eye of the Computer. *Annual Review of Plant Biology* **74**: 387–413.

**Matsumoto-Kitano M, Kusumoto T, Tarkowski P, Kinoshita-Tsujimura K, Vaclavikova K, Miyawaki K, Kakimoto T**. **2008**. Cytokinins are central regulators of cambial activity. *Proceedings of the National Academy of Sciences* **105**: 20027–20031.

**Mayer KFX, Schoof H, Haecker A, Lenhard M, Jügens G, Laux T**. **1998**. Role of WUSCHEL in Regulating Stem Cell Fate in the Arabidopsis Shoot Meristem. *Cell* **95**: 805–815.

**Meng WJ, Cheng ZJ, Sang YL, Zhang MM, Rong XF, Wang ZW, Tang YY, Zhang XS**. **2017**. Type-B ARABIDOPSIS RESPONSE REGULATORs specify the shoot stem cell niche by dual regulation of WUSCHEL. *The Plant Cell* **29**: 1357–1372.

**Mironova V V., Omelyanchuk NA, Yosiphon G, Fadeev SI, Kolchanov NA, Mjolsness E, Likhoshvai VA**. **2010**. A plausible mechanism for auxin patterning along the developing root. *BMC Systems Biology* **4**: 98.

**Miyashima S, Roszak P, Sevilem I, Toyokura K, Blob B, Heo J, Mellor N, Help-Rinta-Rahko H, Otero S, Smet W, *et al.* 2019**. Mobile PEAR transcription factors integrate positional cues to prime cambial growth. *Nature* **565**: 490–494.

**Mor E**. **2020**. A molecular framework for the control of cell division orientation during plant vascular development. *Universiteit Gent. Faculteit Wetenschappen*: http://hdl.handle.net/1854/LU-8674420.

**Moret B, Marhava P, Aliaga Fandino AC, Hardtke CS, ten Tusscher KHW**. **2020**. Local auxin competition explains fragmented differentiation patterns. *Nature Communications* **11**: 2965.

**Muraro D, Mellor N, Pound MP, Help H, Lucas M, Chopard J, Byrne HM, Godin C, Hodgman C, King JR, *et al.* 2014**. Integration of hormonal signaling networks and

mobile microRNAs is required for vascular patterning in Arabidopsis roots. *Proceedings of the National Academy of Sciences* **111**: 857–862.

**Naito T, Yamashino T, Kiba T, Koizumi N, Kojima M, Sakakibara H, Mizuno T**. **2007**. A link between cytokinin and ASL9 (Asymmetric Leaves 2 Like 9) that belongs to the AS2/LOB (Lateral Organ Boundaries) family genes in Arabidopsis thaliana. *Bioscience, Biotechnology and Biochemistry* **71**: 1269–1278.

**Narutaki A, Kahar P, Shimadzu S, Maeda S, Furuya T, Ishizaki K, Fukaki H, Ogino C, Kondo Y**. **2023**. Sucrose Signaling Contributes to the Maintenance of Vascular Cambium by Inhibiting Cell Differentiation. *Plant And Cell Physiology* **00**: 1-12 pcad039.

**Nieminen K, Immanen J, Laxell M, Kauppinen L, Tarkowski P, Dolezal K, Tahtiharju S, Elo A, Decourteix M, Ljung K, *et al.* 2008**. Cytokinin signaling regulates cambial development in poplar. *Proceedings of the National Academy of Sciences* **105**: 20032–20037.

**Nilsson J, Karlberg A, Antti H, Lopez-Vernaza M, Mellerowicz E, Bhalerao RP, Perrot-Rechenmann C, Sandberg G, Bhalerao RP**. **2008**. Dissecting the Molecular Basis of the Regulation of Wood Formation by Auxin in Hybrid Aspen. *The Plant Cell* **20**: 843–855.

**Ogura N, Sasagawa Y, Ito T, Tameshige T, Kawai S, Sano M, Doll Y, Iwase A, Kawamura A, Suzuki T, *et al.* 2023**. WUSCHEL-RELATED HOMEOBOX 13 suppresses de novo shoot regeneration via cell fate control of pluripotent callus. *Science Advances* **9**: eadg6983.

**Ohashi-Ito K, Saegusa M, Iwamoto K, Oda Y, Katayama H, Kojima M, Sakakibara H, Fukuda H**. **2014**. A bHLH Complex Activates Vascular Cell Division via Cytokinin Action in Root Apical Meristem. *Current Biology* **24**: 2053–2058.

**Olariu V, Peterson C**. **2019**. Kinetic models of hematopoietic differentiation. *Wiley interdisciplinary reviews. Systems biology and medicine* **11**: e1424.

**Parizkova B, Zukauskaite A, Vain T, Grones P, Raggi S, Kubes MF, Kieffer M, Doyle SM, Strnad M, Kepinski S, *et al.* 2021**. New fluorescent auxin probes visualise tissue-specific and subcellular distributions of auxin in Arabidopsis e. *New Phytologist* **230**: 535–549.

**Pernisova M, Grochova M, Konecny T, Plackova L, Harustiakova D, Kakimoto T, Heisler MG, Novak O, Hejatko J**. **2018**. Cytokinin signalling regulates organ identity

via the AHK4 receptor in Arabidopsis. *Development (Cambridge)* **145**: dev163907.

**Pi L, Aichinger E, van der Graaff E, Llavata-Peris CI, Weijers D, Hennig L, Groot E, Laux T**. **2015**. Organizer-Derived WOX5 Signal Maintains Root Columella Stem Cells through Chromatin-Mediated Repression of CDF4 Expression. *Developmental Cell* **33**: 576–588.

**Qian P, Song W, Zaizen-Iida M, Kume S, Wang G, Zhang Y, Kinoshita-Tsujimura K, Chai J, Kakimoto T**. **2022**. A Dof-CLE circuit controls phloem organization. *Nature Plants* **8**: 817–827.

**Ragni L, Greb T**. **2018**. Secondary growth as a determinant of plant shape and form. *Seminars in Cell and Developmental Biology* **79**: 58–67.

**Ragni L, Nieminen K, Pacheco-Villalobos D, Sibout R, Schwechheimer C, Hardtke CS**. **2011**. Mobile gibberellin directly stimulates Arabidopsis hypocotyl xylem expansion. *The Plant Cell* **23**: 1322–1326.

**Rienstra J, Hernandes-Garcia J, Weijers D**. **2023**. To bind or not to bind: how Auxin Response Factors select their target genes. *Journal of Experimental Botany* **erad259**.

**Roosjen M, Kuhn A, Mutte S, Boeren S, Krupar P, Koehorst J, Fendrych M, Friml J, Weijers D**. An ultra-fast, proteome-wide response to the plant hormone auxin. *bioRxiv*: https://doi.org/10.1101/2022.11.25.517949.

**Roszak P, Heo J-O, Blob B, Toyokura K, Sugiyama Y, de Luis Balaguer MA, Lau WWY, Hamey F, Cirrone J, Madej E, *et al.* 2021**. Cell-by-cell dissection of phloem development links a maturation gradient to cell specialization. *Science* **374**: eaba5531.

**De Rybel B, Adibi M, Breda AS, Wendrich JR, Smit ME, Novák O, Yamaguchi N, Yoshida S, Van Isterdael G, Palovaara J, *et al.* 2014**. Integration of growth and patterning during vascular tissue formation in Arabidopsis. *Science* **345**: 1255215.

**De Rybel B, Mähönen AP, Helariutta Y, Weijers D**. **2016**. Plant vascular development: From early specification to differentiation. *Nature Reviews Molecular Cell Biology* **17**: 30–40.

**De Rybel B, Möller B, Yoshida S, Grabowicz I, Barbier de Reuille P, Boeren S, Smith RS, Borst JW, Weijers D**. **2013**. A bHLH Complex Controls Embryonic Vascular Tissue Establishment and Indeterminate Growth in Arabidopsis. *Developmental Cell* **24**: 426–437.

**Sachs T**. **1991**. Cell polarity and tissue patterning in plants. *Devlopment* **91**: 83–93.

**Salvi E, Rutten JP, Di Mambro R, Polverari L, Licursi V, Negri R, Dello Ioio R, Sabatini S, Ten Tusscher K**. **2020**. A Self-Organized PLT/Auxin/ARR-B Network Controls the Dynamics of Root Zonation Development in Arabidopsis thaliana. *Developmental Cell* **53**: 431-443.e23.

**Sanio KG**. **1873**. Anatomie der gemeinen Kiefer (Pinus sylvestris L.). In: Jahrb Wiss Bot. 50–126.

**Santner A, Calderon-Villalobos LIA, Estelle M**. **2009**. Plant hormones are versatile chemical regulators of plant growth. *Nature Chemical Biology* **5**: 301–307.

**Sarkar AK, Luijten M, Miyashima S, Lenhard M, Hashimoto T, Nakajima K, Scheres B, Heidstra R, Laux T**. **2007**. Conserved factors regulate signalling in Arabidopsis thaliana shoot and root stem cell organizers. *Nature* **446**: 811–814.

**Savina MS, Pasternak T, Omelyanchuk NA, Novikova DD, Palme K, Mironova V V., Lavrekha V V. 2020**. Cell Dynamics in WOX5-Overexpressing Root Tips: The Impact of Local Auxin Biosynthesis. *Frontiers in Plant Science* **11**: Article 560169.

**Schaller GE, Bishopp A, Kieber JJ**. **2015**. The yin-yang of hormones: Cytokinin and auxin interactions in plant development. *The Plant Cell* **27**: 44–63.

**Schuster C, Gaillochet C, Medzihradszky A, Busch W, Daum G, Krebs M, Kehle A, Lohmann JU**. **2014**. A regulatory framework for shoot stem cell control integrating metabolic, transcriptional, and phytohormone signals. *Developmental Cell* **28**: 438–449.

**Sehr EM, Agusti J, Lehner R, Farmer EE, Schwarz M, Greb T**. **2010**. Analysis of secondary growth in the Arabidopsis shoot reveals a positive role of jasmonate signalling in cambium formation. *Plant Journal* **63**: 811–822.

**Sheen J, Müller B**. **2008**. Cytokinin and auxin interaction in root stem-cell specification during early embryogenesis. *Nature* **453**: 1094–1097.

**Shi D, Lebovka I, Lopez-Salmeroń V, Sanchez P, Greb T**. **2019**. Bifacial cambium stem cells generate xylem and phloem during radial plant growth. *Development (Cambridge)* **146**: dev171355.

**Šimášková M, O'Brien JA, Khan M, Van Noorden G, Ötvös K, Vieten A, De Clercq I, Van Haperen JMA, Cuesta C, Hoyerová K, *et al.* 2015**. Cytokinin response factors regulate PIN-FORMED auxin transporters. *Nature Communications* **6**: 8717.

**Smet W, Sevilem I, de Luis Balaguer MA, Wybouw B, Mor E, Miyashima S, Blob**

**B, Roszak P, Jacobs TB, Boekschoten M, *et al.* 2019**. DOF2.1 Controls Cytokinin-Dependent Vascular Cell Proliferation Downstream of TMO5/LHW. *Current Biology* **29**: 520–529.

**Smetana O, Mäkilä R, Lyu M, Amiryousefi A, Sánchez Rodríguez F, Wu MF, Solé-Gil A, Leal Gavarrón M, Siligato R, Miyashima S, *et al.* 2019**. High levels of auxin signalling define the stem-cell organizer of the vascular cambium. *Nature* **565**: 485–489.

**Smit ME, McGregor SR, Sun H, Gough C, Bågman AM, Soyars CL, Kroon JT, Gaudinier A, Williams CJ, Yang X, *et al.* 2020**. A PXY-mediated transcriptional network integrates signaling mechanisms to control vascular development in Arabidopsis. *The Plant Cell* **32**: 319–335.

**Steiner E, Israeli A, Gupta R, Shwartz I, Nir I, Leibman-Markus M, Tal L, Farber M, Amsalem Z, Ori N, *et al.* 2020**. Characterization of the cytokinin sensor TCSv2 in arabidopsis and tomato. *Plant Methods* **16**: 152.

**Subkhankulova T, Camargo Sosa K, Uroshlev LA, Nikaido M, Shriever N, Kasianov AS, Yang X, Rodrigues FSLM, Carney TJ, Bavister G, *et al.* 2023**. Zebrafish pigment cells develop directly from persistent highly multipotent progenitors. *Nature Communications* **14**: 1258.

**Suer S, Agusti J, Sanchez P, Schwarz M, Greb T**. **2011**. WOX4 imparts auxin responsiveness to cambium cells in arabidopsis. *The Plant Cell* **23**: 3247–3259.

**Sukparangsi W, Morganti E, Lowndes M, Mayeur H, Weisser M, Hammachi F, Peradziryi H, Roske F, Hölzenspies J, Livigni A, *et al.* 2022**. Evolutionary origin of vertebrate OCT4/POU5 functions in supporting pluripotency. *Nature Communications* **13**: 5537.

**Thomson M, Liu SJ, Zou LN, Smith Z, Meissner A, Ramanathan S**. **2011**. Pluripotency factors in embryonic stem cells regulate differentiation into germ layers. *Cell* **145**: 875–889.

**To JPC, Deruère J, Maxwell BB, Morris VF, Hutchison CE, Ferreira FJ, Schaller GE, Kieber JJ**. **2007**. Cytokinin regulates type-A Arabidopsis response regulator activity and protein stability via two-component phosphorelay. *Plant Cell* **19**: 3901–3914.

**To JPC, Haberer G, Ferreira FJ, Deruère J, Mason MG, Schaller GE, Alonso JM, Ecker JR, Kieber JJ**. **2004**. Type-A Arabidopsis response regulators are partially

redundant negative regulators of cytokinin signaling. *The Plant Cell* **16**: 658–671.

**Tognetti VB, Bielach A, Hrtyan M**. **2017**. Redox regulation at the site of primary growth: Auxin, cytokinin and ROS crosstalk. *Plant Cell and Environment* **40**: 2586–2605.

**Tomlin CJ, Axelrod JD**. **2007**. Biology by numbers: Mathematical modelling in developmental biology. *Nature Reviews Genetics* **8**: 331–340.

**Torii K, Inoue K, Bekki K, Haraguchi K, Kubo M, Kondo Y, Suzuki T, Kubota A, Uemoto K, Shimizu H, *et al.* 2022**. A guiding role of the Arabidopsis circadian clock in cell differentiation revealed by time-series single- cell RNA sequencing. *Cell Reports* **40**: 111059.

**Turley EK, Etchells JP**. **2022**. Laying it on thick: A study in secondary growth. *Journal of Experimental Botany* **73**: 665–679.

**Uggla C, Moritz T, Sandberg G, Sundberg B**. **1996**. Auxin as a positional signal in pattern formation in plants. *Proceedings of the National Academy of Sciences* **93**: 9282–9286.

**Ulmasov T, Murfett J, Hagen G, Guilfoyle TJ**. **1997**. Aux/IAA Proteins Repress Expression of Reporter Genes Containing Natural and Highly Active Synthetic Auxin Response Elements. *The Plant Cell* **9**: 1963–1971.

**Ursache R, Andersen TG, Marhavy P, Geldner N**. **2018**. A protocol for combining fluorescent proteins with histological stains for diverse cell wall components. *The Plant Journal* **93**: 399–412.

**Ursache R, Miyashima S, Chen Q, Vatén A, Nakajima K, Carlsbecker A, Zhao Y, Helariutta Y, Dettmer J**. **2014**. Tryptophan-dependent auxin biosynthesis is required for HD-ZIP III-mediated xylem patterning. *Development (Cambridge)* **141**: 1250–1259.

**Wallner ES, López-Salmerón V, Belevich I, Poschet G, Jung I, Grünwald K, Sevilem I, Jokitalo E, Hell R, Helariutta Y, *et al.* 2017**. Strigolactone- and Karrikin-Independent SMXL Proteins Are Central Regulators of Phloem Formation. *Current Biology* **27**: 1241–1247.

**Wallner ES, Tonn N, Shi D, Jouannet V, Greb T**. **2020**. SUPPRESSOR OF MAX2 1-LIKE 5 promotes secondary phloem formation during radial stem growth. *The Plant Journal* **102**: 903–915.

**Wang Z, Oron E, Nelson B, Razis S, Ivanova N**. **2012**. Distinct lineage specification

roles for NANOG, OCT4, and SOX2 in human embryonic stem cells. *Cell Stem Cell* **10**: 440–454.

**Wickham H**. **2016**. ggplot2: Elegant Graphics for Data Analysis. *Springer-Verlag New York*.

**Woudenberg S, Renema J, Tomescu AMF, De Rybel B, Weijers D**. **2022**. Deep origin and gradual evolution of transporting tissues: Perspectives from across the land plants. *Plant Physiology* **190**: 85–99.

**Wybouw B, De Rybel B**. **2019**. Cytokinin – A Developing Story. *Trends in Plant Science* **24**: 177–185.

**Xiao W, Molina D, Wunderling A, Ripper D, Vermeer JEM, Ragni L**. **2020**. Pluripotent Pericycle Cells Trigger Different Growth Outputs by Integrating Developmental Cues into Distinct Regulatory Modules. *Current Biology* **30**: 4384–4398.

**Xie M, Chen H, Huang L, O'Neil RC, Shokhirev MN, Ecker JR**. **2018**. A B-ARR-mediated cytokinin transcriptional network directs hormone cross-regulation and shoot development. *Nature Communications* **9**: 1604.

**Yadav RK, Perales M, Gruel J, Girke T, Jönsson H, Venugopala Reddy G**. **2011**. WUSCHEL protein movement mediates stem cell homeostasis in the Arabidopsis shoot apex. *Genes and Development* **25**: 2025–2030.

**Yanagisawa S**. **2002**. The Dof family of plant transcription factors. *Trends in Plant Science* **7**: 555–560.

**Yang BJ, Minne M, Brunoni F, Plačková L, Petřík I, Sun Y, Nolf J, Smet W, Verstaen K, Wendrich JR, *et al.* 2021**. Non-cell autonomous and spatiotemporal signalling from a tissue organizer orchestrates root vascular development. *Nature Plants* **7**: 1485–1494.

**Ye L, Wang X, Lyu M, Siligato R, Eswaran G, Vainio L, Blomster T, Zhang J, Mähönen AP**. **2021**. Cytokinins initiate secondary growth in the Arabidopsis root through a set of LBD genes. *Current Biology* **31**: 3365–3373.

**Yokoyama A, Yamashino T, Amano YI, Tajima Y, Imamura A, Sakakibara H, Mizuno T**. **2007**. Type-B ARR transcription factors, ARR10 and ARR12, are implicated in cytokinin-mediated regulation of protoxylem differentiation in roots of Arabidopsis thaliana. *Plant and Cell Physiology* **48**: 84–96.

**Zeng J, Dong Z, Wu H, Tian Z, Zhao Z**. **2017**. Redox regulation of plant stem cell fate. *The EMBO Journal* **36**: 2844–2855.

**Zhang J, Eswaran G, Alonso-Serra J, Kucukoglu M, Xiang J, Yang W, Elo A, Nieminen K, Damén T, Joung JG, *et al.* 2019**. Transcriptional regulatory framework for vascular cambium development in Arabidopsis roots. *Nature Plants* **5**: 1033–1042.

**Zhang F, May A, Irish VF**. **2017**. Type-B ARABIDOPSIS RESPONSE REGULATORs Directly Activate WUSCHEL. *Trends in Plant Science* **22**: 815–817.

**Zhang W, Swarup R, Bennett M, Schaller GE, Kieber JJ**. **2013**. Cytokinin Induces Cell Division in the Quiescent Center of the Arabidopsis Root Apical Meristem. *Current Biology* **23**: 1979–1989.

**Zhang W, To JPC, Cheng CY, Eric Schaller G, Kieber JJ**. **2011**. Type-A response regulators are required for proper root apical meristem function through post-transcriptional regulation of PIN auxin efflux carriers. *The Plant Journal* **68**: 1–10.

**Zhao Y**. **2014**. Auxin Biosynthesis. *The Arabidopsis Book* **12**: e0173.

**Zhao J**. **2022**. Roles of strigolactone signaling in the vascular development during secondary growth of Arabidopsis thaliana. *Heidelberg University, Faculty of Biosciences*: DOI 10.11588/heidok.00032055.

**Zhao Z, Andersen SU, Ljung K, Dolezal K, Miotk A, Schultheiss SJ, Lohmann JU**. **2010**. Hormonal control of the shoot stem-cell niche. *Nature* **465**: 1089–1092.

**Zhou Y, Liu X, Engstrom EM, Nimchuk ZL, Pruneda-Paz JL, Tarr PT, Yan A, Kay SA, Meyerowitz EM**. **2015**. Control of plant stem cell function by conserved interacting transcriptional regulators. *Nature* **517**: 377–380.

**Zubo YO, Clabaugh I, Yamburenko M V, Worthen JM, Street IH, Franco-Zorrilla JM, Zhang W, Hill K, Raines T, Solano R, *et al.* 2017**. Cytokinin induces genome-wide binding of the type-B response regulator ARR10 to regulate growth and development in Arabidopsis. *Proceedings of the National Academy of Sciences* **114**: E5995–E6004.

**Zürcher E, Liu J, Di Donato M, Geisler M, Müller B**. **2016**. Plant development regulated by cytokinin sinks. *Science* **353**: 1027–1030.

**Zürcher E, Tavor-Deslex D, Lituiev D, Enkerli K, Tarr PT, Müller B**. **2013**. A robust and sensitive synthetic sensor to monitor the transcriptional output of the cytokinin signaling network in planta. *Plant Physiology* **161**: 1066–1075.

# 8. Appendix

## 8.1 Code

### 8.1.1 ImageJ Code

ImageJ/ Fiji code (macro) for semi-automated high-throughput phenotyping of *Arabidopsis* hypocotyl cross-sections. This code was generated by Dr. Marjorie Guichard with contributions and finalization by me.

**Macro_Phenotyping_Hypocotly_CrossSections**

```
/*
_____AIM OF THE MACRO_____
This is a script for semi-automated high-throughput phenotyping of hypocotyl cross-sections of Arabidopsis thaliana.
It enables 2D measurement of hypocotyl area, vasculature area, xylem vessel area and xylem area in A. thaliana WT and mutant hypocotyls with cell wall stain.
This script was developed by Dr. Marjorie Guichard with contributions and finalization by M.Sc. Aylin S. Haas.

_____REQUIREMENTS_____
STARTING POINT: none
_____PROCESSING SUMMARY_____
1-Image pre-processing
2-Measure the whole hypocotyl area
3-Measure the vasculature area
4-Measure the xylem vessel area
5-Save the measurements
6-Save the Z-projection with a scale bar
7-Save the selections used for analysis

NOTE: Steps highlighted with "*****" can be adjusted depending of the type of processed images

_____BEFORE STARTING_____
//Use the macro MACRO_Save_as_tiff in order to save all images from a .lif project in the respective folder
//close Fiji and open it again, open this macro again
//Now press 'Run' to run this script and start the analysis.

_____START OF SCRIPT_____*/

//Get input and output directories
indir = getDirectory("Choose INPUT Directroy");
//outdir = getDirectory("Choose OUTPUT Directroy"); // in case you want to select a custom output directory

//To eased up the naming process - initial step
GenotypeName = "";
PlantNumber = "";
```

```
//create the empty result table
filelist = getFileList(indir); // to know how many rows should be in the table at max
TotalRowsToCreate = newArray(lengthOf(filelist)); // to know how many rows should be in the table at max
Table.create("Measurement_full");
Table.setColumn("Image_Name", TotalRowsToCreate);
Table.setColumn("Genotype", TotalRowsToCreate);
Table.setColumn("Plant", TotalRowsToCreate);
Table.setColumn("HypocotylArea",TotalRowsToCreate);
Table.setColumn("VasculatureArea",TotalRowsToCreate);
Table.setColumn("XylemVesselArea",TotalRowsToCreate);
Table.setColumn("XylemArea",TotalRowsToCreate);
Table.setColumn("Phloem+CambiumArea",TotalRowsToCreate);
rowIndex = -1;// useful to fill the result table at the end of the process - initialisation number
// to name the result table and create the result folder

outdir = indir+"Results"; // ******change the name of the experiment, or remove this line in case of custom directory
File.makeDirectory(outdir); // remove this line in case you want to select a custom directory

//process all the images contained in input directory
for (i = 0; i < lengthOf(filelist); i++) {
   if (endsWith(filelist[i], ".tif")) {
      rowIndex = rowIndex+1;// useful to fill the result table at the end of the process
      open(indir + File.separator + filelist[i]);

      //Some cleaning
                  run("Select None");// some cleaning
                  roiManager("reset");// some cleaning
                  run("Clear Results");// some cleaning

      ///////1
                  //Image pre-processing
                  //get image
                  name = getTitle();

                  //get the name of the image without ".tif"
                  dotIndex = indexOf(name, ".tif");
                  nameWOtif = substring(name, 0, dotIndex);

                  //Get the plant labels (input genotype and plant number)
                  selectWindow(name);
                  Dialog.create("What is this image?");
                  Dialog.addString("What is the genotype?" , GenotypeName);
                  Dialog.addString("What is the plant number?", PlantNumber);
                  Dialog.show();
                  GenotypeName = Dialog.getString();
                  PlantNumber = Dialog.getString();
                  PlantNumberTable = GenotypeName + "_" + PlantNumber;

                  //select cell wall stain channel if you took the image with two channels
                  //run("Split Channels");
                  //selectWindow("C1-" + name); //Get the first channel = Direct Red 23 stained Cell wall
                  //(channel two is autofluorescence, stored in channel 2 by using TauSeparation while imaging)
```

```
//make Z maximum projection
run("Z Project...", "projection=[Max Intensity]");

// Make the images 8bit and if needed substract Background
rename("Z-projection_Ori");
run("8-bit");
run("Subtract Background...", "rolling=50"); //***** vary the value from 10 to 50.
run("Set Measurements...", "area redirect=None decimal=2"); // just to be sure that area will be measured in the next steps
//////


///////2
//measure the whole hypocotyl area
selectWindow("Z-projection_Ori");
run("Select None");// some cleaning
roiManager("reset");// some cleaning
run("Clear Results");// some cleaning
run("Duplicate...", "title=Hypocotyl_area");
setAutoThreshold("Huang dark");
setOption("BlackBackground", true);
run("Convert to Mask");
run("Options...", "iterations=10 count=1 black do=Nothing"); //***** vary the iteration value from 5 to 20
run("Dilate");

//checking image (in order for this to work, the outlines of the hypocotyl need to be completely closed
waitForUser("Are you happy?");
//continuing
run("Fill Holes");
run("Erode");
run("Analyze Particles...", "size=5000-Infinity add");
selectWindow("Z-projection_Ori");
roiManager("Select", 0);
getSelectionCoordinates(HypocotylAreaCoordinatesX, HypocotylAreaCoordinatesY); // to keep track of this information
        run("Measure");
        HypocotylArea = getResult("Area", 0);


//////3
//measure the vasculature area
selectWindow("Z-projection_Ori");
run("Select None");// some cleaning
run("Duplicate...", "title=vasculature_area");
setAutoThreshold("Huang dark");
setOption("BlackBackground", true);
run("Convert to Mask");
//checking image (in order for this to work, the outlines of the hypocotyl need to be completely closed
waitForUser("Now please select the vasculature area by drawing a line with the freehand selection tool. Then press OK.");
run("Clear Outside");
run("Options...", "iterations=5 count=1 black do=Nothing"); //***** vary the itereation value from 1 to 5
run("Dilate");
//checking image (in order for this to work, the outlines of the hypocotyl need to be completely closed
```

```
waitForUser("Are you happy?");
run("Fill Holes");
run("Erode");
//continuing
run("Analyze Particles...", "size=3000-Infinity add");
selectWindow("Z-projection_Ori");
roiManager("Select", 1);
getSelectionCoordinates(VasculatureAreaCoordinatesX, VasculatureAreaCoordinatesY); // to keep track of this information
        run("Measure");
        VasculatureArea = getResult("Area", 1);
///////

///////4
//take the third duplicate and measure the xylem vessel area and xylem area
selectWindow("Z-projection_Ori");
run("Select None");// some cleaning
run("Duplicate...", "title=xylem_vessel_area");
waitForUser("Now please select the xylem vessel area by drawing a line with the freehand selection tool. Then press OK.");
roiManager("Add");
roiManager("Select", 2);
getSelectionCoordinates(XylemVesselAreaCoordinatesX, XylemVesselAreaCoordinatesY); // to keep track of this information
        run("Measure");
        XylemVesselArea = getResult("Area", 2);
        //measuring xylem area
run("Convex Hull");
roiManager("Add");
roiManager("Select", 3);
getSelectionCoordinates(XylemAreaCoordinatesX, XylemAreaCoordinatesY); // to keep track of this information
run("Measure");
XylemArea = getResult("Area", 3);

///////




///////5
//Create result table and save the measurements as csv
//Fill the result table
Table.set("Image_Name", rowIndex, name);
Table.set("Genotype", rowIndex, GenotypeName);
Table.set("Plant", rowIndex, PlantNumberTable);
Table.set("HypocotylArea",rowIndex, HypocotylArea);
Table.set("VasculatureArea",rowIndex, VasculatureArea);
Table.set("XylemArea",rowIndex, XylemArea);
Table.set("XylemVesselArea",rowIndex, XylemVesselArea);
Table.set("XylemArea",rowIndex, XylemArea);
Table.set("Phloem+CambiumArea",rowIndex, VasculatureArea-XylemArea);
Table.update;
Table.save(outdir + File.separator + "Results.csv");
///////
```

```
                    /////6
                    //Save the Z-projection with a scale bar

                    //add scalebar
                    selectWindow("Z-projection_Ori");
                    run("Scale Bar...", "width=100 height=8 font=28 color=White background=None location=[Lower Right]
bold overlay");
                    run("Flatten");
                    //generate new file name
                    newname = nameWOtif + "_processed.tif";
                    //save hte image on which the analysis will be done as a tif file
                    saveAs("tiff", outdir + File.separator + newname);
                    ///////

                    /////7
                    //Save the selections used for the analysis
                    roiManager("reset");
                    selectWindow("Z-projection_Ori");
                    makeSelection("polygon", HypocotylAreaCoordinatesX, HypocotylAreaCoordinatesY);
                    roiManager("add");
                    roiManager("select", 0);
                    roiManager("rename", "Hypocotyl_area");
                    makeSelection("polygon", VasculatureAreaCoordinatesX, VasculatureAreaCoordinatesY);
                    roiManager("add");
                    roiManager("select", 1);
                    roiManager("rename", "Vasculature_area");
                    makeSelection("polygon", XylemVesselAreaCoordinatesX, XylemVesselAreaCoordinatesY);
                    roiManager("add");
                    roiManager("select", 2);
                    roiManager("rename", "Xylem_vessel_area");
                    makeSelection("polygon", XylemAreaCoordinatesX, XylemAreaCoordinatesY);
                    roiManager("add");
                    roiManager("select", 3);
                    roiManager("rename", "Xylem_area");
                    roiManager("Select", newArray(1,3));
                    roiManager("XOR");
                    roiManager("add");
                    roiManager("select", 4);
                    roiManager("rename", "Phloem_area");
                    toSelect = newArray(0,1,2,4);
                    roiManager("select", toSelect);
                    roiManager("save", outdir + File.separator + nameWOtif + "_ROI.zip");
                    //////

                    //some cleaning
                    run("Close All");
   }
}
run("Close All");
showMessage("Tada!");
```

### 8.1.2 MATLAB Code

For the 1D cambium growth model, I was involved in the generation of the equations describing the core GRN for the 1D model, but the 1D model layout and code was built by Prof. Dr. Victoria V. Mironova, Dr. Viktoriya Lavrekha M.Sc. Daria Azarova and help of Dr. Maria Savina, with minor input from me.

In this chapter, the MATLAB codes of the 1D cambium growth model are listed. The main MATLAB script hast to be run in a folder containing all the scripts listed in this chapter as individual files. The video file of the wild type model can then be easily generated. The parameters can be adjusted in the code function ‘pass_params’, to obtain the video file of the *wox4* model.

**Main MATLAB script of 1D cambium growth model**

```
%%%1D model for bifacial cell fate decision-making and birdirectional
growth directed by balancing auxin and cytokinin signalling

% % This is the main script for the WT model.

% % The ODEs are described in the script
"differentiation_growth_no_growth" and "differentiation_growth".
% % Cell type definition happens as follows described in the script
"define_cell_type".
% % Parameters are passed in the additional scripts.
% % In order to create the wox4 mutant model, the parameter values of
aWOX4 and n_step_of_calculation need to be adjusted in the pass_params.m
file.
clear all

% Setting up the model: Obtaining auxin and cytokinin distribution in
statics, before cell growth, division, etc. as initial data for the
dynamic model
M_params = pass_params();
N_cells = M_params(1);
lengths = zeros(N_cells,1);
lengths(:) = M_params(2);
%Stating characteristics of the time for calculating the stationary
solution
time = M_params(3);
dt = M_params(4);
printTime = 0:dt:time;

E_params = pass_e_params(M_params); %all parameters to run equestions
tau = M_params(30); %Parameter for defining cell types
tau_st = M_params(31); %Parameter for defining cell stemness
S = M_params(32); %number of varibale sets : substances and cell
characteristics

%Setting up an array of zeros which size depends on S and the number of
cells
%Generally the function "zeros(n)" returns an n-by-n matrix of zeros
%In this case it is an S*N_cells-by-1 matrix of zeros
Y=zeros(S*N_cells,1);
```

```
%Defining non zeros initial values for a correct run of the ode23s
function
for j=1:N_cells
    Y(j) = M_params(42);           %first N_cells - AUXIN
    Y(N_cells+j) = lengths(j);     % second N_cells - cell length
    Y(2*N_cells+j) = M_params(43); % third  N_cells - CYTOKININ
    Y(4*N_cells+j) = M_params(44); % fifth N_cells - WOX4
    Y(5*N_cells+j) = M_params(45); % sixth  N_cells - AS
    Y(6*N_cells+j) = M_params(46); % seventh N_cells - CS

end

%%% Calculation of the differential equations (numerical solution of
differential equations) using the ode23s function.
%%% Obtaining the initial concentration of all substances in all cells.
options = [];
[T, res3] = ode23s(@no_differentiation_growth_activatory, printTime, Y,
options, N_cells, E_params);
%%% Defining the initial cell types dependend on AS and CS for all cells.
%%% The variable "res3" contains all values of all calculation steps of
all substances.
%%% The last calculation step is considered "end"
cell_type = zeros(1,N_cells);
for i = 1:N_cells
    as_i = res3(end, 5*N_cells+i);
    cs_i = res3(end, 6*N_cells+i);

    res3(end, 3*N_cells+i) = define_cell_type(as_i, cs_i, tau, tau_st);
    cell_type(i) = define_cell_type(as_i, cs_i, tau, tau_st);
end

% Preparing the dynamic calculation %%
% specify the number of caluclation steps, if increased the model runs
longer
n_step_of_calculation = M_params(33);
% save and load data of the calculation using function @cell which
returns a sz1-by-sz2 cell array of empty matrices where sz1, sz2 indicate
the size of each dimension
Yres = cell(n_step_of_calculation+1,1);
Rez = cell(n_step_of_calculation,1);

% Setting the time of calculating the dynamics of the cells growth and
division
% "printTime_dynamics" is a vector specifying the interval of integration
% for @ode function
time_dynamics = M_params(34);
printTime_dynamics = 0:dt:time_dynamics;

Kgrow = M_params(35); % constant of cell growth rate
size_min_div = M_params(36); % cell length threshold for cell division
minimum
size_max_div = M_params(37); % cell length threshold for cell division
maximum
aux_diff = M_params(38);   % minimum auxin concentration for xylem cell
differentiation
cyt_diff = M_params(39);   % minimum cytokinin concentration for phloem
cell differentiation
length_diff_xylem = M_params(40); % minimum cell length for xylem cell
differentiation
length_diff_phloem = M_params(41); % minimum cell length for phloem cell
differentiation
```

```
N_cells_initial = size(lengths,1);

auxin = zeros(1,N_cells_initial);
cell_length = zeros(1,N_cells_initial);
cyt = zeros(1,N_cells_initial);
cell_type = zeros(1,N_cells_initial);
wox4 = zeros(1,N_cells_initial);
as = zeros(1,N_cells_initial);
cs = zeros(1,N_cells_initial);

options = [];
Y = res3(end, :);

% Calculation of cell division and differentiation %%

%%% An additional variable to save every step of calculation is needed,
%%% because the cell division is not moderated by the @ode function.
%%% After every step of the numerical solution of the differential
equations,
%%% it needs to be decided if a cell will devide or differentiate.
%%% When a cell divides, a new cell is added to the ensemble.
%%% When a cell differentiates, it is deleted from the ensemble.
Yres{1} = Y;
k = N_cells_initial;

%Setting up counter for PXY+, PXY+ SMXL5+, SMXL5+, xylem, phloem cells
%get and save the statistic data
SMXL5_count = 0;
PXY_count = 0;
SMXL5_PXY_count = 0;
xylem_count = 0;
phloem_count = 0;
division_count = 0;
%arrays in which the number of each cell type is written at each
calculation step
arrSMXL5_count = zeros(n_step_of_calculation+1,1);
arrPXY_count = zeros(n_step_of_calculation+1,1);
arrSMXL5_PXY_count = zeros(n_step_of_calculation+1,1);
arrphloem_count = zeros(n_step_of_calculation+1,1);
arrxylem_count = zeros(n_step_of_calculation+1,1);
arrdivision_count = zeros(n_step_of_calculation+1,1);

%%% The main part of calculating cell growth and division
for m = 1:n_step_of_calculation

    %resetting the value of the cell type counter at each calculation
step
    SMXL5_count = 0;
    PXY_count = 0;
    SMXL5_PXY_count = 0;

    %%% Calculation of the differential equations(numerical solution of
differential equations)using the ode15s function.
    %%% "printTime_dynamics" is a vector specifying the interval of
integration.
    %%% "Yres{m}" is a vector of initial conditions for every step of
calculation.
    %%% After "options" all parameters listed above are inserted for
function @differentiation_growth_activatory

    [T, res3] = ode15s(@differentiation_growth_activatory,
printTime_dynamics, Yres{m}, options, Kgrow, k, E_params);
```

```
    Rez{m} = res3;

    %checking the types of cells, and if necessary, changing them
    for i=1:k
        as_i=res3(end-1, 5*k+i);
        cs_i=res3(end-1, 6*k+i);

        type_i = define_cell_type(as_i, cs_i, tau, tau_st);
        res3(end, 3*k+i) = type_i;
    end

    k0=k; % current cell count

    Ycur=zeros(S*k,1);

    for i=1:k
        auxin(i)=res3(end, i);
        cell_length(i)=res3(end, k+i);
        cyt(i) = res3(end, 2*k+i);
        cell_type(i) = res3(end-1, 3*k+i);

      if cell_type(i)==1
              PXY_count=PXY_count+1;
      elseif cell_type(i)==3
          SMXL5_PXY_count=SMXL5_PXY_count+1;
      elseif cell_type(i)==2
           SMXL5_count=SMXL5_count+1;
      end
        wox4(i) = res3(end, 4*k+i);
        as(i) = res3(end, 5*k+i);
        cs(i) = res3(end, 6*k+i);

        Ycur(i)=res3(end, i);
        Ycur(k+i)=res3(end, k+i);
        Ycur(2*k+i)=res3(end, 2*k+i);
        Ycur(3*k+i)=res3(end, 3*k+i);
        Ycur(4*k+i)=res3(end, 4*k+i);
        Ycur(5*k+i)=res3(end, 5*k+i);
        Ycur(6*k+i)=res3(end, 6*k+i);
    end
    %cell division

    kdiv=k0; % current cell count

    %%% In this loop(from "for" to respective "end")the cells are checked
and divided.
    for i=k:-1:1
        %%% here checking the conditions for division: cell type, cell
length
        if res3(end, 3*k+i)==3 && res3(end, k+i)>=size_min_div &&
res3(end, k+i)<=size_max_div && res3(end,i)>=0.1

            SMXL5_PXY_count=SMXL5_PXY_count+1; % new stem cell after
division
            division_count=division_count+1;

            kdiv=kdiv+1; %the number of cells that will be obtained after
cell division
            Ydiv=zeros(S*kdiv,1); %creating a new cell

            for j=1:kdiv %filling in new and old cells with data
```

```
                if j<i
                    Ydiv(j) = auxin(j);
                    Ydiv(kdiv+j) = cell_length(j);
                    Ydiv(2*kdiv+j) = cyt(j);
                    Ydiv(3*kdiv+j) = cell_type(j);
                    Ydiv(4*kdiv+j) = wox4(j);
                    Ydiv(5*kdiv+j) = as(j);
                    Ydiv(6*kdiv+j) = cs(j);

                elseif j==i

                    Ydiv(j)=auxin(j);
                    Ydiv(j+1)=auxin(j);

                    Ydiv(kdiv+j)=cell_length(j)/2;
                    Ydiv(kdiv+j+1)=cell_length(j)/2;

                    Ydiv(2*kdiv+j) = cyt(j);
                    Ydiv(2*kdiv+j+1) = cyt(j);

                    Ydiv(3*kdiv+j) = cell_type(j);
                    Ydiv(3*kdiv+j+1) = cell_type(j);

                    Ydiv(4*kdiv+j) = wox4(j);
                    Ydiv(4*kdiv+j+1) = wox4(j);

                    Ydiv(5*kdiv+j) = as(j);
                    Ydiv(5*kdiv+j+1) = as(j);

                    Ydiv(6*kdiv+j) = cs(j);
                    Ydiv(6*kdiv+j+1) = cs(j);

                elseif j>i+1
                    Ydiv(j)=auxin(j-1);
                    Ydiv(kdiv+j)=cell_length(j-1);
                    Ydiv(2*kdiv+j)=cyt(j-1);
                    Ydiv(3*kdiv+j)=cell_type(j-1);
                    Ydiv(4*kdiv+j) = wox4(j-1);
                    Ydiv(5*kdiv+j) = as(j-1);
                    Ydiv(6*kdiv+j) = cs(j-1);

                end
            end

            Ycur=Ydiv; %fill in new and old cells with data

            auxin = Ycur(1:kdiv);
            cell_length = Ycur(kdiv+1:2*kdiv);
            cyt = Ycur(2*kdiv+1:3*kdiv);
            cell_type = Ycur(3*kdiv+1:4*kdiv);
            wox4 = Ycur(4*kdiv+1:5*kdiv);
            as = Ycur(5*kdiv+1:6*kdiv);
            cs = Ycur(6*kdiv+1:7*kdiv);

            k=kdiv;
        end
    end
    if k0~=k
        %display a message about cell division in the matlab console
        disp 'division happened';

    end
```

```
    %cell differentiation = cell is removed from the cell ensemble

    %%% Condition for cell differentiation to phloem: checking CYTOKININ
concentration in the cell and the cell length
    if Ycur(3*k)>cyt_diff && Ycur(2*k)>length_diff_phloem
        kdeath=k-1;
        Ydeath=zeros(S*kdeath,1);
        for i=1:kdeath
           Ydeath(i)=Ycur(i);
           Ydeath(kdeath+i)=Ycur(k+i);
           Ydeath(2*kdeath+i)=Ycur(2*k+i);
           Ydeath(3*kdeath+i)=Ycur(3*k+i);
           Ydeath(4*kdeath+i)=Ycur(4*k+i);
           Ydeath(5*kdeath+i)=Ycur(5*k+i);
           Ydeath(6*kdeath+i)=Ycur(6*k+i);
        end
        Ycur=Ydeath;
        k=kdeath;

        phloem_count=phloem_count+1;
        %display a message about cell differentiation in the matlab
console
        disp 'SMXL5 cell differention happened';

    end
    %%% Condition for cell differentiation to xylem: checking AUXIN
concentration in the cell and the cell length
    if Ycur(1)>aux_diff && Ycur(k+1)>length_diff_xylem
        kdeath=k-1;
        Ydeath=zeros(S*kdeath,1);
        for i=1:kdeath
           Ydeath(i)=Ycur(i+1);
           Ydeath(kdeath+i)=Ycur(k+i+1);
           Ydeath(2*kdeath+i)=Ycur(2*k+i+1);
           Ydeath(3*kdeath+i)=Ycur(3*k+i+1);
           Ydeath(4*kdeath+i)=Ycur(4*k+i+1);
           Ydeath(5*kdeath+i)=Ycur(5*k+i+1);
           Ydeath(6*kdeath+i)=Ycur(6*k+i+1);
        end
        Ycur=Ydeath;
        k=kdeath;

        xylem_count=xylem_count+1;
        %display a message about cell differentiation in the matlab
console
        disp 'PXY cell differention happened';

    end

    %write data for the next step of calculation
    Yres{m+1}=Ycur;

    arrSMXL5_count(m)=SMXL5_count;
    arrPXY_count(m)=PXY_count;
    arrSMXL5_PXY_count(m)=SMXL5_PXY_count;
    arrphloem_count(m)=phloem_count;
    arrxylem_count(m)=xylem_count;
    arrdivision_count(m)=division_count;

    clear res3
```

```
end
disp 'end of calculation';

% Preparing recording of the video
%%% Before drawing the whole video, the maximal length of the cell
%%% ensebmles from each calculation step needs to be considered.

length_max = 0;
g_max = 0;
i_max = 0;
for iu = 2:size(Yres,1)
    g_max_iu=size(Yres{iu},1)/S;
    if g_max_iu>g_max
        g_max = g_max_iu;
        i_max = iu;
    end
    length_iu = 0;
    for i=1:g_max_iu
        length_iu = length_iu+Yres{iu}(g_max_iu+i);
    end
    if length_iu>length_max
        length_max = length_iu;
    end
end

length_max = length_max+1;
% Recording the video
%%% In order to make the video file: drawing a figure from every one
(two, five,
%%% or ten...) calculation result and join them together one by one -
frame(s) = getframe(gcf)
disp 'recording video'
s=1;
for j=1:2:(size(Yres,1))-1 % set the start and finish time points for the
video
    g=max(size(Yres{j},1),size(Yres{j},2)) ;

    %the connection between the cellular state and the color of cells in
the video
    cellstate1=ones(1,g/S)*0.98;
    cellstate2=ones(1,g/S)*0.25;
    cellstate3=ones(1,g/S)*0.75;

    %arrays storing the length of cells for each state needed for marking
cells in a cell ensemble
    X1=zeros(4,g/S);
    Y1=zeros(4,g/S);
    X2=zeros(4,g/S);
    Y2=zeros(4,g/S);
    X3=zeros(4,g/S);
    Y3=zeros(4,g/S);

    %arrays of concentrations of substances in each cell
    auxin_p = zeros(1,g/S);
    cyt_p = zeros(1,g/S);
    cell_size_p = zeros(1,g/S);
    cell_type_p = zeros(1,g/S);
    wox4_p = zeros(1,g/S);
    as_p = zeros(1,g/S);
    cs_p = zeros(1,g/S);
```

```
    %arrays needed to mark the cell ensemble, taking into account the
size of the cells
    x = zeros(1,g/S);
    X = zeros(4,g/S);
    Y = zeros(4,g/S);
    c = zeros(1,g/S);

    Y(4,:) = -0.2;
    Y(3,:) = -0.2;
    for i=1:g/S
        auxin_p(i) = Yres{j}(i);
        cyt_p(i) = Yres{j}(2*g/S+i);
        cell_type_p(i) = Yres{j}(3*g/S+i);
        cell_size_p(i) = Yres{j}(g/S+i);
        wox4_p(i) = Yres{j}(4*g/S+i);
        as_p(i) = Yres{j}(5*g/S+i);
        cs_p(i) = Yres{j}(6*g/S+i);
    end

    %filling the lattice of cells with cell sizes in the cell ensemble in
the video
    for i=1:g/S
        if i==1
            X(2,i)=cell_size_p(i);
            X(3,i)=cell_size_p(i);
        else
            X(2,i)=X(2,i-1)+cell_size_p(i);
            X(3,i)=X(3,i-1)+cell_size_p(i);
            X(1,i)=X(2,i-1);
            X(4,i)=X(3,i-1);
        end
        x(i) = abs(X(1,i)+X(2,i))/2;
        c(i) = Yres{j}(2*g/S+i);

        %painting over the cells in the cell ensemble in accordance with
the cell type
        if cell_type_p(i) == 3
            cellstate1(:) = 0.82;
            X1(:,i) = X(:,i);
            Y1(:,i) = Y(:,i);
            stem_coordX = (X1(1,i)+X1(2,i))/2;
        elseif cell_type_p(i) == 2
            cellstate2(:) = 0.55;
            X2(:,i) = X(:,i);
            Y2(:,i) = Y(:,i);
        else
            cellstate3(:) = 0.65;
            X3(:,i) = X(:,i);
            Y3(:,i) = Y(:,i);
        end
    end
    %after color preparation for cell type drawing the figure.
    fig = figure ('visible','off','Color','w');
    hold on;

    %drawing the cells of the cell ensemble
    patch([[0;0.0001;0.0001;0],X1],[[0;0;-0.0001;-
0.0001],Y1],[cellstate1,cellstate1(1)],'EdgeColor','black','LineStyle','-
','LineWidth',0.3);
    patch([[0;0.0001;0.0001;0],X2],[[0;0;-0.0001;-
0.0001],Y2],[cellstate2,cellstate2(1)],'EdgeColor','black','LineStyle','-
','LineWidth',0.3);
```

```
    patch([[0;0.0001;0.0001;0],X3],[[0;0;-0.0001;-
0.0001],Y3],[cellstate3,cellstate3(1)],'EdgeColor','black','LineStyle','-
','LineWidth',0.3);
    map_cells = [0.95, 0.95, 0.95
                 0.45, 0.45, 0.45
                 0.75, 0.75, 0.75
                 ];
    colormap(gray);
    caxis([0,1]);

    %creating graphs of the concentration of the substances in each cell
    hAuxin = plot(x, auxin_p,'g-s');%, 'DisplayName', 'Auxin');
    hCyt = plot(x, cyt_p,'b-s');%, 'DisplayName', 'Cytokinin');
    hWOX4 = plot(x, wox4_p,'r-');%, 'DisplayName', 'WOX4');
    hAS = plot(x, as_p,'c-');%, 'DisplayName', 'AS');
    hCS = plot(x, cs_p,'m-');%, 'DisplayName', 'CS');
    legend([hAuxin,hCyt,hWOX4,hAS,hCS],'AUXIN','CYTOKININ','WOX4', 'AS',
'CS');

    axis([0 length_max -0.3 5]); % same axis for all figures in video

    % adding different types of cell counters to the video

    str_SMXL5_count_cell=['SMXL5+  = ' num2str(arrSMXL5_count(j))]; %
make string from text and numbers
    text(2,4.5,str_SMXL5_count_cell,'FontSize',7) % funtion @text creates
text object: text(x,y,'string','PropertyName',PropertyValue....)

    str_PXY_count_cell=['PXY+ = ' num2str(arrPXY_count(j))];
    text(2,3.5,str_PXY_count_cell,'FontSize',7)

    str_SMXL5_PXY_count_cell=['SMXL5+ PXY+ = '
num2str(arrSMXL5_PXY_count(j))];
    text(2,2.5,str_SMXL5_PXY_count_cell,'FontSize',7)

    str_xylem_count_cell=['xylem = ' num2str(arrxylem_count(j))];
    text(7,4.5,str_xylem_count_cell,'FontSize',7)

    str_phloem_count_cell=['phloem = ' num2str(arrphloem_count(j))];
    text(7,3.5,str_phloem_count_cell,'FontSize',7)

    str_division_count_cell=['Stem cell divisions = '
num2str(arrdivision_count(j))];
    text(7,2.5,str_division_count_cell,'FontSize',7)

    title ('cambium');

    hold off;

    frame(s) = getframe(gcf); %save figure to frame and put it in the
arrays of frames
    s = s+1;
    close(fig);

    %displaying amessage on the matlab console about the percentage of
the video that has already been recorded
    if j==round(size(Yres,1)/2)
        disp 'recording video 50% '
    end

    if j==round(size(Yres,1)/4)
        disp 'recording video 25% '
```

```
    end
end
%collecting the frames drawn in the previous block into the video
%Name the video
mov = VideoWriter('Cellular_model_WT.mp4','MPEG-4');
mov.FrameRate = 50;
open(mov)
writeVideo(mov,frame)
close(mov)
fprintf('END\n');

%end of script
```

**Function** ‘define_cell_type’

```
%Script for defining the cell type upon differentation based on auxin
signalling (AS)
% and  cytokinin signalling (CS) ratio
% % Cell type 1, xylem precursor (PXY+) if AS > CS + tau
% % Cell type 2, phloem precursor (SMXL5+) if AS + tau < CS
% % Cell type 3, stem cell (PXY+/SMXL5+) if CS - tau < AS < CS + tau

function type = define_cell_type(as,cs,tau,tau_st)

p = abs(as-cs);

    if (abs(as-cs))/(as+cs) < tau_st
        type = 3;

    else
       if p > tau
           if as+tau > cs
                type = 1;
           end;
           if cs+tau > as
                type = 2;
            end;
       else
           if as+p > cs
                type = 1;
           end;
           if cs+p > as
                type = 2;
           end;
       end;
    end;
 end
```

**Function** ‘delution’

```
function res = delution(substance, L)

res = substance/L;
end
```

**Function** 'differentiation_growth_activatory'

```
function dy = differentiation_growth_activatory(t, y, Kgrow,k,e_params)
dy=zeros(7*k,1);

alpha = e_params(1);          %alpha - Auxin flow rate
aks = e_params(3);            %aks - Auxin synthesis constant
akd = e_params(3);            %akd - Auxin degradation constant
aD = e_params(4);             %aD - Auxin diffusion constant
a_lat_comp = e_params(5);     %a_lat_comp - Auxin lateral compensation

betta = e_params(6);          %betta - Cytokinin flow rate
cks = e_params(7);            %cks - Cytokinin synthesis constant
ckd = e_params(8);            %ckd - Cytokinin degradation constant
cD = e_params(9);             %cD - Cytokinin diffusion constant
c_lat_comp = e_params(10);    %c_lat_comp - Cytokinin lateral compensation

kdWOX4 = e_params(11);
kdAS = e_params(12);
kdCS = e_params(13);

h1 = e_params(14);             %h for WOX4

aWOX4 = e_params(15);
aAS = e_params(16);
aCS = e_params(17);

q_Auxin_AS = e_params(18);
q_WOX4_AS = e_params(19);
q_CS_AS = e_params(20);

q_Cytokinin_CS = e_params(21);
q_WOX4_CS = e_params(22);
q_AS_CS = e_params(23);

h2 = e_params(24);          %h for AUXIN
h3 = e_params(25);          %h for CYTOKININ


    for i=1:k

        AUXIN = y(i);
        CYTOKININ = y(2*k+i);

        WOX4 = y(4*k+i);
        AS = y(5*k+i);
        CS = y(6*k+i);

        length_i = y(k+i);
        cyt_i = y(2*k+i);

        aux_sinth_i = -akd*y(i) - (1-a_lat_comp)*(2*length_i)*aD*y(i);
%auxin accumulation and degradation for each cell
        cyt_sinth_i = -ckd*cyt_i -(1-c_lat_comp)*(2*length_i)*cD*cyt_i;
%cytokinin accumulation and degradation for each cell

        %cell type dependent synthesis
        if y(3*k+i) == 1 || y(3*k+i) == 3
            aux_sinth_i = aux_sinth_i+aks;
        elseif y(3*k+i) == 2
            cyt_sinth_i = cyt_sinth_i+cks;
        end;
```

```
        if i==1
            dy(i) = alpha + aD*y(i+1) - aD*y(i); %auxin influx, border
condition and diffusion for the first xylem cell
            dy(2*k+i) = cD*y(2*k+i+1) - cD*cyt_i; %cytokinin border
condition and diffusion

        elseif i==k
            dy(i) = aD*y(i-1)-aD*y(i); %border condition for auxin: flux
and influx by passive transport in the border (phloem) cell
            dy(2*k+i) = betta - cD*cyt_i + cD*y(2*k+i-1); %cytokinin
influx from phloem, border condition for passive transport

        else
            dy(i) = aD*y(i+1)+aD*y(i-1) - 2*aD*y(i); %auxin passive
transport between i, next and previous cells
            dy(2*k+i) = cD*y(2*k+i+1)+ cD*y(2*k+i-1) - 2*cD*cyt_i;
%cytokinin passive transport between i, next and previous cells

        end;

       %Equations for interaction
       %dWOX4
       dy(4*k+i) = (1-(abs(AS-CS)/(AS+CS)))*aWOX4-(kdWOX4*WOX4);
       %dAS
       dy(5*k+i) =
aAS*((WOX4^h1)+(AUXIN^h2)/(1+(WOX4^h1/q_WOX4_AS)+(AUXIN^h2/q_Auxin_AS)+(C
S^h1/q_CS_AS)))-(kdAS*AS);
       %dCS
       dy(6*k+i) =
aCS*((WOX4^h1)+(CYTOKININ^h3)/(1+(WOX4^h1/q_WOX4_CS)+(CYTOKININ^h3/q_Cyto
kinin_CS)+(AS^h1/q_AS_CS)))-(kdCS*CS);


        %auxin
        dy(i) = delution((dy(i)+aux_sinth_i),length_i);
        %cytokinin
        dy(2*k+i) = delution((dy(2*k+i)+cyt_sinth_i),length_i);
        %dWOX4
        dy(4*k+i) = delution(dy(4*k+i),length_i);
        %dAS
        dy(5*k+i) = delution(dy(5*k+i),length_i);
        %dCS
        dy(6*k+i) = delution(dy(6*k+i),length_i);



        %cell growth
        if y(3*k+i) == 3 || y(k+i)<1

            dy(k+i) = Kgrow;
        elseif y(3*k+i) == 2 && y(2*k+i)>=1.5
            dy(k+i) = Kgrow;
        elseif y(3*k+i) == 1 && y(i)>=1.5
            dy(k+i) = Kgrow;
        else
            dy(k+i) = 0;
        end;

    end;

end
```

**Function** 'no_differentiation_growth_activatory'

```
function dy = no_differentiation_growth_activatory(t, y,
N_cells,e_params)

alpha = e_params(1);          %alpha - Auxin flow rate
aKd = e_params(3);            %akd - Auxin degradation constant
aD = e_params(4);             %aD - Auxin diffusion constant + PIN347
a_lat_comp = e_params(5);     %a_lat_comp - Auxin lateral compensation

betta = e_params(6);         %betta - Cytokinin flow rate
cKd = e_params(8);           %ckd - Cytokinin degradation constant
cD = e_params(9);            %cD - Cytokinin diffusion constant
c_lat_comp = e_params(10);    %c_lat_comp - Cytokinin lateral compensation

kdWOX4 = e_params(11);
kdAS = e_params(12);
kdCS = e_params(13);

h1 = e_params(14);             %h for WOX4

aWOX4 = e_params(15);
aAS = e_params(16);
aCS = e_params(17);

q_Auxin_AS = e_params(18);
q_WOX4_AS = e_params(19);
q_CS_AS = e_params(20);

q_Cytokinin_CS = e_params(21);
q_WOX4_CS = e_params(22);
q_AS_CS = e_params(23);

h2 = e_params(24);          %h for AUXIN
h3 = e_params(25);          %h for CYTOKININ

k = N_cells;
dy = zeros(7*k,1);

     for i=1:k
        AUXIN = y(i);
        CYTOKININ = y(2*k+i);

        WOX4 = y(4*k+i);
        AS = y(5*k+i);
        CS = y(6*k+i);


        length_i = y(k+i);
        cyt_i = y(2*k+i);

        aux_sinth_i = -aKd*y(i)-(1-a_lat_comp)*(2*length_i)*aD*y(i)-
y(i)*dy(k+i); %auxin accumulation and degradation for each cell
        cyt_sinth_i = -cKd*cyt_i -(1-c_lat_comp)*(2*length_i)*cD*cyt_i -
cyt_i*dy(k+i); %cytokinin accumulation and degradation for each cell

        if i==1
            dy(i) = alpha + aD*y(i+1) - aD*y(i); %auxin influx, border
condition and diffusion for the first xylem cell
            dy(2*k+i) = cD*y(2*k+i+1) - cD*cyt_i; %cytokinin border
condition and diffusion
```

```
        elseif i==k
            dy(i) = aD*y(i-1) - aD*y(i); %border condition for auxin:
flux and influx by passive transport in the border (phloem) cell
            dy(2*k+i) = betta - cD*cyt_i + cD*y(2*k+i-1); %cytokinin
influx from phloem, border condition for passive transport

        else
            dy(i) = aD*y(i+1) + aD*y(i-1) - 2*aD*y(i); %auxin passive
transport between i, next and previous cells
            dy(2*k+i) = cD*y(2*k+i+1) + cD*y(2*k+i-1) - 2*cD*cyt_i;
%cytokinin passive transport between i, next and previous cells

        end;

       %Equations for interaction
       %dWOX4
       dy(4*k+i) = (1-(abs(AS-CS)/(AS+CS)))*aWOX4-(kdWOX4*WOX4);
       %dAS
       dy(5*k+i) =
aAS*((WOX4^h1)+(AUXIN^h2)/(1+(WOX4^h1/q_WOX4_AS)+(AUXIN^h2/q_Auxin_AS)+(C
S^h1/q_CS_AS)))-(kdAS*AS);
       %dCS
       dy(6*k+i) =
aCS*((WOX4^h1)+(CYTOKININ^h3)/(1+(WOX4^h1/q_WOX4_CS)+(CYTOKININ^h3/q_Cyto
kinin_CS)+(AS^h1/q_AS_CS)))-(kdCS*CS);

       %delution function
        %auxin
        dy(i) = delution((dy(i)+aux_sinth_i),length_i);
        %cytokinin
        dy(2*k+i) = delution((dy(2*k+i)+cyt_sinth_i),length_i);
        %dWOX4
        dy(4*k+i) = delution(dy(4*k+i),length_i);
        %dAS
        dy(5*k+i) = delution(dy(5*k+i),length_i);
        %dCS
        dy(6*k+i) = delution(dy(6*k+i),length_i);

       %no cell grows for get initial concentrations of substances in the
       %cell ensemble
       dy(k+i) = 0;

    end;
end
```

**Function** 'pass_e_params'

```
function e_params = pass_e_params(M_params)
%Passing parameters for equestion
e_params = zeros(1,25);
%Passing auxin and cytokinin parameters
e_params(1) = M_params(5);    %alpha - Auxin flow rate
e_params(2) = M_params(6);    %aks - Auxin synthesis constant - PIN1
e_params(3) = M_params(7);    %akd - Auxin degradation constant
e_params(4) = M_params(8);    %aD - Auxin diffusion constant + PIN347
e_params(5) = M_params(9);    %a_lat_comp - Auxin lateral compensation

e_params(6) = M_params(10);   %betta - Cytokinin flow rate
e_params(7) = M_params(11);   %cks - Cytokinin synthesis constant
e_params(8) = M_params(12);   %ckd - Cytokinin degradation constant
e_params(9) = M_params(13);   %cD - Cytokinin diffusion constant
```

```
e_params(10) = M_params(14);  %c_lat_comp - Cytokinin lateral
compensation

%Passing the parameters of the gene regulatory network
e_params(11) = M_params(15);  %kdWOX4
e_params(12) = M_params(16);  %kdAS
e_params(13) = M_params(17);  %kdCS

e_params(14) = M_params(18);  %h for WOX4

e_params(15) = M_params(19);  %aWOX4
e_params(16) = M_params(20);  %aAS
e_params(17) = M_params(21);  %aCS

e_params(18) = M_params(22);  %q_Auxin_AS
e_params(19) = M_params(23);  %q_WOX4_AS
e_params(20) = M_params(24);  %q_AS_CS

e_params(21) = M_params(25);  %q_Cytokinin_CS
e_params(22) = M_params(26);  %q_WOX4_CS
e_params(23) = M_params(27);  %q_AS_CS

e_params(24) = M_params(28);  %h for AUXIN
e_params(25) = M_params(29);  %h for CYTOKININ

end
```

**Function** 'pass_params'

```
function model_params = pass_params()
model_params = zeros(1,46);

model_params(1) = 11;      %N_cells
model_params(2) = 1;       %length of cell

%Stating characteristics of the time for calculating the stationary
solution
%before starting the dynamics and before starting the growth and division
of cells.
model_params(3) = 5000;    %time
model_params(4) = 10;      %dt

%Passing auxin and cytokinin parameters
model_params(5) = 1.1;     %alpha - Auxin flow rate
model_params(6) = 0.01;    %aks - Auxin synthesis constant - PIN1
model_params(7) = 0.006;   %akd - Auxin degradation constant
model_params(8) = 0.4;     %aD - Auxin diffusion constant + PIN347
model_params(9) = 0.85;    %a_lat_comp - Auxin lateral compensation

model_params(10) = 0.18;   %betta - Cytokinin flow rate
model_params(11) = 0.0036; %cks - Cytokinin synthesis constant
model_params(12) = 0.007;  %ckd - Cytokinin degradation constant
model_params(13) = 0.085;  %cD - Cytokinin diffusion constant
model_params(14) = 0.9;    %c_lat_comp - Cytokinin lateral compensation

model_params(15) = 1;      %kdWOX4
model_params(16) = 1;      %kdAS
model_params(17) = 1;      %kdCS

model_params(18) = 2;      %h for WOX4
```

```
model_params(19) = 0.4;     %aWOX4 %for WT model: aWOX4= 0.4 %for mutant
model: aWOX4= 0.2
model_params(20) = 1;       %aAS
model_params(21) = 1;       %aCS

model_params(22) = 1;       %q_Auxin_AS
model_params(23) = 1;       %a_WOX4_AS
model_params(24) = 1;       %q_CS_AS

model_params(25) = 1;       %q_Cytokinin_CS
model_params(26) = 1;       %q_WOX4_CS
model_params(27) = 1;       %q_AS_CS

model_params(28) = 2;       %h for AUXIN
model_params(29) = 2;       %h for CYTOKININ

model_params(30) = 0.001;  %tau - Parameter for defining cell types
model_params(31) = 0.03;   %tau_st - Parameter for defining cell stemness
model_params(32) = 7;       %S - number of varibale sets : substances and
cell characteristics

model_params(33) = 2000;   %n_step_of_calculation %2000 for WT model,
%1000 for wox4 mutant model
model_params(34) = 100;     %time_dynamics

model_params(35) = 10^(-4); %Kgrow - constant of cell growth rate
model_params(36) = 1.5;      %size_min_div - cell length threshold for
cell division minimum
model_params(37) = 2.5;      %size_max_div - cell length threshold for
cell division maximum
model_params(38) = 1.5;      %aux_diff - minimum auxin concentration for
xylem cell differentiation
model_params(39) = 1.5;      %cyt_diff - minimum cytokinin concentration
for phloem cell differentiation
model_params(40) = 3;        %length_diff_xylem - minimum cell length for
xylem cell differentiation
model_params(41) = 3;        %length_diff_phloem - minimum cell length for
phloem cell differentiation

%initial concentration condition of variables
model_params(42) = 0.01;     %variable - AUXIN
model_params(43) = 0.1;      %variable - CYTOKININ
model_params(44) = 0.01;     %variable - WOX4
model_params(45) = 0.01;     %variable - AS
model_params(46) = 0.01;     %variable - CS

end
```

## 8.2 Publications

**Haas AS**, Shi D, Greb T. (2022) Cell Fate Decisions Within the Vascular Cambium – Initiating Wood and Bast Formation. *Frontiers in Plant Science*. 13:864422.

DOI: https://doi.org/10.3389/fpls.2022.864422

Parts of this publication are presented in this thesis with corresponding reference.

## 8.3 Abbreviations

Abbreviations introduced in the text this work or commonly used in molecular biology are listed below.

| | |
|---|---|
| *Agrobacterium* | *Agrobacterium tumefaciens* |
| *Arabidopsis* | *Arabidopsis thaliana* |
| AHK | ARABIDOPSIS HISTIDINE KINASE |
| AHP | ARABIDOPSIS HISTIDINE PHOSPHOTRANSFER |
| ANAC | NAC DOMAIN CONTAINING PROTEIN |
| ANT | ANTEGUMENTA |
| ARF | AUXIN RESPONSE FACTOR |
| ARR | ARABIDOPSIS RESPONSE REGULATOR |
| APL | ALTERED PHLOEM DEVELOPMENT |
| ATP | adenosine triphosphate |
| BP/KNAT1 | BREVIPEDICELLUS/KNOTTED-1LIKE |
| ChIP | Chromatin Immunoprecipitation |
| CLE | CLAVATA3/EMBRYO SURROUNDING REGION- related |
| *Col-0* | *Arabidopsis* Columbia ecotype |
| CSC | (Vascular) cambium stem cell |
| DEG | Differentially expressed gene |
| Dex | Dexamethasone |
| DNA | Desoxyribonucleic acid |
| DOF | DNA-BINDING WITH ONE FINGER |
| DR5 | Auxin signalling sensor (Direct repeat 5) |
| *E. coli* | *Escherichia coli* |
| EDTA | Ethylenediaminetetraacetic acid |
| EMSA | Electrophoretic Mobility Shift Assay |
| ER | Endoplasmic reticulum |
| EtOH | Ethanol |
| GFP | Green fluorescent protein |
| GO | Gene ontology |
| GR | glucocorticoid receptor |
| GRN | Gene regulatory network |
| HAM | HAIRY MERISTEM |
| HD-ZIP III | Class III HOMEODOMAIN LEUCINE ZIPPER |
| IAA | Indole-3-acetic-acid |
| IPT | ISOPENTYL TRANSFERASE |
| KMD | KISS ME DEADLY |
| LBD | LATERAL ORGAN BOUNDARIES DOMAIN |

| | |
|---|---|
| LHW | LONESOME HIGHWAY |
| LM | Low melting |
| LOG | LONELY GUY |
| logFC | log2 Fold Change |
| M | Molar |
| mCherry | Monomeric Cherry |
| MP | MONOPTEROS (ARF5) |
| MS | Murashige and Skoog |
| ODE | Ordinary differential equation |
| PBS | Phosphate buffered saline |
| padj | p adjusted |
| PCR | Polymerase chain reaction |
| PEAR | PHLOEM EARLY DOF |
| PFA | Paraformaldehyde |
| PIN | PIN-FORMED |
| PUP | PURINE PERMEASE |
| PXY | PHLOEM INTERCALETED WITH XYLEM |
| RAM | Root apical meristem |
| RFP | Red fluorescent protein |
| RNA | Ribonucleic acid |
| RT | Room temperature |
| SAM | Shoot apical meristem |
| SAUR | SMALL AUXIN UPREGULATED |
| SDS | Sodium dodecyl sulfate |
| SMXL | SUPPRESSOR OF MAX2 1-LIKE |
| TCS | Two component system sensor |
| T-DNA | Transfer DNA |
| TMO | TARGET OF MONOPTEROS |
| WOL | WOODEN LEG |
| WOX | WUSCHEL RELATED HOMEOBOX |
| WUS | WUSCHEL |
| YFP | Yellow fluorescent protein |

## 8.4 List of figures in the main text

## 8.5 List of tables in the main text